THESIS

DUNE EROSION NEAR SEA WALLS

XBEACH VALIDATION

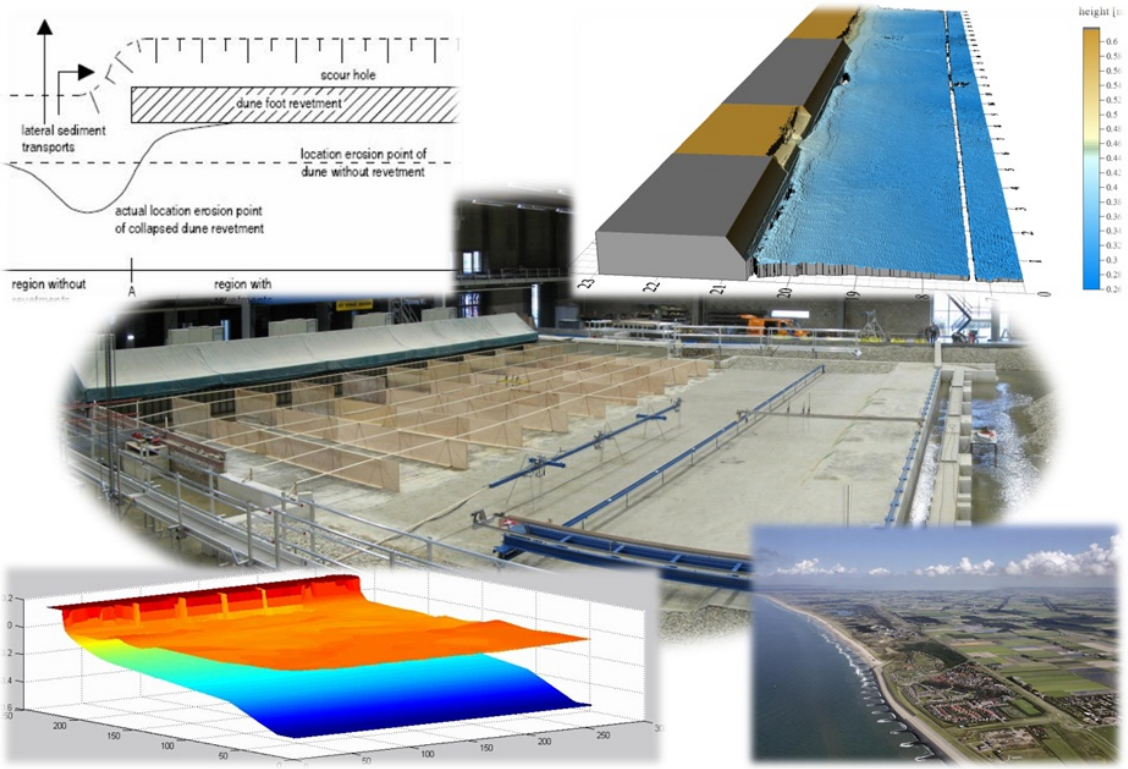

ING B.B. DE VRIES

DELFT UNIVERSITY OF TECHNOLOGY & DELTARES
21 JUNE 2011

TU Delft
Delft University of Technology

Deltares
Enabling Delta Life

DUNE EROSION NEAR SEA WALLS

XBEACH VALIDATION

MASTER THESIS

BY

ING B.B. DE VRIES

STUDENTNUM: 1368486

DELFT UNIVERSITY OF TECHNOLOGY

FACULTY OF CIVIL ENGINEERING AND GEOSCIENCES

SECTION OF HYDRAULIC ENGINEERING

IN CONJUNCTION WITH

DELTARES

DELFT, 21 JUNE 2011

GRADUATION COMMITTEE:
PROF.DR.IR. M.J.F. STIVE (CHAIRMAN)
IR. P.F.C. VAN GEER
IR. A.R. VAN DONGEREN
IR. J.S.M. VAN THIEL DE VRIES
Ir. P.B. Smit

TU Delft
Delft University of Technology

Deltares
Enabling Delta Life

Preface

This report presents the findings of the master thesis on the subject dune erosion near seawalls. The thesis was carried out in the framework of the Master program at the faculty of Civil Engineering & Geoscienes at Delft University of Technology. The project was executed at Deltares. The subject of the thesis originates from the Rijkswaterstaat programme “Strength and Loads on Water Defenses (SBW)”. This programme requires new assessment software to assess the coastal protection in complex situations.

When I started the project the information on the interaction between dunes and structures was limited. I want to thank my supervisors Ap, Jaap and Pieter for their feedback throughout the project. They really helped me to get a grasp on the matter and set the boundaries for this project. They showed a lot of patience when reviewing the draft reports. I specifically want to thank Pieter for the countless hours he spend helping me when I was struggling with Matlab again. Ap en Jaap for their help when XBeach didn’t do what I wanted it to do.

In general I thank the many people that gave me help and support without which I could not have presented this report to you now.

Delft, September 2011

B.B. de Vries

Summary

Introduction

The Dutch coastline mainly consists of dunes and sea-dikes. Every 6 years the strength of the water defenses is checked by the Dutch authorities. At the connection between dunes and sea-dikes the assessment rules prescribe additional erosion of the dunes next to the structure. The prescribed amount of additional erosion is based on expert judgement and was not validated with measurements. Assessors questioned the accuracy of the assessment rules for a combination of dunes and structures in planform.

The alongshore exchange of sediment is important for the development of additional erosion near structures. The present 1D assessment model DUROS+ can not assess the transition between dunes and structures. They need to be assessed in a dedicated manner, which takes time and money. Therefore the Dutch Dune Safety Assessment demands advanced models to assess the coastal protection in complex situations. One such model is XBeach. XBeach is a two-dimensional (2DH) model that predicts the morphological changes in the coastal zone during a storm. XBeach fully includes the longshore direction, which makes it a useful tool to assess sea defenses in complex situations.

Storm impact on a dune-dike system

During a storm dunes erode and provide sediment to the beach. The foreshore rises and the wave height and hence the wave force F_x in front of the dunes decreases. Subsequently the wave-induced water level setup increases. The surface of seawalls prevent erosion by cutting off the supply of sediment to the beach. Waves in front of a seawall remain high throughout the storm and can even increase. Subsequently the wave-induced water level setup decreases.

Over the transition the amount of sediment available for erosion with respect to the dunes decreases. The longshore distance over which the supply of sediment changes depends on the shape and size of the connection. The longshore gradient in the sediment supply causes a difference in elevation of the foreshore. The difference in wave-induced water level setup between dunes and seawalls cause a water level gradient over the transition. The water level gradient drives a current which transports sediment from the dunes to the seabed in front of the seawall. The loss of sediment to the dike profile causes the foreshore of dunes near the connection to rise slower. More and higher waves reach the dunes near the connection during the storm which results in more erosion.

Obliquely incident waves generate a longshore current which transports sediment along the shore. The velocity and transport capacity of the longshore current depend on the dissipation of wave energy. Seawalls reflect incoming waves and the dissipation of wave energy is limited. Consequently the velocity and transport capacity of the longshore current is limited. In a dune transect the dissipation of wave energy and hence the transport capacity of the longshore current is larger. Subsequently there is a longshore gradient in transport capacity in the transition zone.

The amount of additional erosion near structures depends on the angle of wave incidence with respect to the shore. Dunes situated downstream of the connection experience a significant increases in erosion (Steetzel, 1993). Near the upstream connection the decreasing transport capacity of the longshore current causes sediment to be deposited on the seabed in front of the structure. Sediment will pile up against the structure resulting in less erosion near the connection compared to dunes under identical longshore uniform conditions.

Model behaviour of a dune-dike system

The behaviour of a dune-dike system was investigated with exploratory 2DH simulations of a simple closed abrupt connection between dunes and a dike. Dune erosion is quantified by the retreat point R* and the erosion volume A. The behaviour of an undisturbed dune and dike transect is modeled with 1D models. Undisturbed means that there is no influence of a dune-dike connection on process behaviour.

The dune erosion process is simulated correctly by XBeach. After the storm the beach has become wider. The dune foot has moved in landward direction while the waterline moved seaward. The vertical position of the dune foot hardly changed. The behaviour of a dike transect during a storm is modeled well in a qualitative sense. The erosion depth near the toe of a structure is underestimated. This is likely to be caused by an underestimation of the suspended sediment concentration near the toe of the dike (Deltares, 2010).

XBeach predicts additional erosion to develop next to the dune-dike connection. The longshore variation in wave height, wave force F_x and wave-induced water level setup in the transition zone are predicted by XBeach. The resulting water level gradient drives the longshore current in the transition zone. In a situation with normally incident waves the dune crest retreat ΔR^* increased with 24.7% next to the connection. The maximum increase of the erosion volume A near the connection is predicted to be 22.2%.

The longshore current can have a profound impact on the development of additional erosion near structures. XBeach predicts dune erosion of an undisturbed dune stretch in a situation with obliquely incident waves to be more than for normally incident waves. The dune crest retreat increased with 16.5% and the erosion volume with ±15%. This is associated with additional stirring by the longshore current (J.A. Roelvink 2011, pers. comm. 7 September).

When the dunes are situated upstream of the connection sediment will pile up against the structure. Consequently dune erosion next to the connection is less than the erosion in an undisturbed dune stretch. The influence of the dune-dike connection on the additional erosion is isolated from the effect of the longshore current. In this case XBeach predicts the dune retreat near the connection to be 35.4% less than in the undisturbed dune stretch. The erosion volume is predicted to be 32.1% less near the connection. The combined effect of the connection and the longshore current results in a decrease of ΔR^* near the connection of 24.7%. The erosion volume decreases with 22.2%.
In the transition zone there is a gradient in the velocity and transport capacity of the longshore current. Sediment transported by the longshore current is deposited on the seabed in front of the structure. As the foreshore in front of the structure rises the velocity and transport capacity of the longshore current increases. Consequently the sediment is deposited further downstream of the connection.

When dunes are situated downstream of the connection the erosion next to the connection increases significantly. For the isolated effect of the dune-dike connection XBeach predicts the maximum increase of ΔR^* next to the connection to be 56.6%. The erosion volume increased with 64.7%. This is caused by the increasing velocity and transport capacity of the longshore current. The eroded sediment is partially deposited on the foreshore downstream of the connection. Waves in this deposition area break sooner and dunes behind it show less erosion than an undisturbed dune stretch. XBeach predicted dunes in the deposition area to show 28.3% less retreat and a decrease of 22.9% in the erosion volume. For the combined effect of the connection and the longshore current the maximum increase of ΔR^* next to the connection is 82.5%. The maximum increase of the erosion volume is 89.4%.

Experiments in the Delta Basin

The influence of structures on dune erosion was investigated in a series of pilot experiments. The experiments were carried out with normally incident long-crested waves and were aimed at 4 different closed abrupt connections between a dune and a structure. Two configurations of dunes and hard structures were investigated. Each configuration was tested with 2 different wave peak periods T_p. The experiments proved the development of additional erosion near structures. The connections investigated in the experiments were:

1 The connection between a dike and an unprotected dune,
2 The connection between a dike and a dune that is protected by a dune revetment,
3 A breach in a dike with a body of sand,
4 A breach in a dune revetment.

A large number of measurements were taken before, during and after an experiment. To measure the morphological evolution use was made of a wheel profiler, 6 Argus video cameras and a hand-held surface scanner. The Argus video system measured among others the dune crest position every 6 seconds from which the dune crest retreat ΔR^*Argus was derived. From the wheel profiler measurements the erosion volume A_{WP} and the dune crest retreat ΔR^*_{WP} were derived. These measurements were used in the model-data comparison. The hydrodynamics were measured using two types of wave gauges and electro-magnetic flow meters. The wave height measurements were used to calibrate the hydrodynamic conditions in XBeach.

Analysis of the measurements revealed a longshore variation in wave height during the experiments. At the center of the basin the waves were largest. At the right side wall they were smaller. This caused a longshore variation in dune erosion. In some cases gully formation increased the amount of additional erosion near structures. The amount of additional erosion fell well within the standard deviation of the measurements. The effect of additional erosion was very local. Various disturbing processes made the experiments unsuitable to derive a reliable quantification of the additional dune erosion near structures.
Due to the longshore variation in dune erosion statistical parameters were used to compare measurements and prediction. The used parameters were the mean, the standard deviation, the minimum and the maximum of the dataset. Disturbances in space and time were omitted from the model-data comparison.

Model-data comparison

The measurements of the experiments are compared with XBeach predictions. The predictive capabilities of XBeach proved to be good. The measured wave height H_{m0} was used to calibration the wave height in XBeach. In XBeach the wave height is controlled by the breaker parameter γ in the Roelvink formulation for the wave dissipation model (Roelvink *et al.*, 2010). The best representation of the wave height H_{m0} in the Delta Basin is given by $\gamma = 0.54$. This is close to the default value of 0.55.

In XBeach the erosion in a dike breach is a function of the breach width and the wave period. The erosion increases for a smaller breach width. This is associated with the fraction of sediment volume lost to the scour hole in front of the adjacent dikes compared to the total amount of eroded sediment. Wider breaches supply more sediment to the foreshore than narrower breaches. Therefore wider breaches lose relatively less sediment to the scour holes which results in less erosion in wider breaches. The breach erosion increases for an increasing wave period. The erosion in dike breaches (B1, B2 & B3) during the Delta Basin experiments was disturbed. It was influenced by the longshore variation in wave height and gully formation. Therefore no quantitative comparison of the erosion in the breaches was made.

In dune revetment sections large differences between measurements and prediction were observed. XBeach underestimates the erosion above the dune revetment. To erode the dunes above the revetment waves must reach the dune front. Therefore wave runup is an important process for erosion above the revetment. Currently XBeach only simulates long wave runup.

The erosion in the revetment breach (B11) is predicted well. The predicted dune crest retreat shows a close resemblance with the measurements. The erosion volume is slightly underestimated. This is caused by a different shape of the predicted profile. The comparison between a dune revetment breach (B11) and a dike breach (B2) with an equal width revealed that the erosion in breach B11 is less than breach B2. This is associated with the fact that the foreshore of the revetment raised more than the foreshore of the dike. Consequently the wave height in B11 is less than in B2.

For experiments V1 (Dune stretch D1 & D2) and V3 (Dune stretch D11) with a wave period of T_p = 2.07 seconds the predictive capabilities of XBeach are very good. In experiments V1 & V3 the predicted bottom elevation $\overline{z_{b,Pred}}$ above SSL shows a close resemblance with the measured bottom elevation $\overline{z_{b,WP}}$. The predicted mean erosion volume $\overline{A_{Pred}}$ is slightly underestimated. This is explained by the fact that the foreshore in XBeach raised more than in the experiments. The development in time of $\overline{A_{Pred}}$ is simulated well by XBeach. Also the development in time of the predicted mean dune crest retreat $\overline{\Delta R^*_{Pred}}$ shows a close resemblance with the measured time development of $\overline{\Delta R^*_{Argus}}$.
The performance of XBeach for experiments V2 (Dune stretch D1 & D2) and V4 (Dune stretch D11) with a wave period of T_p = 1.55 seconds is relatively good. The predicted shape of the mean bottom elevation above SSL is similar to $\overline{z_{b,WP}}$ derived from the profile measurements, but has an offset in seaward direction. In both experiments a bar developed seaward of x = ±18.5 m which was not predicted by XBeach. The development in time of $\overline{\Delta R^*_{Pred}}$ is not simulated properly by XBeach. The predicted rate of dune crest retreat decreases too rapidly in XBeach. The predicted mean erosion volume $\overline{A_{Pred}}$ is underestimated. This is partially explained by the fact that the foreshore in XBeach raised more than in the experiments. The development in time of $\overline{A_{Pred}}$ is simulated well by XBeach. Generally the performance of XBeach for experiments V2 & V4 is less than in experiments V1 & V3 but is still considered to be relatively good.

The peak frequency of the Jonswap spectrum proved to have a relatively large influence on the amount of dune erosion predicted by XBeach. The effect of the wave period for 2DH models with a large depth scale (n_d = 60) is not properly simulated by XBeach. The configuration of dunes and hard structures has little influence on the effect of the wave period. The stability of XBeach for small depth scales is highly dependent on the calculation grid. Neumann boundaries can generate unwanted longshore currents in a situation with normally incident waves.

Contents

1 Introduction

1.1 General

The Netherlands is located in a low-lying delta and as long as the country exists there has been a battle against the water. Not only the sea possess a threat, but also rivers such as the Rhine and the Meuse. In the past millennium there have been countless floods causing the loss of many lives and property. The most recent major flood is the 1953 North Sea flood in which 1,835 people lost their lives. Due to climate change and global warming the sea level rises and as the amount of precipitation increases so does the river discharge. In the near future the threat posed by nature is likely to increase. With 9 million people living below mean sea level (MSL) and over 65% of the gross domestic product being earned in this region flood protection is indispensable for the Dutch people, see Figure 1.1.

Figure 1.1: Holland without flood protection: Blue areas are prone to flooding (Rijkswaterstaat, 2004)

The first dikes in the Netherlands were build by the Romans. Due to the industrial revolution and the invention of the steam engine large quantities of earth and water could be moved relatively easy. Huge engineering projects to reclaim land from the sea and to tame the rivers were executed in the 20th century. Twenty days after the 1953 North Sea flood a committee was installed to advise on measures to prevent flooding of the Netherlands resulting in the Delta Works. Along with the Zuiderzee Works they have been declared one of the Seven Wonders of the Modern World by the American Society of Civil Engineers.

The Dutch coastline has a length of 432 km and mainly consists of dunes and sandy beaches. With a combined length of 254 km they form the primary sea defense (Technische Adviescommissie voor de Waterkeringen, 1995). During a storm the dunes erode, but as long as their function, flood protection, is maintained this is not a problem. At some locations however the rate of dune erosion is too large during design conditions. Due to a structural loss of sediment and a global sea level rise the narrow stretch of dunes is thinning down. Along the North Sea shore the total loss of sediment is in the order of 4 million m^3 per year (Vellinga, 1986). Beach nourishments are a good and flexible solution to the structural long term erosion problems. However they are not suitable for every location along the North Sea coast. To prevent breakthrough at these locations during a storm reinforcement works are necessary. Structures that are mainly used along the Dutch coastline to reduce the amount of dune erosion during storm conditions are:

- Seawalls,
- Revetments,
- Sea-dikes.

In the past decades many seawalls, dune revetments and sea-dikes have been built to counteract the coastal erosion and to prevent further retreat of the dunes. A seawall is a nearly vertical structure at the transition between the beach and the mainland. It bridges the height difference between the low-lying beach and mainland. It generally requires staircases to access the beach. On the mainland a boulevard, parking area or road is often situated, see Figure 1.2. The seaward surface of a seawall is usually smooth and impermeable and they are considered to be an easy to build coastal protection. By cutting off the supply of sediment to the beach by a hard and impermeable surface storm erosion is prevented. Sea-dikes , such as the Hondsbossche Zeewering, are similar to seawalls with the main difference that there is hardly any or no beach in front of the sea-dike and they generally have a more gently slope. Presently 34 km of the Dutch coastline consist of sea-dikes (Technische Adviescommissie voor de Waterkeringen, 1995).

Figure 1.2: Seawall at El Malecon de Havana, Cuba[1]

A revetment is similar to a seawall with the main difference that they are more gently sloping. Revetments can be rough as well as smooth depending on the concrete elements used. By using specific concrete elements it is possible for vegetation to grow on the revetment. These nature friendly banks are mainly applied in inland regions were the water level is relatively constant and wave attack is mild. Moreover revetments are not always applied over the entire vertical distance from the beach to the mainland.

When the quality of the water defenses is not looked after carefully flooding is inevitable. Therefore the Dutch authorities check the strength of the water defenses in the Netherlands every six years. The assessment rules are provided by the Dutch government in “De veiligheid van de primaire waterkeringen in Nederland” shortly VTV (Ministerie van Verkeer en Waterstaat, 2007).

1.2 Problem definition

The Dutch coastline mainly consists of dunes and sea-dikes with a combined length of 288 km. To assess the safety of the connection between a dune and a hard structure the VTV provides rules. The assessment rules prescribe additional erosion of the dunes next to the structure based on expert judgement (Steetzel, 1995). In 2008 Rijkswaterstaat commissioned Deltares to make an inventory of problems and questions regarding the use of the assessment rules in the safety assessment (Boers, 2008). The present assessment rules for the connection between a dune and a hard structure had not been validated with measurements. Therefore assessors questioned the accuracy of the them.

The Rijkswaterstaat program “Strength and Loads on Water Defenses” (SBW) is aimed at establishing new assessment rules for future assessment of water defenses. In particular it is focused on water defenses that can’t be accurately assessed with the current assessment rules. Hybrid water defenses, a combination of dunes and hard structures, fall in this category. In 2008

[1] Retrieved from:http://lebbeuswoods.wordpress.com/2010/01/01/on-the-malecon/

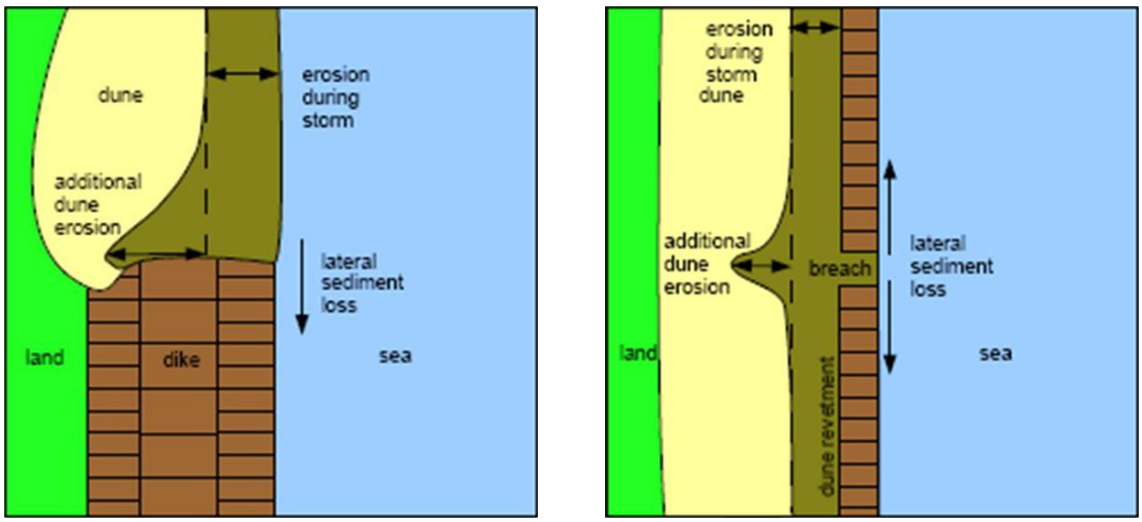

(a) At a dune-dike connection *(b) At a breach in a revetment*

Figure 1.3: Additional dune erosion (Boers et al., 2011)

Rijkswaterstaat commissioned the execution of a series of pilot experiments to get a better understanding of the influence of structures on dune erosion. The main objective was to qualitatively verify the hypothesis that near the connection between dunes and a structure the dunes next to the structure experience additional erosion during a storm. When this is verified the present assessment rules were to be reviewed with the measurements.

For a normative storm surge the dune erosion values prescribed in VTV are obtained with the numerical model DUROS+ (Expertisenetwerk Water Veilig, 2007). This empirical model is validated against many experiments. Although the model has been applied many times it is not generic. It is based on the assumption that the coastline is alongshore uniform. It is therefore inadequate to assess situations where there are significant longshore interactions. In the behaviour of hybrid defenses under storm conditions longshore variations play an important role, see Figure 1.3. Presently hybrid defenses can not be assessed with software. Assessors have to assess hybrid defenses in a dedicated manner which takes time and money. Therefore the Dutch Dune Safety Assessment demands advanced models to assess the coastal protection in complex situations.

1.3 Project objective

1.3.1 Main question

The development of the numerical model XBeach was initiated by United States Army Corps of Engineers after the devastating effects of the 2004/2005 hurricanes on the barrier islands and coastline near the Gulf of Mexico. XBeach fully includes the longshore direction and contains the essential processes to predict dune erosion. This makes it a useful tool to assess the safety of sea defenses in situations where the longshore effect influences the amount of dune erosion. XBeach is still under development and is validated against a broad range of laboratory and field experiments. The objective of this master thesis is to validate the numerical model XBeach with the results of the Delta Basin experiments. This objective is formulated in the main research question:

"*Is XBeach able to reproduce the dune erosion measured in the experiments?*"

1.3.2 Subquestions

In the Delta Basin a large number of measuring devices were used to monitor the dune erosion experiments. The experiments were not aimed to gather detailed quantitative data. The velocity meters performed poorly and too little wave gauges were installed to obtain sufficient hydrodynamic data for the calibration of XBeach. Therefore this thesis focuses on identifying and validating the processes causing additional dune erosion near hard structures. This is expressed in an additional question:

"*Which physical processes cause additional dune erosion near unerodable structures?*"

XBeach predicts the impact of hurricanes and storms on barrier islands and low-lying sandy beaches based on a set of equations. These equations link the hydrodynamic forcing to the morphological response of the coastal system. Based on model assumptions and initial conditions the equations predict the morphological response of a system to a predefined forcing. These equations however also form the limitations of the model as it can not simulate processes that are not implemented in the model by expressing them in equations. Therefore it is vital to investigate which processes are implemented in the model and how this affects the model results which is expressed in a 2nd subquestion.

"*Does XBeach simulate the identified physical processes responsible for additional dune erosion near structures?*"

To identify the processes present in the Delta Basin during the experiment the measured data is analyzed. This is indispensable to properly validate the XBeach model as it identifies processes that might cause differences between modeling results and the pilot experiments. This is summarized in the next and last subquestion.

"*Which physical processes can be identified in the measured data of the experiments?*"

1.4 Report outline

In Chapter 2 the behaviour of a dune-dike system under storm conditions based on a literature survey is described. Furthermore this chapter describes the fundamental processes responsible for the morphological development of a hybrid water defense during a storm. Chapter 3 is aimed at investigating the model behaviour of XBeach for hybrid water defenses. Subsequently it investigates the capabilities of XBeach to predict the proper behaviour of a dune-dike system under storm conditions. In this chapter it is verified whether or not the model behaviour is consistent with literature. In Chapter 4 the Delta Basin experiments are described in detail. Subsequently the measurements are analyzed to identify processes that are expected to cause differences between the measurements and XBeach predictions. Finally Chapter 5 compares the measured hydrodynamic and morphodynamic properties as observed in the Delta Basin experiments with the properties simulated by XBeach. In Chapter 6 the conclusions and recommendations are presented.

2 Storm impact on a dune-dike system

2.1 Introduction

In the past decades extensive research has been carried out to investigate the process of dune erosion. This provided a detailed insight into the morphological response of a dune system to storm conditions. For “undisturbed” dune and dike systems the behaviour of the governing processes and their development in time is reasonably well understood. Here “undisturbed” means that the conditions along the coast are alongshore uniform and hence there is no influence of a dune-dike connection on the process behaviour. The impact of a storm on a dune or dike system is usually considered to be a 1D cross-shore phenomenon (van Thiel de Vries *et al.*, 2010).

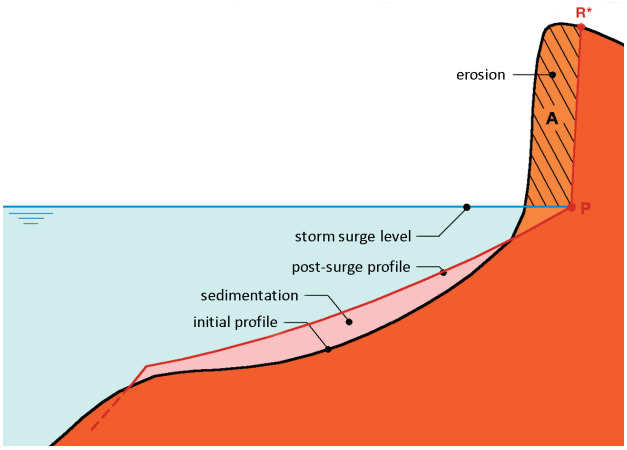

Figure 2.1: Morphological response parameters (Expertisenetwerk Water Veilig, 2007).

Dune erosion can be expressed with numerous parameters each having their own advantages. The most common and widely used parameters are the retreat point R^* and the erosion volume above storm surge level A, see Figure 2.1. The retreat point is defined as the point in a cross-section on ground level to which the dune erosion has progressed. The line connecting the retreat points in longshore direction is called the retreat line. The erosion volume above storm surge level is defined by the surface area A expressed in m^3/m, the erosion volume per m coastline. This surface area is confined by the initial profile, the post-surge profile and the storm surge level (SSL). Section 2.5 gives a summary of the fundamental processes that are responsible for the morphological response of a coastal system to the hydrodynamic conditions.

2.2 Dune erosion under storm conditions[1]

During a storm the mean sea level rises and waves are able to reach the dune face. The waves are much higher than usual and impact the dune face. Episodically lumps of sediment slide on to the beach. In front of the dune the turbulence level is high due to the intense wave action. The eroded sediment is brought into suspension. In front of the dune the amount of sediment in suspension is high. Both short and long waves are important for the hydrodynamics in front of the dune. Long waves are effective in triggering the episodic collapse of the dune front. As the storm progresses the long waves become relatively more important than short waves (van Thiel de Vries, 2009). The generation of (long) infragravity waves is described in Subsection 2.5.1.

During a storm there is a large wave-induced mass flux towards the shore which is associated with the high waves. The onshore directed mass flux is compensated by a strong undertow, see Subsection 2.5.3. The combination of a strong undertow and a high concentration of suspended sediment in front of the dunes result in a large seaward directed transport capacity. Consequently

[1] Derived from (van Thiel de Vries, 2009)

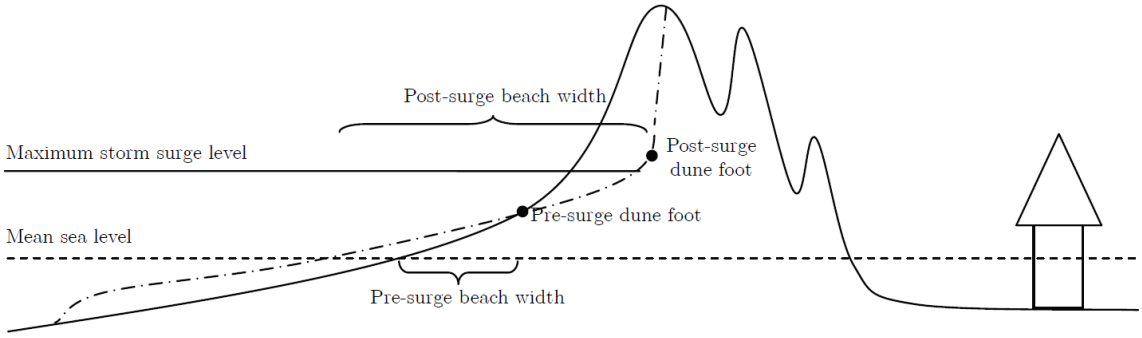

Figure 2.2: Dune erosion under storm conditions (van Thiel de Vries, 2009).

the eroded sediment is transported offshore. Offshore the water depth increases causing the undertow velocity to decrease. The transport capacity of the undertow becomes less and sediment starts to settle. As the storm progresses the bottom in the surfzone rises.

During the storm a new coastal profile is formed. This profile is more efficient in dissipating the energy of the high incoming waves. As the bed level in the surfzone rises the water depth decreases. The breaker point moves in seaward direction and waves start to break further offshore. Consequently there is more time to dissipate the wave energy. The breaking process is described in Subsubsection 2.5.2.2. As the new coastal profile develops less waves reach the dune face. Waves that do reach it are lower and hence carry less energy. The suspended sediment concentration in front of the dune decreases. The undertow is confined within the surfzone and since the breaker point moves seaward sediment is transport further offshore. Although the average volume of a lump of sediment remains relatively constant the time interval between successive lumps increases. Consequently the rate of dune erosion decreases as the storm progresses. The new coastal profile is in better equilibrium with the storm conditions. If the storm duration is long enough the post-surge profile is independent of the initial profile.

After the storm the beach has become wider, see Figure 2.2. The dune foot has moved in landward direction while the waterline moved seaward. The vertical position of the dune foot has hardly changed (van Thiel de Vries, 2009). The post-surge profile is not in equilibrium with the milder post-storm hydrodynamic conditions. Waves, tide and wind start to reshape the foreshore again and the dunes gain eroded sediment back. Without a structural loss due to a gradient in the longshore sediment transport the dunes will recover from the storm. However this takes considerably longer than the time it took to erode them.

The behaviour of dunes between successive storm events is comparable with the seasonal changes of a beach profile. In the summer period the waves are relatively small and sediment is pushed up the beach in the form of migrating sand bars. In this period the beach is rich in

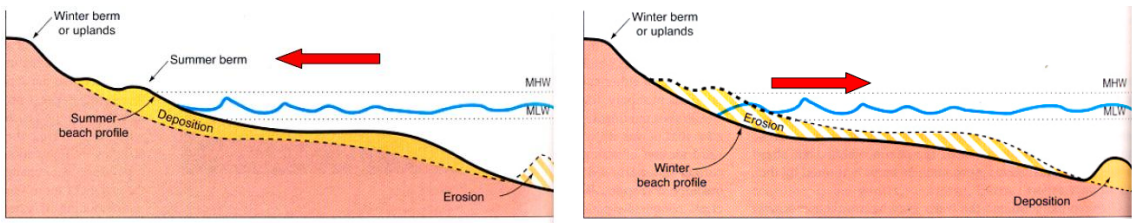

(a) Summer beach profile *(b) Winter beach profile*

Figure 2.3: Seasonal variations in beach profile (Bosboom and Stive, 2010)

sediment and the beach profile is characterized by a steep slope, see Figure 2.3a. In the winter period the waves are higher and more energetic. The sediment is transport seawards and deposited offshore creating sand bars. In the winter the beach is poor in sediment and has a more gentle slope, see Figure 2.3b. During relatively calm periods the sediment is again transported to the beach. “The beach breathes with the seasons” so to speak.

2.3 Storm impact on a sea-dike

Seawalls and sea-dikes are constructed at locations where dunes can not provide the necessary protection against flooding. The volume of sediment available for erosion during a normative storm surge is to small at these locations. Consequently the dune is expected to be breached during the storm. The hard and sand tight surface of seawalls prevent erosion by cutting off the supply of sediment to the beach. As long as the impermeable surface is intact the position of the structure is fixed. The lack of sediment prevents the coastal profile to adjust to the storm conditions. During the storm the dissipation of wave energy due to breaking is limited. The waves attacking the seawall remain high throughout the storm.

Seawalls and sea-dikes tend to reflect incoming waves. Consequently a standing wave pattern might develop in front of the structure. For non-breaking waves the return current associated with the onshore directed mass flux is small, see Subsubsection 2.5.4.2. Consequently the undertow velocities are much smaller than in a dune transect with identical conditions. Waves running down the surface of a seawall cause a high turbulence intensity in front of the seawall. The standing wave pattern in front of the seawall increases the turbulence intensity further. Sediment near the toe of the seawall is brought into suspension. The sediment is transported seaward and a scour hole develops (Roelse, 1993), see Figure 2.4.

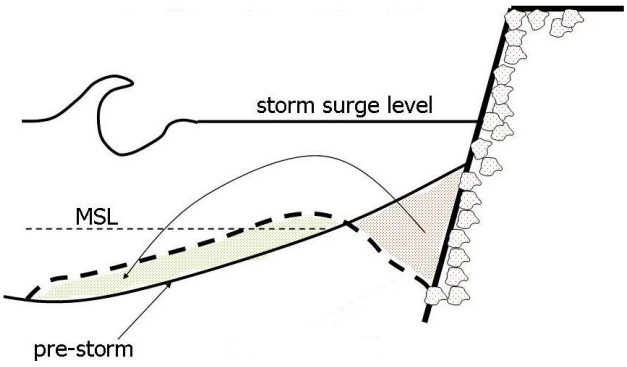

Figure 2.4: Scour hole development in front of a seawall during storm conditions (Bosboom and Stive, 2010).

The wave height in front of the seawall might increase throughout the storm. The wave height is usually depth-limited. As the scour hole grows the water depth near the toe of the dike increases. Consequently the wave height near the toe of the dike increases (Bosboom and Stive, 2010). Since the wave runup depends on the wave height at the dike toe the runup increases throughout the storm.

2.4 Hybrid sea defenses

A hybrid sea defense is a combination of dunes and structures. Generally the construction used to connect the dunes and structure is only surrounded by water during storm surges. Therefore the influence of the connection on the morphological development of their surroundings is confined to storm events (Roelse, 1993). Over the transition from dunes to a structure the amount of sediment available for erosion reduces with respect to the dunes. The longshore distance over which the supply of sediment changes depends on the shape and size of the connection. The longshore gradient in the amount of sediment available for erosion causes a difference in the elevation of the foreshore, see Figure 2.5. In this figure ΔA_0 is the amount of sediment which was refrained from the erosion processes by the structure. Sediment is transported from the

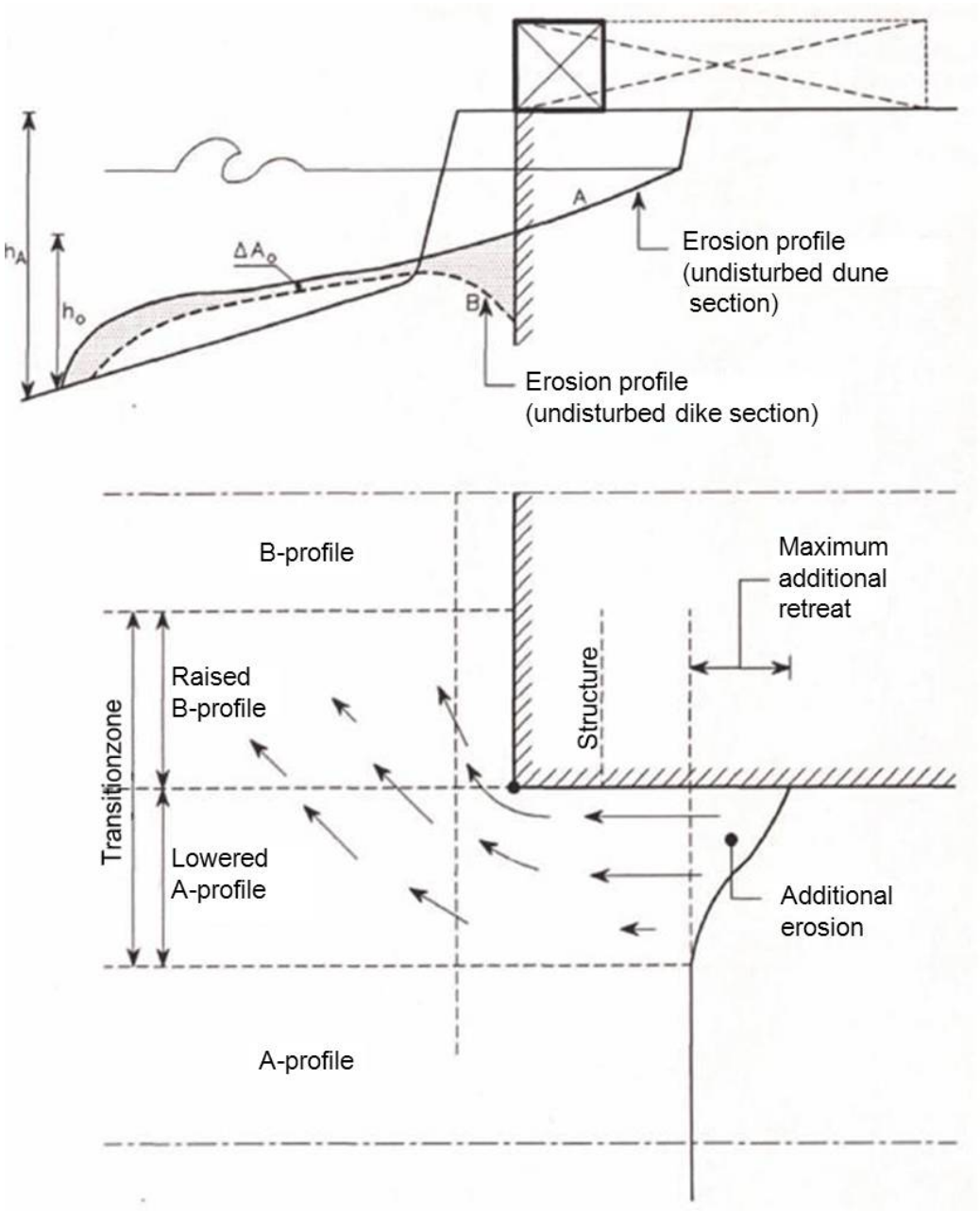

Figure 2.5: Additional erosion near an abrupt connection between dunes and a structure (Steetzel, 1993).

higher dune profile to the lower dike profile (Steetzel, 1995). The loss of sediment to the dike profile causes the dune profile to adjusts slower to the storm conditions than undisturbed dune transects. The foreshore rises slower and the breaker point is closer to the dune face. Waves reaching the dune face remain high for a longer period of time. Within the storm duration more waves are able to reach the dune face. Consequently more sediment is eroded from the dunes which results in a larger dune retreat, see Figure 2.5.

Steetzel does not describe the mechanism behind the transport of sediment from the higher dune profile to the lower dike profile (Steetzel, 1995). However the behaviour of the hydrodynamic processes can give an insight in to the forces which drive the sediment transport. Throughout a storm dunes erode and retreat landwards. The foreshore rises and the wave height in front of

the dunes reduces. Consequently the wave force F_x decreases since it is indirectly proportional to the square of the wave height. Subsequently the wave-induced water level setup increases, see Subsubsection 2.5.4.1. Waves in front of a seawall or sea-dike remain high throughout the storm and might even increases. This leads to a decrease of the water level setup. Due to the difference in wave-induced water level setup between the dunes and the seawalls there is a water level gradient over the connection. This water level gradient drives a current which transports sediment from the dunes to the foreshore of the seawall.

As the dunes retreat wave reflection at the dune face occurs latter than reflection on the adjacent structure. The phase lag in wave reflection causes a differential head to be developed over the connection. The magnitude and sign of the water level gradient depends on wave reflection and consequently oscillates. The oscillating hydraulic gradient drives an oscillating current around the corner of the structure. The oscillating undulation current is expected to stir up sediment in addition to the waves (Boers *et al.*, 2008). Subsequently the sediment is transported towards the seawall by the longshore current in front of the connection. In addition to the undulation current turbulence at the corner of the structure can cause a local scour hole (Roelse, 1993).

2.4.1 Transition connections

There is a large variety in the applied connections between dunes and structures in the Netherlands. Roelse made an overview of the applied connections between dunes, dikes and dune revetments in the province of Zeeland in the Netherlands (Roelse, 1993). The connections are divided in two categories; a relatively abrupt termination of the structure as shown in Figure 2.5 and a more gradual transition from the dunes to a structure as shown in Figure 2.6. Furthermore a distinction is made between open and closed connections (Steetzel, 1995). For a closed connection the landward side of the structure reaches beyond the dune face position after a normative storm surge. For an open connection the dune face position after a normative storm surge reaches beyond the landward side of the structure. Consequently there is a possibility that during a storm sediment from behind the structure is supplied to the beach. This can endanger the stability of the structure. The supply sediment from behind the structure reduces additional erosion next to it.

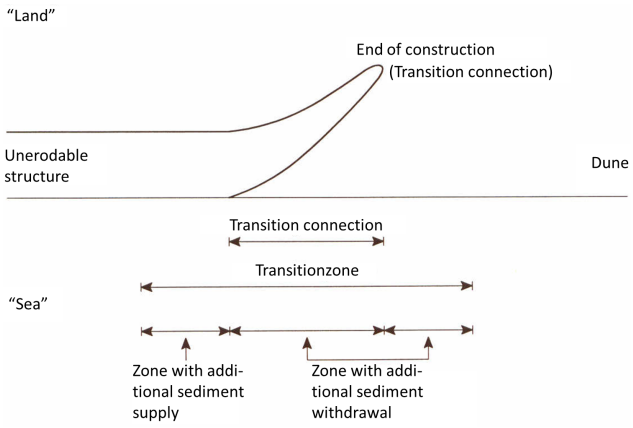

Figure 2.6: Gradual transition between dunes and a structure (Steetzel, 1995).

Steetzel derived guidelines to estimate the amount of additional erosion near abrupt transitions, see Equation 2.1. In this equation h_a is the difference between the lowest point in the deposition zone and the dune level. $\delta = h_0/h_a$, with h_0 the difference between the lowest point in the deposition zone and the intersection between the undisturbed dune erosion profile and the front of the structure, see Figure 2.5. $\Delta\hat{A}_0$ is the amount of sediment refrained from erosion by the structure. For a more gradual transition the amount of additional erosion is less. A detailed derivation of the guidelines is presented in (Steetzel, 1993) and (Steetzel, 1995).

$$\Delta R_r = \frac{\Delta \hat{A}_0}{h_a}\left(\frac{1}{\sqrt{\delta}+\delta}\right) \tag{2.1}$$

2.4.2 Effects of oblique incident waves

Waves coming in under an angle with respect to the shoreline generate a longshore current, see Subsubsection 2.5.4.4. This current transports sediment along the shore. The velocity of the longshore current depends on the dissipation of wave energy. Seawalls and sea-dikes tend to reflect incoming waves and the dissipation of wave energy due to breaking is limited. Consequently the velocity of the longshore current and hence its transport capacity in front of a seawall is limited, see Subsubsection 2.5.4.4. In a dune transect the dissipation of wave energy is much higher than in dike transect with identical conditions. Therefore the velocity and hence the transport capacity of the longshore current are higher in a dune stretch. Furthermore when a structure influences the supply of sediment to the beach it will effect the amount of sediment transported by the longshore current. Subsequently a longshore gradient in the sediment transport exists over the upstream and downstream connections of the hybrid defense. The dunes near the downstream connection experience a significant increases in erosion (Steetzel, 1993). Near the upstream connection the decreasing transport capacity of the longshore current causes sediment to be deposited on the foreshore of the structure. Depending on the amount of sediment deposited on the foreshore the scour hole in front of the structure might (partially) be filled up.

In the case that 2 structures are close to each other e.g. a breach in a sea-dike the sediment deposited on the foreshore is transported by the longshore current. The sediment is subsequently deposited on the foreshore in front of the downstream structure. Between the structures the amount of erosion increases significantly. The retreat point R^* will move in landward direction over a large distance (Steetzel, 1993).

2.5 Hydrodynamic processes related to morphological change

This section describes the fundamental processes that are responsible for the morphological response of a coastal system to the hydrodynamic conditions. It is mainly derived from the process description given in the Coastal Dynamics lecture notes (Bosboom and Stive, 2010).

2.5.1 Wave groups

Far out at sea the water surface elevation looks irregular and random. In fact the water surface is determined by many waves with different periods, heights and directions. The waves form groups which transport wave energy E with the group velocity c_g. The formation of wave groups is best explained by an example. Consider two monochromatic waves with an equal height traveling in the same direction. The waves have slightly different frequencies ω_1 & ω_2 and therefore slightly different wave numbers k_1 & k_2 and velocities. The wave phases θ_1 & θ_2 are usually assumed to be a random number between 0 and 2π. For a detailed description of wave properties, such as the propagation speed and energy balance, see (Holthuijsen, 2007). When the waves are in phase they reinforce each other resulting in a surface elevation η of twice the wave height. When the waves are 180° out of phase the crest of one wave coincides with the trough of the 2nd wave and the waves cancel each other out resulting in a zero surface elevation. The wave group is mathematically described by the summation of the monochromatic waves.

$$\eta = a\sin(\omega_1 t - k_1 x + \theta_1) + a\sin(\omega_2 t - k_2 x + \theta_2) \tag{2.2}$$

$$\eta = 2a \underbrace{\sin\left(\frac{\omega_1+\omega_2}{2}t - \frac{k_1+k_2}{2}x + \frac{\theta_1+\theta_2}{2}\right)}_{\text{Fast}} \underbrace{\cos\left(\frac{\omega_1-\omega_2}{2}t - \frac{k_1-k_2}{2}x + \frac{\theta_1-\theta_2}{2}\right)}_{\text{Slow}} \tag{2.3}$$

In Figure 2.7 the surface elevation η is plotted in blue. The red line represents the low frequency motion of Equation 2.3. The length L_g and period T_g of the wave group and hence the propagation speed c_g is calculated from the difference in wave frequencies.

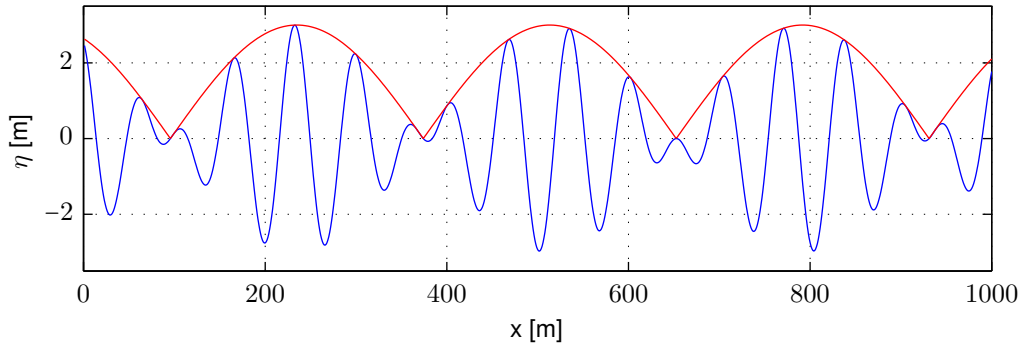

Figure 2.7: Wave group of two monochromatic waves with a slightly different period. The blue line represents the surface elevation η, the red line the low frequentie motion of Equation 2.3.

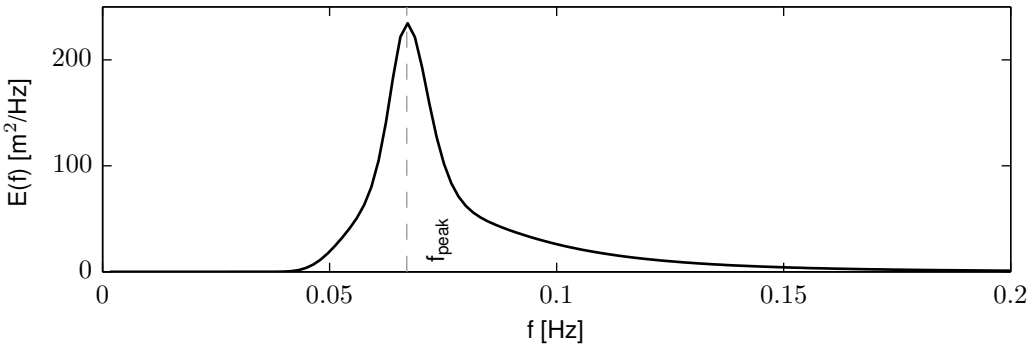

Figure 2.8: Jonswap spectrum giving the wave energy as a function of frequency.

$$L_g = \frac{2\pi}{k_2 - k_1} = \frac{2\pi}{\Delta k} \tag{2.4}$$

$$T_g = \frac{2\pi}{\omega_2 - \omega_1} = \frac{2\pi}{\Delta \omega} \tag{2.5}$$

$$c_g = \lim_{\Delta k \to (0)} \frac{\Delta \omega}{\Delta k} = \frac{d\omega}{dk} = \left[\frac{1}{2} + \frac{kd}{\sinh(2kd)}\right]\frac{\omega}{k} = nc \tag{2.6}$$

In the last equation n denotes the ratio between the group velocity c_g and the wave celerity c. In deep water where the wave celerity is unaffected by the water depth n = 0.5. The wave energy is transported in the direction of wave propagation with only half the wave speed. When a wave group reaches shallow water its propagation speed reduces and becomes equal to the wave celerity c_0. In shallow water n = 1. When the waves start to break as they reach the surfzone the wave group is destroyed.

The surface elevation at sea is determined by waves with different periods, heights and direction. A time series of the surface elevation can be decomposed into its constituent frequencies and associating amplitudes using a Fourier Transformation. From this information a wave spectrum can be constructed. A wave spectrum gives the wave energy E as a function of the wave frequency (Holthuijsen, 2007). Although many different spectra forms exist the Jonswap spectrum, Figure 2.8, is most widely used. As individual mono-chromatic waves interact with each other they create wave groups. For each bi-chromatic pair a wave group is generated making the groups more irregular.

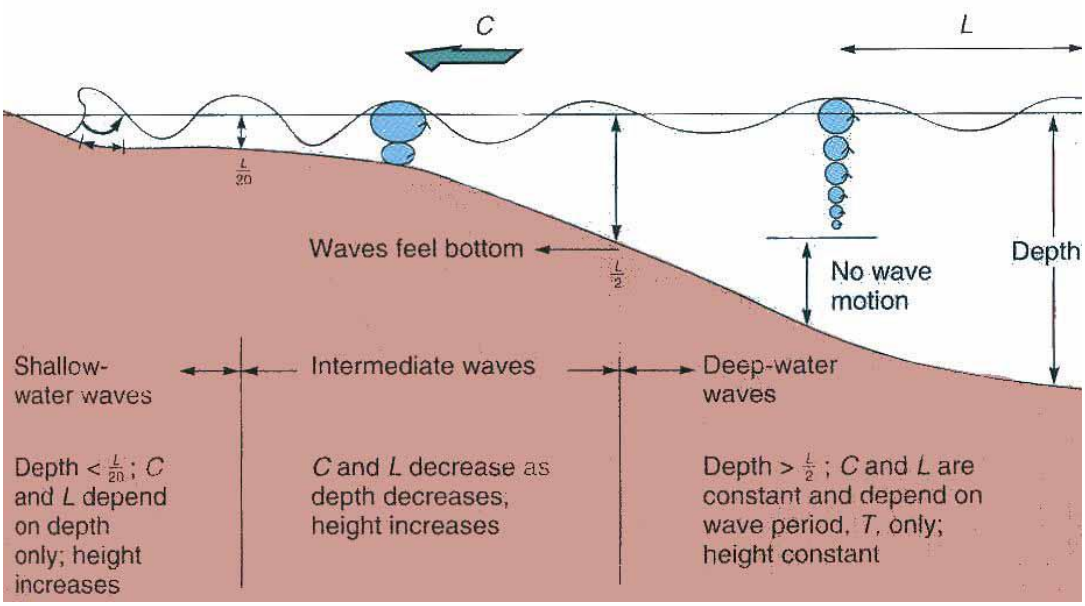

Figure 2.9: Wave transformation (Bosboom and Stive, 2010)

2.5.2 Wave transformation

2.5.2.1 Shoaling

As a wave reaches shallower water the propagation speed reduced. The wave length and height H are indirectly influenced by this change in wave speed. Since a wave has a certain length the leading edge of the wave reaches shallower water sooner than the trailing edge. Consequently the leading edge travels with a lower velocity towards the coast than the trailing edge and the wave length L starts to reduce. Although the wave length and wave speed are affected by the change in water depth the energy flux U and wave period remain constant. The energy flux is the rate at which energy is transmitted in the direction of wave propagation. It is defined across a vertical plane perpendicular to the direction of wave propagation extending over the entire depth. Since nc reduces when waves enter shallow water and U remains constant the wave height H must increase. This is called shoaling, see Figure 2.9.

$$U = Ec_g = Enc \tag{2.7}$$

2.5.2.2 Wave breaking

The water depth under the wave crest is larger than the water depth under the wave trough. Since the propagation speed is a function of the water depth in shallow water the wave crest moves faster than the trough. The wave gets shorter and higher and consequently the wave front gets steeper. When the wave front becomes too steep the wave starts breaking. At that moment the velocity of the water particles in the wave crest exceeds the wave celerity. In 1944 Miche expressed the limiting wave steepness with Equation 2.8.

$$\left[\frac{H}{L}\right]_{max} = 0.142 \tanh(kd) \tag{2.8}$$

In shallow water where $\tanh(\text{kd}) \rightarrow$ kd for kd $\rightarrow 0$ waves start breaking when the water depth d is roughly 0.88 times the wave height H.

$$\left[\frac{H}{L}\right]_{max} = 0.142kd \approx 0.88\frac{d}{L} \tag{2.9}$$

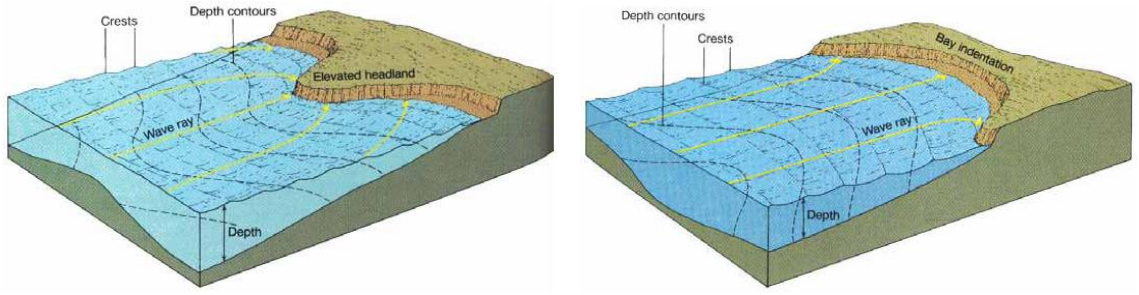

(a) Focus of wave energy *(b) Divergence of wave energy*

Figure 2.10: Refraction patterns (Bosboom and Stive, 2010)

2.5.2.3 Refraction

Refraction occurs when there is a difference in wave speed along the wave crest. When a wave encounters a current the propagation velocity of the wave is affected. Variations in current velocity or direction along the wave crest causes a gradient in the wave propagation velocity along the crest. The wave crest starts to bend depending on the current conditions. This is called current-refraction. When a long-crested wave approaches the shoreline under an angle φ_0 refraction is induced by a variation of the water depth along the wave crest. The crest section in deeper water travels with a higher velocity towards the shore than crest sections in shallower water. The wave crest bends to become parallel to the depth contours. This is called depth-refraction.

As the wave moves towards the shoreline the direction of wave propagation changes, along with the distance between the wave rays. The transported amount of energy remains constant. Depending on the refraction pattern there is either a focus of wave energy or a divergence of energy, see Figure 2.10. Since the wave energy E is a function of the wave height H this is translated into either an increase or decrease of the wave height. Based on Snell's law, Equation 2.10, a refraction coëficient can be derived. With this coëficient the change in wave height can be calculated for a situation with parallel contour lines, see (Bosboom and Stive, 2010).

$$\frac{\sin\theta_1}{c_1} = \frac{\sin\theta_0}{c_0} = \text{constant} \tag{2.10}$$

2.5.2.4 Diffraction

When wave propagation is obstructed by e.g. a breakwater there is a large variation of wave energy along the crest. Initially in the sheltered zone the wave height is zero. Along the diffraction line however the wave height is equal to half the incoming wave height. This causes wave energy to be transfered along the wave crest. This is called diffraction and causes a more smooth gradient in the wave height along the wave crest.

2.5.3 Wave-induced mass and momentum flux

Besides energy waves carry momentum in the direction of wave propagation. Seen from a stationary point in space the particle velocities below wave trough level vary harmonically in time. Below wave trough level the wave averaged mean velocity is zero. Therefore the contribution to the mass flux $\vec{q}$ in the direction of wave propagation is zero. Only the section between the wave trough and wave crest contributes to the mass flux.

When recording velocities at a point between MSL and the wave crest velocities are measured only for a part of the wave period. The measured velocities are always positive hence the water particle travels in the direction of wave propagation. Between wave trough level and MSL velocities are measured for a larger part of the wave period. Both positive and negative velocities are

recorded. Since positive velocities are recorded for a longer period of time the wave averaged mean velocity is still positive. As the wave averaged mean velocity is positive between the wave trough and wave crest mass is transported with a velocity u in the direction of wave propagation. The amount of momentum per unit surface area in the direction of wave propagation integrated over the depth, hence the mass flux $\vec{q}$ is given by:

$$\vec{q} = \overline{\int_{-h}^{\eta} \rho u dz} \tag{2.11}$$

The wave-induced momentum or mass flux is transported in the direction of wave propagation. This momentum flux is equivalent to a stress called radiation stress. Horizontal gradients in the radiation stress give rise to a net force on the water. These forces cause water level variations, set-up and set-down, and drive the longshore current when waves come in under an angle with respect to the shoreline.

The wave-induced momentum flux through a vertical plane at a certain location consists of two parts. The plane is orientated perpendicular to the direction of wave propagation and extends to the bottom. The wave propagates in x-direction towards the coast. The first part is the transfer of momentum ρu_x through the vertical plane with a velocity u_x normal to the plane. The 2nd part is the wave-induced pressure force p_{wave} acting on the plane. By integration over the water depth the associated total wave-averaged transport of x-momentum in x-direction S_{xx} is obtained.

$$S_{xx} = \underbrace{\overline{\int_{-h}^{\eta} (\rho u_x)\, u_x dz}}_{\text{Momentum transfer}} + \underbrace{\overline{\int_{-h}^{\eta} p_{wave} dz}}_{\text{Pressure force}} \tag{2.12}$$

A similar equation exists for the transport of y-momentum in y-direction S_{yy}. However the shear component of the radiation stress, defined as the transport of x-momentum in y-direction S_{xy} is different.

$$S_{yy} = \overline{\int_{-h}^{\eta} (\rho u_y)\, u_y dz} + \overline{\int_{-h}^{\eta} p_{wave} dz} \tag{2.13}$$

$$S_{xy} = \overline{\int_{-h}^{\eta} (\rho u_x)\, u_y dz} + \tau_{xy} \tag{2.14}$$

Using linear wave theory the integrals can be approximated resulting in expressions for the radiation stress.

$$S_{xx} = \left(n - \frac{1}{2} + n\cos^2\theta\right) E \tag{2.15}$$

$$S_{yy} = \left(n - \frac{1}{2} + n\sin^2\theta\right) E \tag{2.16}$$

$$S_{xy} = S_{yx} = n\cos\theta\sin\theta E \tag{2.17}$$

In the equations θ represents the angle of wave incidence with respect to the shoreline. When the wave crest is parallel to the shore the angle of wave incidence is 0. The shear components of the radiation stress S_{xy} & S_{yx} become zero and S_{yy} only consists of the pressure force.

As waves approach the shore under an angle shoaling causes an increase of the wave height. Refraction changes the angle of wave incidence and finally the wave height decreases again due

to wave breaking. This results in horizontal variations in radiation stress which give rise to net wave-induced force. The force in x-direction F_x and in y-direction F_y are give by:

$$F_x = -\left(\frac{\partial S_{xx}}{\partial x} + \frac{\partial S_{xy}}{\partial y}\right) \tag{2.18}$$

$$F_y = -\left(\frac{\partial S_{yy}}{\partial y} + \frac{\partial S_{yx}}{\partial x}\right) \tag{2.19}$$

2.5.4 Wave-induced setup and currents

2.5.4.1 Wave set-up and set-down

As waves approach the shore n increases from 0.5 to 1, see Subsection 2.5.1. Due to shoaling the wave height increases. Together this results in an increase of the radiation stress S_{xx} in landward direction in the shoaling zone. A resulting force F_x acts on the body of water in seaward direction. Since a net force implies acceleration of the water body there is a small difference in water level between both sides of the water column. This water level difference compensates for the resulting force F_x due to radiation stress. The water level is lowest at the landward side of the water column and is called wave set-down. In the surfzone the opposite happens. Due to wave breaking the wave height decreases resulting in a decrease of the radiation stress S_{xx} in landward direction. A resulting force F_x acts on the body of water which is compensated by a water level difference between both sides of the water column. At the landward side of the water column the water level is higher and is therefore called wave set-up. The relationship between the wave force F_x, the radiation stress S_{xx} and the water level set-up is expressed by Equation 2.20. In this equation h_0 is the still water depth and $\overline{\eta}$ is the wave-induced water level set-up.

$$F_x = -\frac{dS_{xx}}{dx} = \rho g\left(h_0 + \overline{\eta}\frac{d\overline{\eta}}{dx}\right) \tag{2.20}$$

The maximum water level depression occurs just outside the breaker zone before waves start breaking. By assuming shallow water the maximum wave set-down can be approximated. In a similar way the maximum wave set-up in the surfzone is approximated resulting in two expressions for the wave set-down and wave set-up. The derivation of Equations 2.21 & 2.22 is described in the lecture notes of Coastal Dynamics (Bosboom and Stive, 2010).

$$\overline{\eta}_{\text{set-down}} = -\frac{1}{16}\gamma H_b \tag{2.21}$$

$$\overline{\eta}_{\text{set-up}} = \frac{5}{16}\gamma H_b \tag{2.22}$$

In which:

- $\overline{\eta}_{\text{set-down}}$ = Maximum water level set-down at point of wave breaking,
- $\overline{\eta}_{\text{set-up}}$ = Maximum water level set-up near the shoreline,
- γ = Breaking index; $\gamma = H_b/h_b$,
- H_b = Wave height at point of breaking,
- h_b = Still-water depth at point of breaking

2.5.4.2 Undertow

As a wave propagates towards the shoreline mass is transported in the direction of wave propagation, see Subsection 2.5.3. Since water can not continuously pile up against the coast the mass flux between wave trough and crest must be compensated. At every point in the cross-shore profile the cross-shore current averaged over the water depth must be zero. The onshore directed mass flux is compensated by an offshore directed return current below wave trough level. For non-breaking waves this return current is small. In the surfzone where waves break the mass transport towards the coast is large. Consequently the offshore directed velocities are high. The large return current in the surfzone is called the undertow. Figure 2.11 displays the cross-shore current distribution over the water depth. Positive velocities are directed onshore and negative velocities are directed offshore.

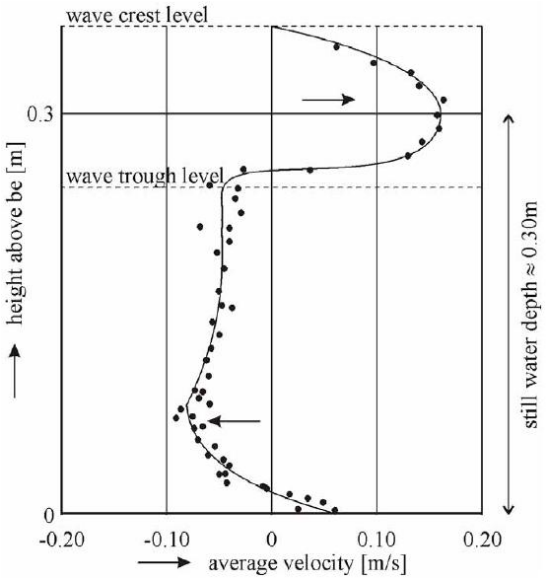

Figure 2.11: Cross-shore current distribution (Boosboom and Stive, 2010)

2.5.4.3 Infragravity waves

Wave groups generates infragravity waves which are important for dune erosion under storm conditions (van Thiel de Vries, 2009). Within a wave group the wave height varies on the wave group scale, see Subsection 2.5.1. Consequently the radiation stress changes as it is a function of the wave height. This causes a resulting force on the water column leading to either a water level set-up or set-down. The result is a long wave motion on the wave group scale which are called infragravity waves. As long as the individual waves which create the wave group are not breaking the long wave is bound to the group. Its wave length, frequency and phase speed are that of the group. Figure 2.12 displays the bound long wave generated by the wave group created by the interaction of two mono-chromatic waves, see Subsection 2.5.1.

As each bi-chromatic pair generates a wave group many infragravity waves with different periods, heights and directions are generated. In analogy with the wave spectrum generated from the individual mono-chromatic waves the bound long waves can be used to create a second order spectrum. This spectrum comprises the information of the short waves including the group

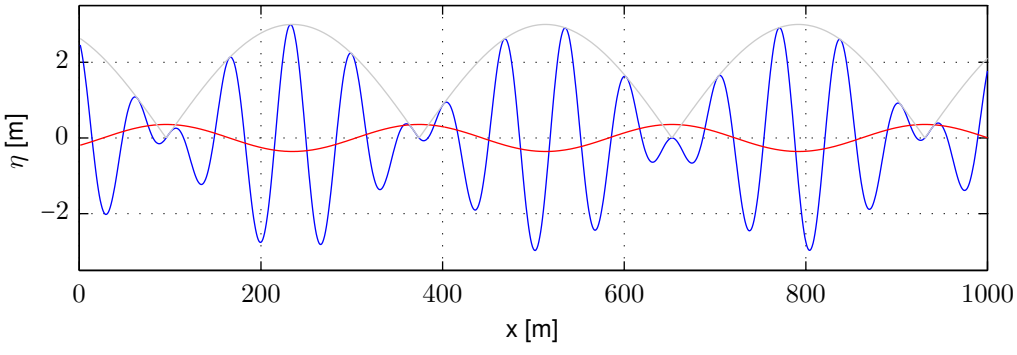

Figure 2.12: Bound long wave (—) generated by the groupiness of the short waves (—)

generated infragravity waves. As can be seen in Figure 2.13 the infragravity waves have less energy than the short waves generating them.

When the waves that create the group enter the surfzone they start breaking. The wave group is destroyed and the bound long wave is released. It continuous traveling towards the coast as a free long wave with the shallow water propagation speed $c_{shallow} = \sqrt{gd}$. At the shore the wave partially breaks and is partially reflected. This generates a time-varying set-up of the water level near the shore which is called surfbeat.

As the short waves creating the wave group approach the shore under an angle φ_0 the infragravity waves generated be the wave group will also have this angle φ_0. When the infragravity waves are released from the wave group they start to refract. Under certain conditions the infragravity waves can become trapped at the shoreline by refraction and reflection causing them to travel along the shore. In that case they are referred to as trapped edge waves.

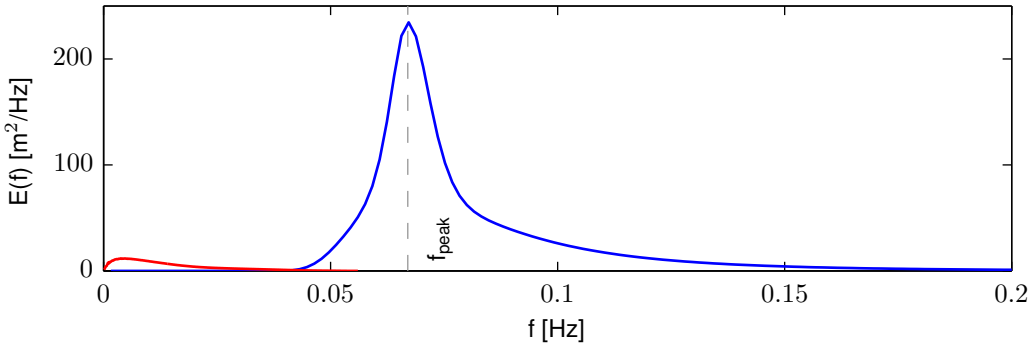

Figure 2.13: Infragravity wave spectrum (—) and short wave spectrum (—).

2.5.4.4 Longshore current

In cross-shore direction the resulting force F_x is compensated by a difference in water level between both sides of the water column. In longshore direction such hydraulic gradient can not develop. In longshore direction the force compensating the resulting force F_y is supplied by the bed shear stress. This stress can only be generated in the presence of a current. This current is called the longshore current and drives the longshore sediment transport. The longshore current is generated in the surfzone and extends to just in the shoaling zone due to turbulent mixing. In the case of a longshore uniform coast the longshore forcing F_y is only present when there is dissipation of energy D_w. By applying Snell's law for refraction and conservation of energy the longshore forcing can be re-written.

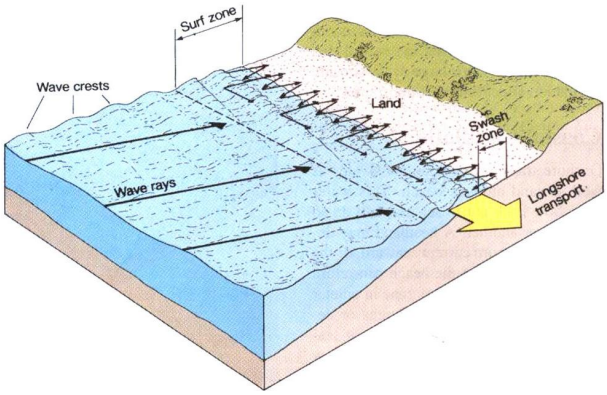

Figure 2.14: Longshore current (Bosboom and Stive, 2010)

$$F_y = -\frac{dS_{yx}}{dx} = \frac{d}{dx}\left(n\cos\theta\sin\theta E\right) \tag{2.23}$$

$$F_y = -\frac{sin\theta}{c}\frac{d}{dx}\left(Ec_g\cos\theta\right) = \frac{D_w}{c_0}\sin\theta_0 \tag{2.24}$$

3 Model behaviour of a dune-dike system

3.1 The XBeach program

3.1.1 Introduction

Hurricanes and storms have a devastating effect on low-lying sandy beaches. For instance on September 16th 2004 hurricane Ivan made landfall near the Gulf Shores in Alabama. As a category 3 hurricane it caused extensive damage to barrier islands and coastal areas, see Figure 3.1. Less than a year later hurricane Katrina developed over the Atlantic Ocean. It made landfall on August 29th near southeast Louisiana and triggered the well-known flooding of New Orleans. The 2004/2005 hurricanes pointed to an urgent need to assess the vulnerability of coastal areas and coastal protection to hurricanes and storm events.

Figure 3.1: Breach through the Pine Beach barrier island after hurricane Ivan passed[1]

This lead to the initiation of the Morphos-3D project by the United Stated Army Corps of Engineers (USACE). The Morphos-3D project is aimed at creating a model to simulate the impact of hurricanes and storms on sandy beaches. In turn this initiated the development of the open-source program XBeach which stands for eXtreme Beach behaviour. XBeach is a two-dimensional (2DH) model that predicts the morphological changes in the coastal zone during a storm. The model solves longshore and cross-shore currents and wave groups which drive infragravity motions, including bound, free and trapped infragravity waves. It is developed with funding and support of the USACE by a consortium of UNESCO-IHE, Deltares, Delft University of Technology and the University of Miami (Roelvink *et al.*, 2010). The XBeach manual, executables and toolboxes are available at `www.xbeach.org`.

3.1.2 Model approach

The interaction between wave groups and long waves is solved with a wave action balance coupled to the non-linear shallow water equations (NSWE). The wave action balance is given by Equation 3.1 and is similar to Delft University's HISWA model (Holthuijsen *et al.*, 1989).

$$\frac{\partial A}{\partial t} + \frac{\partial c_x A}{\partial x} + \frac{\partial c_y A}{\partial y} + \frac{\partial c_\theta A}{\partial \theta} = -\frac{D_w}{\sigma} \qquad \text{with} \qquad A(x,y,t,\theta) = \frac{S_w(x,y,t,\theta)}{\sigma(x,y,t)} \tag{3.1}$$

In this equation A is the wave action, S_w the wave energy and σ represents a radian wave frequency. The x-component and y-component of the wave celerity are c_x & c_y respectively. The 2nd and 3rd left hand side (LHS) terms account for spatial advection of wave energy. Refraction is accounted for by the 4th LHS term in which c_θ is the directional advection speed. D_w accounts for the dissipation of wave energy due to breaking. In the surf zone the wave energy dissipated by breaking D_w is input to a roller energy balance. For a more detailed description of the wave action balance, see (Roelvink *et al.*, 2009).

[1] Adjusted from: `http://coastal.er.usgs.gov/hurricanes/ivan/photos/index.html`

The wave action balance provides the wave forcing for the transport equations of the NSWE, see Equations 3.3 and 3.4. The right hand side of the transport equations express the total force applied to a body of water. Subsequently the left hand side determines the response of the water body to this force.

$$\frac{\partial \eta}{\partial t} + \frac{\partial hu}{\partial x} + \frac{\partial hv}{\partial y} = 0 \tag{3.2}$$

$$\frac{\partial u}{\partial t} + u\frac{\partial u}{\partial x} + v\frac{\partial u}{\partial y} - fv - \nu_h\left(\frac{\partial^2 u}{\partial x^2} + \frac{\partial^2 u}{\partial y^2}\right) = \frac{\tau_{sx}}{\rho h} - \frac{\tau_{bx}}{\rho h} - g\frac{\partial \eta}{\partial x} + \frac{F_x}{\rho h} \tag{3.3}$$

$$\frac{\partial v}{\partial t} + u\frac{\partial v}{\partial x} + v\frac{\partial v}{\partial y} - fu - \nu_h\left(\frac{\partial^2 v}{\partial x^2} + \frac{\partial^2 v}{\partial y^2}\right) = \frac{\tau_{sy}}{\rho h} - \frac{\tau_{by}}{\rho h} - g\frac{\partial \eta}{\partial y} + \frac{F_y}{\rho h} \tag{3.4}$$

In these equations u and v are the flow velocity in x-direction and y-direction respectively, η is the water level and h is the water depth. The 2nd and 3rd LHS terms of the transport equations account for advection. The 4th LHS terms of the transport equations accounts for the Coriolis force. The 5th LHS terms of the transport equations accounts for turbulent viscosity. The 1st and 2nd RHS terms account for the surface shear stress and bed shear stress respectively. The 3rd RHS term in the momentum equations represents the forcing due to water level gradients. The 4th RHS term in the momentum equations gives the wave force applied to a water body.

The sediment transport is modeled with a depth-averaged advection diffusion equation, see Equation 3.5. In this equation C represents the depth-averaged sediment concentration, D_h is the diffusion coefficient, T_s the adaptation for the entrainment of sediment and C_{eq} is the equilibrium concentration (Roelvink *et al.*, 2009).

$$\frac{\partial hC}{\partial t} + \frac{\partial hCu}{\partial x} + \frac{\partial hCv}{\partial y} + \frac{\partial}{\partial x}\left[D_h h\frac{\partial C}{\partial x}\right] + \frac{\partial}{\partial y}\left[D_h h\frac{\partial C}{\partial y}\right] = \frac{hC_{eq} - hC}{T_s} \tag{3.5}$$

3.1.2.1 Avalanching

In the XBeach-model dune face erosion is modeled with an avalanche algorithm. The rate of dune erosion depends on the capacity of the near dune hydrodynamics to transport sediment in offshore direction and on the supply of sediment from the dune. The latest is simulated with an avalanche algorithm. The avalanche algorithm considers a critical wet slope $\phi_{cr,wet}$ and a critical dry slope $\phi_{cr,dry}$, see Figure 3.2. The transition between the critical slopes takes place at a user specified water depth hswitch. The maximum rate of dune erosion in the the avalanche algorithm is specified by dzmax.

When the critical slope between two adjacent grid cells is exceeded sediment is exchanged between these cells to the amount needed to bring the slope back to the critical slope. This exchange rate is limited by a maximum avalanching transport rate dzmax. In the XBeach model the avalanching mechanism is typically triggered when a high infragravity wave reaches the dune front and partly inundates it. The critical underwater slope is suddenly exceeded. The two grid cells at the dune foot are adjusted during the first time step the dune is inundated. In subsequent time steps a chain reaction may take place both in landward points (≥7). Here the critical dry slope may be exceeded due to the lowering of the last wet point (6). In seaward points (3-5) the critical wet slope may be exceeded due to a sediment supply from more landward points (≥6). Consequently sediment is brought from the dry dune into the wet profile where it is transported seaward seaward by undertow and infragravity backwash (Roelvink *et al.*, 2009).

3.1.2.2 Bed-updating

Based on the gradients in the sediment transport the bed level changes according to Equation 3.6. In this equation p is the porosity, f_{mor} is a morphological acceleration factor of O(1-10)

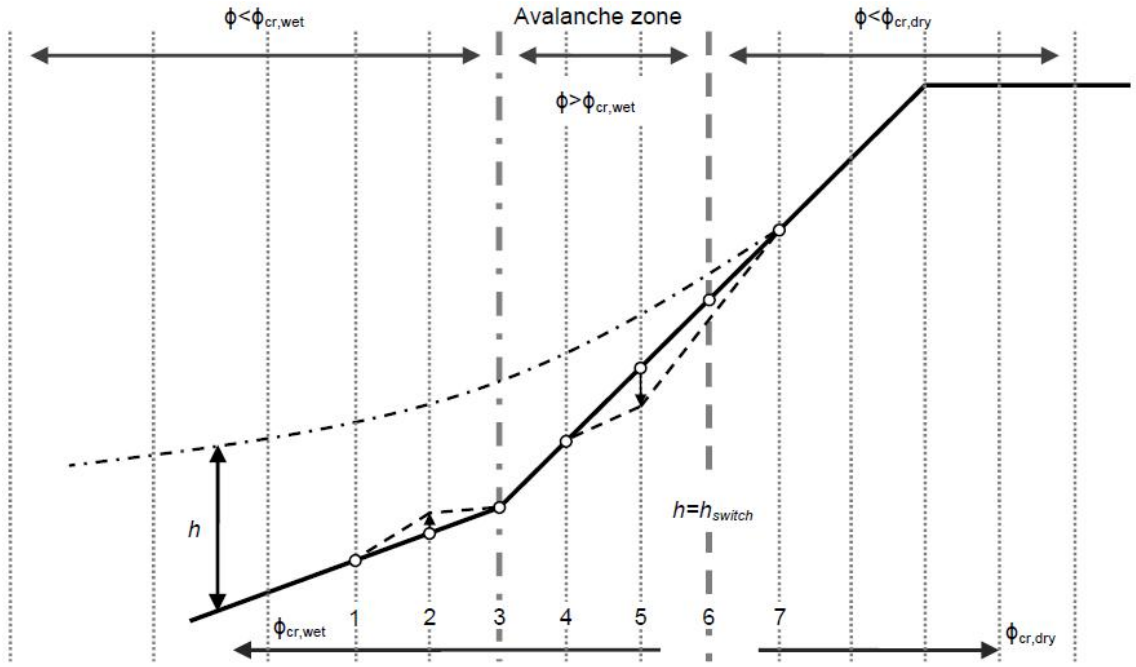

Figure 3.2: Explanation of the avalanching algorithm. The bed is indicated by (—) and the water surface by (−·−). The computational bed level points (−−) are unstable in the avalanche zone. The post avalanche profile is indicated by (−−) (van Thiel de Vries, 2009).

and q_x & q_y represent the sediment transport rates in x- and y-directions respectively (Roelvink *et al.*, 2009).

$$\frac{\partial z_b}{\partial t} + \frac{f_{mor}}{(1-p)}\left(\frac{\partial q_x}{\partial x} + \frac{\partial q_y}{\partial y}\right) = 0 \tag{3.6}$$

3.1.2.3 Boundary conditions

The wave energy density at the offshore boundary is prescribed as a function of y, θ and time. This can be generated for given spectral parameters or using directional spectrum information. At the lateral boundaries the alongshore or along-crest gradient for wave components entering the domain is set to zero. This eliminates the “shadow zones” found in many wave models. At the seaward and, in case of a bay, the landward boundary radiating boundary conditions are prescribed. The radiating boundary condition takes into account the incoming bound long waves. For the lateral boundaries Neumann or Wall boundaries can be used. For Neumann boundaries the longshore water level gradient is prescribed. In case of obliquely incident wave groups this kind of boundary condition gives no large disturbances. For Wall boundaries the mass flux through the boundary is zero (Roelvink *et al.*, 2009).

3.2 Model setup

3.2.1 Modeling approach

Before in Chapter 5 XBeach is validated with measurements a simple closed abrupt connection between dunes and a dike is investigated. The behaviour of a dune-dike system is investigated by dividing the dune-dike connection in 3 regions; an “undisturbed” dune section, an “undisturbed” dike section and the transition between the both sections. Here “undisturbed” means that the conditions along the coast are alongshore uniform and hence there is no influence of a dune-dike connection on the process behaviour. The transition zone is the zone in which the presence of the connection influences its surroundings, see Figure 2.5. The storm impact on a sandy

coastline and sea-dike is considered a 1D cross-shore phenomenon (van Thiel de Vries *et al.*, 2010). Therefore the "undisturbed" dune & dike section is simulated by a 1D model. The 1D dike model is constructed by adding a hard layer to the 1D dune model. The input parameters of both models are identical.

The influence of a dune-dike connection on its surroundings is an inherent 2DH process (van Thiel de Vries *et al.*, 2010). A 2DH "morphodynamic" model is used to simulate the behaviour of a dune-dike connection. A 2nd 2DH model is used to get insight in to the predicted hydrodynamic response to the presence of the connection. In this "hydrodynamic" model morphological change is prevented by setting morfac = 0. The initial bathymetry of this model is equal to the end bathymetry of the "morphodynamic" model which predicted the morphological response of the system. The model simulates the same storm conditions for 1 hour. The "hydrodynamic" model is identical to the "morphodynamic" model except the storm duration.

To quantify the dune erosion predicted by XBeach the retreat point R^* and the erosion volume A are used. These erosion parameters are described in Section 2.1. The output of the "hydrodynamic" model is averaged over the last 5 minutes of the simulation. By omitting the 1st half hour from the averaging procedure spin-up effects are eliminated.

3.2.2 Model input

The input parameter values of the models originate from the Delta Flume experiments of '05/'06. These experiments were used to calibrate the dune erosion process in XBeach. A deviation lies within the use of a different wave spectrum. In the Delta Flume experiments the Pierson-Moskowitz (PM) spectrum was used to generate waves. In the XBeach model the Jonswap spectrum with identical spectrum parameters H_{m0} and f_p was used. The Jonswap spectrum is narrower and has a higher peak frequency than the PM-spectrum. This results in more energetic bound long waves visualized by the bound long wave spectrum. For the lateral model boundaries the Wall condition was used.

The duration of the boundary condition file rt is 30 min. It is reused until the given storm duration of 6 hours is completed. Turning off the random generator (random = 0) insures identical boundary conditions files for every model. To generation long-crested waves the parameter s is 10,000. The waves have an angle of incidence of 0° with respect to the coastline. In the Jonswap spectrum file this translates to mainang = 270. In Table 3.1 on page 23 the input parameters for the models are displayed.

3.2.2.1 Cross-shore profile

The initial profile of the models is similar to that of the Delta Flume experiments of '05/'06, see Figure 3.3. The initial profile is defined by a number of bottom coordinates (x,z). The cross-shore coordinate x increasing in landward direction. The depth z defined positive upward.

3.2.3 Computational grid

The 2DH models have an alongshore length of 650 m to ensure that the lateral model boundaries do not influence the behaviour near the connection. The connection is situated in the middle at y = 325 m. Near the connection the grid spacing is small. Between y = 295 m & y = 355 m the grid spacing dy is 1 m. Towards the lateral model boundaries, y < 295 m & y > 355 m, the grid spacing increases to dy = 4 m. Between y = 0 - 325 m the dunes are located. From y = 325 - 650 m a sea-dike is situated. Figure 3.4 presents the computational grid of the 2DH models including the bottom elevation z_b.

XBeach parameter	1D Dune	1D Dike	2DH Dune-Dike Morphodynamics	2DH Dune-Dike Hydrodynamics
Grid				
nx	94	94	94	94
ny	2	2	235	235
posdown	-1	-1	-1	-1
vardx	1	1	1	1
xfile	x.grd	x.grd	x.grd	x.grd
yfile	y.grd	y.grd	y.grd	y.grd
depfile	bed.dep	bed.dep	bed.dep	bed.dep
thetamin	-90	-90	-90	-90
thetamax	90	90	90	90
dtheta	180	180	20	20
Physical constants				
rho	1000	1000	1000	1000
g	9.81	9.81	9.81	9.81
Time management				
tstart	0	0	0	0
tintg	60	60	60	-
tintm	300	300	300	300
tstop	21600	21600	21600	3600
Boundary conditions				
instat	4	4	4	4
rt	1800	1800	1800	1800
dtbc	0.5	0.5	0.5	0.5
random	0	0	0	0
ARC	1	1	1	1
order	2	2	2	2
epsi	0	0	0	0
Hm0	1.5	1.5	1.5	1.5
fp	0.2041	0.2041	0.2041	0.2041
fnyq	1.0000	1.0000	1.0000	1.0000
mainang	270	270	270	270
s	10000	10000	10000	10000
gammajsp	3.3	3.3	3.3	3.3
wci	0	0	0	0
left	wall	wall	wall	wall
right	wall	wall	wall	wall
Sediment characteristics				
struct	0	1	1	1
ne_layer	-	nebed.dep	nebed.dep	nebed.dep
morfac	1	1	1	0
D50	0.0002	0.0002	0.0002	0.0002

Table 3.1: XBeach model input parameters

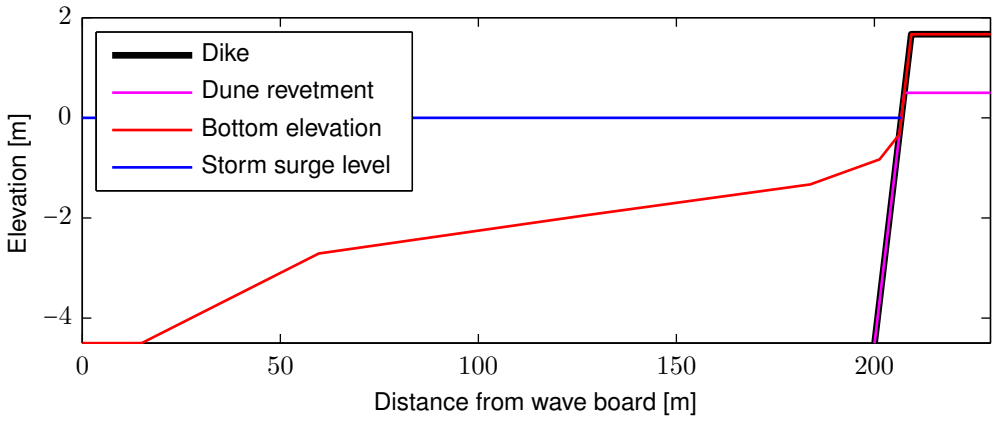

Figure 3.3: Initial profile of Delta Flume experiments.

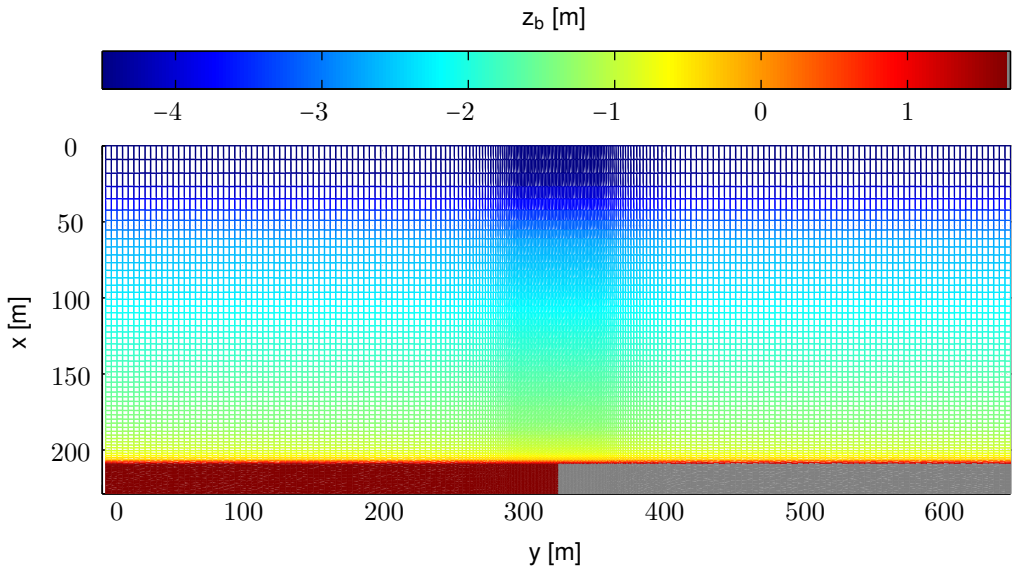

Figure 3.4: Computational grid of the 2DH models indicated by lines. The line color represents the bottom elevation z_b. The dike stretch is indicated by a gray color.

3.2.3.1 Optimal dx_{min}

The calculation time of a model is mainly determined by the number of grid points. Based on the wave speed v and the distance between two adjacent grid points dx XBeach calculates the required time step dt for each point in the model domain. The smallest time step is normative and is applied by XBeach. This process is repeated until the given storm duration is simulated. The grid point spacing in x-direction is calculated based on the CFL-condition, see Equation 3.7. It states that the distance a wave travels in a time step dt must be smaller or equal to the distance between two grid points dx.

$$v\frac{dt}{dx} \leq 1 \tag{3.7}$$

In deep water where the wave celerity is higher the grid point spacing can be larger. In onshore direction the waves slow down and the grid spacing reduces. This ensures that the time step for the initial bottom profile is equal over the entire model domain. During the simulation the bottom elevation changes and so does the time step.

At the shore a minimum spacing dx_{min} is applied. It is chosen such that dune erosion is calculated

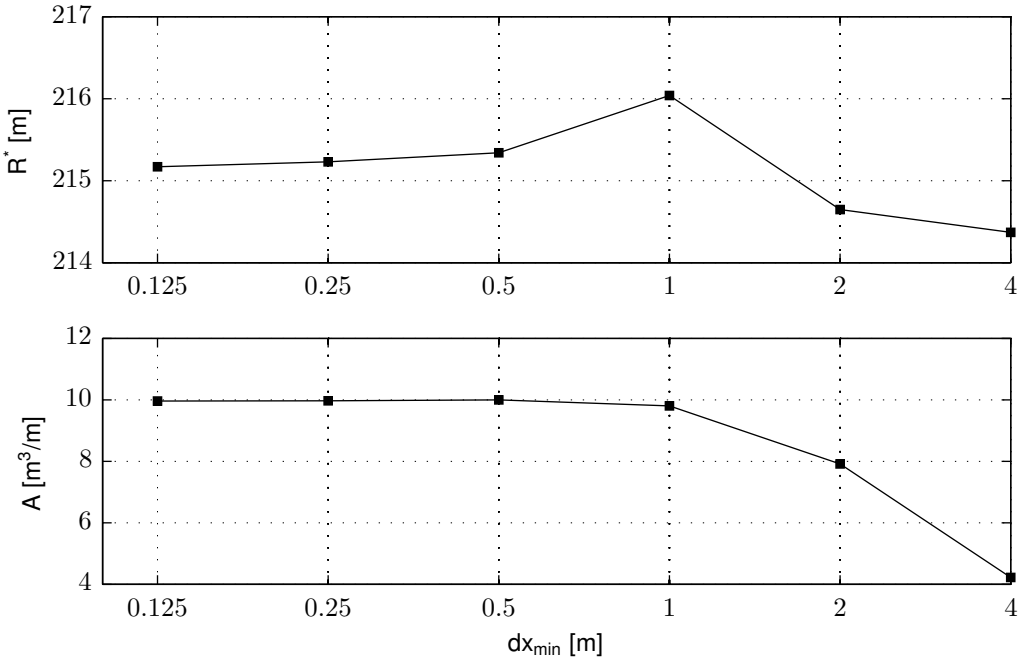

Figure 3.5: Influence of dx_{min} on retreat point R^* and erosion volume A.

accurately while the calculation time is kept as low as possible. As dx_{min} decreases model results become more accurate until a certain limit is reached. A further reduction of dx_{min} will only results in an increase of the calculation time. To determine the optimal onshore grid spacing and obtain an efficient computational grid multiple 1D Dune models were used. The models have identical initial conditions. The only varying parameter is the onshore grid spacing dx_{min} ranging from 0.125 m to 4 m. For each model the retreat point R^* and the erosion volume above storm surge level A is determined.

In the models the retreat point R^* in a transect is defined as the x-coordinate of the grid point which is farthest offshore and from which the bottom elevation is larger than 1.65 m. The dune height at the start of the simulation is 1.67 m. To obtained the erosion volume A the point of intersection with the storm surge level is calculated for the initial profile and end profile. Subsequently the difference above SSL between the initial profile and end profile is numerically integrated over the x-dir with the trapezoidal rule. Figure 3.5 displays R^* & A at the end of each simulation.

The erosion volume A converges to a constant value of 10 m^3/m. For $dx_{min} \geq 1$ m this starts to deviate but only becomes significant upward of dx_{min} = 1 m. This means that for a accurate calculation of the erosion volume the upper limit for the minimum grid spacing is given by dx_{min} = 1 m. The retreat point R^* is relatively constant for small values of dx_{min}. However upward of dx_{min} = 0.5 m the differences become larger. This means that dx_{min} = 0.5 m is the upper limit for an accurate calculation of the retreat point. Based on this data it is argued that the optimal onshore grid spacing is 0.5 m.

3.3 Modeling dune erosion under storm conditions

In this section the consistency between the dune erosion process simulated by XBeach and the erosion process as described in the literature is investigated. The theory on the dune erosion process is described in Section 2.2.

3.3.1 Morphological development

Figure 3.6 displays the bottom elevation at the start of the simulation, after 30 min, after 2 hr and after 6 hr. The time interval between the profile evaluations is 30 min, 1.5 hr and 4 hr respectively. After the storm the beach has become wider. The dune foot moved in landward direction while the waterline moved seaward. The changes in bottom elevation occur landward of x = 170 m. Further seaward the changes in elevation are in the order of millimeters and are considered negligible. This means that the morphologically active zone extends from x = 170 m to the shoreline.

In Figure 3.7 the location of the retreat point during the simulation is displayed. The blue lines indicate the location of the retreat point R^* at the time of profile evaluations. The total dune crest retreat ΔR^*_{tot} during the simulation is 6.06 m. In the 1st 30 min the dune crest retreat is 2.06 m. This accounts for 34% of ΔR^*_{tot}. In the following two time intervals ΔR^* = 2 m which accounts for 2 × 33%. Although the time interval between profile evaluations increases the dune crest retreat in each time interval is roughly equal. The discontinuities in R^* indicates the episodic collapse of the dune front, see Figure 3.7. In the 1st hour collapses of the dune front followed in rapid succession. As the storm progresses the time interval between successive lumps increases and the rate of dune erosion to decreases in time.

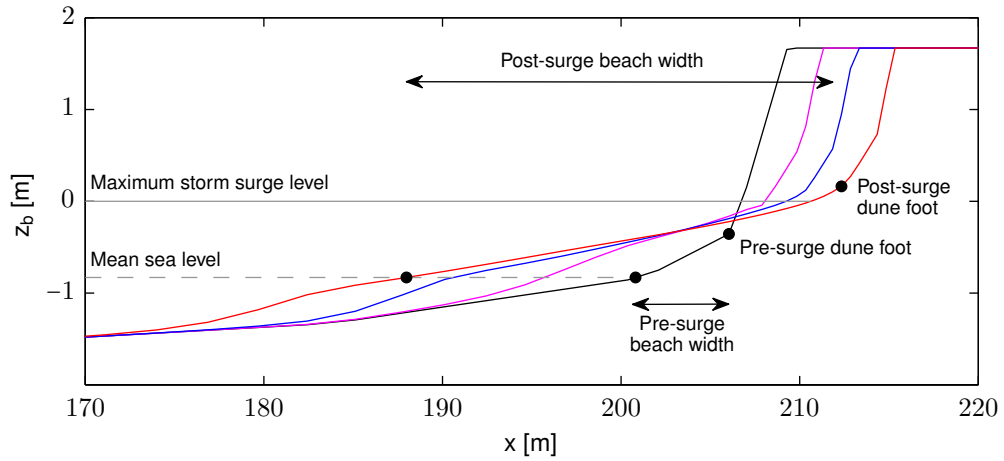

Figure 3.6: Dune erosion predicted by the 1D Dune model. The bottom elevation is evaluated at t = 0:00 hr, the initial cross-shore profile (—), at t = 0:30 hr (—), at t = 2:00 hr (—) and at t = 6:00 hr, the end of the simulation (—).

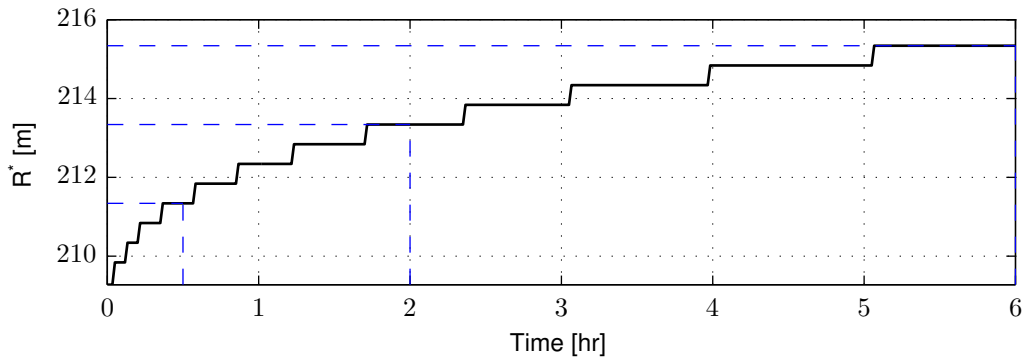

Figure 3.7: Location of the retreat point R^* throughout the simulation.

In Figure 3.8 the development of the suspended sediment concentration in time is displayed. The suspended sediment concentration is highest near the dune front and decreases in seaward direction. Landward from x = 195 m the suspended sediment concentration decrease in time.

Between x = 180 m & x = 195 m however the concentration of suspended sediment increases during the simulation.

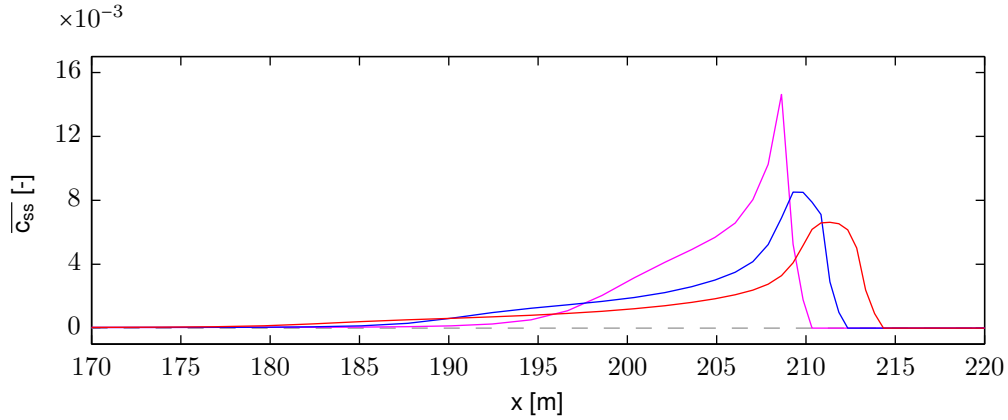

Figure 3.8: Development of the mean suspended sediment concentration in time predicted by the 1D Dune model. The mean suspended sediment concentration is determined between t = 0:25 - 0:30 hr (—), between t = 1:55 - 2:00 hr (—) and between t = 5:55 - 6:00 hr (—).

3.3.2 Hydrodynamic development

In Figure 3.9 the H_{rms} wave height development in time of the short waves and infragravity waves is displayed.[2] During the storm the water depth on the foreshore decreases, see Figure 3.6. The breaker point moves in seaward direction and short waves start to break further offshore. The height of the short waves that reach the dune face become smaller throughout the storm. This is visualized in Figure 3.9 by the short wave height gradient in front of the dune. During the storm this gradient decreases. Subsequently the wave height at for instance 1 m seaward from the dune face becomes smaller throughout the storm. Near x = 207 m the short wave height remains relatively constant throughout the storm. This is associated with a hardly changing bottom elevation between x = 200 m and x = 208 m, see Figure 3.6.

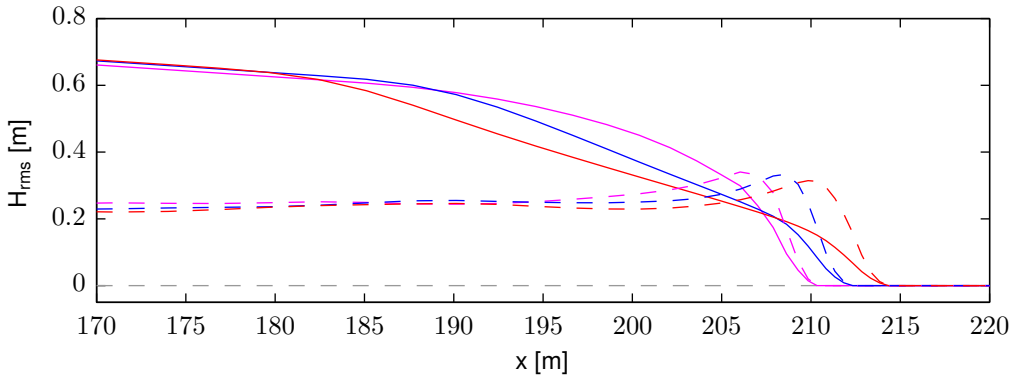

Figure 3.9: H_{rms} wave height development in time predicted by the 1D Dune model. The H_{rms} of the short waves (solid) and of the infragravity waves (dashed) is determined between t = 0:00 - 0:30 hr (—), between t = 0:30 - 2:00 hr (—) and between t = 2:00 - 6:00 hr (—).

The long wave height increases when approaching the dune face due to shoaling. The height of the infragravity waves hardly reduces as the simulation continues. This indicates that there is hardly dissipation of long wave energy due to breaking. As the simulation progresses and the new coastal profile develops long waves become more important which is in accordance with (van Thiel de Vries, 2009).

[2] Calculated with xb_get_hydro.mat (Revision: 4765)

The development of the depth-averaged cross-shore velocity is displayed in Figure 3.10. Negative velocity indicate that the water flows offshore. At the dune face the cross-shore velocity remains relatively high throughout the simulation. On the foreshore the offshore directed flow velocity increases in time. During the simulation the surfzone expands in seaward direction due to the moving breaker point. Since the undertow is confined to the surfzone sediment is transported further offshore.

In Figure 3.11 the development of the sediment transport is displayed. The bulk parameter in XBeach enables the bed load transport and suspended sediment transport to be computed separately (bulk = 0) or combined (bulk = 1). In the simulation the parameter bulk = 1. This means that the depicted sediment transport confines both the bed load transport and the suspended sediment transport. A negative value indicates that the sediment is moved in seaward direction. At the start of the simulation the offshore directed sediment transport is relatively high. At x = ±200 m the sediment transport starts to decrease and the sediment settles on the foreshore. As the simulation continues the sediment transport decreases and the settling point moves offshore. Near the end of the simulation the sediment is deposited seaward from x = ±183 m.

The dune erosion process is simulated correctly by XBeach. The predicted behaviour of a dune transect under storm conditions is consistent with the literature described in Section 2.2.

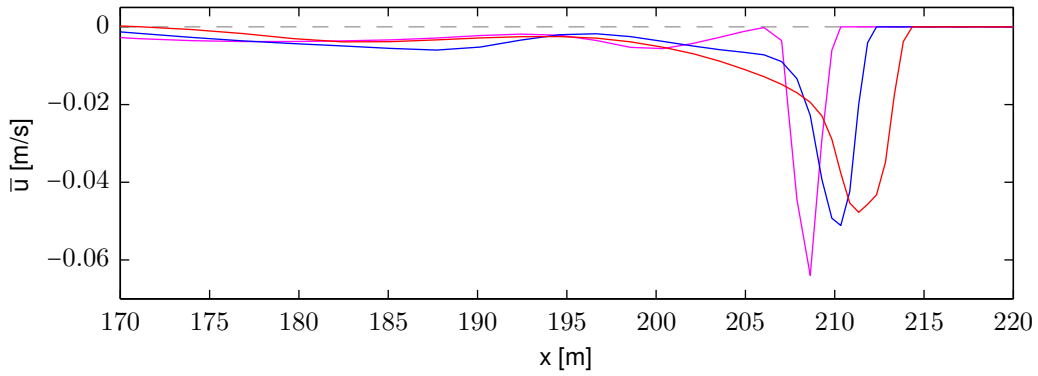

Figure 3.10: Development of the mean cross-shore velocity in time predicted by the 1D Dune model. The mean onshore velocity is determined between t = 0:25 - 0:30 hr (—), between t = 1:55 - 2:00 hr (—) and between t = 5:55 - 6:00 hr (—).

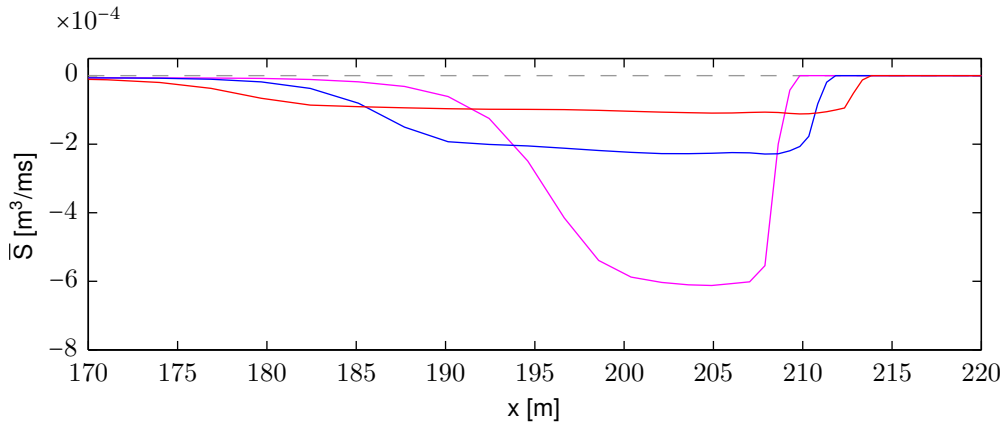

Figure 3.11: Development of the mean sediment transport in time predicted by the 1D Dune model. The mean sediment transport is determined between t = 0:25 - 0:30 hr (—), between t = 1:55 - 2:00 hr (—) and between t = 5:55 - 6:00 hr (—).

3.4 Modeling storm impact on a sea-dike

In this section the consistency between the predicted storm impact on a sea-dike and storm impact described in the literature (Section 2.3) is investigated.

3.4.1 Morphological development

In Figure 3.12 the bottom elevation at the start of the simulation, after 30 min, after 2 hr and after 6 hr is displayed. The time interval between the profile evaluations is 30 min, 1.5 hr and 4 hr respectively. Changes in bottom elevation occur landward of x = 180 m. For x $\leq$ 180 m the changes in elevation are in the order of millimeters and are considered negligible. Therefore it is argued that the morphologically active zone in the 1D Dike model extends from x = 180 m to the shoreline. As sediment is transported seaward a scour hole develops in front of the dike. Figure 3.13 displays the scour depth throughout the storm. Initially the scour depth increases quickly. As the storm progresses the growth rate of the scour depth decreases.

In 1987 Steetzel investigated the behaviour of dune revetments under storm conditions (Steetzel, 1987). In experiment T1 the revetment reached to the top of the dune which can be interpreted as a dike. Experiment T1 is used in the XBeach testbed to validate XBeach against experiments. In the testbed report it was concluded that presently the scour depth at the toe of a dike is underestimated by XBeach (Deltares, 2010).

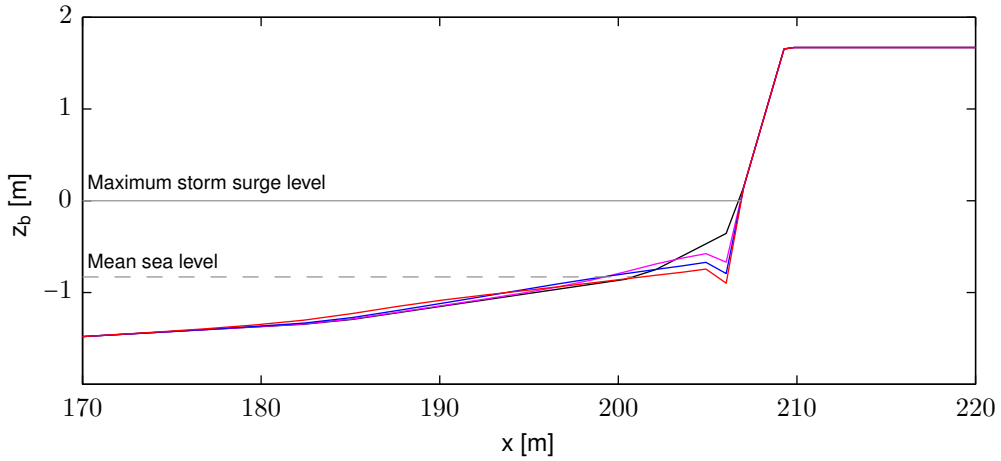

Figure 3.12: Predicted storm impact on a sea-dike by the 1D Dike model. The bottom elevation is evaluated at t = 0:00 hr, the initial cross-shore profile (—), at t = 0:30 hr (—), at t = 2:00 hr (—) and at t = 6:00 hr, the end of the simulation (—).

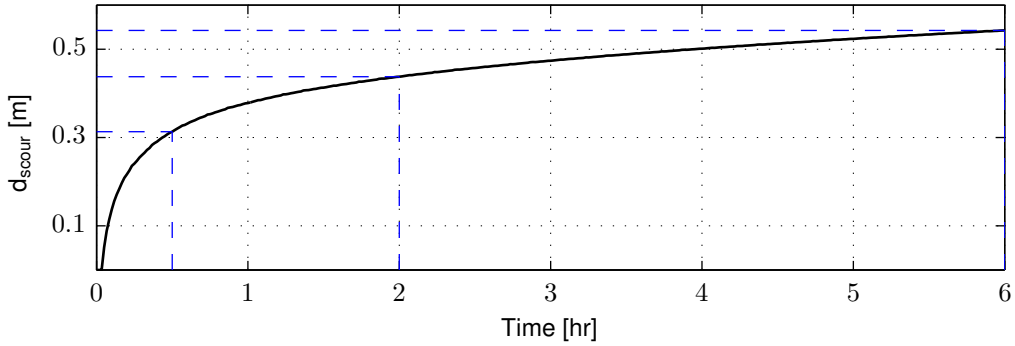

Figure 3.13: Depth of the scour hole in front of the sea-dike throughout the simulation.

Figure 3.14 shows the development of the suspended sediment concentration in time in front of the sea-dike. Near the toe of the dike the suspended sediment concentration is highest. The concentration of suspended sediment decreases in seaward direction. Landward from x = ±197 m the suspended sediment concentration decrease in time. Between x = 180 m & x = 190 m the concentration of suspended sediment increases throughout the simulation.

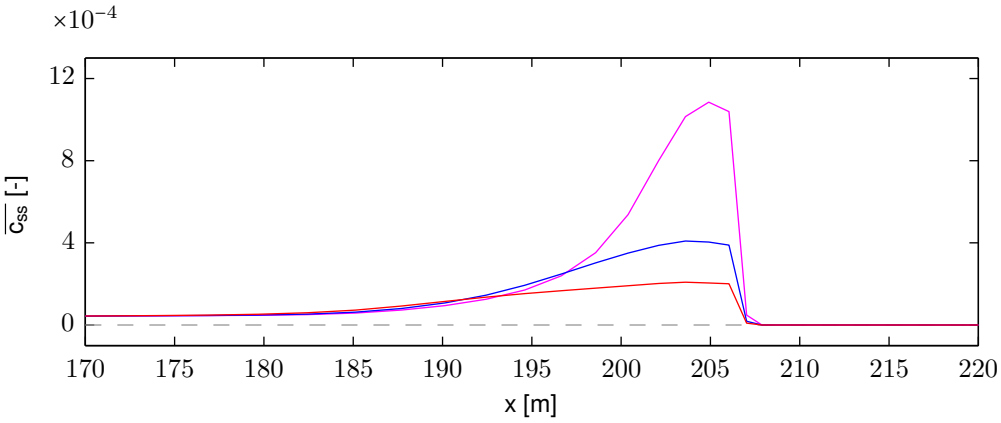

Figure 3.14: Development of the mean suspended sediment concentration in time predicted by the 1D Dike model. The mean suspended sediment concentration is determined between t = 0:25 - 0:30 hr (—), between t = 1:55 - 2:00 hr (—) and between t = 5:55 - 6:00 hr (—).

Compared with the 1D Dune model the predicted concentration of suspended sediment in front of the dike is one order of magnitude smaller. In 1987 Steetzel also investigated an unprotected dune in experiment T5 (Steetzel, 1987). Generally the suspended sediment concentration in front of the dike was a factor 2-4 lower than for an unprotected dune. The XBeach testbed report suggested that the underestimation of the scour depth is caused by an underestimation of the sediment suspension near the dike. The suspended sediment concentration is underestimated with a factor 2 (Deltares, 2010).

The testbed report furthermore concluded that at this stage the erosion volume above a dune revetment is also underestimated. Presently only long wave runup is included in the avalanching algorithm. It was advised to include short wave runup in the avalanching algorithm as well (Deltares, 2010).

3.4.2 Hydrodynamic development

Figure 3.15 displays the H_{rms} wave height development in time of the short waves and infragravity waves is displayed.[3] The short waves that reach the dike remain high and increase slightly throughout the storm. The long wave height increases in landward direction due to shoaling. Throughout the storm the long wave height does not decrease. This indicates that there is hardly any dissipation of long wave energy due to breaking. In front of the dike the long wave height is roughly equal to the short wave height. Throughout the storm the relative importance of long waves with respect to short waves generally remains equal.

The development of the depth-averaged cross-shore velocity is displayed in Figure 3.16. An offshore directed flow of water is indicated by negative velocity. Generally the cross-shore velocities are low. Only from x ≥ 205 m the cross-shore velocities increase to a maximum value of ±4 cm/s. Throughout the storm the cross-shore velocities in front of the dike hardly decrease.

In Figure 3.17 the development of the sediment transport in time is displayed. The bulk parameter

[3] Calculated with xb_get_hydro.mat (Revision: 4765)

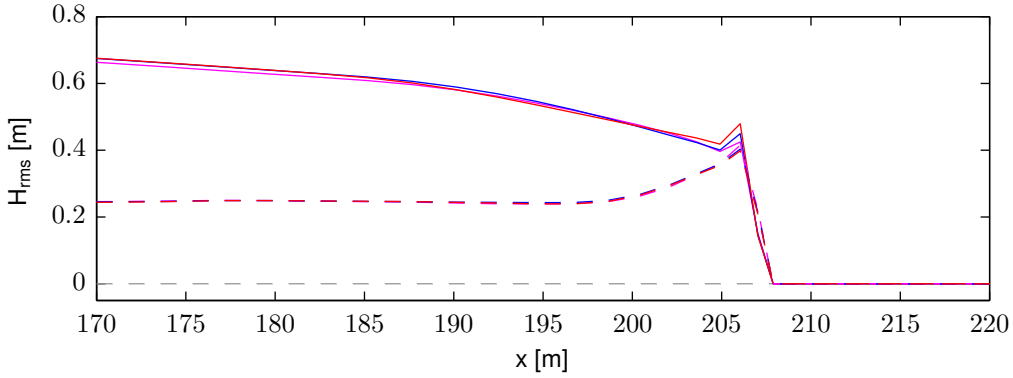

Figure 3.15: H_{rms} wave height development in time predicted by the 1D Dike model. The H_{rms} of the short waves (solid) and of the infragravity waves (dashed) is determined between t = 0:00 - 0:30 hr (—), between t = 1:55 - 2:00 hr (—) and between t = 5:55 - 6:00 hr (—).

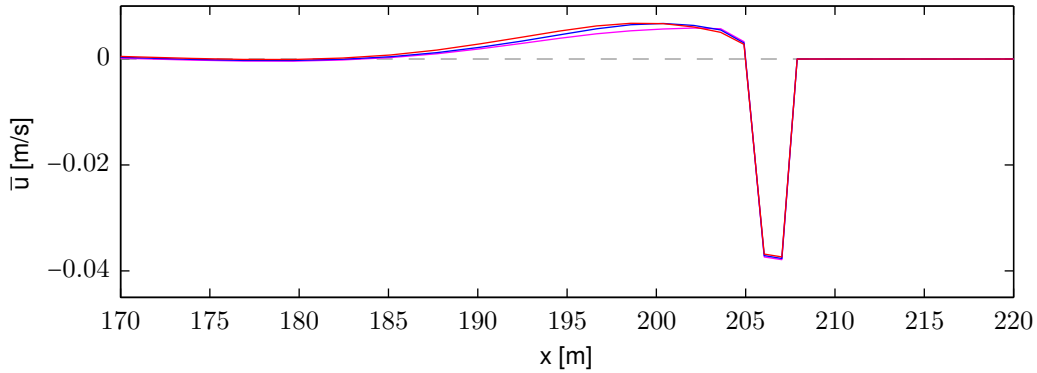

Figure 3.16: Development of the mean onshore velocity in time predicted by the 1D Dike model. The mean onshore velocity is determined between t = 0:25 - 0:30 hr (—), between t = 1:55 - 2:00 hr (—) and between t = 5:55 - 6:00 hr (—).

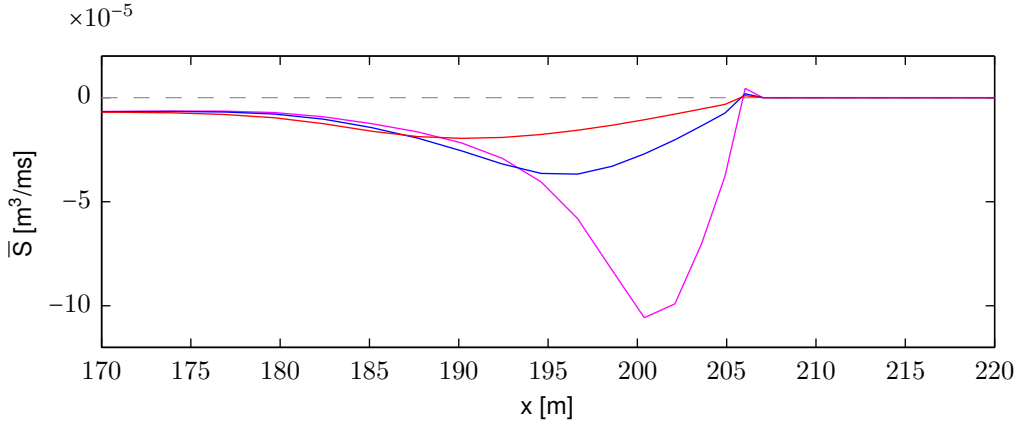

Figure 3.17: Development of the mean sediment transport in time predicted by the 1D Dike model. The mean sediment transport is determined between t = 0:25 - 0:30 hr (—), between t = 1:55 - 2:00 hr (—) and between t = 5:55 - 6:00 hr (—).

enables the bed load transport and suspended sediment transport to be computed separately (bulk = 0) or combined (bulk = 1). The parameter bulk = 1 in the simulation. Hence the depicted sediment transport confines both the bed load transport and the suspended sediment transport. A negative value indicates that the sediment is moved in seaward direction. Compared to a dune transect the sediment transport is relatively low. At the start of the simulation the sediment transport starts to decrease at x = ±200 m and the sediment settles. As the simulation continues the sediment transport decreases and the point at which sediment starts to settle moves offshore. Near the end of the simulation the sediment is deposited seaward from x = ±190 m.

3.5 Modeling the behaviour of a hybrid defense during a storm

In this section the behaviour of a closed abrupt connection between a dune and a dike is investigated with a 2DH model. The setup of this 2DH model is described in Section 3.2. The computational grid and bottom elevation are displayed in Figure 3.4 on page page 24.

3.5.1 Normally incident waves

For undisturbed dune and dike transects the storm impact is considered to be a 1D cross-shore phenomenon (van Thiel de Vries, 2009). Undisturbed means the conditions along the coast are alongshore uniform hence there is no influence of a dune-dike connection. The eroded sediment is transported offshore but remains in the transect. For undisturbed transects the sediment balance or cumulative sedimentation-erosion volume is therefore 0.

At the start of the simulation (t = 0) the cross-shore bottom elevation in each transect is identical. During the storm the bottom in a dune transect rises more and faster than in a dike transect. Consequently a difference in bottom elevation between dune and dike transects develop. This leads to alongshore variations in the hydrodynamics as described in Section 2.4. In the transition zone sediment is transported from the dunes to the dike. Consequently transects in the transition zone do not have a closed cross-shore sediment balance (Steetzel, 1993). This indicates that the sediment balance can give insight into the longshore sediment transport in the transition zone.

For each transect the difference in elevation between the initial profile and final profile is numerically integrated using the trapezoidal rule. This gives the cumulative sedimentation-erosion volume expressed in m^3/m in longshore direction, see Figure 3.18. A negative volume indicates a transect lost sediment to adjacent transects during the storm. Positive volumes show a cross-section gained sediment. Near the dune-dike connection at y = 325 m sediment is transported from the dunes to the dike.

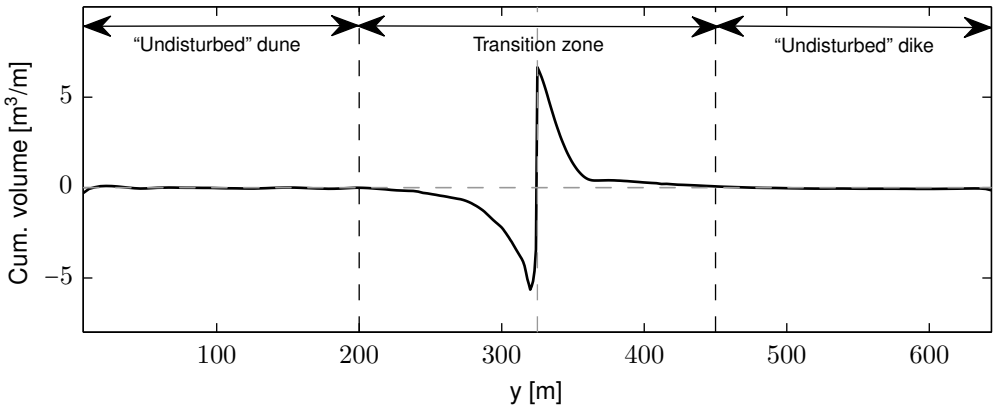

Figure 3.18: Longshore sediment exchange based on the sediment balance for each transect under normally incident waves.

In Figure 3.19 the predicted sedimentation-erosion pattern of a dune-dike system is depicted. A positive value indicates accretion, negative values show erosion. The dunes are brown and dikes are gray. The longshore sediment exchange causes additional dune erosion and hence additional dune retreat next to the connection. Figure 3.19 shows the scour hole that develops in front of the dike during the storm. The scour hole is indicated by a yellow area in front of the dike. In transects close to the connection the scour hole is filled up by sediment from the dunes.

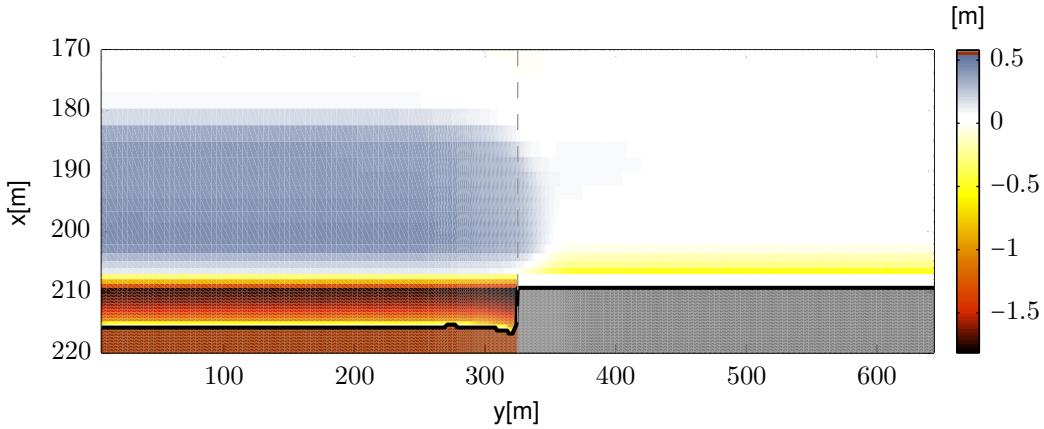

Figure 3.19: Sedimentation-erosion pattern of a dune-dike system under normally incident waves; accretion = +, erosion = -. Dunes are brown, dikes are gray and the retreat line is black.

To quantify the additional dune erosion near the connection the dune crest retreat ΔR^* and the erosion volume A are normalized with the erosion quantities of the 1D Dune model, see Section 3.3. The normalized dune retreat ΔR^*_N is determined by Equation 3.8. In this equation $R^*_{end}(y)$ denotes the retreat point at the end of the simulation for a specific longshore location y. The retreat point in the 1D Dune model is independent y. The normalized erosion volume A_N is calculated with Equation 3.9. For an "undisturbed" dune transects the normalized erosion parameters are 100%.

$$\Delta R^*_N(y) = \frac{\left(R^*_{end}(y) - R^*_0(y)\right)_{2DH}}{\left(R^*_{end} - R^*_0\right)_{1D}} \tag{3.8}$$

$$A_N(y) = \frac{A_{2DH}(y)}{A_{1D}} \tag{3.9}$$

Figure 3.20 displays the normalized dune retreat ΔR^*_N. Near the connection the additional dune

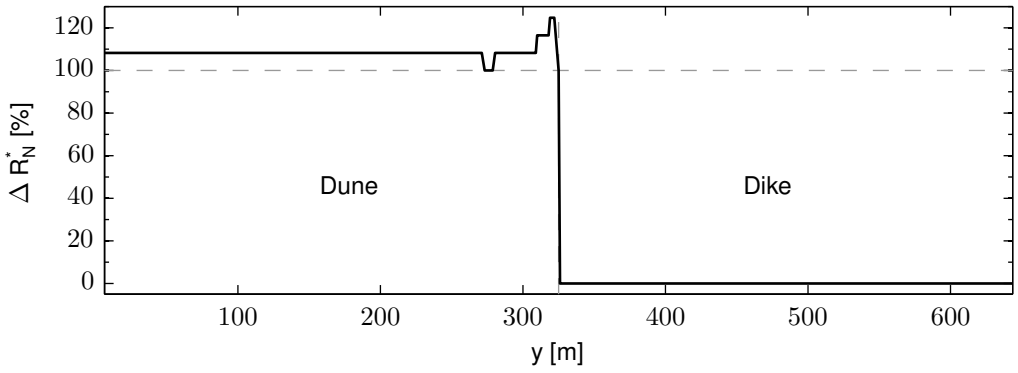

Figure 3.20: Normalized dune retreat $\Delta R^*_N(y)$.

retreat is predicted to be 24.7%. Figure 3.21 shows the normalized erosion volume A_N. XBeach predicts the maximum increase of the erosion volume near the connection to be 22.2%. Outside the region where sediment is transported towards the dike (y≤ ±275 m) the dune retreat and erosion volume increased slightly. This is possibly caused by wave refraction and diffraction around the tip of the dike which generates edge waves. The dune crest retreats one grid cell more than in the 1D Dune model which corresponds to an increase of ±9%. The increase in erosion volume outside the transition zone is ±3%.

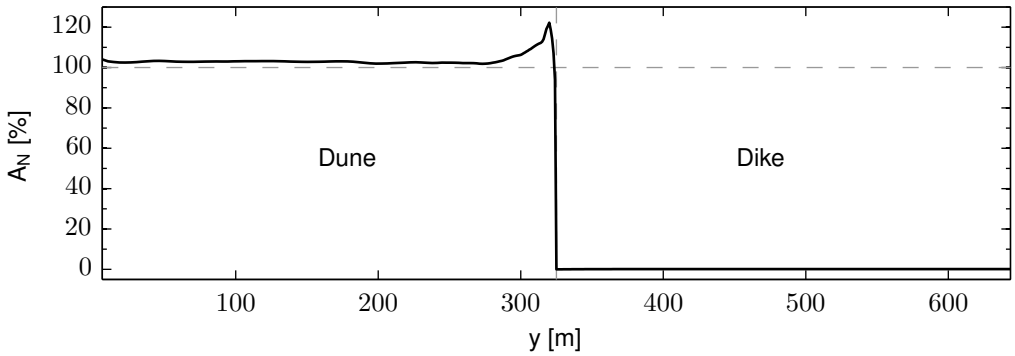

Figure 3.21: Normalized erosion volume above storm surge level $A_N(y)$.

In the upper panel of Figure 3.22[4] the mean wave height predicted by XBeach is displayed. Over the connection there is a longshore variation in wave height. This leads to a longshore variation in the mean wave force F_x, see the 2nd panel from the top in Figure 3.22. Subsequently this results in the expected variation in wave-induced water level setup as shown in the lower panel of Figure 3.22. Furthermore there is a longshore variation in the mean wave force F_y over the connection, see the 3rd panel from the top in Figure 3.22. The gradients in F_y are lower than the gradients in F_x. Gradients in F_y are compensated by the bed shear stress. This stress can only be generated in the presence of a current. In the lower panel the mean still water level including the wave-induced water level setup is depicted. Clearly the water level in front of the dunes (y<325 m) is higher than in front of the dike (y≥325 m). XBeach qualitatively predicts the proper behaviour of the driving forces of the longshore current in front of the connection.

In Figure 3.23 the mean velocity field in front of the coastline is displayed. The current is largely constrained within the morphologically active zone which extends from x = 170 m to the shoreline. Depth-refraction causes waves to bend towards the dune section next to the dike. Due to the longshore current in front of the seawall current refraction tend to bend the waves away from this dune section. Wave current interaction is only applicable with a stationary wave boundary condition. Therefore wave current interaction is not simulated by XBeach in the 2DH models.

3.5.2 Obliquely incident waves

In the following section the angle of wave incidence of the 2DH model is changed to study the effect of oblique incident waves. In the 1st situation (Subsubsection 3.5.2.1) the dunes are situated upstream of the dune-dike connection. In the 2nd situation (Subsubsection 3.5.2.2) the dunes are situated downstream of the closed abrupt dune-dike connection.

When waves come in under an angle with respect to the shoreline a longshore current is generated, see Subsubsection 2.5.4.4. To facilitate the longshore current in the 2DH model Neumann boundaries are used. The parameter epsi = -1 to prevent the water level in the model to rise dur-

[4] H_mean, Fx_mean, Fy_mean and zs_mean output variables of XBeach

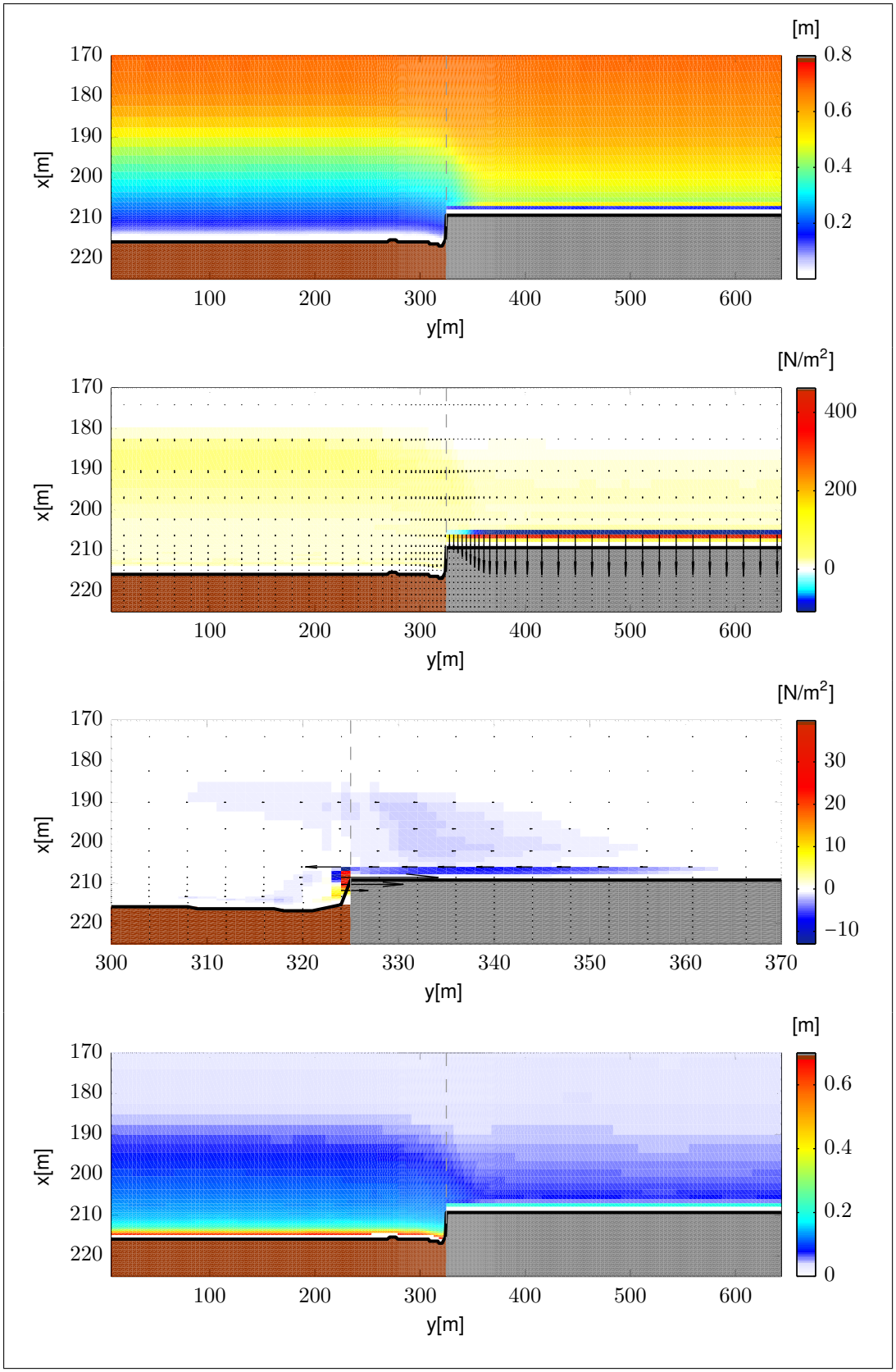

Figure 3.22: XBeach prediction on hydrodynamic conditions in front of a dune-dike connection under normally incident waves. The dunes are brown, the dike is gray and the retreat line is black. Upper panel: Mean short wave height H_{rms}. Second panel from the top: Mean wave force F_x. Third panel from the top: Mean wave force F_y. Lower panel: Mean still water level z_s including the wave-induced water level setup.

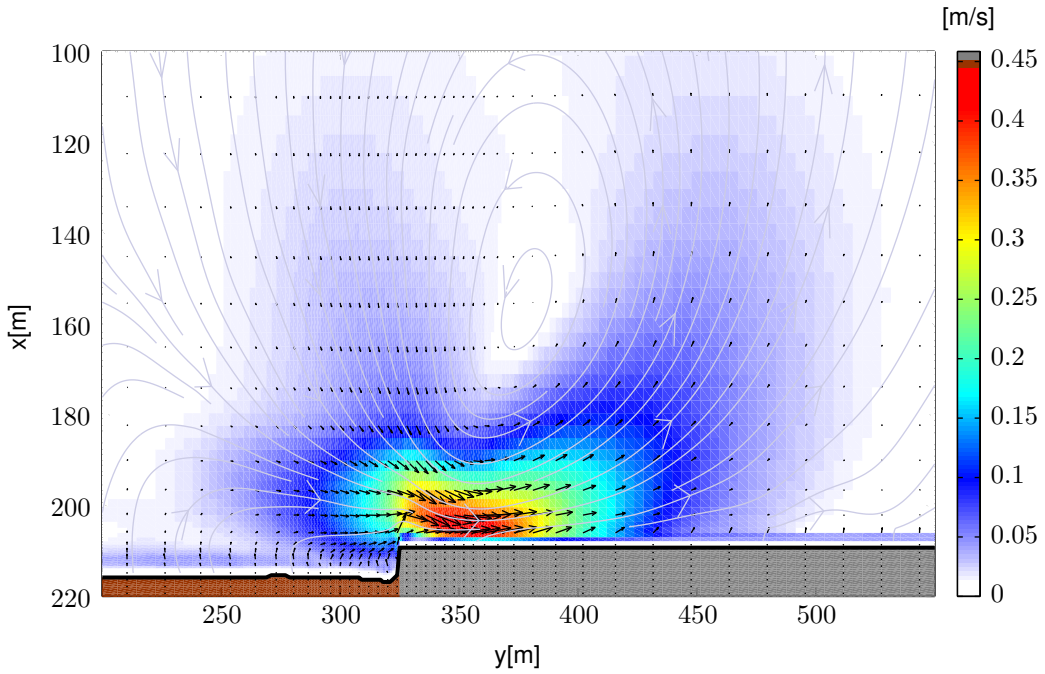

Figure 3.23: Mean velocity field in front of the dune-dike system under normally incident waves: Retreat points of dune (brown) and dike (gray) cross-section are connected by the retreat line (black).

ing the simulation, see Section 3.6. The normalization values for ΔR^* and A are derived from a 2DH Dune model. The model setup is identical to the 2DH "morphodynamic" model for normally incident waves (Figure 3.4) except the dike is replaced by dunes. The 2DH Dune model contains 235 transects from which a mean transects is derived. This mean transect is used to derive the normalization values for ΔR^* and A. The transition from a 1D Dune model to a 2DH Dune model can have an effect on the amount of dune erosion. To quantify this effect the mean transects of a 2DH Dune model with mainang = 270 is compared with the cross-shore profile of the 1D Dune model used in Section 3.3. In the remainder of this chapter the value of mainang is given between brackets. Hence the 2DH Dune model with mainang = 270 is referred to as 2DH (270) Dune model.

3.5.2.1 Dunes situated upstream of the connection

The parameter mainang in the 2DH "morphodynamic" model is changed to mainang = 230. The waves come in from the "southwest" under an angle of 40^o with respect to the shoreline. Other model parameters, except the lateral boundary condition and the epsi parameter, remain equal to the 2DH "morphodynamic" model for normally incident waves and are given in Table 3.1. The waves generate a longshore current flowing from left to right, see Figure 3.24. The velocity of the longshore current depends on the dissipation of wave energy, see Subsubsection 2.5.4.4. In the dune stretch ($y \leq 325$ m) the longshore current velocities are higher and extend more seaward than in the dike stretch ($y \geq 325$ m).

The sediment is transported along the shore from the left model boundary to the right model boundary. The cumulative volume of all transects in the model domain is 368.7 m^3. This indicates that there is a nett transport of sediment into the model through the model boundaries. This was expected and is easily explained. The current velocity and hence the transport capacity of the longshore current are related to the dissipation of wave energy, see Subsubsection 2.5.4.4. In the dune stretch the dissipation of wave energy is larger than in the dike stretch. Consequently the

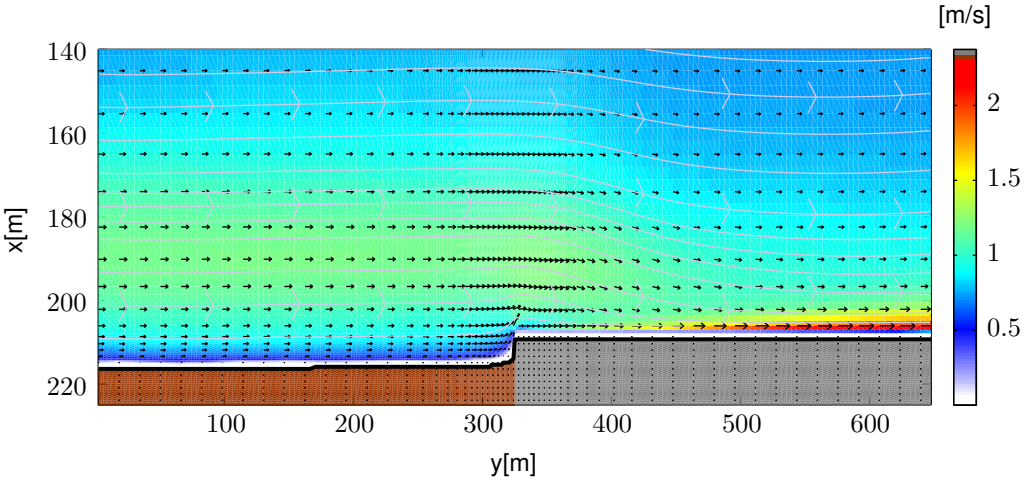

Figure 3.24: Mean velocity field in front of the dune-dike system for mainang = 230: Retreat points of dune (brown) and dike (gray) cross-section are connected by the retreat line (black).

velocity and transport capacity of the longshore current are larger in the dune stretch. Therefore more sediment is transported into the model through the left model boundary than is flowing out of the model through the right model boundary.

The sediment balance of each cross-section can give insight into the longshore sediment transport. For undisturbed transects the eroded sediment is transported seaward but remains in the transect. Undisturbed means that there is no alongshore gradient in the conditions along the coast. Hence the cumulative sedimentation-erosion volume is 0. In Figure 3.25 the sediment balance for the 2DH “morphodynamic” model with mainang = 230 is presented. A negative volume indicates a transect lost sediment to adjacent transects. Cross-section with a positive volume gained sediment during the storm.

Dunes near the connection, between y = 280 m & y = 325 m, gained sediment during the storm. The sediment which is transported along the shore partially piles up against the structure. For y = 325 - 431 m the dike transect gain sediment with a maximum of 11,3 m^3/m at y = 325 m.

Near the dune-dike connection there is a longshore gradient in the velocity and hence transport capacity of the longshore current. At y = 325 m the transport capacity of the longshore current

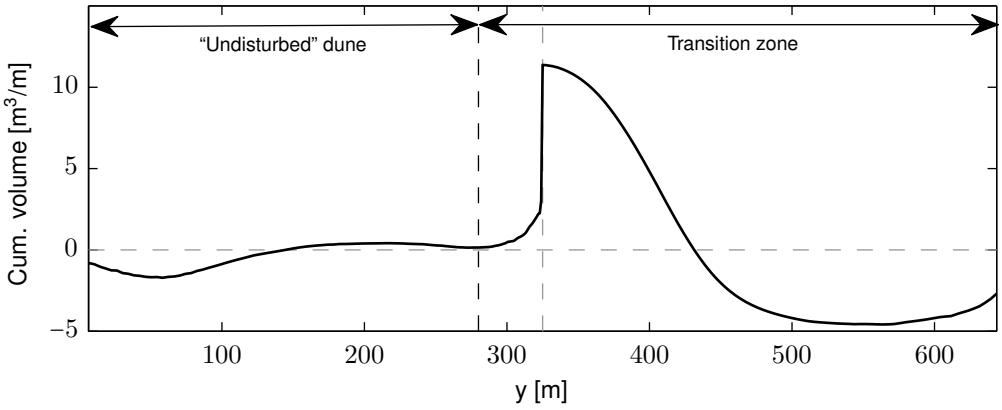

Figure 3.25: Longshore sediment exchange based on the sediment balance for each transect for mainang = 230.

decreases and sediment settles on the foreshore of dike transects close to the connection. The foreshore in the dike transect is raised during the storm and depth-induced wave breaking cause waves to break further offshore. The dissipation of wave energy and hence the velocity and transport capacity of the longshore current in front of the dike increases. Consequently sediment is transported further downstream of the connection. In the simulation sediment is transported 106 m downstream of the connection to y = 431 m, see Figure 3.25. For y ≥ 431 m dike transects lost sediment throughout the storm. This is caused by an increasing velocity and hence transport capacity of the longshore current in front of the dike visible in Figure 3.24 upward of y = 431 m. There is no dike transect that is unaffected by the dune-dike connection in the model domain.

In Figure 3.26 the sedimentation-erosion pattern of the dune-dike system is depicted. A positive value indicates accretion, negative values show erosion. The retreat points R^* of the transects are connected by the retreat line. In Figure 3.27 ΔR^* of the dune stretch is displayed at different time instances. Compared with the undisturbed stretch (y ≤ 280 m) the dunes next to the connection show less erosion. The point at which the erosion decreases significantly moves upstream, see Figure 3.27. At t = 0:30 hr this point lies at y = 315 m. At t = 6:00 hr this point lies at y = 306 m. In front of the dike a scour hole develops during the storm, see Figure 3.26. The scour hole is indicated by a yellow area in front of the dike. Compared with normally incident waves the maximum scour depth is larger. In the region where the dike transects lost sediment (y ≥ 428 m) the scour hole also extends further seaward. Close to the connection the scour hole is filled up

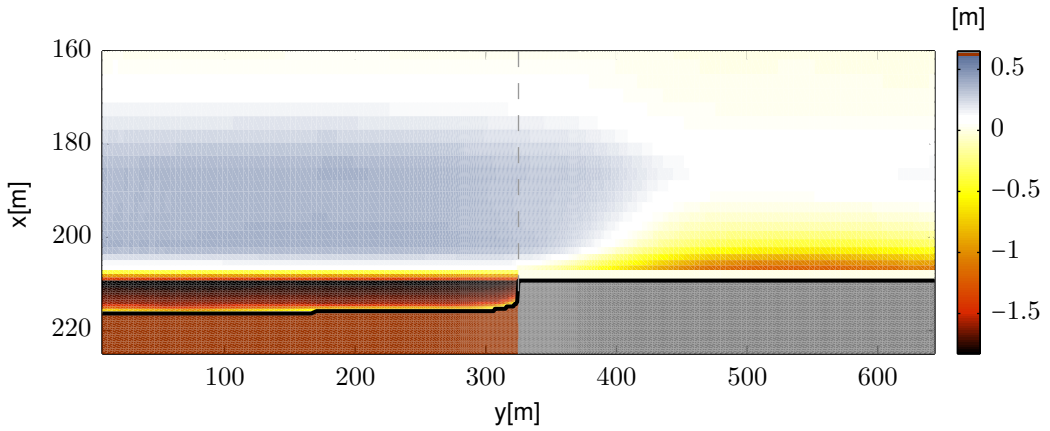

Figure 3.26: Sedimentation-erosion pattern of a dune-dike system for mainang = 230; accretion = +, erosion = -. Dunes are brown, dikes are gray and the retreat line is black.

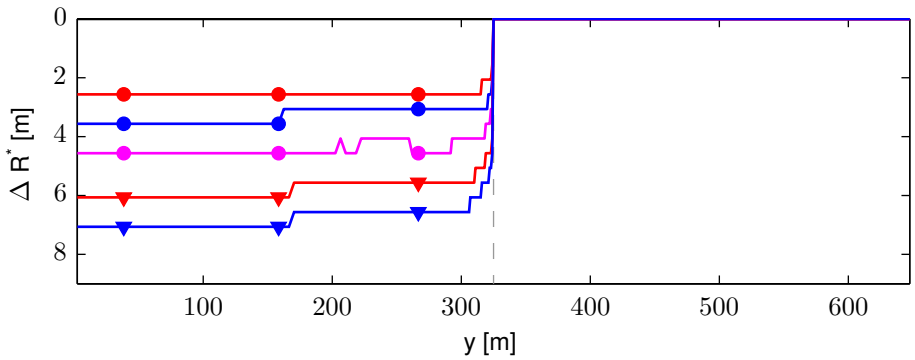

Figure 3.27: Development of ΔR^* of the dune stretch in time for mainang = 230. ΔR^* is displayed at t = 0:30 hr (●), t = 1:00 hr (●), t = 2:00 hr (●), t = 4:00 hr (▼) and t = 6:00 hr (▼).

by the supply of sediment from the dunes. The region in which the scour hole is filled up is larger than for normally incident waves, see Figure 3.26. The blue accretion area in front of the dike is larger compared to normally incident waves and extends to y = ±400 m. For normally incident waves the accretion area in the dike stretch extends to y = ±350 m, see Figure 3.26.

To quantify the dune erosion in the dune-dike system the dune crest retreat ΔR^* and the erosion volume A are normalized with the erosion quantities of the 2DH Dune model. The conditions in the 2DH Dune model are longshore uniform. In Figure 3.28 the bathymetry at t = 6 hr is presented. In Figure 3.30 the mean bottom elevation $\overline{z_b}$ of Figure 3.28 for x = 15 - 22 m is depicted. In this figure the minimum and maximum bottom elevation is given by dashed gray lines. In Figure 3.30 the mean transect of the 2DH Dune model with mainang = 270 is displayed. The figure also presents the bottom elevation of the 1D Dune model (Section 3.3) at t = 6 hr and the mean transect.

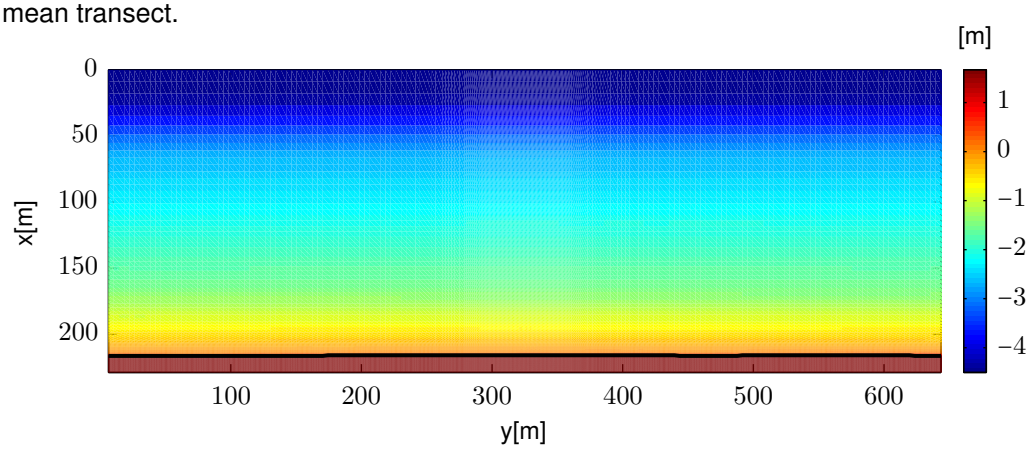

Figure 3.28: Bathymetry of the 2DH Dune model for mainang = 230 at t = 6 hr.

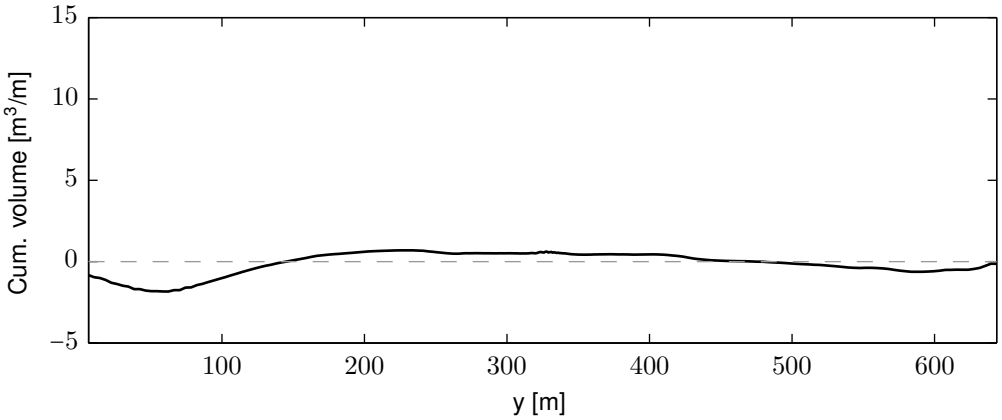

Figure 3.29: Cumulative sedimentation-erosion volume for each transect in the 2DH Dune model with mainang = 230.

Figure 3.28 shows no alongshore variation in the bathymetry. In Figure 3.29 the cumulative sedimentation-erosion volume of the 2DH (230) Dune model is presented. A negative volume indicates a transect lost sediment to adjacent transects. Cross-section with a positive volume gained sediment during the storm. The cumulative volume of all transects in the model domain is 17.2 m^3. Compared to a model domain size of ± 148.000 m^2 this is negligible. This means that the nett transport of sediment into or out of the model domain is very small. This is supported by the fact that the minimum and maximum elevation are close to the mean bottom elevation, see Figure 3.30. Between x = 150 m and x = 210 m the differences between the minimum, maximum

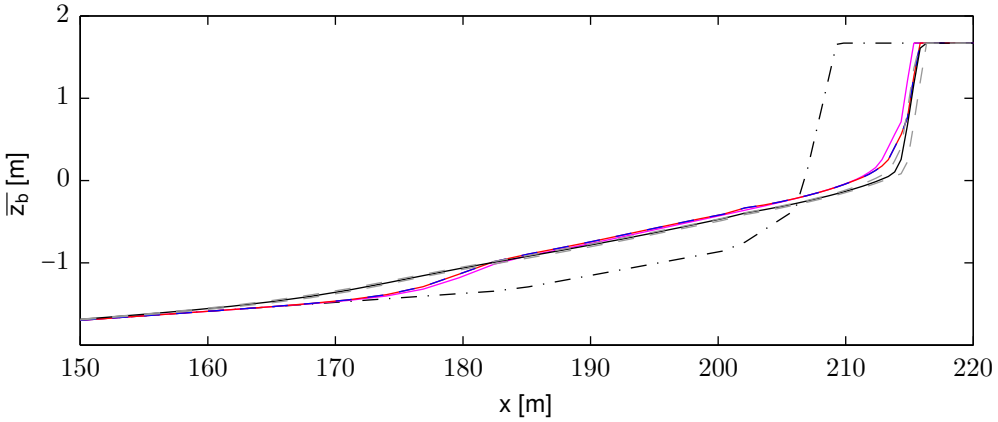

Figure 3.30: Mean final bottom elevation $\overline{z_b}$ of the 2DH Dune model (—) for mainang = 230 and its minimum & maximum measured elevation (– –), the final bottom elevation of the 1D Dune model (—), the mean final bottom elevation $\overline{z_b}$ of the 2DH (270) Dune model with wall boundaries (—), $\overline{z_b}$ of the 2DH (270) Dune model with Neumann boundaries (– –), the initial bottom elevation of both models (– · –), SSL (– · –).

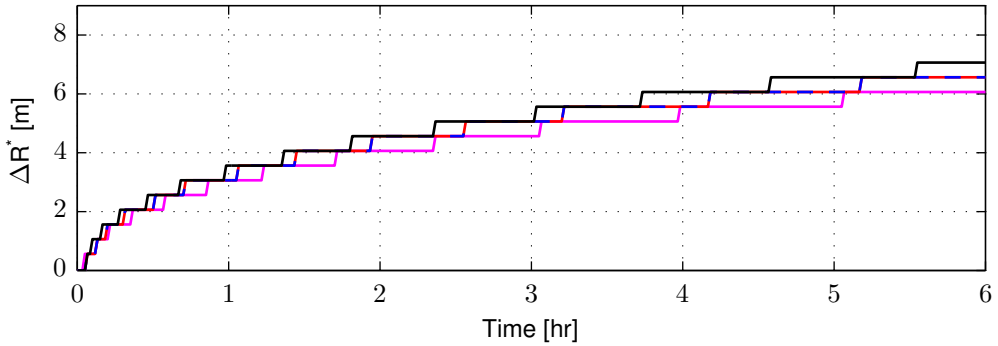

Figure 3.31: Dune crest retreat ΔR^* of the 2DH Dune model (—) for mainang = 230, the 1D Dune model (—), the 2DH (270) Dune model with wall boundaries (—) and the 2DH (270) Dune model with Neumann boundaries (– –).

and mean bottom elevation are negligible. For x ≤ 210 m the differences increase slightly.

The mean transect of the 2DH (270) Dune model with wall boundaries and with Neumann boundaries is identical. This indicates that the lateral boundaries have no effect on the amount of erosion. Although the mean transect of the 2DH (270) models shows more erosion than the 1D Dune model the differences in the bottom profile are little. The 2DH (230) Dune model shows more dune erosion than the 1D Dune model. Between x = 170 m and x = 180 m the foreshore raised considerably more. In addition to the waves the longshore current stirs up sediment (J.A. Roelvink 2011, pers. comm. 7 September). Subsequently the sediment is transported seaward by the undertow. In the case of normally incident waves additional stirring of sediment by the longshore current is absent. This is visualized by the mean suspended sediment concentration $\overline{c_{ss}}$ in Figure 3.32. In this figure solid lines present $\overline{c_{ss}}$ of the 1D Dune model. Dashed lines indicate the mean suspended sediment concentration of the 2DH (230) Dune model. Although the $\overline{c_{ss}}$ of the 2DH (230) Dune model is smaller than $\overline{c_{ss}}$ of the 1D Dune model at the dune face it is larger at the foreshore. Subsequently sediment is transported further offshore compared to normally incident waves, see Figure 3.30.

In the 2DH (230) Dune model changes in bottom elevation occur landward of x = 160 m. Further seaward the changes in elevation are in the order of millimeters and are considered negligible. This means that the morphologically active zone extends from x = 160 m to the shoreline. For normally incident waves the morphologically active zone extends from x = 170 m to the shoreline, see Section 3.3.

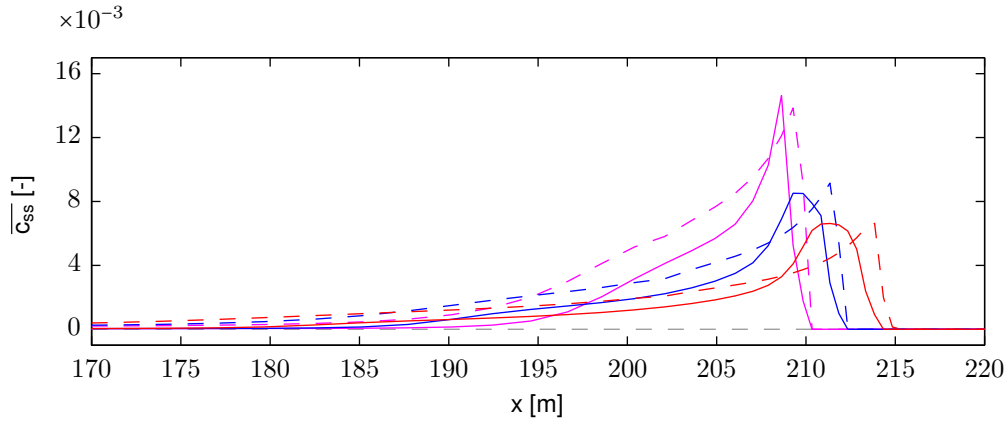

Figure 3.32: Development of the mean suspended sediment concentration in time predicted by the 1D Dune model (solid) and the 2DH Dune model with mainang = 230 (dashed). The mean suspended sediment concentration is determined between t = 0:25 - 0:30 hr (magenta), between t = 1:55 - 2:00 hr (blue) and between t = 5:55 - 6:00 hr (red).

The dune retreat and erosion volume derived from the mean transect of the 2DH (230) Dune model are normalized with the erosion values of the 1D Dune model. This isolates the influence of the longshore current on the erosion process. The mean dune crest retreat of the 2DH (230) Dune model is 7.06 m. This is 1.0 m more than in the 1D Dune model and corresponds with 2 grid cells in x-direction. The dune crest retreat increased with 16,5%. The erosion volume A increased with 1.47 m^3/m to a value of 11.49 m^3/m. This corresponds to an increase of 14.6%.

To isolate the influence of the dune-dike connection on the additional erosion the normalization values are derived from the mean transect of the 2DH (230) Dune model. The normalized dune retreat ΔR^*_N is calculated by Equation 3.8. The normalized erosion volume A_N is determined by Equation 3.9. Figure 3.33 displays the normalized dune retreat ΔR^*_N normalized with erosion values derived from the 2DH (230) Dune model. From y = 170 m ΔR^*_N starts to decrease until a value of 64.6% is reaches at the dune-dike connection. Near the connection the dune crest retreat is 35.4% less than in the undisturbed dune stretch. The normalized erosion volume A_N

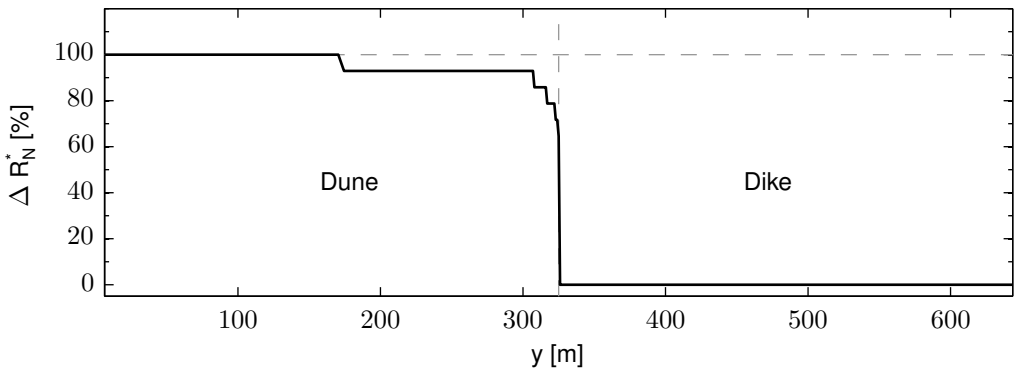

Figure 3.33: Influence of the dune-dike connection on the additional erosion: Normalized dune retreat $\Delta R^*_N(y)$ for mainang = 230.

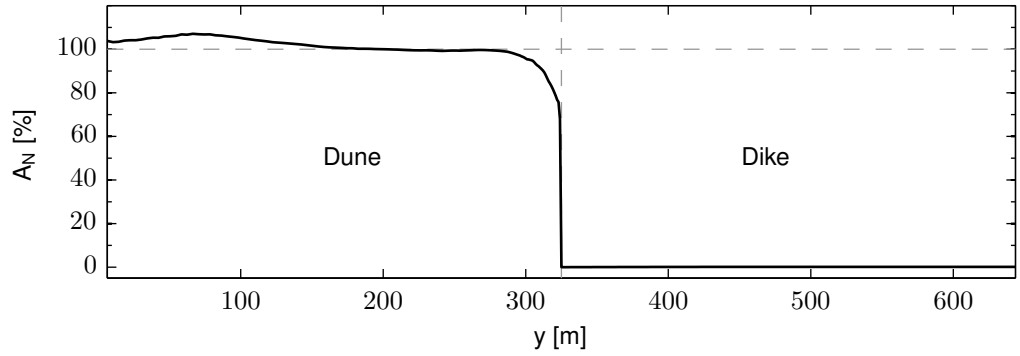

Figure 3.34: Influence of the dune-dike connection on the additional erosion: Normalized erosion volume above storm surge level $A_N(y)$ for mainang = 230.

shows a similar behaviour, see Figure 3.34. Near the connection the erosion volume is 32.1% less than in the undisturbed dune stretch.

The combined effect of the longshore current and the dune-dike connection is obtained by normalization with the erosion values of the 1D Dune model. ΔR^*_N and A_N are calculated by Equations 3.8 3.9 respectively. Figure 3.35 displays the normalized dune retreat ΔR^*_N normalized with erosion values derived from the 1D Dune model. Near the connection the dune crest retreat is 24.7% less than in the 1D Dune model. Near the connection the erosion volume is 22.2% less than in the 1D Dune model, see Figure 3.36.

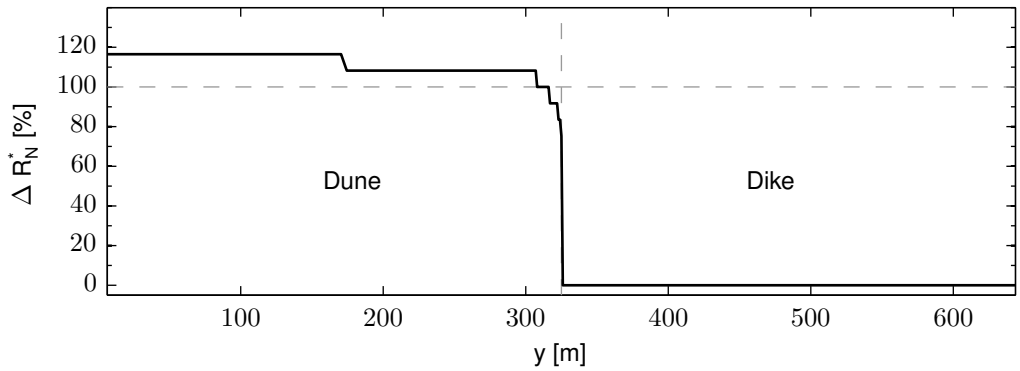

Figure 3.35: Combined influence of the dune-dike connection and longshore current on the additional erosion: Normalized dune retreat $\Delta R^*_N(y)$ for mainang = 230.

In the upper panel of Figure 3.37 the mean wave height predicted by XBeach is displayed. Over the connection there is a longshore variation in wave height. Compared to normally incident waves the longshore variation in wave height extends further down the connection. This leads to a longshore variation in the mean wave force F_x, visible in the 2nd panel from the top in Figure 3.37, and subsequently to a longshore variation in wave-induced water level setup as shown in the lower panel of Figure 3.37. This mechanism is the main driving force behind the morphological response of the coast for normally incident waves. The 3rd panel from the top in Figure 3.37 shows the longshore variation in the mean wave force F_y. The gradients in F_y are lower than the gradients in F_x. Gradients in F_y are compensated by the bed shear stress. This stress can only be generated in the presence of a current. Depending on the angle of wave incidence with respect to the shore the longshore current is determinative for the morphological response of the coastline. XBeach qualitatively predicts the proper behaviour of the driving forces

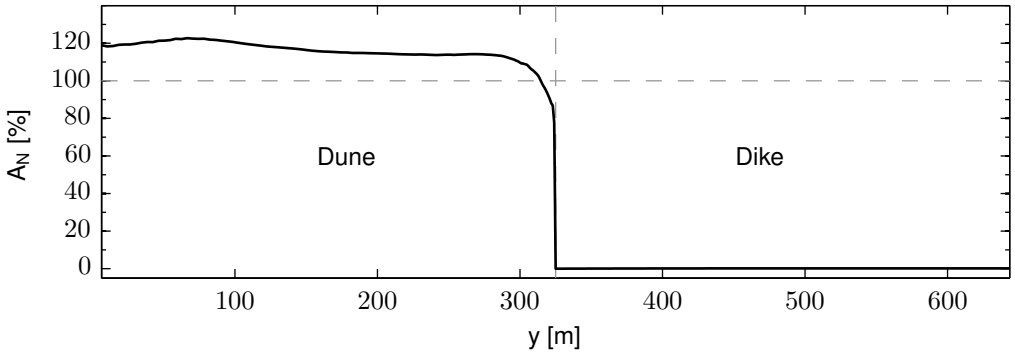

Figure 3.36: Combined influence of the dune-dike connection and longshore current on the additional erosion: Normalized erosion volume above storm surge level $A_N(y)$ for mainang = 230.

of the longshore current.

3.5.2.2 Dunes situated downstream of the connection

The parameter mainang in the 2DH "morphodynamic" model is changed to mainang = 310. The waves come in from the Northwest under an angle of 40° with respect to the shoreline. Other model parameters, except the lateral boundary condition and the epsi parameter, remain equal and are given in Table 3.1. The waves generate a longshore current flowing from right to left, see Figure 3.38. Near the end of the simulation the water circulates around the tip of the dike. This current transport sediment towards the connection.

The sediment balance will again give insight into the longshore sediment transport in the transition zone. In Figure 3.39 the sediment balance for the 2DH "morphodynamic" model with mainang = 310 is presented. The sediment is transported along the shore from the right model boundary to the left model boundary. The cumulative volume of all transects in the model domain is -474.4 m^3. This indicates that there is a nett transport of sediment out of the model through the model boundaries. This was expected and is easily explained. The velocity and transport capacity of the longshore current are related to the dissipation of wave energy, see Subsubsection 2.5.4.4. In the dune stretch the dissipation of wave energy is larger than in the dike stretch. Consequently the velocity and transport capacity of the longshore current are larger in the dune stretch. Therefore more sediment is transported out of the model through the left model boundary than is flowing into the model through the right model boundary.

Since the dune-dike connection is situated downstream the dike stretch is expected to be undisturbed. However at the right model boundary the cumulative sedimentation-erosion volume is negative and remains negative for y ≥ 388 m. It is likely that the amount of sediment transported into the model through the right boundary is too small. In that case the transport capacity of the longshore current is larger than the amount of sediment that is transported. Subsequently sediment is picked up and is transported downstream. These transects have a negative cumulative volume, see Figure 3.39. Between y = 325 m & y = 388 m the cumulative volume is positive.

Downstream of the connection the cumulative sedimentation-erosion volume drops rapidly to a minimum of -18.49 m^3/m. Downstream of the connection the transport capacity of the longshore current increases. The eroded sediment is picked up and is transported downstream. Therefore these transects have a negative cumulative volume. For y = 140 - 260 m the cumulative volume

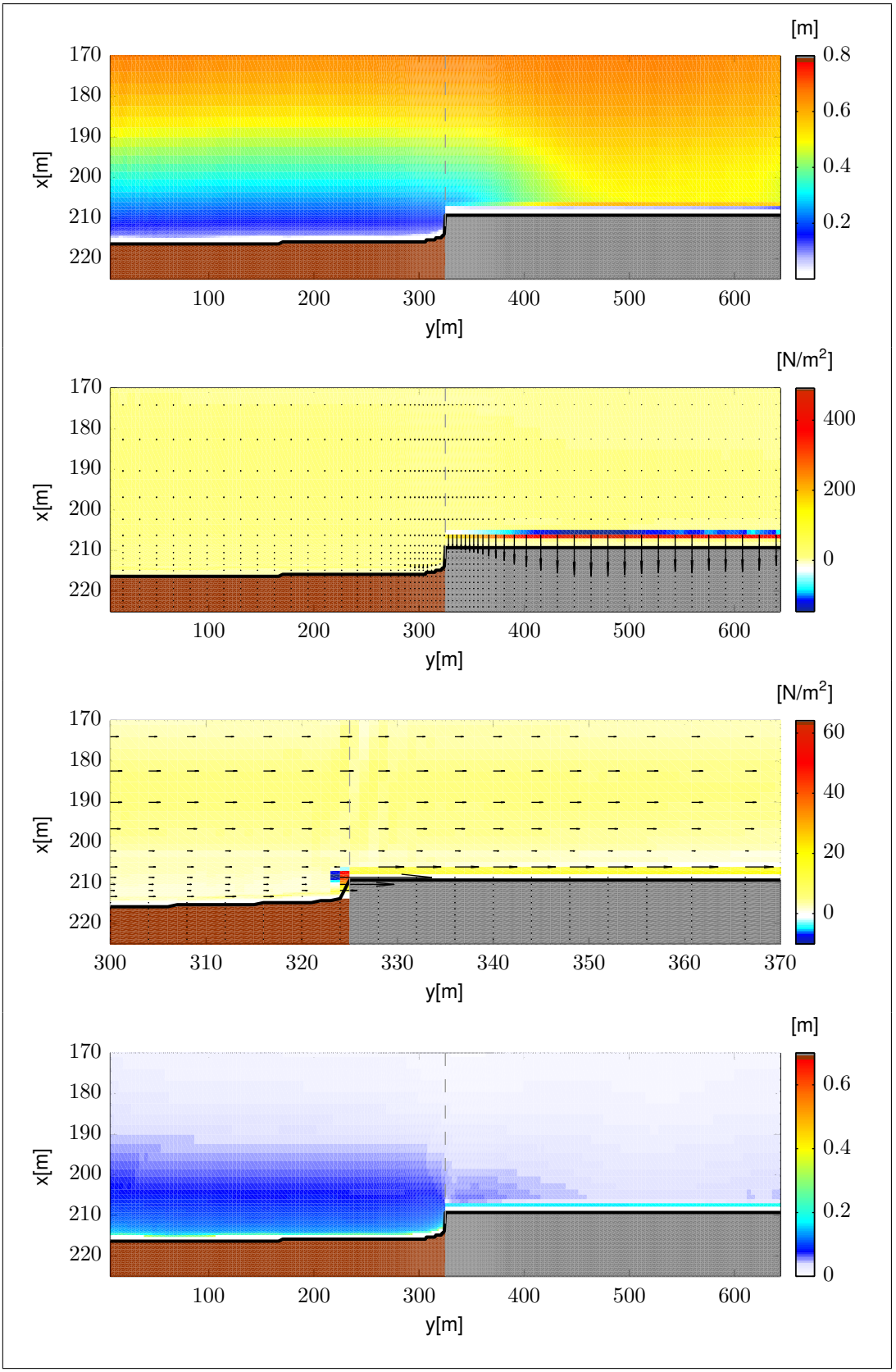

Figure 3.37: XBeach prediction on hydrodynamic conditions in front of a dune-dike connection under normally incident waves. The dunes are brown, the dike is gray and the retreat line is black. Upper panel: Mean short wave height H. Second panel from the top: Mean wave force F_x. Third panel from the top: Mean wave force F_y. Lower panel: Mean still water level z_s including the wave-induced water level setup.

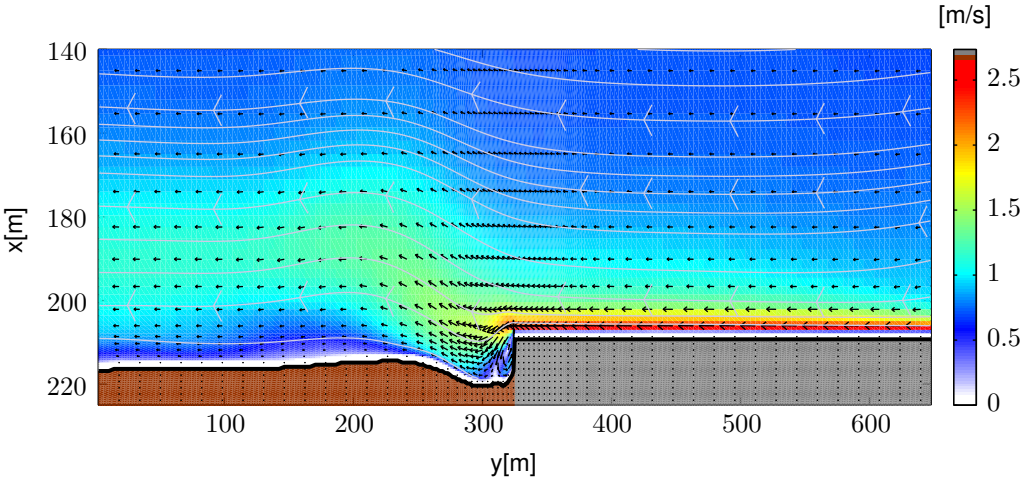

Figure 3.38: Mean velocity field in front of the dune-dike system for mainang = 310: Retreat points of dune (brown) and dike (gray) cross-section are connected by the retreat line (black).

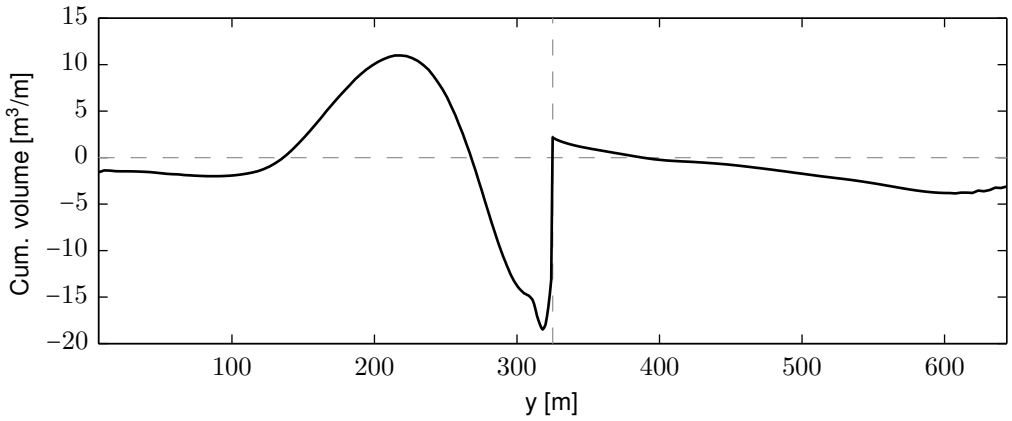

Figure 3.39: Longshore sediment exchange based on the sediment balance for each transect for mainang = 310.

is positive with a maximum of 10.99 m^3/m.

In Figure 3.40 the sedimentation-erosion pattern of the dune-dike system is depicted. Dunes next to the connection erode significantly more. The eroded sediment is partially deposited on the foreshore between y = 140 m & y = 260 m. The additional rise of the foreshore causes dunes behind it to erode less. The scour hole near the connection is not completely filled up. However the scour depth near the connection is smaller than near the right boundary. In Figure 3.41 ΔR^* of the dune stretch is displayed at different time instances. The erosion next to the connection starts to develop at t = 0:30 hr. The erosion increases in time and expands downstream of the connection over time.

To quantify the dune erosion in the dune-dike system the dune crest retreat ΔR^* and the erosion volume A are normalized with the erosion quantities of the 2DH (310) Dune model. The conditions in the 2DH (310) Dune model are longshore uniform. The bathymetry at t = 6 hr is presented in Figure 3.42. In Figure 3.44 the mean bottom elevation $\overline{z_b}$ of Figure 3.42 between x = 15 m and x = 22 m is depicted. In this figure the minimum and maximum bottom elevation is given by dashed gray lines. In Figure 3.44 the mean transect of the 2DH Dune model with mainang = 310 is displayed. The figure also presents the bottom elevation of the 1D Dune model

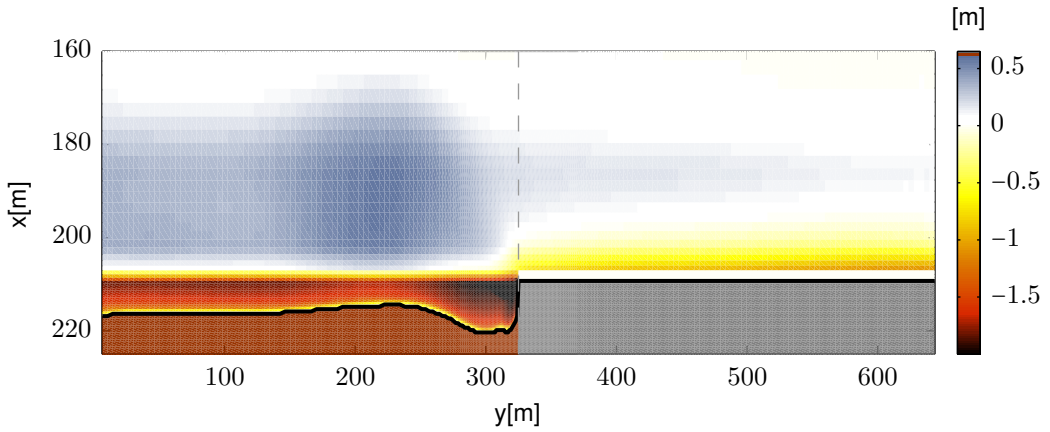

Figure 3.40: Sedimentation-erosion pattern of a dune-dike system for mainang = 310; accretion = +, erosion = -. Dunes are brown, dikes are gray and the retreat line is black.

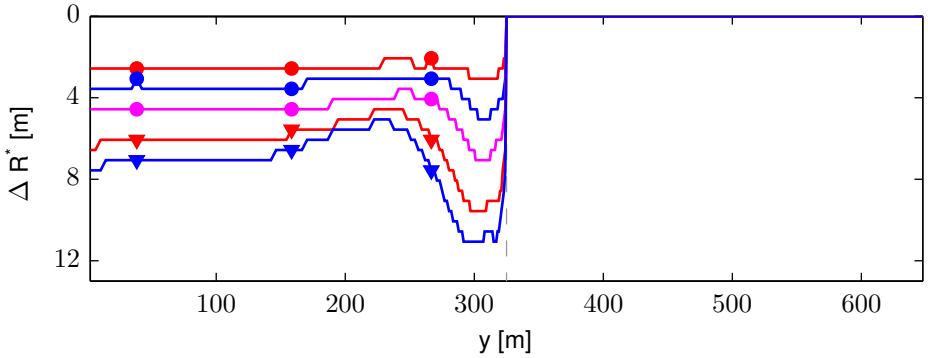

Figure 3.41: Development of ΔR^* of the dune stretch in time for mainang = 310. ΔR^* is displayed at t = 0:30 hr (●), t = 1:00 hr (●), t = 2:00 hr (●), t = 4:00 hr (▼) and t = 6:00 hr (▼).

(Section 3.3) at t = 6 hr and the mean transect.

Figure 3.42 shows no alongshore variation in the bathymetry. In Figure 3.43 the cumulative sedimentation-erosion volume of the 2DH (310) Dune model is presented. A negative volume indicates a transect lost sediment to adjacent transects. Cross-section with a positive volume gained sediment during the storm. Generally the cumulative volume of a transect is negative. Consequently there is a nett transport of sediment out of the model domain. However the cumulative sedimentation-erosion volume of all transects in the model domain is -63.4 m^3. Compared to a model domain size of ± 148.000 m^2 this is still relatively small. This is supported by the fact that the minimum and maximum elevation are close to the mean bottom elevation, see Figure 3.44. Between x = 150 m and x = 210 m the differences between the minimum, maximum and mean bottom elevation are negligible. For x ≤ 210 m the differences increase slightly.

The mean transect of the 2DH (270) Dune model with wall boundaries and with Neumann boundaries is identical. This indicates that the lateral boundaries have no effect on the amount of ero-

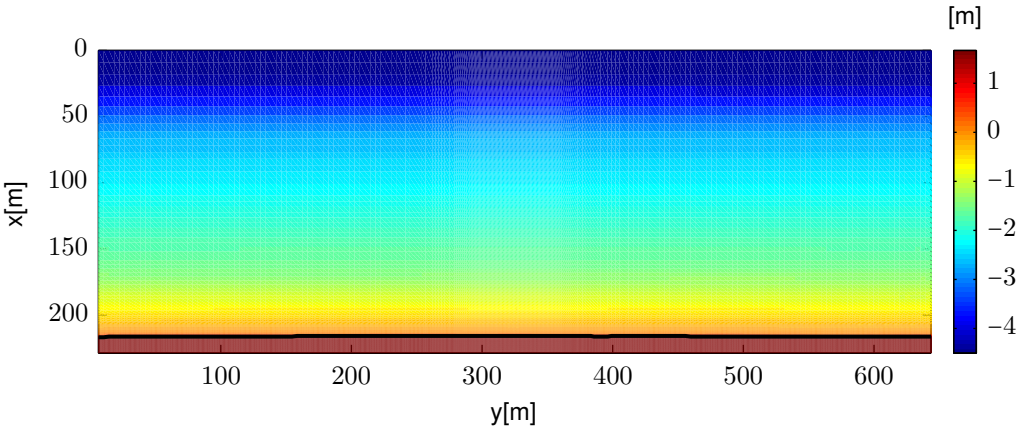

Figure 3.42: Bathymetry of the 2DH Dune model for mainang = 310 at t = 6 hr.

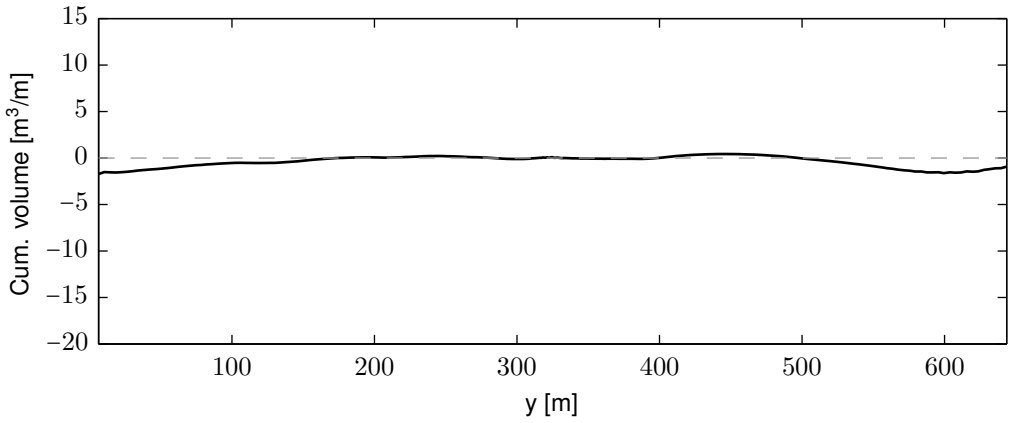

Figure 3.43: Cumulative sedimentation-erosion volume for each transect in the 2DH Dune model with mainang = 310.

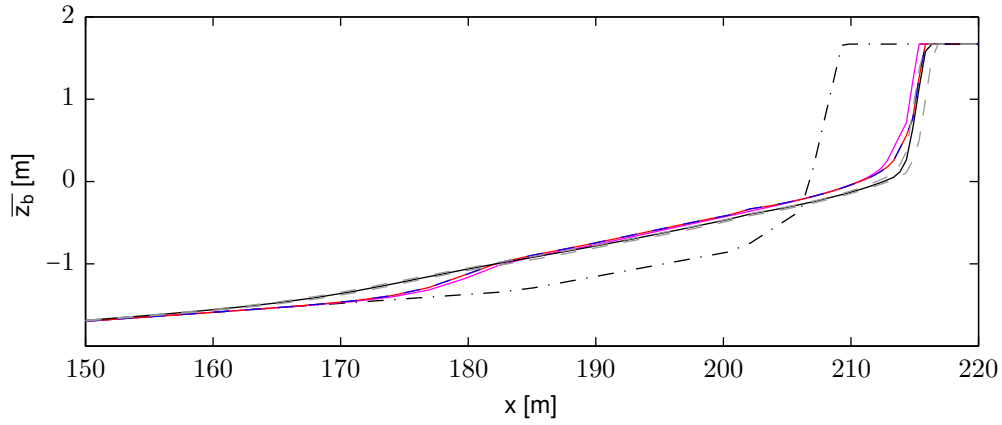

Figure 3.44: Mean final bottom elevation $\overline{z_b}$ of the 2DH Dune model (—) for mainang = 230 and its minimum & maximum measured elevation (– –), the final bottom elevation of the 1D Dune model (—), the mean final bottom elevation $\overline{z_b}$ of the 2DH (270) Dune model with wall boundaries (—), $\overline{z_b}$ of the 2DH (270) Dune model with Neumann boundaries (– –), the initial bottom elevation of both models (– · –), SSL (– · –).

sion. Although the mean transect of the 2DH (270) models shows more erosion than the 1D Dune model the differences in the bottom profile are little. The 2DH Dune model shows more dune erosion than the 1D Dune model. This is caused by the same mechanism as described

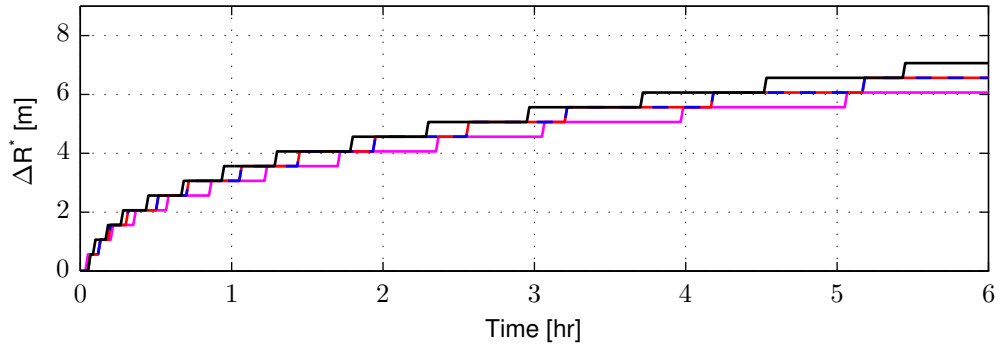

Figure 3.45: Dune crest retreat ΔR^* of the 2DH Dune model (—) for mainang = 230, the 1D Dune model (—), the 2DH (270) Dune model with wall boundaries (—) and the 2DH (270) Dune model with Neumann boundaries (– –).

in Subsubsection 3.5.2.1. In addition to the waves the longshore current stirs up sediment (J.A. Roelvink 2011, pers. comm. 7 September). The sediment is transported seaward by the undertow. This is visualized by the mean suspended sediment concentration $\overline{c_{ss}}$ in Figure 3.46. Although the $\overline{c_{ss}}$ of the 2DH Dune model is smaller than $\overline{c_{ss}}$ of the 1D Dune model at the dune face it is larger at the foreshore. Subsequently sediment is transported further offshore compared to normally incident waves, see Figure 3.44.

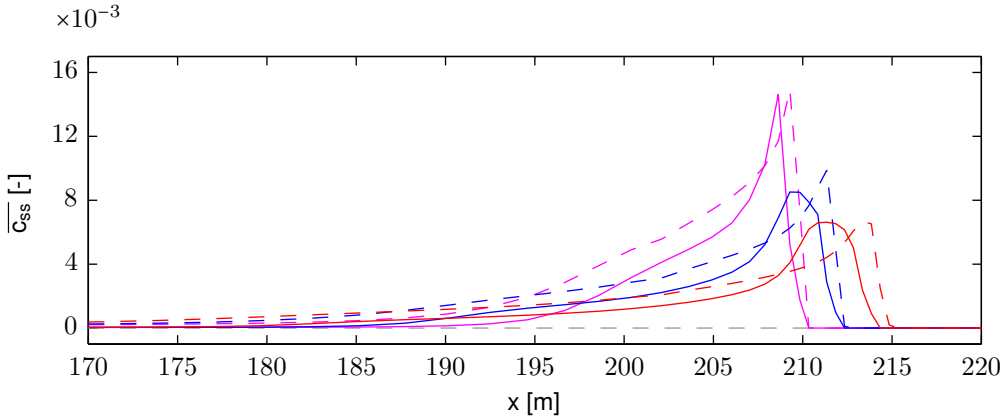

Figure 3.46: Development of the mean suspended sediment concentration in time predicted by the 1D Dune model (solid) and the 2DH Dune model with mainang = 310 (dashed). The mean suspended sediment concentration is determined between t = 0:25 - 0:30 hr (magenta), between t = 1:55 - 2:00 hr (blue) and between t = 5:55 - 6:00 hr (red).

The dune retreat and erosion volume derived from the mean transect of the 2DH (310) Dune model are normalized with the erosion values of the 1D Dune model. This isolates the influence of the longshore current on the erosion process. The mean dune crest retreat of the 2DH (310) Dune model is identical to ΔR^* of the 2DH (230) Dune model, namely 7.06 m. The dune crest retreat in the 2DH (310) Dune model increased with 16.5%. The erosion volume A increased with 1.51 m^3/m to a value of 11.53 m^3/m. This corresponds to an increase of 15.0%.

To isolate the influence of the dune-dike connection on the morphological development of the coast the normalization values are derived from the mean transect of the 2DH (310) Dune model. The normalized dune retreat ΔR^*_N is calculated with Equation 3.8. The normalized erosion volume A_N is determined by Equation 3.9. Figure 3.47 displays the normalized dune retreat ΔR^*_N normalized with erosion values derived from the 2DH (310) Dune model. Near the connection

the dune crest retreat is larger than in the case of an undisturbed dune under obliquely incident waves. The maximum additional dune crest retreat is 56.6%. For y = 146 m - 265 m the dune crest retreat is less than ΔR^* of the undisturbed dune stretch with a minimum of 71.7%. For y $\leq$ 226 m ΔR^*_N increases to a value of 107.1% at the left boundary. The normalized erosion volume A_N shows a similar behaviour, see Figure 3.48. Near the connection the maximum additional erosion volume is 64.7%. Between y = 140 m & y = 261 m the erosion volume is less than the erosion volume of the 2DH Dune model with a minimum of 77.1%.

The combined effect of the longshore current and the dune-dike connection is obtained by normalization with erosion values of the 1D Dune model. ΔR^*_N and A_N are calculated by Equations 3.8 3.9 respectively. Figure 3.49 displays the normalized dune retreat ΔR^*_N normalized with ΔR^* from the 1D Dune model. The maximum additional dune crest retreat is 82.5%. At the left boundary ΔR^*_N has value of 124.7%. The normalized erosion volume A_N shows a similar behaviour. Near the connection the maximum additional erosion volume is 89.4%. At y = 220 m the erosion volume is 11.4% less than the erosion volume of the 2DH Dune model.

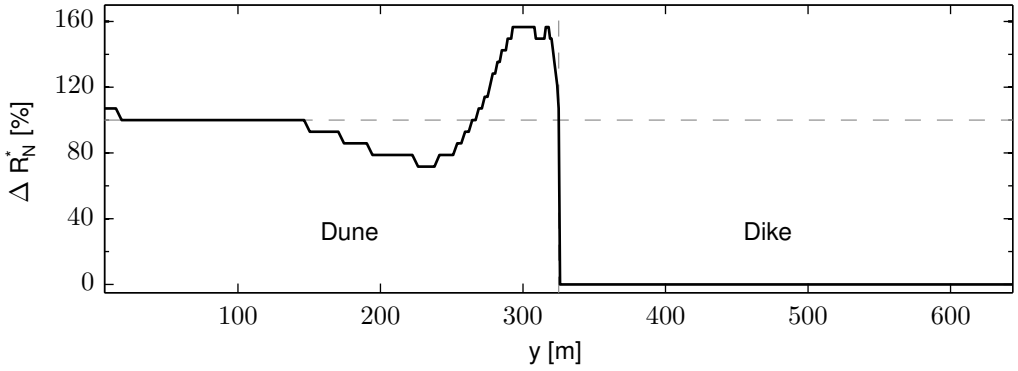

Figure 3.47: Influence of the dune-dike connection on the additional erosion: Normalized dune retreat $\Delta R^*_N(y)$ for mainang = 310.

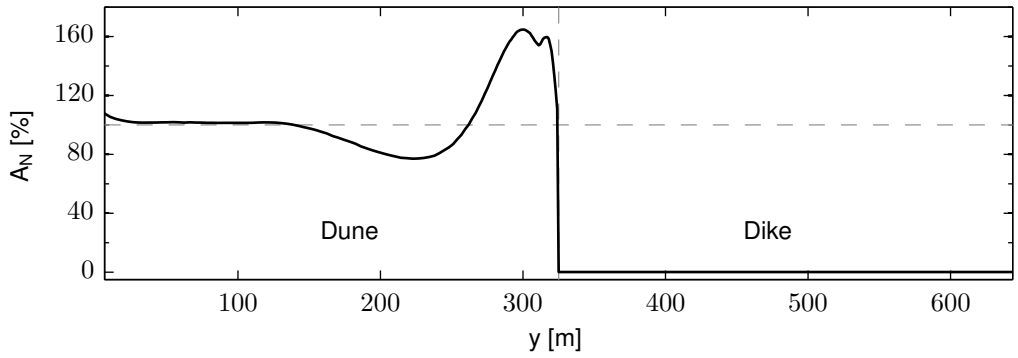

Figure 3.48: Influence of the dune-dike connection on the additional erosion: Normalized erosion volume above storm surge level $A_N(y)$ for mainang = 310.

In the upper panel of Figure 3.51 the mean wave height predicted by XBeach is displayed. Over the connection there is a relatively large longshore variation in wave height. The longshore variation in wave height hardly extends upstream of the connection. This figure also clearly shows that in the area where the eroded sediment is deposited the waves start to break sooner, see Figure 3.40. The gradient in the mean wave height over the connection is relatively large compared to normally incident waves (Figure 3.22). Subsequently the longshore variation in the mean wave force F_x, visible in the 2nd panel from the top in Figure 3.51, and the longshore variation in wave-induced water level setup as shown in the lower panel of Figure 3.51 are larger. However depending on the angle of wave incidence with respect to the shore this mechanism

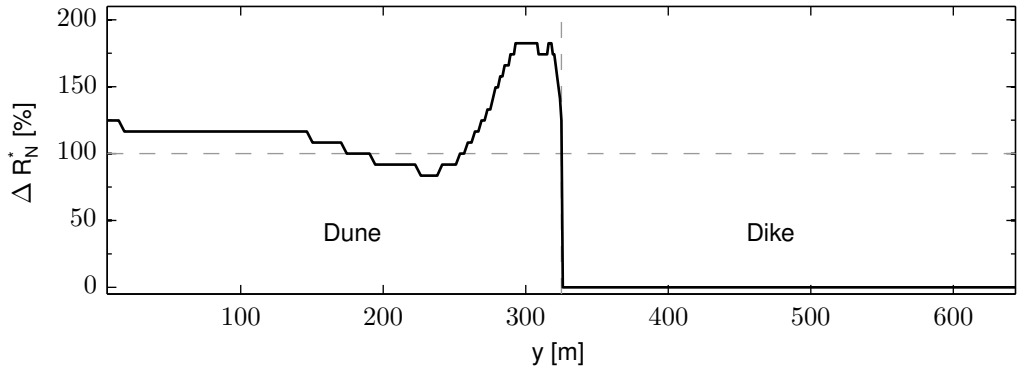

Figure 3.49: Combined influence of the dune-dike connection and longshore current on the additional erosion: Normalized dune retreat $\Delta R^*_N(y)$ for mainang = 310.

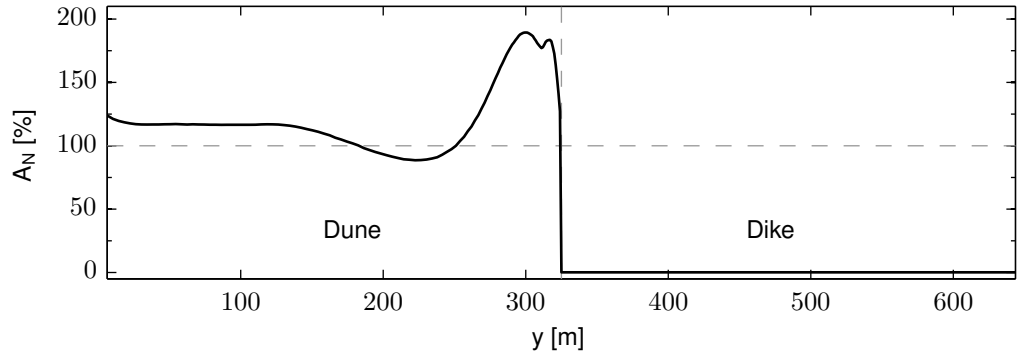

Figure 3.50: Combined influence of the dune-dike connection and longshore current on the additional erosion: Normalized erosion volume above storm surge level $A_N(y)$ for mainang = 310.

is subordinate to the longshore current. XBeach qualitatively predicts the proper behaviour of the driving forces of the longshore current. The 3rd panel from the top in Figure 3.51 shows the longshore variation in the mean wave force F_y. The gradients in F_y over the connection are local and lower than the gradients in F_x. Gradients in F_y are compensated by the bed shear stress.

3.6 Discussion

Exploratory simulations showed unwanted behaviour of Neumann boundaries under certain conditions. Often a flow of water through the model boundaries was generated. In extreme cases the water level in the model raised which accelerated the dune erosion process. The parameter epsi can prevent the water level to rise beyond a certain threshold. However a small and consistent current between the model boundaries influences the morphological development of the coast. This current was also observed for normally incident waves under certain conditions. Therefore the more rigid and stable Wall boundaries are preferred above Neumann boundaries in the case of normally incident waves.

Neumann boundaries allow waves to propagate out of the model domain using a kinematic relationship. Therefore the relationship needs the water level elevation z_s and the wave-induced flow velocities u_w at the model boundary. However currents with a velocity u_{cur} can flow through the boundary. Hence the flow velocity at the boundary u consist of u_{cur} and u_w. To separate the flow velocity at the boundary in u_{cur} and u_w the current velocity is expressed by Equation 3.10. The value of ϵ is given by the XBeach parameter epsi. Subsequently u_w = u - u_{cur}. A detailed

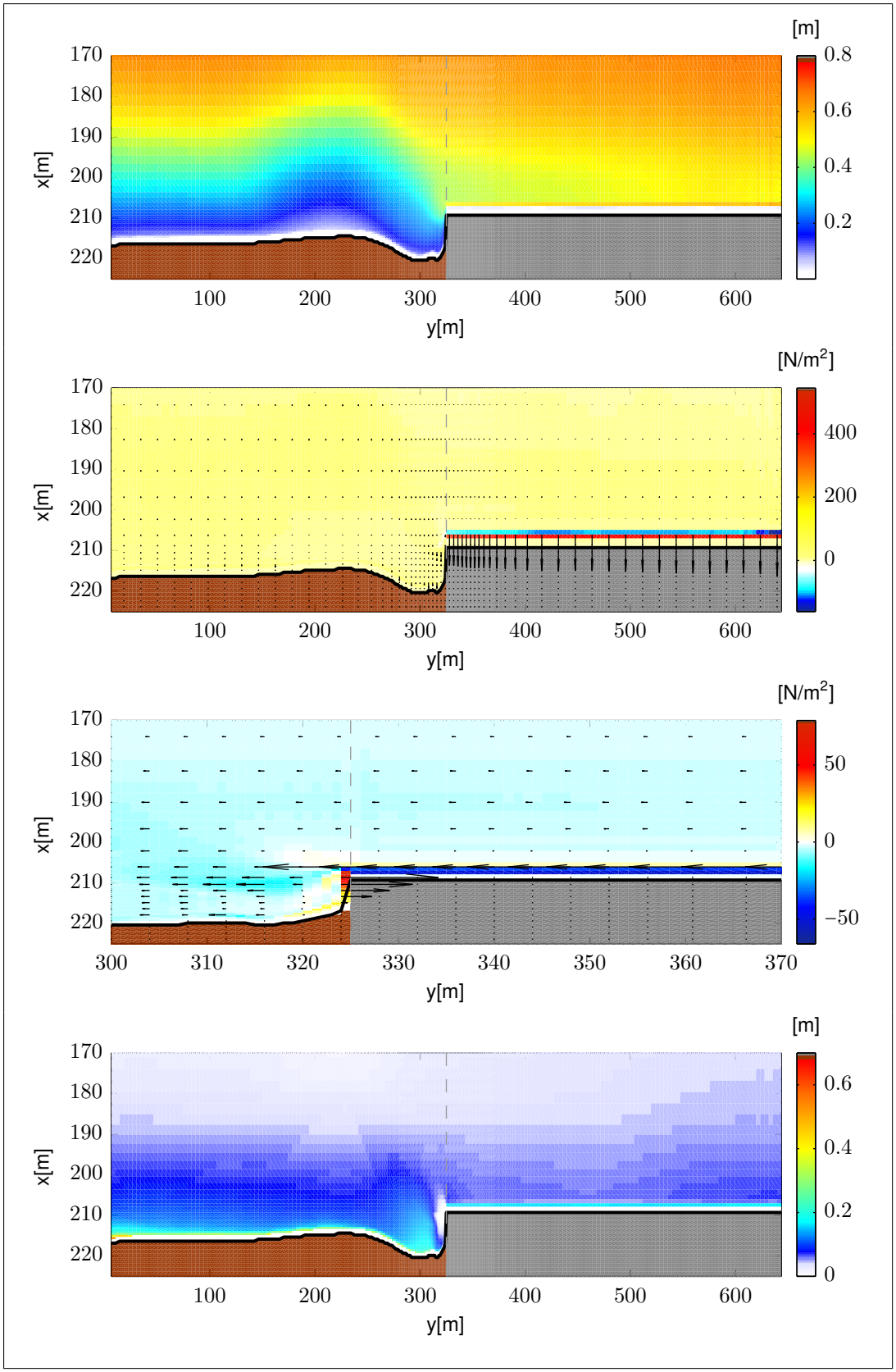

Figure 3.51: XBeach prediction on hydrodynamic conditions in front of a dune-dike connection under normally incident waves. The dunes are brown, the dike is gray and the retreat line is black. Upper panel: Mean short wave height H. Second panel from the top: Mean wave force F_x. Third panel from the top: Mean wave force F_y. Lower panel: Mean still water level z_s including the wave-induced water level setup.

description of the online separation of the flow velocity at the boundary is given in Wenneker *et al.* (2010).

$$u_{cur} = \epsilon u + (1-\epsilon)u_{cur} \qquad \text{with} \qquad \epsilon << 1 \tag{3.10}$$

3.7 Conclusion

The dune erosion process is simulated correctly by XBeach. The predicted behaviour of a dune transect under storm conditions is consistent with the literature described in Section 2.2. The behaviour of a dike transect during a storm is well modeled in a qualitative sense. The development of the dike transect and the hydrodynamics is in agreement with the literature described in Section 2.3. The XBeach testbed report emphasized that the erosion depth near the toe of a dike and a dune revetment is underestimated. This is likely to be caused by an underestimation of the suspended sediment concentration near the toe of the dike. Also the erosion volume above a dune revetment is underestimated (Deltares, 2010). The testbed report concluded that in addition to long wave run-up also short wave runup should be included in the avalanching algorithm.

The behaviour of a dune-dike system under storm conditions and normally incident waves is dictated by a longshore current in the transition zone. This current is responsible for the transport of sediment from the dunes to the dike. It is generated by a longshore water level gradient resulting from a difference in wave-induced water level setup between an undisturbed dune section and an undisturbed dike section. The difference in the wave-induced water level setup is directly related to a longshore gradient in the wave force F_x and hence the wave height at the shoreline. This in turn is a response to the difference in morphological development of the cross-shore profile between a dune and a dike. The morphological development of an “undisturbed” transect is dominated by the supply of sediment to the beach.

XBeach predicts the longshore current in the transition zone, see Figure 3.23. The hydrodynamic response to morphological changes in the bottom profile are modeled well. In the case of normally incident waves XBeach predict an additional dune retreat of 24.7% near the connection, see Figure 3.20. The maximum increase of the erosion volume near the connection is predicted to be 22.2%, see Figure 3.21. Outside the transition zone dune erosion increases with ±3%. This is possibly related to wave refraction and edge waves.

The mean transect of the 2DH (270) Dune model with wall boundaries and with Neumann boundaries is identical. This indicates that the lateral boundaries have no effect on the amount of erosion. Although the mean transect of the 2DH (270) models shows more erosion than the 1D Dune model the differences in the bottom profile are little. The predicted behaviour of a dune-dike connection under storm conditions and normally incident waves is consistent with the literature described in Section 2.4.

Depending on the angle of wave incidence with respect to the shoreline the longshore current has a profound impact on the development of additional erosion near structures. In the case of obliquely incident waves the erosion of an undisturbed dune stretch is more than in the case of normally incident waves, see Figure 3.30. The dune crest retreat increased with 16.5% and the erosion volume with ±15%. This is associated with additional stirring by the longshore current (J.A. Roelvink 2011, pers. comm. 7 September). The morphologically active zone extends ±10 m further seaward to x = 160 m compared with normally incident waves.

When the dunes are situated upstream of the connection sediment will pile up against the structure. Subsequently the erosion near the connection is less than the erosion of undisturbed dune

stretches. The influence of the dune-dike connection on the additional erosion is isolated from the effect of the longshore current. In this case XBeach predicts the dune retreat near the connection to be 35.4% less than in the undisturbed dune stretch, see Figure 3.33. The erosion volume is predicted to be 32.1% less near the connection. The combined effect of the connection and the longshore current results in a decrease of ΔR^* near the connection of 24.7%. The erosion volume decreases with 22.2%.
Over the connection there is a gradient in the current velocity and transport capacity of the longshore current. Sediment transported by the longshore current is deposited in front of the structure. As the foreshore in front of the dike is raised the velocity and transport capacity of the longshore current increases. Subsequently the sediment is deposited further downstream of the connection.

When the dunes are situated downstream of the connection the erosion near the structure increases significantly. The sediment is partially deposited on the foreshore further downstream of the connection, see Figure 3.40. Waves in this deposition area break sooner and dunes behind it show less erosion than an undisturbed dune stretch. For the isolated effect of the dune-dike connection XBeach predicts dunes in the deposition area to show 28.3% less dune crest retreat and decrease of 22.9% in the erosion volume compared to the undisturbed dune stretch, see Figures 3.47 and 3.48. The maximum additional dune crest retreat near the connection is 56.6%. The erosion volume shows a maximum increase of 64.7%. For the combined effect of the connection and the longshore current these values are 82.5% and 89.4% respectively. The predicted behaviour of a dune-dike system under storm conditions and oblique incident waves is consistent with the literature which is described in Subsection 2.4.2.

4 Experiments in the Delta Basin

4.1 Introduction

In 2007 Rijkswaterstaat commissioned the execution of pilot experiments on dune erosion near unerodable structures. The main objective was to qualitatively verify the hypothesis that at the connection between a dune and a structure additional erosion of the dunes next to the structure develops during a storm. When this is verified the present assessment rules were to be reviewed with the measurements. This chapter, except Section 4.7 to Section 4.9, is an abstract of the report of the pilot experiments (Boers *et al.*, 2008).

The experiments were to be carried out by Deltares in the framework of the Rijkswaterstaat programme “Strength and Loads on Water Defenses (SBW)”. This programme is aimed at establishing new assessment rules for the future assessment of water defenses. In particular this programme is focused on water defenses that can’t be accurately assessed with the current assessment rules. The hybrid water defenses, a combination of dunes and structures, fall in this category. The current assessment rules for hybrid defenses are based on a theoretical derivation carried out by Steetzel in 1995 (Steetzel, 1995).

In the previous decades dune erosion research was mainly focused on cross-shore sediment transport. Wave flumes are adequate to facilitate this kind of research since there is no variation in longshore direction. Especially the Delta Flume was used extensively to carry out large scale experiments. Since the transition between a dune and a dike also involves longshore sediment transport wave flumes are not suitable. For this reason the pilot experiments were carried out in the Delta Basin.

With a surface area of 50 m $\times$ 50 m and a maximum water depth of 1 m the Delta Basin is amongst the largest wave basins in the world. It is equipped with a wave generator consisting of 80 independently controlled paddles. Each paddle has a width of 0.33 m. The total width of the Delta Basin is 26.42 m. In 2009 the Delta Basin was modified and a second multi-directional wave generator was added. The wave generators are equipped with Active Reflection Compensation which means that waves that are reflected by the shoreline are absorbed by the wave board and are not reflected back into the model.

From 12 December 2007 until 7 March 2008 the Delta Basin was available for experiments. Within this time span four experiments were carried out with 2 different configurations of dunes and structures, see Figure 4.2. Unfortunately the available amount of time was too short to carry out a reference dune erosion test without any structures. The reference test was intended to investigating the longshore variation in dune erosion caused by various circumstances. In 1981 however Tilmans executed similar experiments (Tilmans, 1981). These experiments showed that the longshore variation in dune erosion without structures under normally incident waves was minor. These experiments are however not fully comparable with the experiments described in this chapter.

The Delta Basin experiments were carried out with normally incident long-crested waves and were aimed at four different closed abrupt connections between a dune and a structure.

1 The connection between a dike and an unprotected dune,
2 The connection between a dike and a dune that is protected by a dune revetment,
3 A breach in a dike with a body of sand,
4 A breach in a dune revetment.

4.2 Model area layout

The model was confined at three sides by a sealing wall of concrete which was constructed in such a way that it was sand- and watertight. At the offshore side the wave generator was situated. The model area was divided in to three areas, the (concrete) foreshore, the test area and the wave damping beaches at the lateral boundaries, see Figure 4.3.

The offshore area is situated between the wave generator and the test area. It was assumed that this area is not influenced by dune erosion and to prevent erosion of the bottom it was made of concrete. A typical problem in wave basins is the possible generation of standing waves traveling along the coast to the model boundaries. The waves are reflected by the boundaries creating a (partially) standing wave pattern. In nature however these waves are not reflected meaning that this phenomenon will not occur in nature under normal circumstances. To prevent the generation of standing waves nine wave guiding walls were constructed in the foreshore, see Figure 4.1 and Figure 4.3. Furthermore wave damping beaches at the sides of the model, consisting of coarse gravel with a slope of 1:5, were constructed to damp any waves traveling along the shore.

In the test area the configurations with different connection types were subjected to waves to study the morphological changes during storm conditions. Dikes and dune revetments were constructed as unerodable immobile structures consisting of a layer of concrete on a fill of sand. The remaining part of the test area consisted of sand with a grain size D_{50} of 125 µm. To prevent any loss of sand from behind or below the concrete the connection between the structure and the dune was made with a sheet of wood. All connections in the experiments are closed and abrupt. Figure 2.5 shows a principal sketch of closed abrupt connection.

In the test area a rail was mounted on thin piles approximately 4 m in front of the dune face. These piles, with a diameter of 20 mm, were so thin that it was assumed that they had a negligible effect

Figure 4.1: Experiment setup in the Delta Basin with at the left side the wooden wave guiding walls and at the bottom the Mobile Measuring Bridge

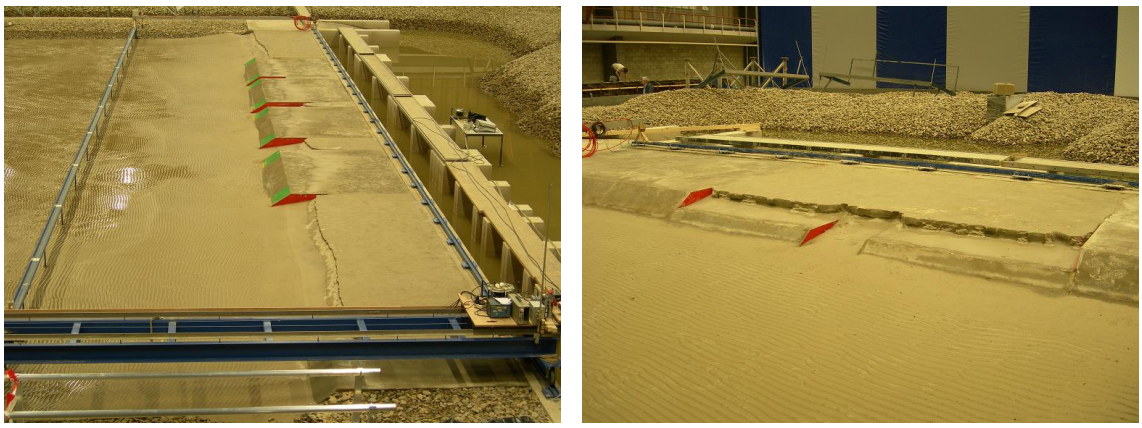

(a) Configuration 1 *(b) Configuration 2*

Figure 4.2: Test area configurations

on the wave propagation and hence the morphology. A second rail was mounted on top of the sealing wall. The rails were used by the Mobile Measuring Bridge (MMB) to support the wheel profiler which measured the cross-shore profile, see Figure 4.1. Subsection 4.5.3 describes the profile measurements taken with the wheelprofiler.

4.2.1 Test area configurations

The first configuration of dunes and hard structures that was tested consisted of one dike section in the middle of the shore with dune sections on either sides. In the dike section breaches were constructed at three locations. The breaches were constructed like a dune and therefore it looks like the model consists of four dike sections, see Figure 4.2a. Each breach was given a different width to investigate the effect of the breach size on the erosion of the dike body. The width of the breaches were 1 m, 0.5 m and 0.25 m.

Since the wave damping beaches could have an effect on the amount of dune erosion the 2nd configuration consisted of two dike sections at the left side of the test area and a (larger) dune section on the right side. In between the dike sections a dune with dune revetment was constructed to investigate the connection between a dike and a dune with revetment. The dune revetment section had a width of 3.5 m and was breached in the middle, with a breach size of 0.5 m, see Figure 4.2b. Both configurations are visualized in Figure 4.3. In this figure D=Dune, H=Dike, B=Breach, DR=Dune Revetment and R=Reference. In Table 4.1 the longshore coordinates y of the different stretches and the location of profile measurements are given.

4.2.2 Cross-shore profile

The cross-shore profile in the Delta Basin is an exact 1:10 reproduction of the cross-shore profile used in the large scale dune erosion experiments in the Delta Flume in the years 2005 and 2006. The results of the Delta Flume experiments were later on used to compare the measured results of the pilot experiments.

The water level in the Delta Basin was 0.45 m above the concrete floor at the waveboard corresponding to a storm surge level of 5 m above mean sea level (MSL) on prototype scale. The dunes and dikes had a crest height of 0.617 m which, on prototype scale, corresponds to a crest height of 15 m above MSL. The dune foot revetment had a crest height of 0.50 m, 8 m above MSL on prototype scale, on top of which a 11.7 cm thick layer of sand was placed giving the dune with revetment also a crest height of 0.617 m, see Figure 4.4.

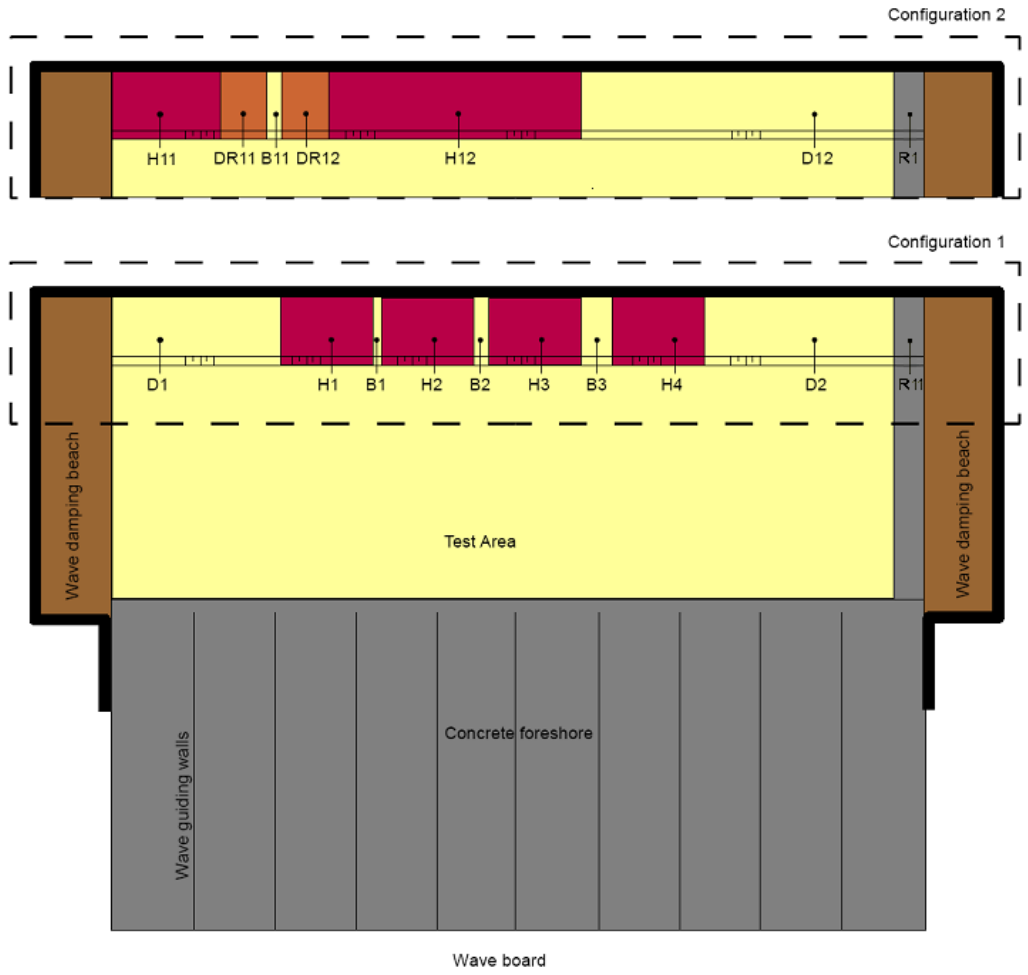

Figure 4.3: Model layout (Boers et al., 2011)

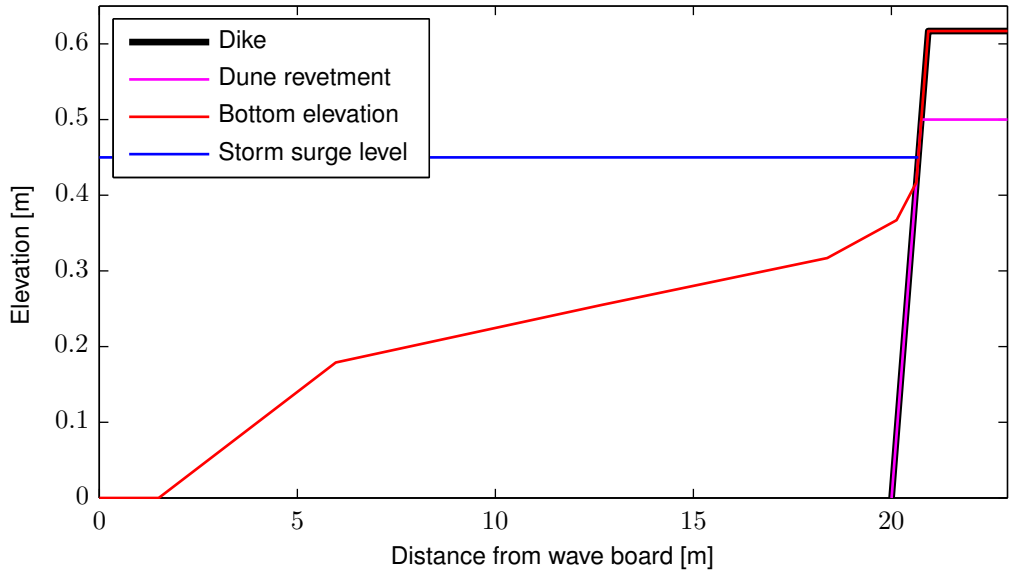

Figure 4.4: Cross-shore profile in the Delta Basin (Boers et al., 2008)

Stretch	Type	Longshore stretch coordinate y [m]	
		Full	Wheelprofiler
Configuration 1			
D1	Dune	0 - 5.53	2.53, 4.03, 4.78, 5.03, 5.28
H1	Dike	5.53 - 8.53	5.78, 6.28, 7.03, 7.78, 8.28
B1	Breach	8.53 - 8.78	8.66
H2	Dike	8.78 - 11.78	9.03, 9.53, 10.28, 11.03, 11.53
B2	Breach	11.78 - 12.28	12.03
H3	Dike	12.28 - 15.28	12.53, 13.03, 13.78, 14.53, 15.03
B3	Breach	15.28 - 16.28	15.78
H4	Dike	16.28 - 19.28	16.53, 17.03, 17.78, 18.53, 19.03
D2	Dune	19.28 - 25.42	19.53, 19.78, 20.03, 20.78, 22.28
R1	Reference	25.42 - 26.42	25.92
Configuration 2			
H11	Dike	0 - 3.53	2.03, 3.03, 3.28
DR11	Revetment	3.53 - 5.03	3.78, 4.03, 4.53, 4.78
B11	Breach	5.03 - 5.53	5.28
DR12	Revetment	5.53 - 7.03	5.78, 6.03, 6.53, 6.78
H12	Dike	7.03 - 15.28	7.28, 7.53, 8.53, 8.78, 9.66, 10.66 11.66 12.66, 13.66 14.78, 15.03
D11	Dune	15.28 - 25.42	15.53, 15.78, 16.78, 17.78, 18.78 19.78, 20.78, 21.78, 22.78, 23.78
R11	Reference	25.42 - 26.42	25.92

Table 4.1: Longshore coordinates of stretches and profiler measurements

4.3 Test Programme

Each configuration was tested with two different wave peak periods T_p. All other hydraulic parameters, such as wave height H_{m0} and water level, remained constant. Table 4.2 gives an overview of the hydrodynamic conditions that were applied for each experiment.

An experiment consisted of three series of wave generation. The first two series had a duration of 15 minutes and the third lasted 60 minutes. The total time of wave generation was 90 minutes. Between two successive series the wave basin was slowly emptied to measure the bathymetry. When the measurements were completed the basin was filled again and the next series of wave generation started. The bathymetry was measured at the beginning of a test (T000), after 15 minutes of wave generation (T015), after 30 minutes (T030) and at the end of an experiment (T090). An overview of the procedure during an experiment is presented in Table 4.3. The measuring activities are described in Section 4.5.

Experiment	H_{m0} [m]	T_p [s]	Configuration
V1	0.15	2.07	1
V2	0.15	1.55	1
V3	0.15	2.07	2
V4	0.15	1.55	2

Table 4.2: Target wave conditions (Boers et al., 2008)

Wave series / Measuring Code	Activity in wave basin	Measuring activity
	Model area construction	
T000	Model is empty	Profile/scan measurements
	Filling the model	Argus fill measurements
	Wave generation (1st series)	Hydraulic measurements
T015	Draining the model	Argus empty measurements
	Model is empty	Profile/scan measurements
	Filling the model	Argus fill measurements
	Wave generation (2nd series)	Hydraulic measurements
T030	Draining the model	Argus empty measurements
	Model is empty	Profile/scan measurements
	Filling the model	Argus fill measurements
	Wave generation (3rd series)	Hydraulic measurements
T090	Draining the model	Argus empty measurements
	Model is empty	Profile/scan measurements

Table 4.3: Testing procedure (Boers et al., 2008)

4.4 Scale relations

To verify whether or not the present assessment rules give an accurate prediction of the amount of additional erosion near structures the measurements must be scaled up to prototype scale. For the scaling from experiment to prototype scaling rules were developed (Vellinga, 1986) which were revised in 2008 (Van Rijn *et al.*, 2008).

The cross-shore profile in the Delta Basin had a depth scale of $n_d = 60$. The length scale n_l of experiments is usually different than the depth scale. The Delta Basin experiments had a length scale of $n_l = 120$. The wave height scale n_H is equal to the depth scale. The wave height in the experiments is 0.15 m which corresponds with a wave height of $H_{m0} = 9$ m on prototype scale. The wave period scale is equal to the square root of the depth scale $n_{T_p} = \sqrt{n_d} = 7.75$. This means that the wave periods in the Delta Basin $T_p = 1.55$ s and $T_p = 2.07$ s correspond with a wave period of $T_p = 12$ s and $T_p = 16$ s on prototype scale. The morphological time scale which scales the storm duration is given by $n_{T_m} = {n_d}^{0.56} = 9.90$ (Boers *et al.*, 2008). A storm duration of 15 hours can then be simulated in the Delta Basin with a test duration of about 1.5 hours. Furthermore the grain size was scaled with a factor of $n_{D_{50}} = 2.37$ and the fall velocity of the sediment with a factor of $n_w = 3.55$.

With a prototype grain size D_{50} of 225 µm the grain size in the Delta Basin should be 95 µm according to the scaling rules. The grain size in the Delta Basin however proved to be 125 µm. The experiment results were afterwards corrected for the larger grain size. Table 4.4 gives an overview of the applied scale relations.

Parameter	Scale	Prototype	Delta Basin
Depth	60		
Length	120		
D_{50}	2.37	225 µm	95 µm
Fall velocity	3.55	2.68 cm/s	0.75 cm/s
Wave height H_{m0}	60	9 m	0.15 m
Wave period T_p	7.75	12 / 16 s	1.55 / 2.07 s
Time	9.90	15 hr	1.52 hr

Table 4.4: Scale relations for the Delta Basin (Boers et al., 2008)

4.5 Measuring programme

A large number of measurements were taken before, during and after an experiment. To measure the morphological evolution and rate of dune erosion use was made of a wheel profiler, 6 Argus video cameras and a hand-held surface scanner. The hydrodynamics were measured using two types of wave gauges and electro-magnetic flow meters. A total station was used to measure the location of the measuring devices. An overview of the used instruments is presented below. The locations of the instruments are displayed in Figure 4.9a and Figure 4.9b on page 64.

- 1 Total station,
- 6 Argus video cameras,
- 1 Wheel profiler,
- 1 Hand-held surface scanner,
- 11 Wave gauges (WHM),
- 3 Directional wave gauges (GRSM),
- 1 Electro-magnetic flow meter (SHM),
- 14 Sediment grain size sieve.

4.5.1 Wave gauges

A wave gauge is an instrument that measures the resistance of an electric current that is flowing between two silvered copper wires. The current flows from one wire, through the water, to the second wire. When the wires are completely submerged the resistance is small. When they are totally emerged the current is unable to flow between the wires resulting in an infinitely high resistance. This means that the resistance is a measure for the surface elevation of the water. By placing three wave gauges (WHM) in close proximity to each other, with different distances between them the incoming and reflected waves can be distinguished mathematically (Massel, 1996).

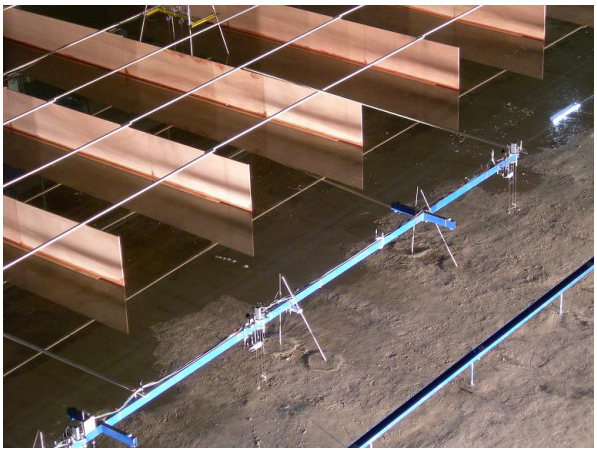

Figure 4.5: Wave gauges in a longshore transect

A GRSM consists of one wave gauge (WHM) and two electro-magnetic flow meters (SHM). The electro-magnetic flow meters measured the flow velocity at 0.12 m beneath the mean water level in cross-shore and longshore direction. The combined data of the surface elevation and the flow velocities makes it possible to derive the wave energy density as a function of the wave direction.

With this information also alongshore traveling waves can be distinguished.

Between two successive series of wave generation the wave gauges measured the water level when the wave basin was emptied or filled. This data together with the measurements from the Argus video system made it possible to derive the bathymetry. During wave generation the wave gauges measured the surface elevation from which the hydrodynamic conditions were derived.

Three wave gauges were placed at the center of the wave basin in front of the wave board. The gauges (WHM01, WHM02 and WHM03) were meant to measure the incoming and reflected waves at deep water. In the surfzone three gauges (WHM04, WHM05 and WHM06) were positioned to measure the propagation and dissipation of wave energy in front of the dune. For both configurations the longshore position of these wave gauges is different, see Figure 4.9a and Figure 4.9b. Outside the surfzone six pairs of wave gauges (WHM81 & WHM91, WHM82 & WHM92 and WHM83 & WHM93) were placed to measure the uniformity of the wave propagation in front of the dune. The data from these gauges can be used to identify any waves traveling along the shore. Two wave gauges (WHM71 and WHM72) were placed at the side walls of the basin in the concrete foreshore to monitor the uniformity of wave propagation along the wave board.

4.5.2 The Argus video system

This section is derived from the paper by (Van Geer *et al.*, 2009). In this paper the Argus video system and the techniques used to process the camera recordings are described. Four video cameras were configured according to the ARGUS system and placed above the model. The cameras were calibrated and their position and orientation calculated. With this information every pixel of an ARGUS image is related to a certain horizontal position (x,y) given the elevation of that point. The system uses this information and the difference in color intensity to determine the position of the waterline. By combining the data of the Argus video cameras and water level measurements the bathymetry of the model was obtained. Figure 4.6 displays the composed bathymetry which results from combining the obtained bathymetry with the known location of dunes and structures and the measured dune crest position.

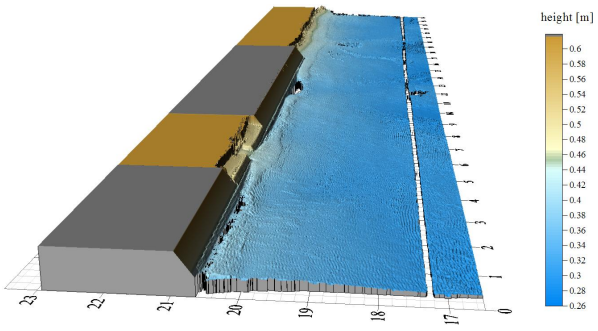

Figure 4.6: Composed bathymetry using the Argus video system (Van Geer et al.*, 2009)*

Measuring the bathymetry using the Argus video system has some disadvantages. When during the experiments a scour hole developed the water stayed in it when emptying the basin. This means that the video system could not measure the bathymetry of the scour hole. Moving foam on the water surface was sometimes interpreted as a moving water line giving false information about the bathymetry. Using a weighted moving average the foam could often be identified and was excluded from the measurements.

Two cameras were mounted right and left of the model to measure the dune crest regression during wave attack. During an experiment the dune crest was illuminated from the landside. This results in a shade at the dune front. The shade is characterized by a sudden increase in the intensity of the red color in cross-shore direction, see Figure 4.7. Consequently the position of the dune crest can be identified. Every 6 seconds a picture was taken from the dune crest resulting in the development of the dune crest retreat as the experiment progresses.

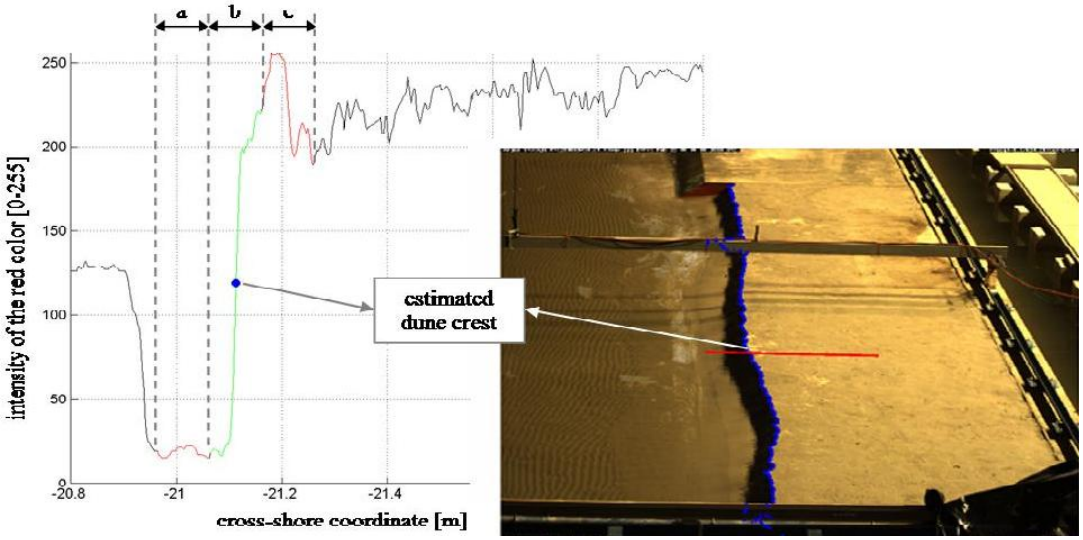

Figure 4.7: Argus dune crest position measuring technique (Boers et al., 2011)

4.5.3 Wheel profiler

The bottom elevation in a cross-shore transect was measured by a wheel profiler between x = 17.5 m to x = 22.93 m. Stretches R1 & R11 near the right model boundary were used as a reference for the profile measurements, see Figure 4.3. These reference stretches were constructed like a dike section. The profiler was installed on a carriage that moves in cross-shore, from onshore to offshore, direction over the Mobile Measuring Bridge (MMB). The MMB moves over two rails in alongshore direction, see Figure 4.1. Every 20 mm the profiler touches the surface with a wheel with a diameter of 40 mm. As soon as it feels resistance the wheel is pulled up. Due to this no unstable parts of the dune face collapsed due to the profiler measurements. The diameter of the wheel causes two disadvantages. The first one is that when the profiler reaches the dune face it moves down at least 20 mm offshore from the dune front. The second disadvantage is that all the details of a ripple bed are filtered out.

4.5.4 Hand-held surface scanner

Near the different connections more detailed measurements were taken with a hand-held surface scanner. The system consists of a laser and a camera which hangs under a certain known angle with respect to the laser. A laser beam is projected on the connection and the straight line is deformed by the 3D surface. The laser beam is captured by the camera and the data is interpreted by the system. The location of the hand-held scanner is determined by a electro-magnetic field between a transmitter and a receiver on the scanner. The position of the magnetic field transmitter is measured with the total station and remains fixed. The main disadvantage of this system is that it is very sensible to magnetic sources other than its own transmitter. Since the floor of the Delta Basin contains an unknown number of magnets, used in previous experiments, the magnetic field of the transmitter was distorted. Due to this not all surface scans had a good quality, but as long as the transmitter was within a distance of 450 mm from the receiver the results were acceptable. Despite this the hand-held scanner gives a high density recording of the bottom elevation near the connection.

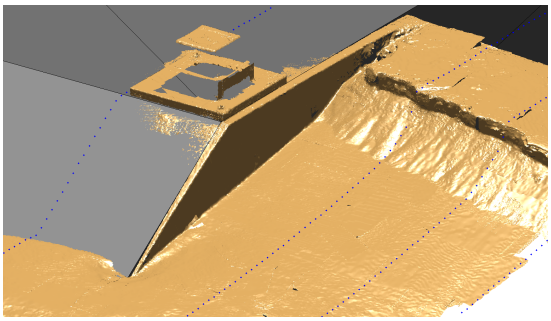

Figure 4.8: Surface scan of a dune-dike connection. Blue point are the wheelprofiler measurements

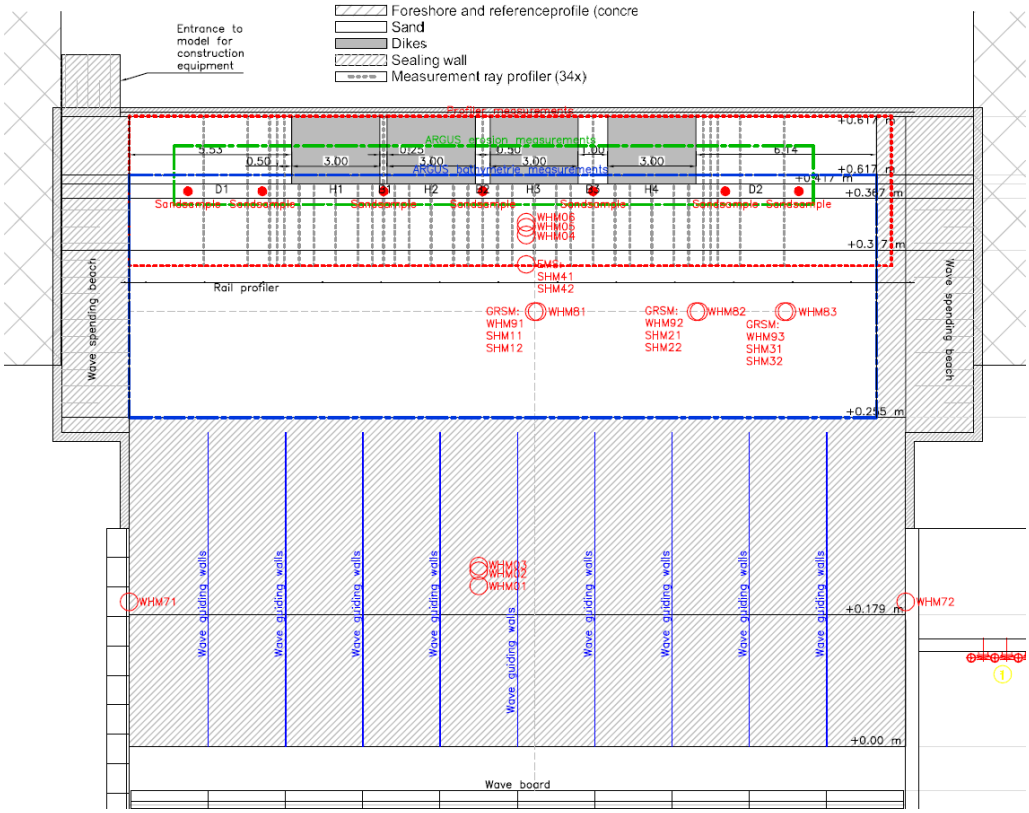

Figure 4.9a: Instrument location configuration 1 (Boers et al., 2008)

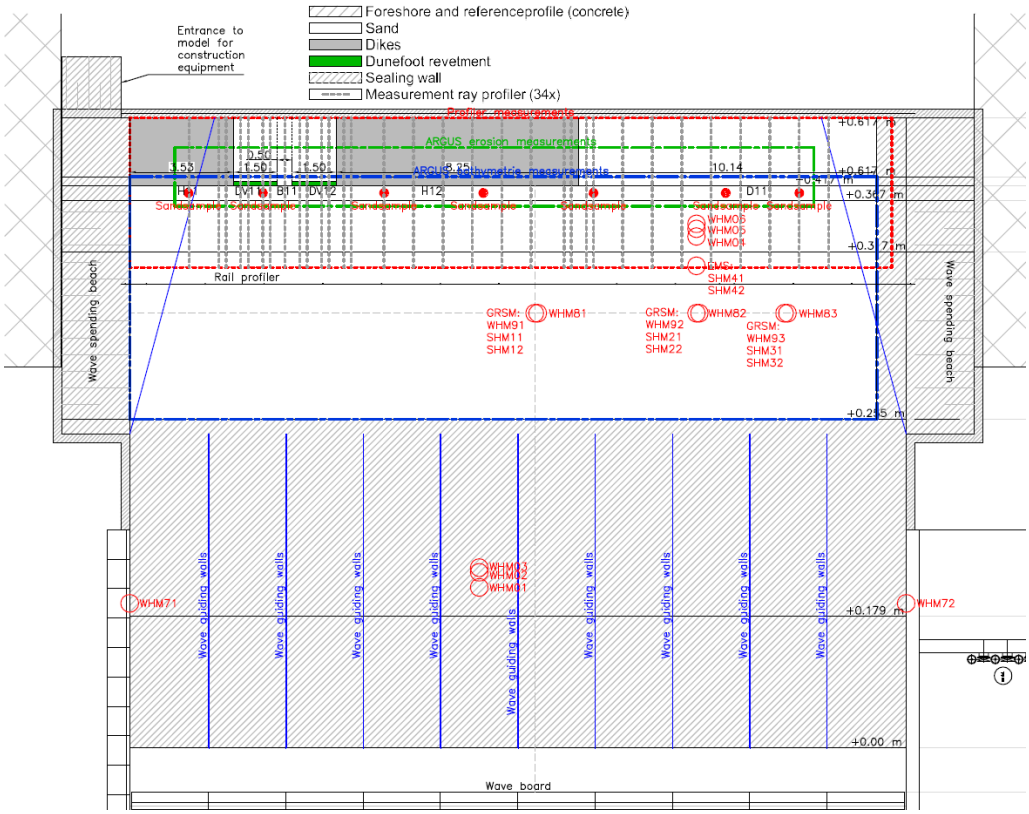

Figure 4.9b: Instrument location configuration 2 (Boers et al., 2008)

4.6 Data analysis

4.6.1 Hydraulic conditions

Throughout the experiments the wave gauges functioned properly except WHM92 during experiment V1. The flow velocity and water level measurements give the possibility to derive a directional wave spectrum at the GRMS locations which can reveal alongshore traveling waves and hence a standing wave pattern. However the velocity measurements suffered from a temporal drift, a sudden offset in the signal and inexplicable spikes. This gives the velocity measurements little accuracy making them unsuitable to derive a directional wave spectrum. Nevertheless analysis of the hydraulic measurements did not reveal a standing wave pattern Boers *et al.* (2008).

The wave damping beaches at the lateral boundaries of the model functioned as intended and dissipated the energy of incoming waves. Consequently wave diffraction caused a local longshore variation of the wave height near the lateral boundaries. The dune sections close to the model boundaries received less wave energy resulting in less dune erosion. The region of influence of the wave damping beaches was defined as the longshore distance at the waterline between the model boundary and the diffraction line. The angle between the diffraction line and the shore normal axis is $\pm 15^{o}$. This means that over a distance of 2.24 m the wave damping beaches influence the morphological development. This is observed in Figure 4.12 where at the left model boundary the dune retreat ΔR^{*} decreases.

On the other hand measurements show a large global longshore variation in wave height. Already near the wave board a difference in wave height of 1 cm was observed between wave gauges WHM71 and WHM72. However at the foreshore the guiding walls prevented variations in wave height to spread in longshore direction. Consequently the waves were relatively long-crested and the wave spectra at the measurement locations between the guiding walls were quite uniform.

Roughly 5 meters from the wave board the waves started breaking. As higher waves start to break sooner they dissipate more energy. Consequently it is expected that further onshore the longshore variation in wave height is less. However a wave height difference of 1.5 cm was measured between wave gauges WHM81 & WHM91 at the basin center and WHM83 & WHM93 near the lateral boundary. The wave gauges WHM83 & WHM93 were located such that they were well out of the region of influence of the wave damping beaches. At the center of the basin the largest waves were recorded. At the side wall the waves were smaller. The wave height measurements for wave gauges WHM82 & WHM92 located between the basins center and the

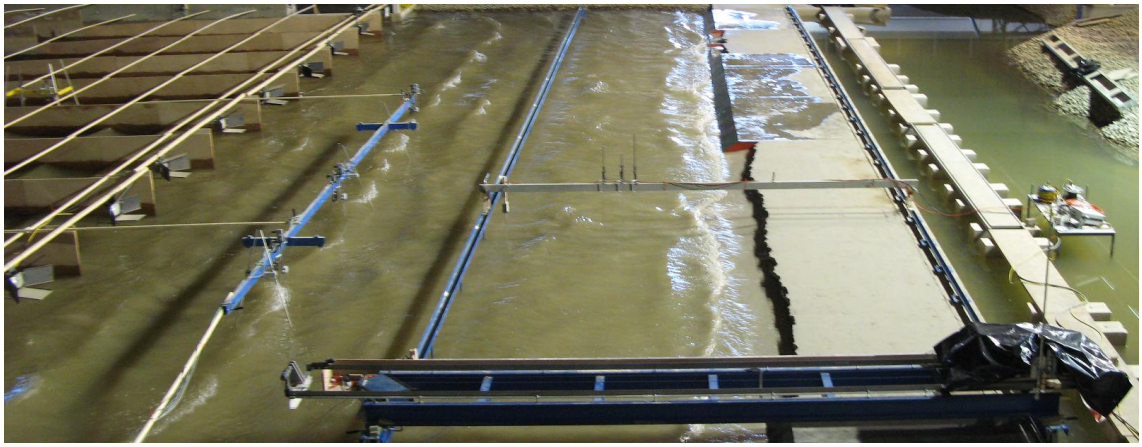

Figure 4.10: Longshore variation in wave breaking observed from the white foam on the waves

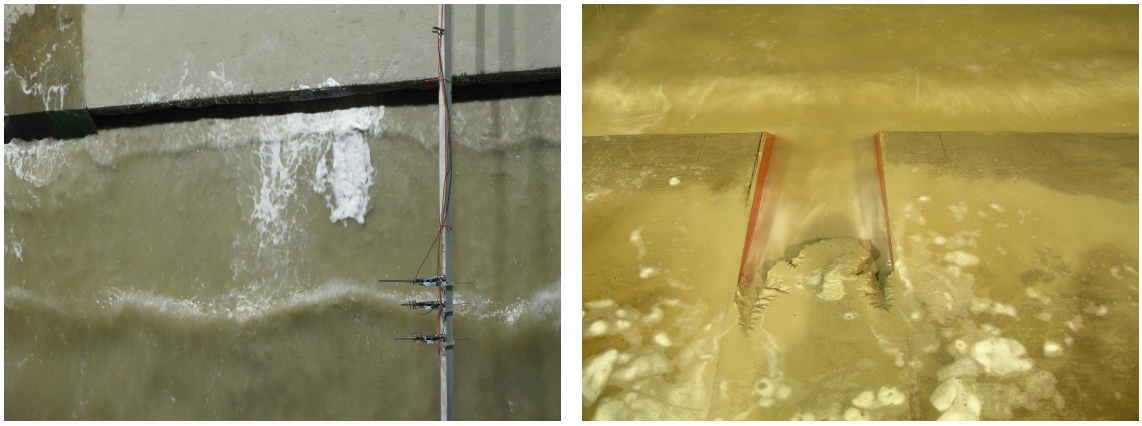

(a) Rip current *(b) Gully formation*

Figure 4.11: Hydrodynamic observations

lateral boundary corresponds to either the measurements of WHM81 & WHM91 for a peak period of T_p = 2.07 s or to WHM83 & WHM93 for a peak period of T_p = 1.55 s. Furthermore the wave spectra of the incident and reflected waves of the measurement locations were not uniform.

The cause of the longshore variations in wave height is not obvious. Since the measurements were carried out in pairs and the wave height difference within each pair was small instrumental errors are unlikely. However a small phase lag in the waves when leaving the guiding walls could explain the wave height differences. As waves at one location start to break sooner they dissipate more energy. Consequently the wave height at the wave gauge is less resulting in a flat wave spectrum. At another location waves are still shoaling causing the measured wave height to be higher and the spectrum to be more peaked, see Figure 4.10. The cause of this phase lag is expected to lie within the wave generation and hence the wave board steering. This causes particular stretches of coast to receive more wave energy which has a profound impact on the development of the coastline.

The alongshore variation in the hydraulic conditions might explain the observed circulation cells. They were identified by foam that moved offshore concentrated at a location, see Figure 4.11a. Circulation cells contributed to the longshore variation of the offshore bathymetry and consequently influences the offshore hydraulic conditions. As waves reached the shoreline a fraction ran up over the dikes. Since the backflow of water was sometimes concentrated near a connection between a dune and a structure a gully was formed due to flow erosion. At some point in time waves were able to propagate into the gully increasing the erosion rate and deepening the gully. This resulted in additional erosion near the connection, see Figure 4.11b.

Gully formation played a significant role in the morphological development of the breaches (B1, B2 & B3) in experiment V1 and the connection between a dike and a dune with revetment in experiment V3. Both experiments had a wave peak period of T_p = 1.55 s. For experiment V2 with a wave period T_p = 2.07 s gully formation was less. As the dune front retreats wave reflection occurs latter than reflection on the adjacent dike. This causes a differential head to be developed over the connection which in turn drives an undulation current. This current causes a scour hole to develop at the connection. The reflected waves were expected to develop into edge waves. However the wave gauges were located too far offshore to distinguish edge waves from a directional wave spectrum. Consequently their presence was never proven.

4.6.2 Morphological response

During the experiments a scour hole developed in front of the dike and dune revetment. Although the scour depth in front of a dike was generally larger than the depth in front of a dune revetment it showed a large longshore variation. This longshore variability also emerged in the dune crest position in the first 15 minutes of wave generation. As the experiment continued the longshore variations increased but diminished further offshore, see Figure 4.13a. As the morphological development is a response to the hydrodynamic forcing the longshore variation in wave height might have caused these longshore morphological variations. Nonetheless the longshore variations in dune crest position make it difficult to distinguish an undisturbed dune section and hence quantify the additional erosion near unerodable structures.

The dune retreat in the breaches (B1, B2 & B3) of configuration 1 showed large differences especially in experiment V1, see Figure 4.12. In both experiments the dune retreat is largest for breach B2. The breaches suffered from gully formation mainly during experiment V1 which significantly increased the amount of erosion near the structure. The breach with the largest dune retreat B2 was situated near the center of the basin. Here measurements showed that the wave height was largest so the increased dune retreat in breach B2 is explainable. Measurements also showed that to the right of WHM81 & WHM91 the wave height was less. This explains the reduced dune retreat of breach B3 with respect to the retreat in breach B2. To the left of WHM81 & WHM91 no wave gauges were located. This makes it impossible to conclude that the reduced dune retreat of breach B1 is also caused by a lower wave height.

Between two successive series of wave generation the wave basin was slowly emptied to measure the bathymetry. Once empty profile measurements were taken which usually took a few hours. The next series of wave generation was performed the following day leaving the wave basin empty overnight. As the sediment dried up the unstable dune front collapsed providing sediment to the beach. When the next series of wave generation commenced the sediment on the beach prevented waves from reaching the dune front. Before dune regression could continue the sediment on the beach had to be transported offshore usually taking a few minutes.

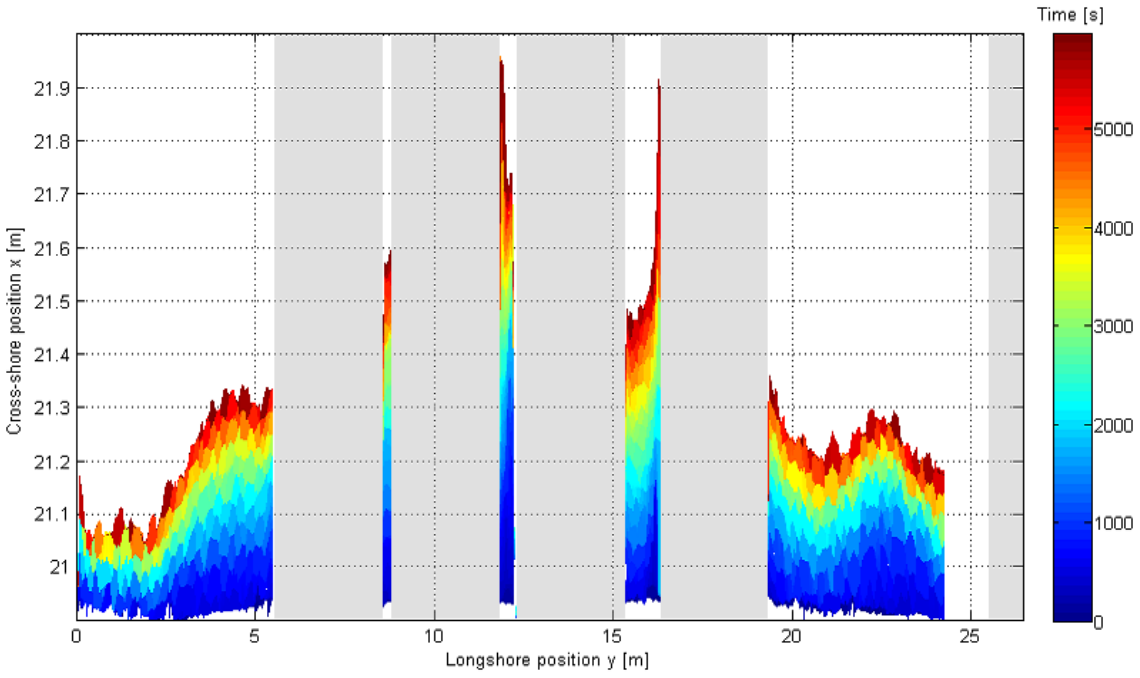

Figure 4.12: Dune crest position during experiment V1 (Boers et al., 2008)

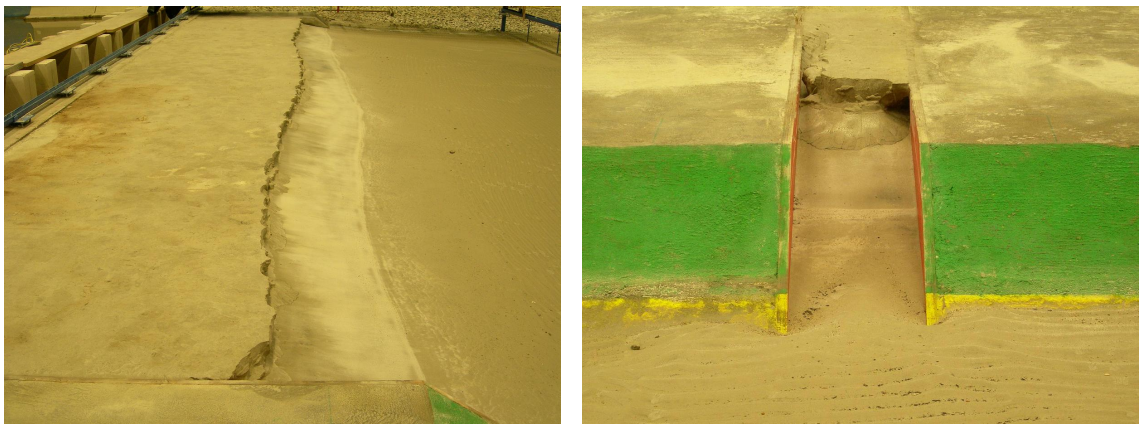

(a) Longshore variation in dune crest position *(b) Cave and gully formation*

Figure 4.13: Morphologic observations

At the connection between a dune and a structure the formation of caves was sometimes observed. After collapse they developed into gullies, see Figure 4.13b. It was hypothesized that the presence of a hard element resulted in a local focus of the wave energy but this was never verified. Further offshore the longshore variations in bathymetry were smoothed out and bed ripples emerged. The bed ripples were also observed on the concrete foreshore indicating that sediment moved well beyond the boundaries of the morphological measuring devices.

4.6.2.1 Argus dune crest measurements

The Argus dune crest measurements were quite successful. The measurement started just before the first waves were generated and continued a few minutes after the last waves reached the shore. During experiments V3 and V4 the support beam of the wave gauges obstructed the view of the Argus video cameras on the dune crest between y = 17.57 m and y = 18.1 m. In between these coordinates the dune crest position was interpolated. In the area from y > 24.12 m the wheelprofiler carriage obstructed the view of the Argus video cameras on the dune crest.

At the beginning of an experiment the dune profile was still intact and the sloping surface prevented a proper shade to develop at the dune crest. In this case the Argus video system interpreted the moving waterline as the dune crest resulting in a large cross-shore variation of the measured crest position. As the sloping surface was eroded and a stronger shadow line developed at the dune crest the measured dune crest position stabilized. In Figure 4.14 the dune crest position over time is displayed for a location in the breach of the dune revetment. It shows the large cross-shore variation of the dune crest position in the first few minutes of the experiment. Also the overnight collapse of the dune front is distinguished at t = 16.4 minutes.

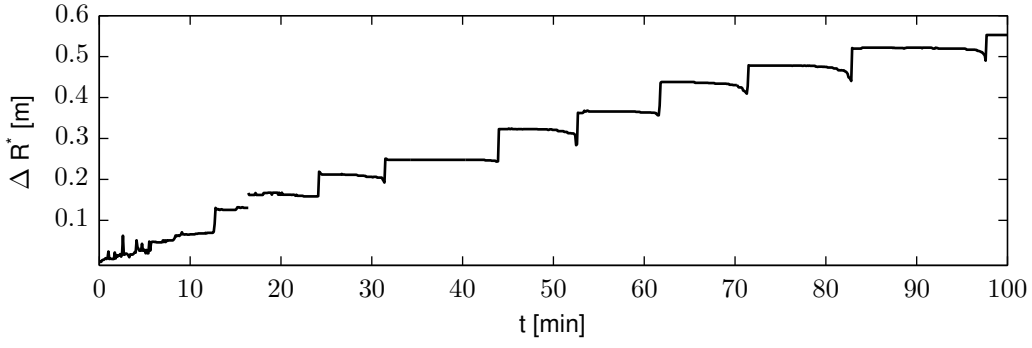

Figure 4.14: Dune crest position measurement of experiment V3 at y = 5.23 m

As the dune front becomes unstable due to undercutting of the dune foot it starts collapsing. A lump of sediment subsides and slides down on the beach. Since the Argus video cameras were placed under an angle with respect to the vertical this subsidence is interpreted as a forward moving dune front. As the lump of sediment subsides further a shadow line develops at the new dune front. This is visualized as a sudden jump in the dune crest position. In Figure 4.14 the forward moving dune front just before a jump in the dune crest position can clearly by distinguished.

4.6.2.2 Wheelprofiler measurements

During construction the wheelprofiler was used to check whether or not the constructed model setup was similar to the designed setup. The measurements revealed that the maximum difference in bottom elevation between the constructed and intended profile was in the order of 1 cm. During the experiments the measurements showed that sediment moved out of the profiles. This indicates that sediment was transported either in longshore direction or beyond the offshore boundary of the wheelprofiler. Figure 4.15 displays the mean bottom elevation of the 8 profile measurements taken in dune sections D11 at the end of experiment V3. The range of the measurements is expressed by the minimum and maximum measured values given by a dashed gray lines. They give an idea of the longshore morphological variations.

4.6.3 Quantifying additional dune erosion

The additional dune erosion near a structure was relatively small and fell well within the standard deviation of the measurements. For a peak period T_p of 2.07 seconds additional erosion only developed after 30 minutes. On prototype scale this means that additional erosion for T_p = 16 s only starts developing after a storm duration of 5 hours. Compared with the value prescribed in the current assessment rules the additional erosion was minor. However for a wave period of T_p = 1.55 s the additional erosion can be up to 50% larger than the erosion of an undisturbed dune. For breach B2 with a width of 0.5 m the erosion volume was up to 125% larger. Comparison of the measurements revealed that the current assessment rules overpredict the additional erosion near structures with a factor of 2 or more. The caves penetrating deep into the dune were identified as a safety hazard as they might cause the dune to fail.

The remainder of this section is obtained from the paper by Boers for the Coastal Sediments conference of 2011 (Boers *et al.*, 2011). The impact of structures on dune erosion is expressed by Equation 4.1. A linear regression analysis was used to determine the enhancement factor for each connection type. In the analysis no distinction was made between the effect of the wave

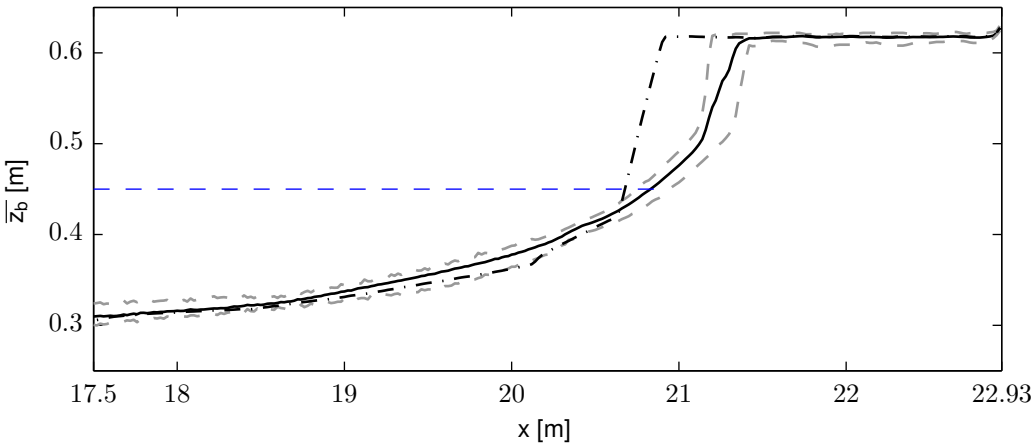

Figure 4.15: Mean bottom elevation of dune sections D11 (—) including the mean initial profile (– · –), the minimum & maximum measured values (– –) and the SSL (– –).

period, duration of wave generation or the breach width. Also the effect of gully formation which has a distinct effect on the development of additional erosion near structures was not taken into account. On the other hand measurements taken in the region of influence of the wave damping beaches were not used in the analysis. When correlation between additional dune erosion and the erosion of an undisturbed dune section is strong these conditions have a minor influence on the enhancement factor. Furthermore it is not clear to what extend the connections mutually influence each other.

For the analysis measurements from the hand-held surface scanner were used to determine the amount of additional erosion with respect to the mean erosion measured by the surface scanner. A linear regression T-test confirmed that within the measurement boundaries of the hand-held surface scanner the different conditions have a minor influence on the enhancement factor. In Table 4.5 the enhancement factors resulting from the regression analysis and the corresponding standard error for each connection type is given.

$$A_{con} = \alpha_{con} A_{dune} \tag{4.1}$$

In which:

- A_{con} = Maximum erosion volume above SSL at the connection [m^3/m],
- α_{con} = Enhancement factor [-],
- A_{dune} = Erosion volume above SSL for an undisturbed dune section [m^3/m],

Connection type	Enhancement factor α_{con}	Standard error σ_α
Dune and dike	1.27	0.08
Dike and dune revetment	1.51	0.16
Breach in a dike body	1.88	0.13
Breach in a dune revetment	1.52	0.22

Table 4.5: Erosion enhancement factors (Boers et al., 2008)

4.7 Data used in the XBeach comparison

In Chapter 5 measurements of the experiments are compared with the XBeach prediction. The wheelprofiler measurements and the dune crest position measured by the Argus video system are used to compare the dune crest retreat ΔR^*, the erosion volume A and the bottom profile z_b. The wave height measurements are used to calibrate the wave height H_{m0} in XBeach. The above is summarized by:

- ΔR^* → Argus dune crest position measurements & Wheelprofiler measurements,
- A → Wheelprofiler measurements,
- z_b → Wheelprofiler measurements,
- H_{m0} → Wave height measurements

To compare the bottom profile both the wheelprofiler measurements and the predicted bottom elevation are interpolated onto a grid with a constant size of dx = 0.02 m. From the dune crest position measurements disturbance in both time and space were excluded. Subsequently the dune retreat is calculated by subtracting the crest position at t=0 from the crest position at time t, see Equation 4.2.

$$\Delta R^*(t,y) = R^*(t,y) - R^*(0,y) \tag{4.2}$$

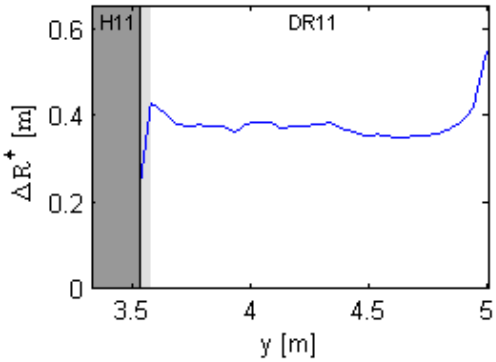

(a) ΔR^* derived from dune crest position measurements near connection H11-DR11 at t = 90 min of experiment V3

(b) Photo of connection H11-DR11 at t = 90 min of experiment V3

Figure 4.16: Inaccuracy of dune crest position measurements near structures

4.7.1 Omitted measurements due to disturbance in space

Near a structure the dune crest position measurements showed little dune crest retreat. The measured crest position near a structure was compared with photo's taken during the experiments. Figure 4.16a shows the dune crest retreat derived from dune crest position measurements ΔR^*_{ARGUS} at connection H11-DR11. In the light gray area ΔR^* reduces. In the experiment however additional erosion developed at connection H11-DR11, see Figure 4.16b. This revealed that near a structure the dune crest position was not measured accurately. Therefore these measurements were excluded. Measurements taken within the region of influence of the wave damping beaches have also been excluded from the analysis.

In the upper panel of Figure 4.17 the dune crest position of experiment V1 is presented at the end of the experiment. The lower panel presents this information for experiment V3. The location of dunes, dikes, breaches and dune revetment sections is given by the stretch code at the top of the figure. Here a D stands for Dune, H=Dike, B=Breach, DR=Dune Revetment and R=Reference. In Figure 4.17 dikes have a dark gray color. The locations from which the measurements were

Stretch	Type	Longshore stretch coordinates y [m]	
		Full	Comparison
Configuration 1			
D1	Dune	0 - 5.53	2.24 - 5.45
B1	Breach	8.53 - 8.78	8.58 - 8.68
B2	Breach	11.78 - 12.28	11.83 - 12.13
B3	Breach	15.28 - 16.28	15.33 - 16.28
D2	Dune	19.28 - 25.42	19.38 - 24.18
Configuration 2			
DR11	Revetment	3.53 - 5.03	3.58 - 4.98
B11	Breach	5.03 - 5.53	5.03 - 5.53
DR12	Revetment	5.53 - 7.03	5.58 - 6.93
D11	Dune	15.28 - 25.42	15.48 - 24.18

Table 4.6: Longshore coordinates of comparison stretches

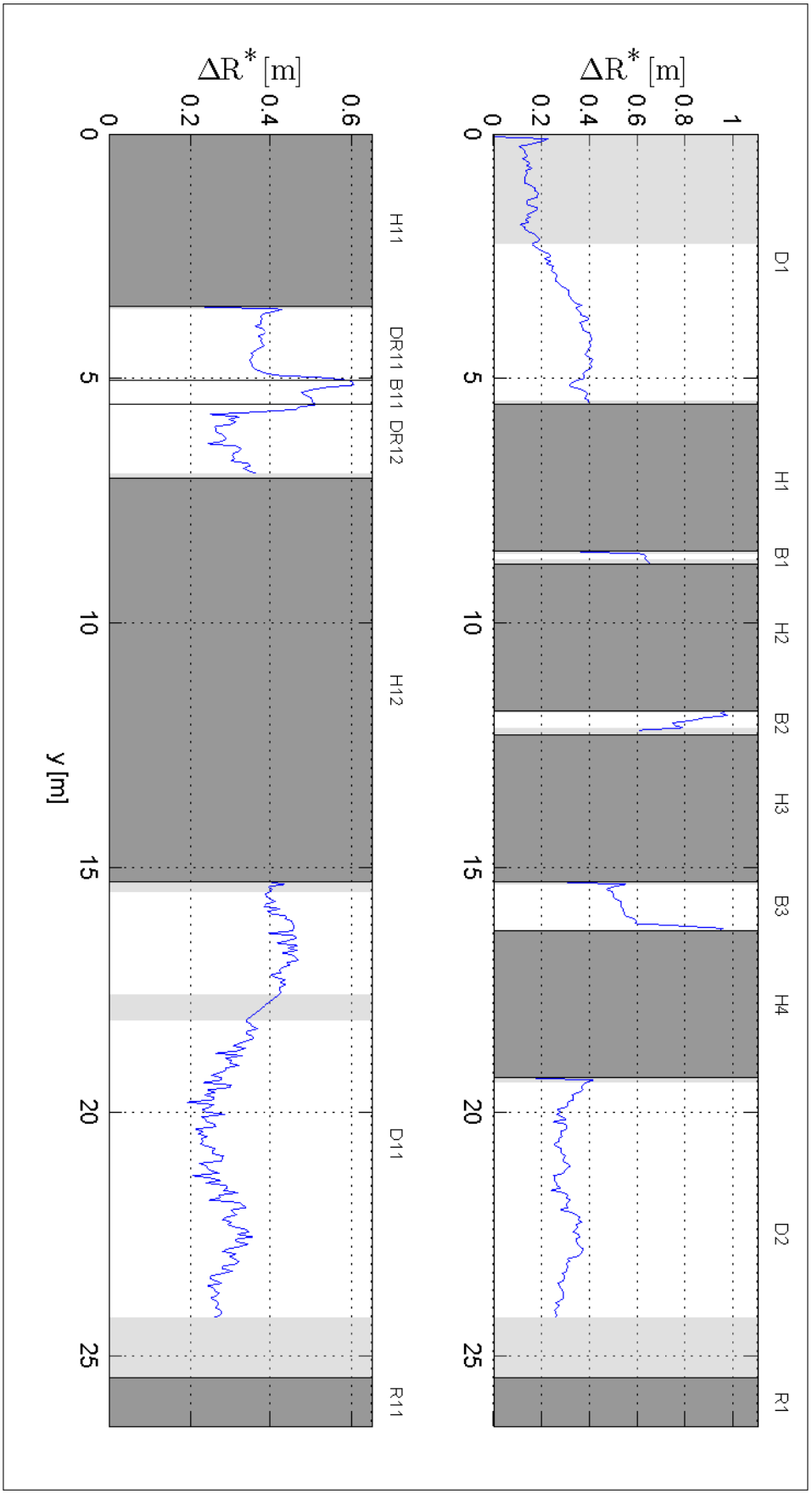

Figure 4.17: Spacial disturbances in dune crest position measurements; Structures have a dark gray color, locations from which the measurements were excluded have a light gray color. Measurements in white area's are used in the comparison. Upper panel: Configuration 1 with the dune crest retreat of experiment V1 at t = 90 min which is at the end of T030. Lower panel: Configuration 2 with the dune crest retreat of experiment V3 at t = 90 min.

excluded have a light gray color. Measurements in the white stretches are used to compare with the XBeach prediction and are therefore comparison stretches. Table 4.6 presents the longshore coordinates of the entire stretches and the comparison stretches.

4.7.2 Omitted measurements due to disturbance in time

At the beginning of each experiment (T000) the dune crest position showed a large cross-shore variation. This was caused by the sloping surface of the initial profile. As the sloping surface was eroded by the waves the measured dune crest position stabilized which usually toke a couple of minutes. This phenomenon is clearly visible in the first 5 minutes of Figure 4.12. These first minutes are therefore excluded from analysis. The dune crest position measurements started before the first waves were generated and continued a few minutes after the last waves reached the shoreline. This means that the record length of the dune crest position is longer than the duration of the experiment. Outside the period of wave generation the dune crest position does not change and therefore these measurements are excluded.

In Figure 4.18 the mean dune crest retreat $\overline{\Delta R^*_{ARGUS}}$ of dune section D11 of experiment V3 is displayed. Gray parts denote the time intervals which are excluded from the analysis. Measurements in white area's are used in the comparison. Table 4.7 gives these time intervals. The combined length of the time intervals for a test is 90 minutes. Note that for each experiment the initial record length of the dune crest position measurements is different.

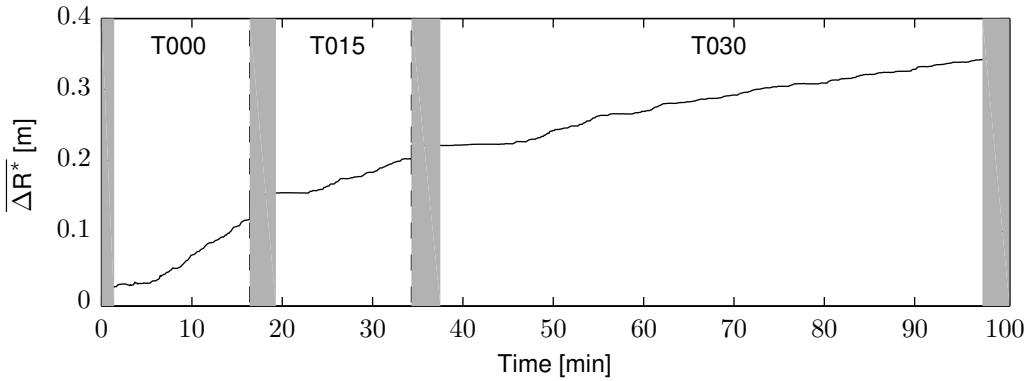

Figure 4.18: Mean dune crest retreat $\overline{\Delta R^*_{ARGUS}}$ for dune section D11 of experiment V3. Time intervals from which the measurements were excluded are gray.

Experiment	T000	T015	T030
V1	3.7 - 18.7	19.7 - 34.7	38.1 - 98.1
V2	3.0 - 18.0	21.7 - 36.7	38.0 - 98.0
V3	1.4 - 16.4	19.3 - 34.3	37.5 - 97.5
V4	3.1 - 18.1	24.0 - 39.0	41.5 - 101.5

Table 4.7: Time intervals of dune crest position measurements for comparison

4.7.3 Resulting comparison figures

For each experiment a spatial overview is created of the dune crest retreat ΔR^* and the erosion volume A at the end of an experiment. The spatial overview is identical to Figure 4.17 except that in the lower panel the erosion volume is displayed. During the experiments a longshore variation in dune erosion developed, see Subsection 4.6.2. Therefore statistical parameters are used to compare measurements and prediction. The used parameters are the mean, the standard deviation, the minimum and the maximum of the dataset.

The upper panel of Figure 4.19 displays the development in time of the mean dune crest retreat $\overline{\Delta R^*}$ of dune sections D1 & D2 in experiment V1. The mean dune crest retreat derived from the dune crest position measurements $\overline{\Delta R^*_{ARGUS}}$ is blue, its standard deviation is given by a dashed blue line. Black dots indicate the mean dune crest retreat derived from the 10 profile measurements in D1 & D2 ($\overline{\Delta R^*_{WP}}$). The whiskers represent the standard deviation in the profile measurements. The middle panel of Figure 4.19 displays the development in time of the mean erosion volume $\overline{A}$ of dune sections D1 & D2 in experiment V1. Black dots indicate the mean erosion volume derived from the profile measurements in D1 & D2 ($\overline{A_{WP}}$). The whiskers represent the standard deviation. In the lower panel of Figure 4.19 the bottom elevation is shown. The final mean bottom elevation based on profile measurements $\overline{z_{b,WP}}$ has a solid black line. The mean initial profile is a dashed black line. Gray dashed lines indicate the minimum and maximum bottom elevation measured within the comparison stretches.

4.8 Conclusion

The longshore variations in wave height considerable influenced the morphological development of the coastline. Especially the differences in dune crest retreat and erosion volume between the breaches B2 and B3 might be related to this. The lack of wave gauges at the left of the basins center prevents concluding that the reduced dune retreat of breach B1 with respect to breach B2 is also caused by a lower wave height. Gully formation significantly influenced the amount of additional erosion especially for the breaches in a dike body and the connection between a dike and dune with revetment. The transport of sediment to the concrete foreshore might cause differences between the XBeach simulations and the measurements.

The amount of additional dune erosion fell well within the standard deviation of the measurements. For a peak period T_p of 2.07 seconds additional erosion only developed after 30 minutes. The existence of additional erosion near structures was proven with measurements of the hand-held surface scanner. The surface scanner produced a very detail high density recording of the bottom elevation. Given the fact that the region where measurement were taken is relatively small it is concluded that the effect of additional erosion is very local. Furthermore the lack of current data due to poor performance of the electro-magnetic flow meters and too little wave gauges makes a proper analysis of the hydrodynamic conditions virtually impossible.

The longshore variations in wave height and morphological development of the shoreline are relatively large compared with the additional erosion. Considering the relatively large influence of gully formation and the mutual influence of the connections on each other it is concluded that the experiments are not suitable to derive a reliable quantification of the additional erosion near structures.

The experiments were initially aimed at verifying the hypothesis that unerodable structures cause additional erosion of the dunes next to it. The experiments provided the necessary information to accomplish the objective and proved the existence of additional erosion near hard structures. Therefore they were certainly useful. Furthermore they provided valuable insights into processes that influenced the development of additional erosion near hard structures.

4.9 Recommendations

The insights obtained from the pilot experiments are formulated in recommendations regarding the model setup for future research to additional dune erosion near hard structures.

- Measure the wave height along a longshore transect at the shoreline and at various distances

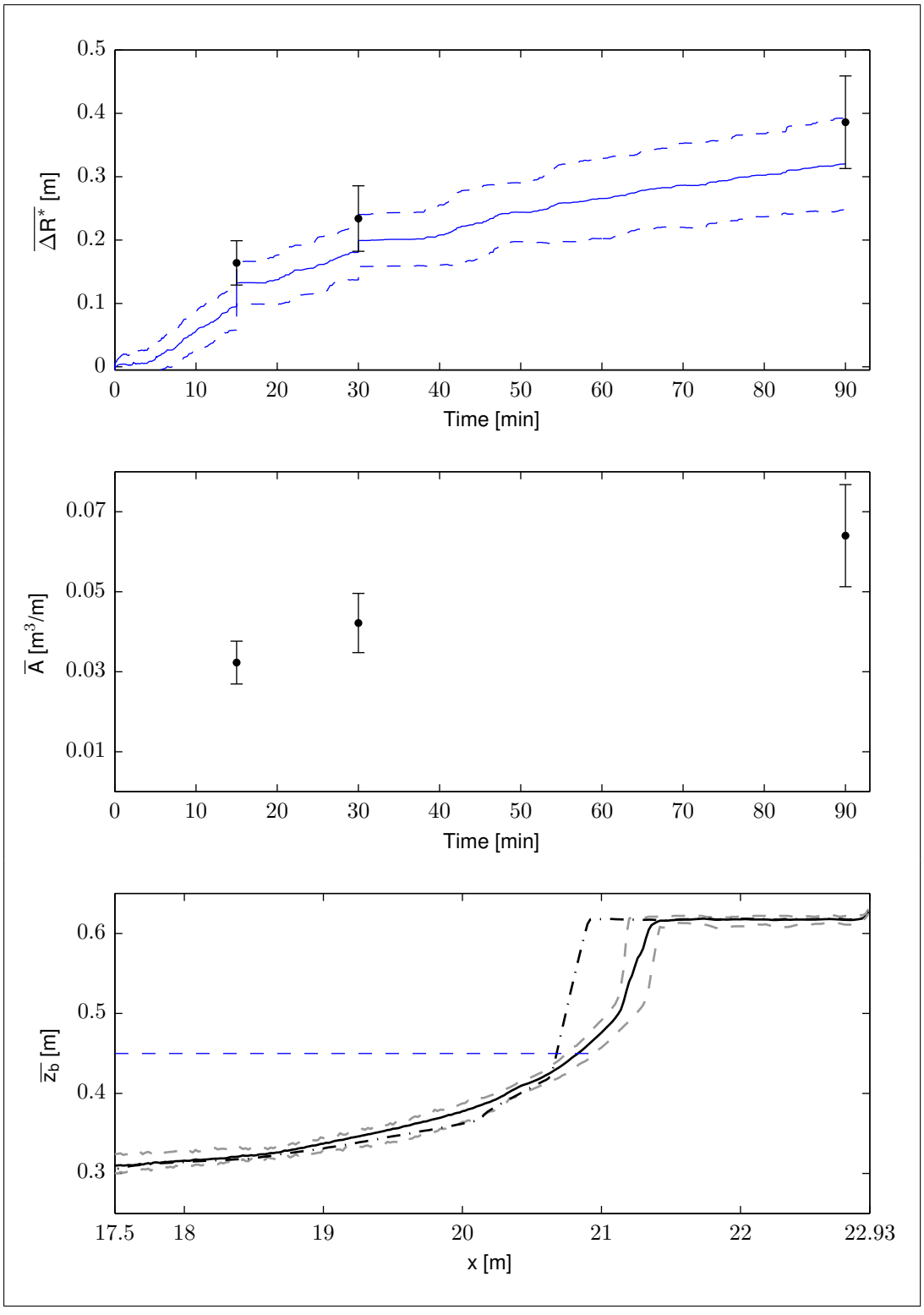

Figure 4.19: Mean erosion parameters of D11 in Experiment V3. Upper panel: Mean dune crest retreat $\overline{\Delta R^*}$ of 1. Argus measurements (—) and its standard deviation (– –), 2. Profile measurements (•) and its standard deviation (whiskers). Middle panel: Mean erosion volume $\overline{A}$ of profile measurements (•) and its standard deviation (whiskers). Lower panel: Mean final bottom elevation $\overline{z_b}$ (—) and the initial bottom elevation (– · –) of profile measurements , SSL (– –) and minimum & maximum measured elevation (– –)

from it. Preferably measure the surface elevation of the entire model domain with for instance laser altimeters suspended from the roof of the building.

- Limit the longshore variations in wave height as much as possible. Measure the wave height in a longshore transect at the wave board and at various distances from it.
- Use reliable velocity meters and measure the current velocities along a longshore transect at various distances from the shoreline.
- Increase the density of velocity meters in front of the connection to accurately measure the longshore current in front of it.
- Prevent the development of gully formation by either preventing waves from running over the dunes and dikes or prevent water on the dune and dike surface to flow back to the wave basin.
- Investigate one connection per test to be constructed at the center of the model domain to eliminate the mutual influence of connections.
- Investigate the influence of the angle of wave incidence and the shape of the connection on the development and magnitude of the additional erosion near hard structures.

5 Model-data comparison

5.1 Introduction

In this chapter a model-data comparison is performed between the measurements from the Delta Basin experiments described in Chapter 4 and the response of the coastal system predicted by XBeach. The XBeach model is described in Chapter 3. The simulation analysis of Chapter 3 showed that XBeach is able to qualitatively predict the behaviour of a dune-dike connection under storm conditions.

To assess the performance of XBeach the measured and predicted dune crest retreat ΔR^*, erosion volume A and cross-shore bottom profile z_b are compared. After discussing the model setup, calibration and model input in Section 5.3 the model performance for breach sections, dune revetment sections and dune sections is assessed in Section 5.4. The location of breaches, dune revetments and dunes is given in Section 4.2.

5.2 Comparison approach

To assess the capabilities of XBeach to simulate the Delta Basin experiments the dune crest retreat ΔR^*, the erosion volume A and the bottom profile are compared. In Section 4.7 the measurements used in the comparison are described. From the predicted bathymetry the dune crest retreat ΔR^* is calculated by Equation 4.2. The predicted dune crest retreat is denoted by ΔR^*_{Pred}. The dune crest position R^* is defined as the x-coordinate of the grid point which is farthest offshore and from which the bottom elevation is larger than 0.615 m.

The dune crest retreat ΔR^* is also derived from the profile measurement with Equation 5.1. Profiler measurements were taken at T000, T015, T030 and T090, see Table 4.3. $R^*_{WP}(90,y)$ denotes the retreat point derived from wheelprofiler measurements taken after 90 minutes of wave generation. Subsequently T000, T015 and T030 denote measurements taken after 0, 15 and 30 minutes of wave generation respectively. Since $\Delta R^*_{WP}(90,y)$ is defined by the difference in the location of R^* between T090 and T000 the diameter of the profilers wheel has no influence on the value of $\Delta R^*_{WP}(90,y)$. The longshore coordinate at which profile measurements were taken are given in Table 4.1.

$$\Delta R^*_{WP}(t,y) = R^*_{WP}(t,y) - R^*_{WP}(0,y) \qquad \text{with t = [15, 30, 90]} \tag{5.1}$$

To obtain the erosion volume A the point of intersection with the still water level is calculated for the initial profile and end profile. Subsequently the difference above SSL between the initial profile and end profile is numerically integrated over the x-dir with the trapezoidal rule for each cross-section. This procedure is applied to both the profile measurements and the XBeach prediction and results in the erosion volume A expressed in m^3/m. To compare the bottom profile both the wheelprofiler measurements and the predicted bottom elevation are interpolated onto a grid with a constant size of dx = 0.02 m.

During the experiments a longshore variation in dune erosion developed due to various physical processes, see Subsection 4.6.2. This longshore variation is not expected to arise in the XBeach prediction. Therefore statistical parameters are used to assess the performance of XBeach. The used parameters are the mean, the standard deviation, the minimum and the maximum of the measured and predicted erosion parameters. Both the mean dune crest retreat derived from

the Argus dune crest position measurements $\overline{\Delta R^*_{Argus}}$ and the predicted mean dune crest retreat $\overline{\Delta R^*_{Pred}}$ are calculated by Equation 5.2. In this equation n is the number of locations within the comparison stretches (Table 4.6) were ΔR^* is measured. $\overline{\Delta R^*(15)}$ represents the mean dune crest retreat after 15 min of wave generation. This results in the measured dune crest retreat $\overline{\Delta R^*_{Argus}}$ in a stretch as a function of time. Similarly the predicted ΔR^*_{Pred} is use to derive the predicted mean dune crest retreat $\overline{\Delta R^*_{Pred}}$ using the same equation. Similarly the measured mean erosion volume $\overline{A}_{WP}$ is calculated by Equation 5.3. At the locations of profile measurements (Table 4.1) the predicted erosion volume is used to calculate $\overline{A}_{Pred}$ with Equation 5.3.

$$\overline{\Delta R^*(t)} = \overline{\sum_{i=1}^{n} \Delta R^*(t,i)} \qquad \text{with t = [15, 30, 90]} \tag{5.2}$$

$$\overline{A(t)} = \overline{\sum_{i=1}^{n} A(t,i)} \qquad \text{with t = [15, 30, 90]} \tag{5.3}$$

To compare the bottom profile the mean bottom elevation for each point in a transect is calculated by Equation 5.4. This equation is used to calculate both the measured and predicted mean bottom elevation $\overline{z_{b;WP}}$ and $\overline{z_{b;Pred}}$. In this equation i is the number of profile measurements taken in a dune stretch. The minimum and maximum measured values are derived to visualize the longshore variation in $z_{b;WP}$.

$$\overline{z_b(t,x)} = \overline{\sum_{i=1}^{n} z_b(t,x,i)} \qquad \text{with t = [15, 30, 90]} \tag{5.4}$$

5.3 Model setup & Calibration

The Delta Basin experiments had a depth scale of n_d = 60, see Section 4.4. The scale dependency of XBeach was recently investigated by (Brandenburg, 2010) which has led to the implementation of a depth scale in XBeach. It scales multiple numerical parameters with the applied depth scale. Furthermore it was recommended to set the parameter turb = 0 for n_d > 20.

5.3.1 Computational grid

For experiments V1-V4 a 2DH model was constructed. Experiment V1 & V2 both have the same configuration of dunes and hard structures, namely configuration 1. The only difference is the wave period with T_p = 2.07 s for experiment V1 and T_p = 1.55 s for experiment V2. Experiments V3 & V4 use configuration 2 with T_p = 2.07 s for experiment V3 and T_p = 1.55 for experiment V4, see Section 4.2. The 2DH models have an alongshore length of 26.42 m and a cross-shore length of 22.88 m. In the upper right panel of Figure 5.1 the computational grid of configuration 1 including the bottom elevation z_b is displayed. The location of dunes, dikes, breaches and dune revetment sections is given by the stretch code at the top of the figure. Here D stands for Dune, H=Dike, B=Breach, DR=Dune Revetment and R=Reference, see Figure 4.3 and Table 4.1. Dikes have the same height as dunes, z_b = 0.167 m.

In the upper left of Figure 5.1 the grid spacing in x-direction is displayed. At the offshore wave boundary Δx is largest with Δx = 0.9 m. In landward direction Δx decreases to a minimum of Δx = 0.05 m at the water line. In the lower panel of Figure 5.1 the grid spacing in y-direction Δy is displayed. In dune stretches D1 & D2 the grid spacing is uniform with Δy = 0.1 m. To predict the morphological development in breaches more accurately Δy is smaller in breaches B1, B2 & B3. To limit the number of grid cells and hence the simulation time, Δy increases at dike sections (H1, H2, H3 & H4). Figure 5.2 on page 81 displays this information for configuration 2.

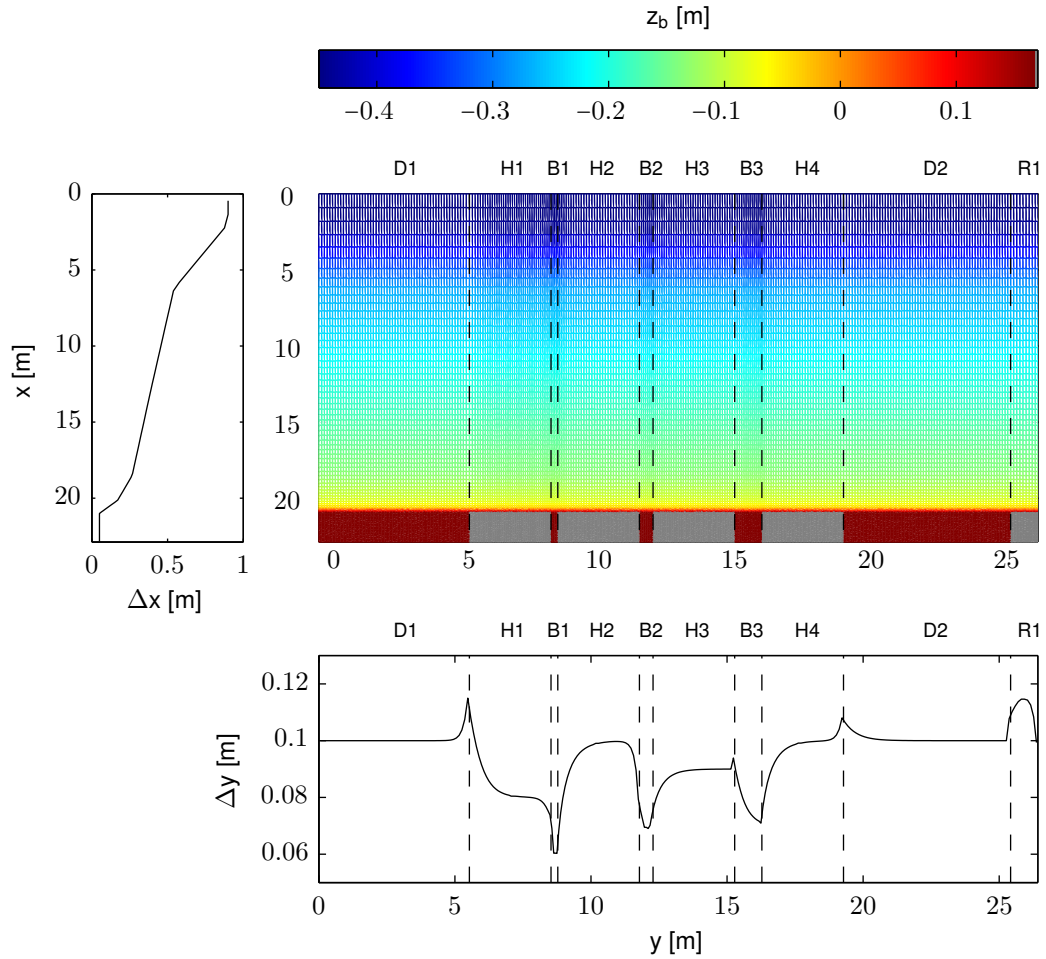

Figure 5.1: Computational grid for configuration 1, experiments V1 & V2. Upper right panel: The computational grid including the bottom elevation z_b. In the stretch code at the top of the figure a D stands for Dune, H=Dike, B=Breach, DR=Dune Revetment and R=Reference. Upper left panel: Grid spacing in x-direction. Bottom panel: Grid spacing in y-direction.

5.3.2 Model boundaries

The wave damping beaches at the lateral boundaries of the Delta Basin dissipate the energy of incoming waves and prevent them from being reflected back into the model. In XBeach this property is modeled with Neumann boundary conditions. They allow waves to propagate out off the model domain by forcing no alongshore gradient at the boundary. At the same time the sealing wall behind the damping beaches prevents water to flow out off the model. This property is simulated in XBeach with Wall boundary conditions. XBeach however only allows one boundary condition type for each lateral boundary. This prevents both properties to be simulated simultaneously. In the models of the experiments Wall boundaries are applied. This choice is explained in Section 5.5.

The waveboard is simulated by a 2D weakly-reflective absorbing-generating wave boundary. The wave boundary applies 2nd order steering to generate waves from the imposed Jonswap spectrum. The spectrum parameters f_p and H_{m0} are equal to the target wave conditions in the experiments, see Table 4.2. The waveboard in the Delta Basin is equipped with Active Reflection Compensation (ARC). This prevents waves from being reflected back into the model. The absorbing wave boundary condition mimics the ARC of the waveboard in the Delta Basin. In Table 5.1 the input parameters of the XBeach models are displayed.

XBeach parameter	V1	V2	V3	V4
Grid				
nx	94	94	94	94
ny	282	282	210	210
posdown	-1	-1	-1	-1
vardx	1	1	1	1
xfile	x.grd	x.grd	x.grd	x.grd
yfile	y.grd	y.grd	y.grd	y.grd
depfile	bed.dep	bed.dep	bed.dep	bed.dep
thetamin	-45	-45	-45	-45
thetamax	45	45	45	45
dtheta	10	10	10	10
Physical constants				
rho	1000	1000	1000	1000
depth scale	60	60	60	60
Time management				
tstart	120	120	120	120
tintg	6	6	6	6
tsmean	tsmean.txt	tsmean.txt	tsmean.txt	tsmean.txt
tstop	5520	5520	5520	5520
Boundary conditions				
instat	4	4	4	4
rt	900	900	900	900
dtbc	0.05	0.05	0.05	0.05
random	0	0	0	0
ARC	1	1	1	1
order	2	2	2	2
Hm0	0.15	0.15	0.15	0.15
fp	0.4831	0.6452	0.4831	0.6452
fnyq	1.9324	2.5808	1.9324	2.5808
mainang	270	270	270	270
s	10000	10000	10000	10000
gammajsp	3.3	3.3	3.3	3.3
wci	0	0	0	0
break	roelvink2	roelvink2	roelvink2	roelvink2
gamma	0.54	0.54	0.54	0.54
left	wall	wall	wall	wall
right	wall	wall	wall	wall
back	wall	wall	wall	wall
Sediment characteristics				
struct	1	1	1	1
ne_layer	nebed.dep	nebed.dep	nebed.dep	nebed.dep
turb	0	0	0	0
D50	0.000125	0.000125	0.000125	0.000125

Table 5.1: XBeach input parameters for models of experiments

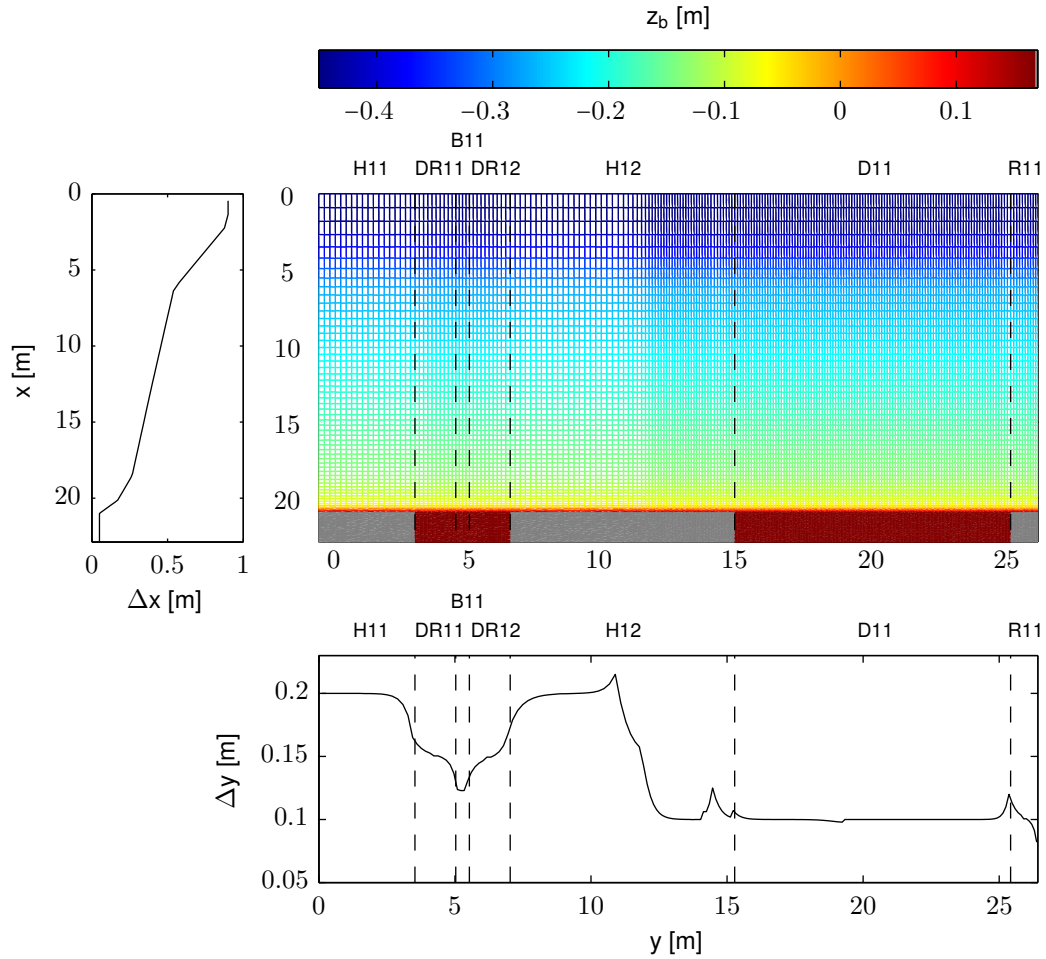

Figure 5.2: Computational grid for configuration 2, experiments V3 & V4. Upper right panel: The computational grid including the bottom elevation z_b. In the stretch code at the top of the figure a D stands for Dune, H=Dike, B=Breach, DR=Dune Revetment and R=Reference. Upper left panel: Grid spacing in x-direction. Bottom panel: Grid spacing in y-direction.

5.3.3 Cross-shore profile

The cross-shore profile is derived from the intended initial cross-shore profile in the Delta Basin experiments, see Subsection 4.2.2. The intended cross-shore profile is defined by a number of bottom coordinates (x,z). In Figure 5.3 the intended initial profile is presented by a red line. Dots indicate x-coordinates that define the initial profile of dunes, dikes and dune revetment sections. To prevent numerical distortions XBeach requires the grid spacing between adjacent grid cells to vary less than 15%.

At certain locations the bottom coordinates that define the intended profile are close to each other. Placing grid cells exactly on the x-coordinates of the intended profile yields a small grid spacing at these locations. This results in a inefficient computational grid and a long calculation time. Therefore the bottom elevation of the intended profile was interpolated to an efficient computational grid.[1] This caused the initial cross-shore profile in XBeach to deviated slightly from the intended profile, see Figure 5.3.

[1] Interpolated with xb_grid_xgrid.mat (Revision: 4892)

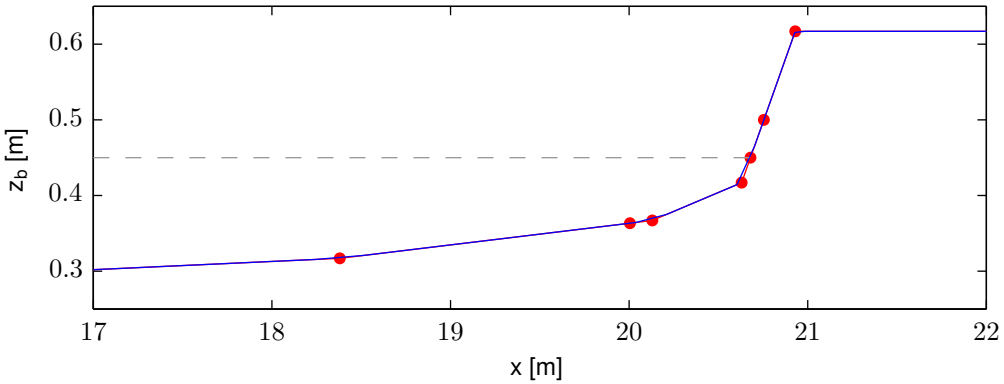

Figure 5.3: Intended initial cross-shore profile in the Delta Basin experiments (—), the interpolated initial XBeach profile (—) and the SSL (– –).

5.3.4 Wave height calibration

The hydrodynamic calibration is carried out using the measured wave height H_{m0} in cross-shore direction. In XBeach the wave height is controlled by the breaker parameter γ in the Roelvink formulation for the wave dissipation model (Roelvink *et al.*, 2010). To calibrate the wave height H_{m0} a 1D Dune model is used with the input parameters of experiment V3, see Table 5.1. In contrast to the 2DH model of experiment V3 the 1D Dune model has only 1 directional bin (thetamin = -90, thetamax = 90 & dtheta = 180). The number of grid cells in y-direction is ny = 2.

From the simulation results the wave height H_{m0} is calculated over the cross-shore profile for 3 time intervals. The time intervals correspond with the 3 series of wave generation in the Delta Basin experiments (T000, T015 and T030), see Table 4.3. The predicted wave height at the wave gauge location is obtained by interpolation between the nearest points in the computational grid. The difference between the measured and predicted wave height is expressed in a root mean square error (RMSE) for each time period. To obtain the sensitivity of γ 8 models with different values for γ were used. The upper panel of Figure 5.4 displays the cumulative error magnitude for different values of γ. For γ = 0.54 the cumulative error magnitude is smallest. Therefore γ = 0.54 is considered to give the best representation of the wave height H_{m0} in the Delta Basin. This is close to the default value for γ which is 0.55 (Roelvink *et al.*, 2010).

In the lower three panels of Figure 5.4 the wave height predicted by XBeach for γ = 0.54 and the measured wave height for T000, T015 & T030 are displayed. Roughly 5 m from the waveboard waves start breaking. This was also observed in the experiments, see Subsection 4.6.1. Between the breaker point and the wave board the shoaling zone is clearly visible. At x = 6.42 m and x = 16.28 m the longshore variation in wave height in the Delta Basin is visible.

5.4 Model-data comparison

For each experiment V1-V4 a spatial overview of the dune crest retreat ΔR^* and the erosion volume A at the end of an experiment is presented in Figures 5.15 - 5.18 on Pages 100 - 103. The location of dunes, dikes, breaches and dune revetment sections is given by the transect code at the top of the figure. Here a D stands for Dune, H=Dike, B=Breach, DR=Dune Revetment and R=Reference. The longshore coordinates of the stretches are given in Table 4.1. A dike profile is also indicated by a dark gray plane. The information in light gray areas is not used in the comparison. In these areas the measurements were distorted, see Section 4.7. The setup of a spatial overview is explained by a global description of Figure 5.15 below. The results of the spatial overviews for breaches B1, B2 & B3 is described in Subsection 5.4.1. Sections 5.4.2,

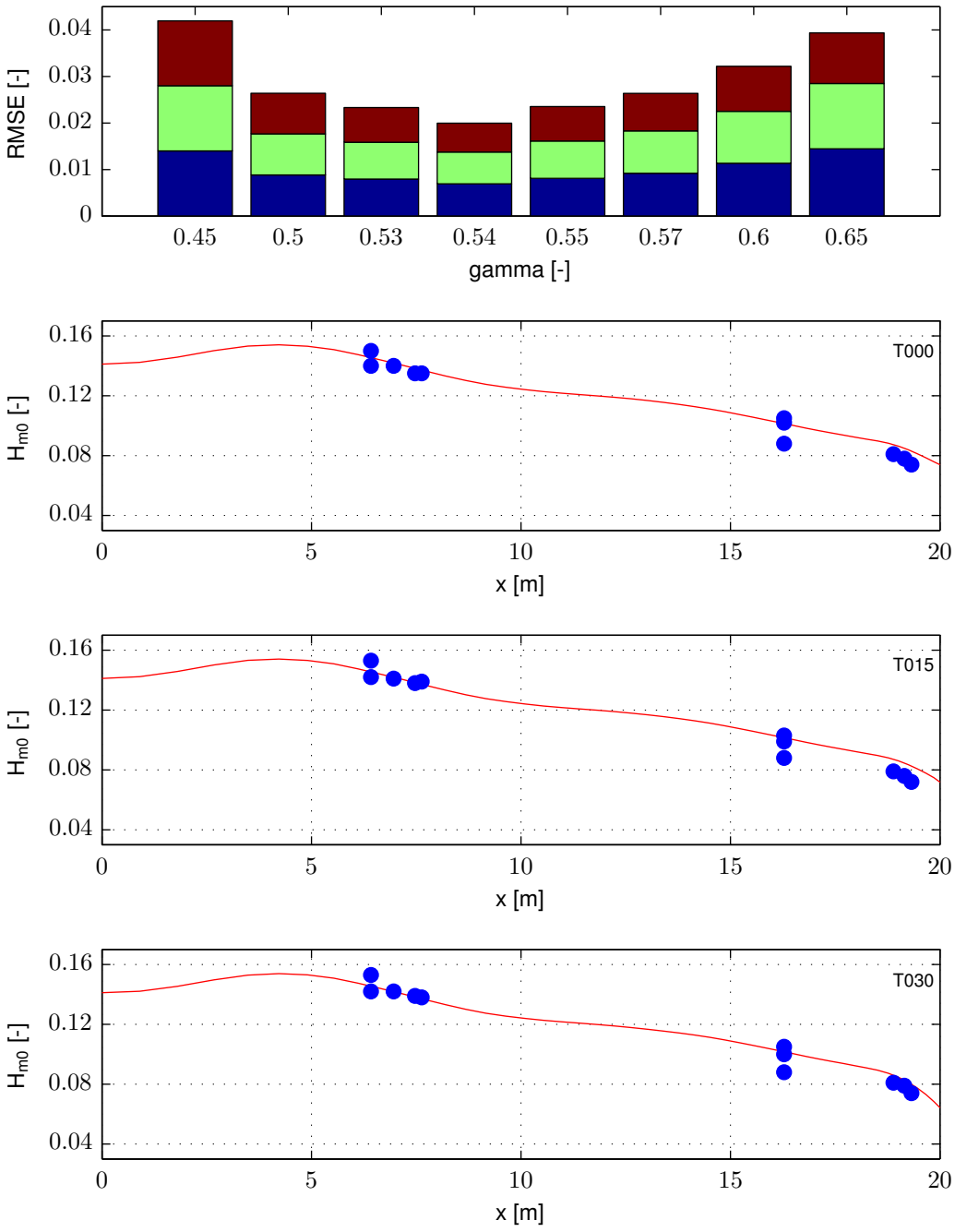

Figure 5.4: Wave height calibration for experiment V3. Upper panel: RMSE for different values of γ. The RMSE is divided in an error for T000 (blue), T015 (green) and T030 (red). Second panel from the top: Comparison of the wave height measurements (blue) and the XBeach prediction with γ = 0.54 (red) for T000. Third and fourth panel from the top: Comparison of the wave height measurements (blue) and the XBeach prediction with γ = 0.54 (red) for T015 & T030 respectively.

5.4.3 and 5.4.4 describe the results for dune revetment stretches, the revetment breach B11 and dune stretches respectively.

In the upper panel of Figure 5.15 the dune crest retreat, derived from the dune crest position measured by the Argus video system ΔR^*_{Argus}, is displayed by a blue line. Black dots indicate the dune crest retreat derived from profile measurements ΔR^*_{WP}. Generally the dune crest retreat derived from profile measurements $\Delta R^*_{WP;T090}$ is larger than ΔR^*_{Argus}, see the upper panel of Figure 5.15. The dune retreat predicted by XBeach is presented by a red line. In the lower panel of Figure 5.15 the erosion volume derived from profile measurements A_{WP} is given by black dots. A red line indicates the predicted erosion volume A_{Pred}.

The XBeach prediction of ΔR^* and A shows a zigzag pattern, see the red line in the upper and lower panel of Figure 5.15. This pattern is associated with the presence of circulation cells in front of the coast. The circulation cells are made visible by the mean flow velocity in front of the coast, see Figure 5.5. In Figure 5.5 the mean flow velocity of experiment V1 is displayed between y = 0.5 m and y = 3.5 m. A black line denotes the dune crest position from which ΔR^*_{Pred} in Figure 5.15 was derived. The dunes in this figure have a brown color. Offshore from x = 21.1 m five areas can be distinguished with a relatively high mean onshore velocity. In between the areas the flow is directed offshore. In the Delta Basin experiments circulation cells in front of the coast were also observed, see Subsection 4.6.1. Whether the circulation cells in XBeach result from the zig-zag pattern in the shoreline or vice versa is unclear. The coupling of the hydrodynamics and morphodynamics make it difficult to determine whether the hydrodynamics or the morphodynamics initiated the behaviour visible in Figure 5.5.

5.4.1 Breach sections B1, B2 & B3

Breaches in a dike section (B1, B2 & B3) were investigated in experiment V1 & V2 (Figures 5.15 & 5.16). In experiment V1 the measured erosion in breach B2 is larger than in breaches B1 &

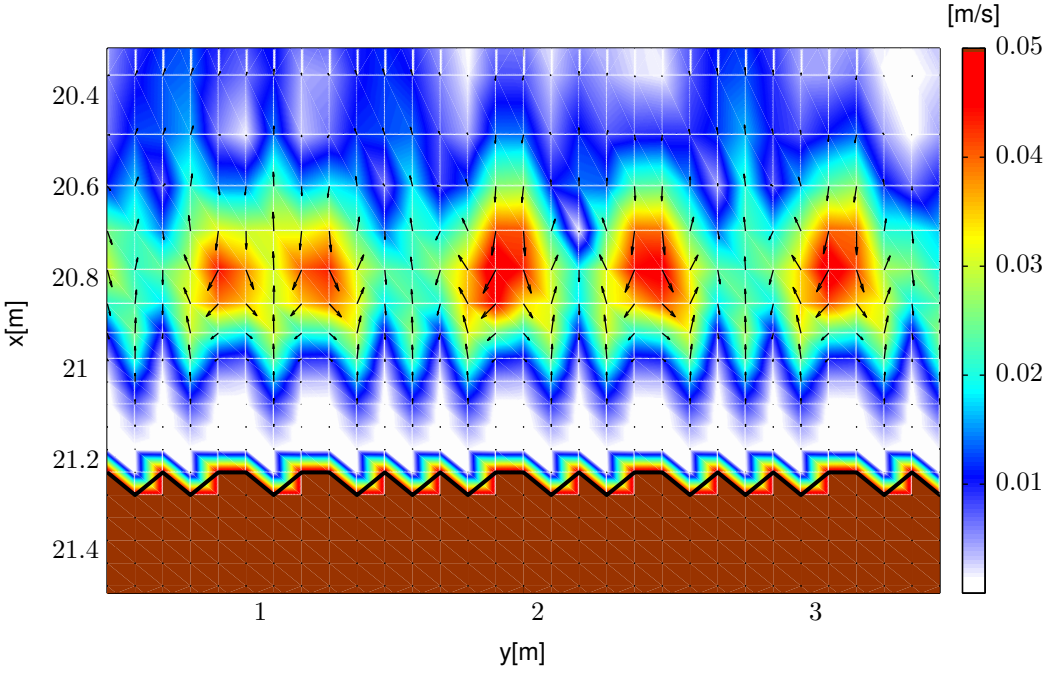

Figure 5.5: Predicted mean velocity in front of dune section D1 in experiment V1. A black line denotes the location of R^*_{Pred}. Dunes have a brown color. The current pattern indicates the presence of circulation cells in front of the coast.

B3. This is shown by both the dune crest retreat ΔR^*_{Argus} & ΔR^*_{WP} and the erosion volume A_{WP} in Figure 5.15. The measured dune crest retreat ΔR^*_{Argus} in B1 & B3 is ±0.6 m. In B1 & B3 the erosion volume $A_{WP} \approx 0.1$ m^3/m. Compared with dune sections D1 & D2 the measured erosion in the breaches is higher. Near a structure the measured dune retreat in a breach increases which is seen at connection B3-H4. The predicted dune crest retreat in B1 & B3 is similar to the measured dune retreat. For B2 however the measured erosion is larger than the predicted erosion. At the end of the experiment ΔR^*_{Argus} is ±62% larger and A_{WP} is ±69% larger than the predicted values, see Figure 5.15. XBeach shows an increasing breach erosion with a decrease of the breach width. The measurements do not show a relationship between the breach width and the breach erosion. This is caused by various disturbing processes that influenced the erosion of the breaches, see below.

In experiment V2 the measured erosion in breach B2 is also larger than in B1 & B3, see Figure 5.16. However the differences between the measured erosion in the breaches is smaller. For all breaches in a dike section the dune crest retreat $\Delta R^*_{Argus}/\Delta R^*_{WP} \approx 0.6$ m and $A_{WP} \approx 0.1$ m^3/m. The measured erosion is much larger than the predicted erosion in the breaches. Similar to experiment V1 XBeach shows an increasing breach erosion with a decrease of the breach width. The increase in ΔR^*_{Argus} at the connection with a dike section is small.

5.4.1.1 Disturbing processes

Gully formation significantly influenced the morphological development of the breaches during the experiments. Especially breach B2 suffered from gully formation which increased the erosion in the breach. In the Delta Basin experiment there was a longshore variation in wave height. The wave gauges showed that at the center of the basin the wave height was largest. This increased the erosion in breach B2 even further and explains why the measured erosion in B2 is largest in both experiments. In Section 4.6 the disturbing processes present in the experiments are described in detail. Both gully formation and the longshore variation in wave height were not simulated by XBeach. Therefore a quantitative comparison of the measured and predicted breach erosion is meaningless. The remainder of this section focuses on the predicted erosion in the breaches.

5.4.1.2 Predicted erosion in breach B1, B2 & B3

Both experiments show that XBeach predicts an increasing erosion with a decrease of the breach width. Tables 5.2 and 5.3 presents the mean dune crest retreat $\overline{\Delta R^*_{Pred}}$ and the erosion volume $\overline{A_{Pred}}$ for breaches B1, B2 & B3 in experiment V1 & V2. In Figure 5.6 this data is visualized. At t = 90 min in experiment V1 the mean dune crest retreat in the smallest breach (B1) is ±20% larger than in the largest breach (B3). For B2 this is 7%. The mean erosion volume shows slightly higher values with 28% and 10% for breach B1 and B2 respectively. For experiment V2 at t = 90 min $\overline{\Delta R^*_{Pred}}$ in B1 is ±32% larger than B3. For B2 this is 16%. For $\overline{A_{Pred}}$ these values are 39% and 19% for breach B1 and B2 respectively. The erosion in a dike breach is a function of the breach width and the wave period. For a smaller breach width the erosion increases. When the wave period increases the breach erosion also increases.

This behaviour is explained by the fraction of sediment volume lost to the scour hole in front of the adjacent dikes compared with the total amount of eroded sediment. Figure 5.7 shows the bathymetry of experiment V1 at t = 90 min. The dike sections between the breaches have a length of 3 m. The wider breach (B3) at the right of Figure 5.7 supplies more sediment to the foreshore than the narrower breaches (B1 & B2). Therefore B3 lose relatively less sediment to the scour holes in front of the adjacent dike. More sediment is deposited in front of breach B3 which consequently results in less erosion.

Time	$\overline{\Delta R^*_{Pred}}$ [10^{-3} m]			$\overline{A_{Pred}}$ [10^{-4} m^3/m]		
[min]	B1	B2	B3	B1	B2	B3
15	186	169	153	259	211	209
30	306	269	249	442	367	342
90	596	531	496	918	788	718

Table 5.2: Mean erosion in breaches (B1, B2 & B3) of experiments V1

Time	$\overline{\Delta R^*_{Pred}}$ [10^{-3} m]			$\overline{A_{Pred}}$ [10^{-4} m^3/m]		
[min]	B1	B2	B3	B1	B2	B3
15	116	113	106	183	162	150
30	186	175	164	307	263	233
90	416	363	314	657	565	474

Table 5.3: Mean erosion in breaches (B1, B2 & B3) of experiments V2

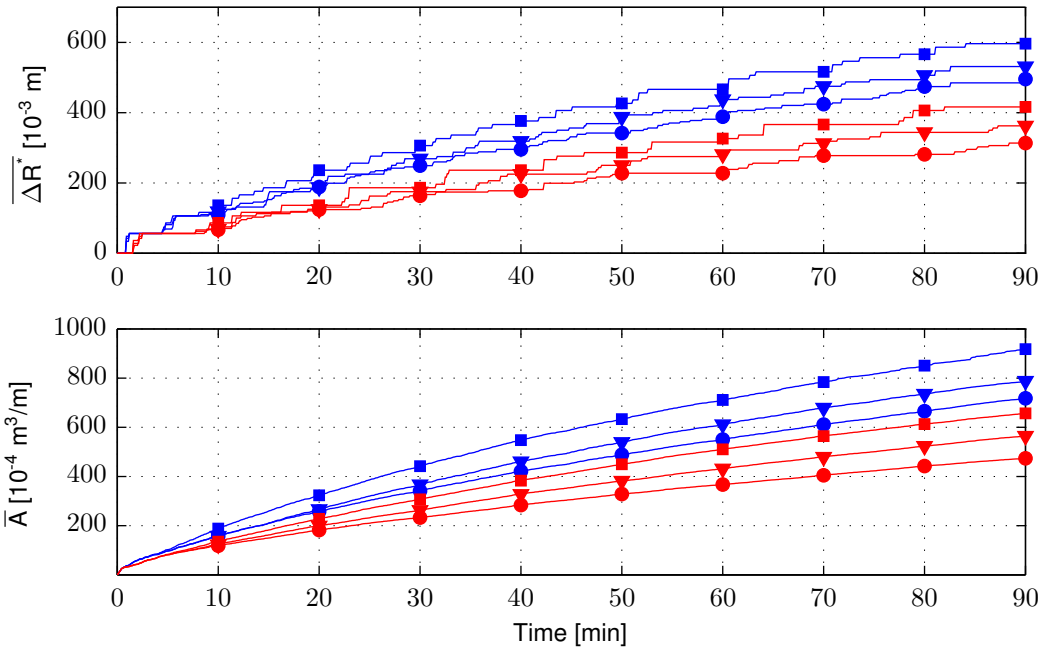

Figure 5.6: Mean erosion in breaches (B1, B2 & B3) of experiments V1 & V2. Upper panel: $\overline{\Delta R^*_{Pred}}$ in B1 experiment V1 (■), $\overline{\Delta R^*_{Pred}}$ in B2 experiment V1 (▼), $\overline{\Delta R^*_{Pred}}$ in B3 experiment V1 (●), $\overline{\Delta R^*_{Pred}}$ in B1 experiment V2 (■), $\overline{\Delta R^*_{Pred}}$ in B2 experiment V2 (▼), $\overline{\Delta R^*_{Pred}}$ in B3 experiment V2 (●). Lower panel: $\overline{A_{Pred}}$ in B1 experiment V1 (■), $\overline{A_{Pred}}$ in B2 experiment V1 (▼), $\overline{A_{Pred}}$ in B3 experiment V1 (●), $\overline{A_{Pred}}$ in B1 experiment V2 (■), $\overline{A_{Pred}}$ in B2 experiment V2 (▼), $\overline{A_{Pred}}$ in B3 experiment V2 (●).

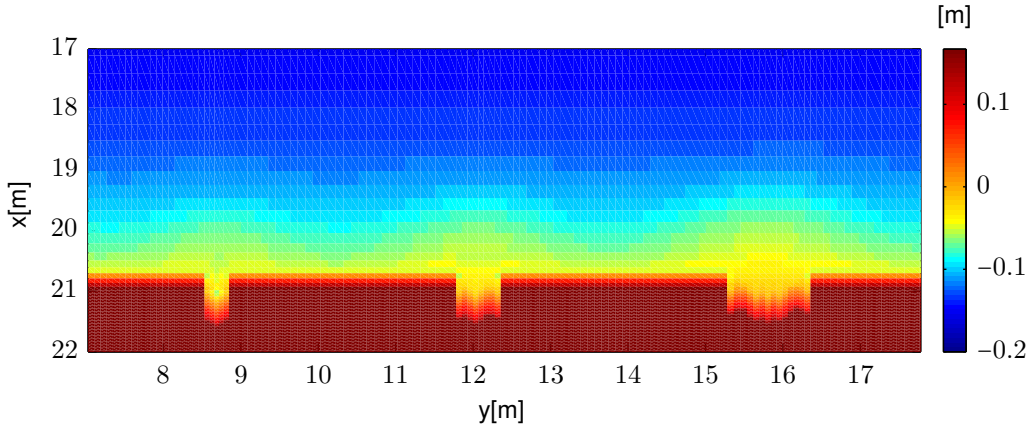

Figure 5.7: Bathymetry of experiment V1 at t = 90 min. Breach B1 is situated left, B2 in the middle and B3 is situated right.

5.4.2 Dune revetment sections DR11 & DR12

Configuration 2 contained two dune revetment sections DR11 & DR12 which were investigated in experiment V3 & V4. In Figure 5.17 both ΔR^* and A indicate that the predicted amount of erosion above the revetment is much less than the measured erosion. At the connection with structures DR11-H11 and DR12-H12 the measured dune crest retreat ΔR^*_{Argus} & ΔR^*_{WP} increases. This is also visible in the erosion volume A_{WP}, see the lower panel of Figure 5.17. XBeach predicts a slight increase in the erosion at connections DR11-H11 & DR12-H12. Above the revetment the measured erosion is less than in the revetment breach (B11). This is also predicted by XBeach.

In experiment V4 (Figure 5.18) both the dune crest retreat ΔR^*_{Argus} & ΔR^*_{WP} and the erosion volume A_{WP} increases significantly towards structures H11 & H12. XBeach however does not predict additional erosion at the connection between a dune with revetment and a dike (DR11-H11 & DR12-H12), see Figure 5.18. In accordance with experiment V3 the predicted amount of erosion above the revetment is much less than the measured erosion.

To quantify the difference between the predicted and measured erosion above the revetment the mean erosion parameters are compared. Within the dune revetment sections 2×4 profile measurements were taken, see Table 4.1. The measured and predicted mean erosion volume above the revetment $\overline{A_{WP}}$ and $\overline{A_{Pred}}$ is calculated by Equation 5.3 with n = 8. The dune crest position was measured with a resolution of dy = 0.05 m. The combined length of the dune revetment sections DR11 & DR12 from which measurements are usable is 2.75 m, see Table 4.6. Within DR11 & DR12 ΔR^*_{Argus} is known at 57 locations. Subsequently the mean dune crest retreat $\overline{\Delta R^*_{Argus}}$ is calculated by Equation 5.2 with n = 57. The predicted ΔR^*_{Pred} at these 57 locations are use to derive the predicted $\overline{\Delta R^*_{Pred}}$ with the same equation. In Table 5.4 the mean predicted and measured erosion parameters are presented which are also displayed in Figure 5.9.

At t = 15 min the difference between $\overline{\Delta R^*_{Argus}}$ and $\overline{\Delta R^*_{Pred}}$ is small. The mean erosion volume however shows larger differences at t = 15 min, see the lower panel of Figure 5.9. In Figure 5.8 the predicted and measured mean bottom elevation of dune revetment sections DR11 & DR12 at t = 15 min in experiment V3 are displayed. In this figure the black dot indicates the mean predicted retreat point $\overline{R^*_{Pred}}$, the red dot indicates the mean retreat point derived from profile measurements $\overline{R^*_{WP}}(15)$. Both measured and predicted retreat point lie close to each other. The erosion volume $\overline{A_{Pred}}$ derived from the predicted mean bottom elevation is less than $\overline{A_{WP}}$. This is visible in Figure 5.9 at t = 15 min.

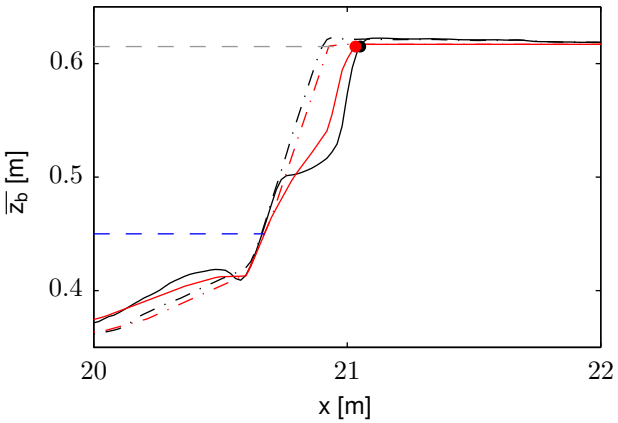

Figure 5.8: Mean bottom elevation of revetment sections DR11 & DR12 at t = 15 min of experiment V3. This figure shows at t = 15 min $\overline{z_{b,WP}}$ (—) and $\overline{z_{b,Pred}}$ (—). The initial profiles at t = 0 min $\overline{z_{b,WP}}$ (– · –) and $\overline{z_{b,Pred}}$ (– · –). The retreat point based on profile measurements (•) and R^* of XBeach (•). An elevation of 0.615 m is represented by (– –) and SSL by (– –).

The initial profile above SSL of XBeach lies onshore of the mean initial profile of the experiments, see the dashed-dotted lines in Figure 5.8. Onshore there is a small difference in elevation. This is partially caused by the difference between the intended initial profile in the Delta Basin and the initial profile of XBeach as described in Subsection 5.3.3. Furthermore measurements revealed

Time [min]	$\overline{\Delta R^*}$ [10^{-3} m]				$\overline{A}$ [10^{-4} m^3/m]			
	V3		V4		V3		V4	
	$\overline{\Delta R^*_{Argus}}$	$\overline{\Delta R^*_{Pred}}$	$\overline{\Delta R^*_{Argus}}$	$\overline{\Delta R^*_{Pred}}$	$\overline{A_{WP}}$	$\overline{A_{Pred}}$	$\overline{A_{WP}}$	$\overline{A_{Pred}}$
15	96	108	51	58	192	107	142	49
30	179	121	114	59	279	116	205	71
90	347	180	269	79	453	153	361	79

Table 5.4: Mean erosion above dune revetment (DR11 & DR12) of experiments V3 & V4

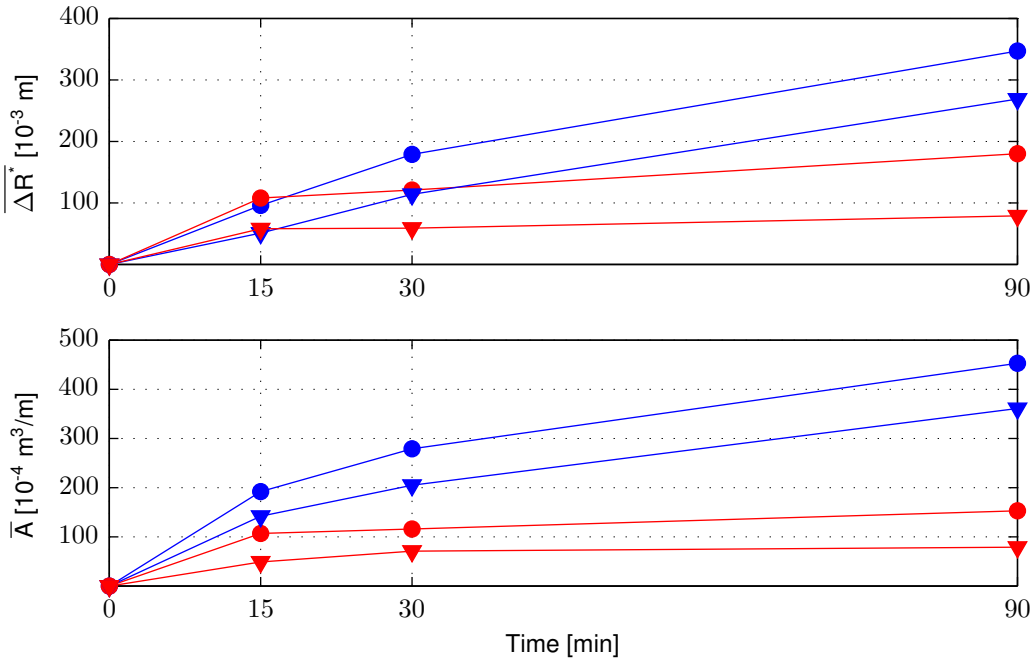

Figure 5.9: Mean erosion above dune revetment (DR11 & DR12) of experiments V3 & V4. Upper panel: $\overline{\Delta R^*_{Argus}}$ in experiment V3 (●), $\overline{\Delta R^*_{Pred}}$ in experiment V3 (●), $\overline{\Delta R^*_{Argus}}$ in experiment V4 (▼) and $\overline{\Delta R^*_{Pred}}$ in experiment V4 (▼) Lower panel: $\overline{A_{WP}}$ in experiment V3 (●), $\overline{A_{Pred}}$ in experiment V3 (●), $\overline{A_{WP}}$ in experiment V4 (▼), $\overline{A_{Pred}}$ in experiment V4 (▼).

that the maximum difference in bottom elevation between the initial profile constructed in the Delta Basin and the intended profile was in the order of 1 cm.

For experiment V3 $\overline{A_{WP}}$ is ±79% larger than $\overline{A_{Pred}}$ at t = 15. For experiment V4 this is even 190%. After t = 15 min the erosion above the dune revetment hardly increases. In time the difference between the predicted and measured erosion parameters increase. For experiment V3 at t = 90 min $\overline{\Delta R^*_{Argus}}$ is 93% larger and $\overline{A_{WP}}$ is 196% larger than the predicted values. For experiment V4 this is 240% and 357% respectively.

An explanation for the difference between the measurements and prediction is that to erode the dunes above the revetment waves must reach the dune front. Therefore wave runup is an important process in the development of the erosion above the revetment. Currently XBeach only simulates long wave runup. In the testbed report it is hypothesized that in addition to long wave runup also short wave runup should be included in the avalanching algorithm (Deltares, 2010).

5.4.3 Breach in a dune revetment B11

A breach in a dune revetment (B11) was investigated in experiment V3 & V4 and had a width of 0.5 m. For experiment V3 the measured and predicted dune crest retreat are roughly equal to 0.5 m. The predicted erosion volume A_{Pred} however is less than the measured erosion volume A_{WP}, see Figure 5.17. Figure 5.10 displays the measured and predicted bottom elevation in the breach. The initial profile of XBeach deviates slightly from the mean initial profile of the experiments, see the dashed-dotted lines in Figure 5.10. This is partially caused by interpolation of the intended initial profile to the XBeach computational grid. Furthermore the maximum difference in bottom elevation between the constructed initial profile and the intended profile was in the order of 1 cm. In Figure 5.10 dots present R^* derived from profile measurements and from XBeach. The location of R^*_{WP} and R^*_{Pred} is almost identical. Above SSL $\overline{z_{b,WP}}$ is steeper than $\overline{z_{b,Pred}}$. Therefore A_{Pred} is smaller than A_{WP}. Compared with dune section D11 the breach erosion is somewhat higher. For experiment V4 ΔR^*_{Argus}, ΔR^*_{WP} and ΔR^*_{Pred} show a close resemblance. Also A_{Pred} is less than A_{WP}, see Figure 5.18. This is comparable with experiment V3.

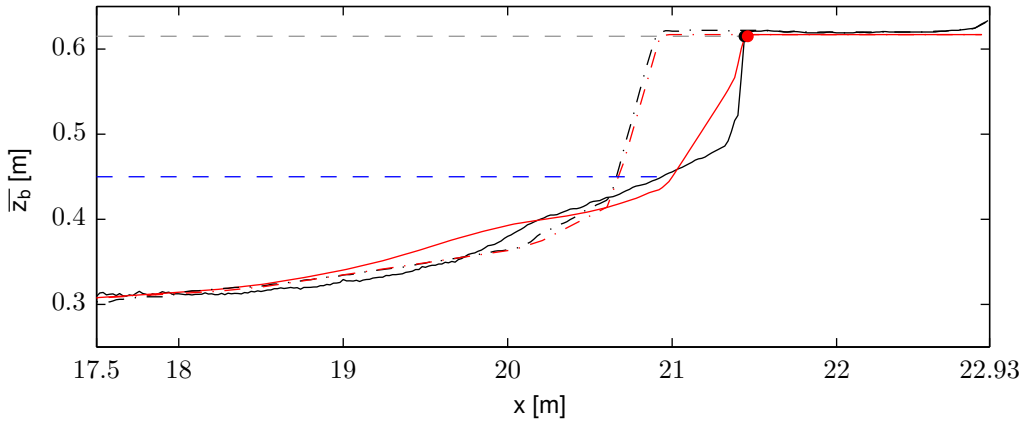

Figure 5.10: Predicted final mean bottom elevation of breach B11 $\overline{z_{b,Pred}}$ (—) and profile measurement $\overline{z_{b,WP}}$(—), the initial bottom elevation of XBeach (– · –) and profile measurements (– · –), SSL (––), the retreat point based on profile measurement (•) and R^* of XBeach (•). An elevation of 0.615 m is indicated by (––).

In XBeach the breach in the dune revetment (B11) shows less erosion compared with the erosion of a breach in a dike with the same width (B2) in experiments V1 & V2. To quantify the erosion in the breaches the dune retreat ΔR^*_{Pred} and the erosion volume A_{Pred} is averaged over the breach width for t = 15 min, 30 min and 90 min using Equations 5.2 & 5.3 respectively. In Table 5.5 the mean dune retreat $\overline{\Delta R^*_{Pred}}$ and the mean erosion volume $\overline{A_{Pred}}$ is given for experiment V1 & V3 which both have a wave period of T_p = 2.07 s. In Table 5.6 these values are given for experiment V2 & V4 which have a wave period of T_p = 1.55 s. In Figure 5.11 the erosion values given in these tables are depicted.

Time	$\overline{\Delta R^*_{Pred}}$ [10^{-3} m]		$\overline{A_{Pred}}$ [10^{-4} m^3/m]	
[min]	B2	B11	B2	B11
15	169	166	211	210
30	269	246	367	311
90	531	476	788	655

Table 5.5: Mean breach erosion experiment V1 & V3

Time	$\overline{\Delta R^*_{Pred}}$ [10^{-3} m]		$\overline{A_{Pred}}$ [10^{-4} m^3/m]	
[min]	B2	B11	B2	B11
15	113	116	162	153
30	175	146	263	236
90	363	296	565	453

Table 5.6: Mean breach erosion experiment V2 & V4

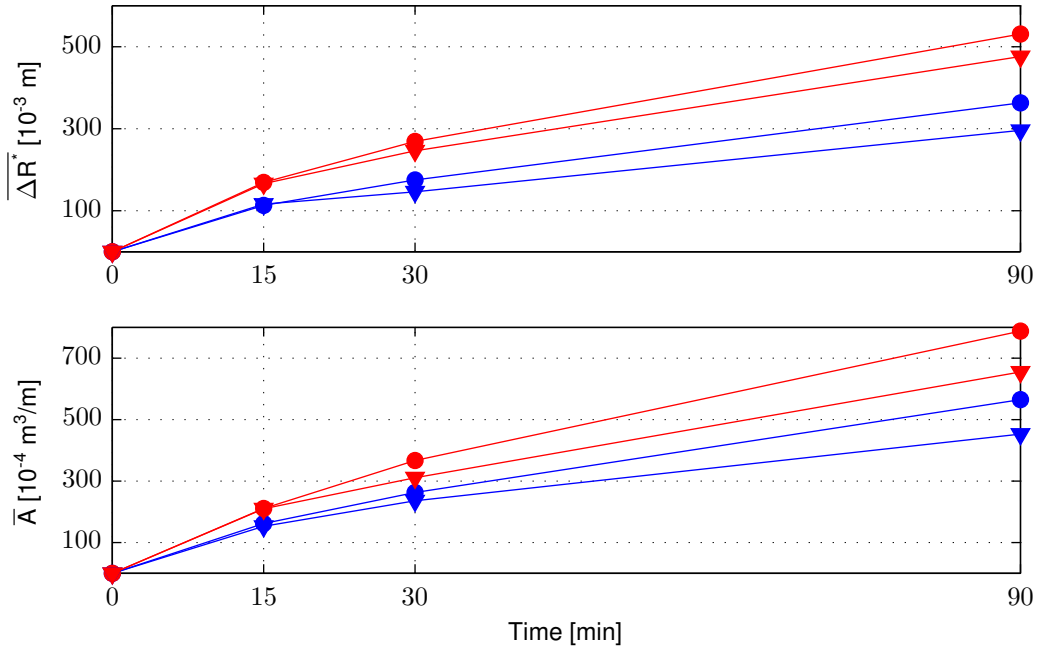

Figure 5.11: Mean breach erosion of B2 & B11. Upper panel: Mean dune crest retreat of B2 in experiment V1 (●), B11 in V3 (▼), B2 in V2 (●) and B11 in V4 (▼). Lower panel: Mean erosion volume of B2 in V1 (●), B11 in V3 (▼), B2 in V2 ● and B11 in V4 (▼).

Figure 5.11 shows that differences in $\overline{\Delta R^*_{Pred}}$ and $\overline{A_{Pred}}$ between B2 & B11 start to develop after t = 15 min. Only near the end of the simulation the differences become significant. At t = 90 min $\overline{\Delta R^*_{Pred}}$ of B2 in experiment V1 is 11% larger than $\overline{\Delta R^*_{Pred}}$ of B11 in experiment V3. Between experiment V2 & V4 this difference increases to 22%. The mean erosion volume shows comparable differences. At t = 90 min the mean erosion volume of B2 in experiment V1 is 20% larger than $\overline{A_{Pred}}$ of B11 in experiment V3. Between experiment V2 & V4 the difference again increases to 24%.

XBeach predicts less erosion in a dune revetment breach (B11) than in a breach in a dike section (B2) with an equal breach width of 0.5 m. A possible explanation is that the wave height near the dune revetment breach is lower than near breach B2. In Figure 5.12 the mean bottom elevation is presented for dune revetment sections DR11 & DR12 and dike sections H11 & H12 in experiment V3, see Figure 5.17. The depth of the scour hole in front of the structures is equal. However the foreshore in front of the revetment is higher than the foreshore in front of the dike. Consequently waves in front of the revetment start to break sooner and dissipate more energy. This results in a smaller wave height near breach B11 compared to B2.

5.4.4 Dunes

5.4.4.1 Temperal development

Dune sections were investigated in all four experiments V1-V4. The upper panel of Figure 5.15 presents a spatial overview of the measured and predicted dune crest retreat at t = 90 min of experiment V1. In dune section D2 the dune crest retreat measured by the Argus system shows a mild variation in longshore direction. ΔR^*_{WP} shows a similar variation. In D1 the longshore variation in ΔR^*_{Argus} & ΔR^*_{WP} is much larger. The longshore variation in ΔR^*_{Argus} & ΔR^*_{WP} is reflected in the erosion volume A_{WP}, see the lower panel of Figure 5.15. XBeach does not predict a longshore variation in dune erosion. The zig-zag pattern in ΔR^*_{Pred} and A_{Pred} is associated with circulation cells in front of the shore, see Figure 5.5.

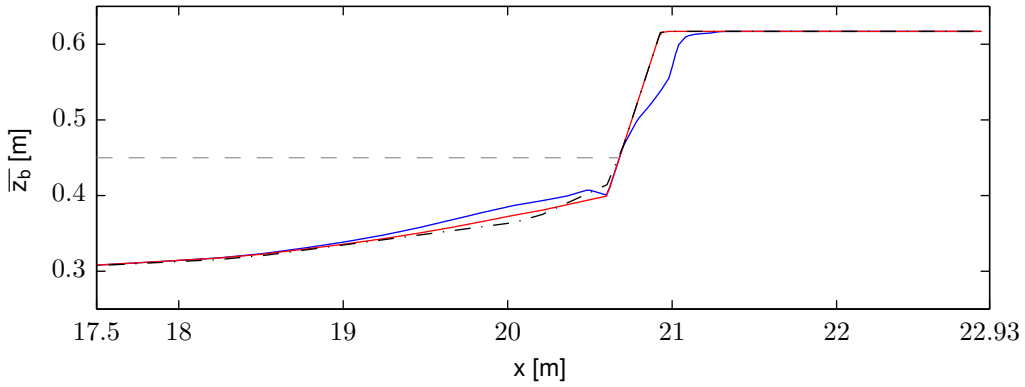

Figure 5.12: Mean bottom elevation $\overline{z_{b,Pred}}$ of dune revetment sections DR11 & DR12 (—), $\overline{z_{b,Pred}}$ of dike sections H11 & H12 (—), the SSL (– –) and the initial XBeach profile (– · –).

Experiment V2 investigated configuration 1 with a smaller wave period of T_p = 1.55 s. Compared with experiment V1 the longshore variation in the measured dune erosion in D1 & D2 increased. This is visualized by ΔR^*_{Argus}, ΔR^*_{WP} and A_{WP} in the upper and lower panel of Figure 5.16 respectively. XBeach does not predict these large variations in dune erosion. A similar behaviour is observed in dune section D11 in experiments V3 & V4 in Figures 5.17 and 5.18 respectively. Since the measured dune erosion shows large longshore variations comparison of the erosion in dune sections is focused on the development of the measured and predicted mean erosion in time. The remainder of this section explains the setup of Figure 5.19.

The upper panel of Figure 5.19 compares the development in time of $\overline{\Delta R^*_{Argus}}$, $\overline{\Delta R^*_{WP}}$ and $\overline{\Delta R^*_{Pred}}$ of dune sections D1 & D2 in experiment V1. In this panel $\overline{\Delta R^*_{Pred}}$ is red, $\overline{\Delta R^*_{Argus}}$ is blue. The standard deviation in the Argus measurements is given by a dashed blue line. Black dots indicate the mean dune crest retreat $\overline{\Delta R^*_{WP}}$ derived from the 10 profile measurements in D1 & D2. The whiskers represent the standard deviation in the profile measurements. Both $\overline{\Delta R^*_{Argus}}$, $\overline{\Delta R^*_{WP}}$ and $\overline{\Delta R^*_{Pred}}$ were calculate with Equation 5.2.

The middle panel of Figure 5.19 compares the development in time of $\overline{A_{WP}}$ and $\overline{A_{Pred}}$ of dune sections D1 & D2 in experiment V1. In this panel $\overline{A_{Pred}}$ is a solid red line. The standard deviation in the prediction is given by a dashed red line. Black dots indicate the mean erosion volume $\overline{A_{WP}}$ derived from the profile measurements in D1 & D2. The whiskers represent the standard deviation. Both $\overline{A_{WP}}$ and $\overline{A_{Pred}}$ were calculate with Equation 5.3.

In the lower panel of Figure 5.19 the bottom elevation is compared. The final predicted mean bottom elevation $\overline{z_{b,Pred}}$ is the solid red line. The final mean bottom elevation based on profile measurements $\overline{z_{b,WP}}$ is a solid black line. The mean initial profile in XBeach is given by a dashed red line. The mean initial profile in the experiments is a dashed black line. The figure also presents gray dashed lines which indicate the minimum and maximum bottom elevation measured within the comparison stretch. The dimensions of the comparison stretches are given in Table 4.6.

Figures 5.20, 5.21 and 5.22 on Pages 105 - 107 present this statistical information for the dune sections of experiment V2, V3 and V4 respectively. The following sections describe the results presented in these figures in detail.

5.4.4.2 Experiment V1; Dune section D1 & D2

In experiment V1 two dune section were investigated D1 & D2. Near the wave damping beach at y = 0 the measured dune erosion decreases, see section D1 in Figure 5.15. Near structures XBeach predicts additional dune erosion which is among others visible at connection D1-H1 in Figure 5.15. In experiment V1 the foreshore raised very little near x = 20 m, see lower panel of Figure 5.19. Furthermore the erosion volume above SSL is larger than the sedimentation volume below SSL. The erosion volume A is equal to the surface area confined by the initial profile and the final profile above SSL. The sedimentation volume is equal to the surface area confined by the initial profile and the final profile below SSL.

Above SSL the final $\overline{z_b}$ predicted by XBeach generally lies between the minimum and maximum measured bottom elevation, see lower panel of Figure 5.19. The predicted foreshore is higher than the measured elevation of the foreshore. Despite this difference the bottom profile predicted by XBeach shows a close resemblance with the measurements. For x≤19 m the predicted profile is almost identical to the measured elevation. The initial mean profiles deviate slightly from each other, see Figure 5.13 and the lower panel of Figure 5.19.

The predicted mean erosion volume $\overline{A_{Pred}}$, displayed in the middle panel of Figure 5.19, is smaller than $\overline{A_{WP}}$. Only at t = 90 min $\overline{A_{Pred}}$ falls within the standard deviation of the measurements. The predicted mean dune crest retreat $\overline{\Delta R^*_{Pred}}$ in the upper panel of Figure 5.19 is generally larger than one times the standard deviation of the Argus measurements. Regarding $\overline{\Delta R^*_{WP}}$ derived from profile measurements $\overline{\Delta R^*_{Pred}}$ falls within the standard deviation of the measurements for t = 30 min & t = 90 min.

There is only a minor difference between the predicted and measured mean bottom elevation $\overline{z_b}$ above SSL. Despite this the difference between $\overline{\Delta R^*_{Pred}}$ and $\overline{\Delta R^*_{WP}}$ is much larger, see the upper panel of Figure 5.19. This is caused by the definition of the retreat point R^*. It is defined as the x-coordinate of the grid point which is farthest offshore and from which the bottom elevation is larger than 0.615 m. Figure 5.13 zooms in on the lower panel of Figure 5.19. The dashed gray line lies at z_b = 0.615 m. The black and red dot represent R^* based on profile measurements and XBeach respectively. A cross-shore difference is clearly visible which explains why in the upper panel of Figure 5.19 $\overline{\Delta R^*_{Pred}}$ is larger than $\overline{\Delta R^*_{WP}}$.

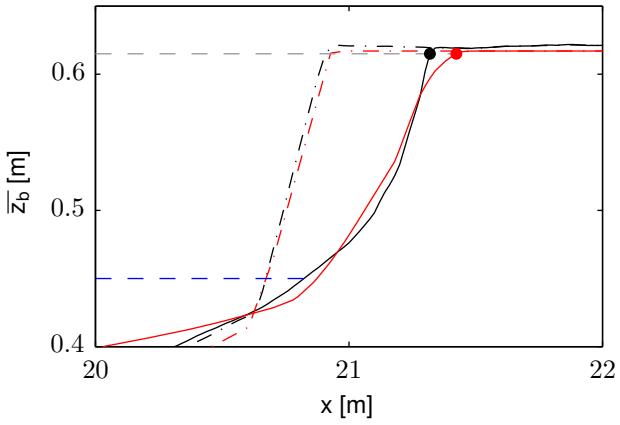

Figure 5.13: Mean bottom elevation of Figure 5.19 with the retreat point based on profile measurements (•) and R^* of XBeach (•). A elevation of $\overline{z_b}$ = 0.615 m is represented by (−−).

The initial profile above SSL of XBeach lies onshore of the mean initial profile of the experiments, see the dashed lines in Figure 5.13. Onshore there is a small difference in elevation. This is partially caused by the difference between the intended initial profile in the Delta Basin and the initial profile of XBeach as described in Subsection 5.3.3. Furthermore measurements revealed that the maximum difference in bottom elevation between the initial profile constructed in the Delta Basin and the intended profile was in the order of 1 cm.

The difference in the initial profiles explains why $\overline{A_{Pred}}$ in the middle panel of Figure 5.19 is less than $\overline{A_{WP}}$. During the experiments sediment was transported beyond the seaward boundary of the wheelprofiler (x = 17.5 m). Sediment ended up on the concrete offshore area between the wave guiding walls were a 1 cm thick layer of sand was observed, see Subsection 4.6.2. XBeach predicts a larger rise of the foreshore which makes the profile more efficient in dissipating the incoming wave energy. Therefore XBeach is expected to predict less dune erosion than was measured in the experiments.

Despite some differences the overall performance of XBeach is rather good especially regarding the mean bottom elevation in the lower panel of Figure 5.19. In Table 5.7 the magnitude of the measured and predicted $\overline{\Delta R^*}$ and $\overline{A}$ are displayed for both experiment V1 & V2.

5.4.4.3 Experiment V2; Dune section D1 & D2

In experiment V2 the 2 dune section D1 & D2 were investigated with a wave period of T_p = 1.55 s, see Table 4.2. In this experiment the foreshore raised only little near x = 20 m, see the lower panel of Figure 5.20. The predicted rise of the foreshore is higher than the measured elevation of the foreshore. Seaward from x = ±18.5 m a bar developed in the experiments. In XBeach the difference between the initial and final profile offshore from x = 18.5 m is negligible which indicates that XBeach predicts little morphological activity seaward of x = 18.5 m. Despite this difference $\overline{z_{b,Pred}}$ lies between the minimum and maximum measured bottom elevation offshore from x = ±19.5 m. For x≤19 m the predicted profile is almost identical to the measured elevation. Above SSL the shape of the predicted bottom profile is similar to the measured bottom profile but has an offset in seaward direction.

The middle panel of Figure 5.20 clearly shows that $\overline{A_{Pred}}$ is less than $\overline{A_{WP}}$. Throughout the experiment this difference remains relatively constant. At t = 15 min $\overline{A_{Pred}}$ is 39% smaller than $\overline{A_{WP}}$. For t = 30 min & t = 90 min this is 41.8% and 39.5% respectively.

For t ≤ 15 min $\overline{\Delta R^*_{Pred}}$ is larger than $\overline{\Delta R^*_{Argus}}$ and lies above the standard deviation of the Argus measurements. For 15 min < t < 74 min $\overline{\Delta R^*_{Pred}}$ lies within the standard deviation of the measurements. For t ≥ 74 min $\overline{\Delta R^*_{Pred}}$ is larger than $\overline{\Delta R^*_{Argus}}$ one and lies above the standard deviation, see the upper panel of Figure 5.20. At t = 90 min $\overline{\Delta R^*_{Pred}}$ is 22.4% smaller than $\overline{\Delta R^*_{Argus}}$. This would indicates that the rate of dune crest retreat decreases to rapidly in XBeach. In Table 5.7 the magnitude of the measured and predicted mean erosion parameters $\overline{\Delta R^*}$ and $\overline{A}$ for experiment V1 & V2 are displayed. In Subsubsection 5.4.4.6 the influence of the wave period on the amount of dune erosion is described.

Time [min]	$\overline{\Delta R^*}$ [10^{-3} m]				$\overline{A}$ [10^{-4} m^3/m]			
	V1		V2		V1		V2	
	$\overline{\Delta R^*_{Argus}}$	$\overline{\Delta R^*_{Pred}}$	$\overline{\Delta R^*_{Argus}}$	$\overline{\Delta R^*_{Pred}}$	$\overline{A_{WP}}$	$\overline{A_{Pred}}$	$\overline{A_{WP}}$	$\overline{A_{Pred}}$
15	86	146	70	104	258	195	251	153
30	161	226	143	135	403	293	378	220
90	316	394	313	243	629	575	655	395

Table 5.7: Mean dune erosion (D1 & D2) of experiments V1 & V2

5.4.4.4 Experiment V3; Dune section D11

In experiment V3 one dune section (D11) was investigated. The measurements show a large longshore variation in dune erosion visible in both the dune crest retreat ΔR^*_{Argus} & ΔR^*_{WP}, in the upper panel of Figure 5.17, and the erosion volume A_{WP} in the lower panel of Figure 5.17. Unlike XBeach the measurements show no additional erosion near connection D11-H12 within the comparison stretch of D11. The performance of XBeach in experiment V3 is very similar to the performance in experiment V1. Above SSL the predicted mean bottom elevation $\overline{z_{b,Pred}}$ shows a close resemblance with $\overline{z_{b,WP}}$, see the lower panel of Figure 5.21. It generally lies within the minimum and maximum measured elevation except near x = 21 m. In the experiment the foreshore raised only little. Similar to experiments V1 & V2 XBeach predicts a larger rise of the foreshore. For x ≤ 18.5 m the predicted and measured bottom elevation is almost identical.

The predicted mean erosion volume $\overline{A_{Pred}}$ is smaller than $\overline{A_{WP}}$ and only falls within the standard deviation of the measurements at t = 90 min, see the middle panel of Figure 5.21. Throughout the experiment the difference between $\overline{A_{Pred}}$ and $\overline{A_{WP}}$ expressed in m^3/m remains relatively constant. At t = 15 min $\overline{A_{Pred}}$ is $144{\cdot}10^{-4}$ m^3/m smaller than $\overline{A_{WP}}$. For t = 30 min & t = 90 min this is $157{\cdot}10^{-4}$ m^3/m and $115{\cdot}10^{-4}$ m^3/m respectively. Since $\overline{A_{Pred}}$ and $\overline{A_{WP}}$ increases in time the relative difference decreases throughout the experiment. At t = 15 min $\overline{A_{Pred}}$ is 44.6% smaller than the measured erosion volume. For t = 30 min & t = 90 min this is 37.2% and 18% respectively.

For t ≥ 15 min the predicted mean dune crest retreat $\overline{\Delta R^*_{Pred}}$ lies around the standard deviation of the Argus measurements. Compared with $\overline{\Delta R^*_{WP}}$ derived from profile measurements $\overline{\Delta R^*_{Pred}}$ at t = 15 min, 30 min and 90 min is almost equal, see the upper panel of Figure 5.21. Despite some differences the overall performance of XBeach is very good especially regarding the mean bottom elevation. Table 5.8 gives the magnitude of the predicted and measured mean erosion parameters $\overline{\Delta R^*}$ and $\overline{A}$ for experiment V3 & V4.

5.4.4.5 Experiment V4; Dune section D11

In experiment V4 dune section D11 was investigated with a wave peak period of T_p = 1.55 s, see Table 4.2. In accordance with previous experiments the foreshore raised little near x = 20 m. XBeach predicts the foreshore to rise higher than the measured elevation of the foreshore, see the lower panel of Figure 5.22. Seaward from x = ±19 m a bar developed in the experiments. The difference between the initial and final profile in XBeach for x ≤ 19 is negligible. This indicates that XBeach predicts little morphological activity seaward of x = 19 m. Despite this difference $\overline{z_{b,Pred}}$ generally lies between the minimum and maximum measured bottom elevation offshore from x = ±19 m. Above SSL the shape of the predicted bottom profile is similar to the measured bottom profile but has an offset in seaward direction.

The predicted mean erosion volume $\overline{A_{Pred}}$ is less than the measured $\overline{A_{WP}}$ and falls outside the standard deviation of the measurements, see the middle panel of Figure 5.22. The difference between $\overline{A_{WP}}$ and $\overline{A_{Pred}}$ increases throughout the experiment. At t = 15 min $\overline{A_{Pred}}$ is $150{\cdot}10^{-4}$ m^3/m smaller than $\overline{A_{WP}}$. For t = 30 min & t = 90 min this is $179{\cdot}10^{-4}$ m^3/m and $266{\cdot}10^{-4}$ m^3/m respectively. The relative difference remains constant throughout the experiment. At t = 15 min $\overline{A_{Pred}}$ is 46.0% smaller than $\overline{A_{WP}}$. For t = 30 min & t = 90 min this is 45.5% and 41.5% respectively. This indicates that despite the difference in magnitude the development of $\overline{A}$ in time is simulated well by XBeach.

The behaviour of the predicted mean dune crest retreat $\overline{\Delta R^*_{Pred}}$ compared with the measured $\overline{\Delta R^*_{Argus}}$ is similar to the behaviour in experiment V2. For t ≤ 15 min $\overline{\Delta R^*_{Pred}}$ is larger than the $\overline{\Delta R^*_{Argus}}$ and lies above the standard deviation of the Argus measurements. For 15 min < t < 75

min $\overline{\Delta R^*_{Pred}}$ lies within the standard deviation of the measurements. For t ≥ 75 min $\overline{\Delta R^*_{Pred}}$ is larger than $\overline{\Delta R^*_{Argus}}$ and lies above the standard deviation, see the upper panel of Figure 5.20. At t = 15 min the predicted $\overline{\Delta R^*_{Pred}}$ is 57.8% larger than $\overline{\Delta R^*_{Argus}}$. For t = 30 min this is 5.2%. For t = 90 min $\overline{\Delta R^*_{Pred}}$ is 21.7% smaller than $\overline{\Delta R^*_{Argus}}$. This indicates that the rate of dune crest retreat decreases to rapidly in XBeach. In Table 5.8 the magnitude of the predicted and measured mean erosion parameters $\overline{\Delta R^*}$ and $\overline{A}$ for experiment V3 & V4 are displayed. In Subsubsection 5.4.4.6 the influence of the wave period on the amount of dune erosion is described.

Time [min]	$\overline{\Delta R^*}$ [10^{-3} m]				$\overline{A}$ [10^{-4} m^3/m]			
	V3		V4		V3		V4	
	$\overline{\Delta R^*_{Argus}}$	$\overline{\Delta R^*_{Pred}}$	$\overline{\Delta R^*_{Argus}}$	$\overline{\Delta R^*_{Pred}}$	$\overline{A_{WP}}$	$\overline{A_{Pred}}$	$\overline{A_{WP}}$	$\overline{A_{Pred}}$
15	95	149	64	101	323	179	278	150
30	181	225	142	134	422	265	393	214
90	321	385	300	235	640	525	641	375

Table 5.8: Mean dune erosion (D11) of experiments V3 & V4

5.4.4.6 Influence of the wave period

In the Delta Basin the wave period decreased with 25.1% from T_p = 2.07 s for experiments V1 & V3 to T_p = 1.55 s for experiments V2 & V4. Based on research by van Gent to the influence of the wave period on dune erosion a decrease in the dune erosion is expected. The effect of the wave period on dune erosion reduces in time (Van Gent *et al.*, 2008). The decrease in dune erosion is calculated by subtracting the magnitude of the erosion parameters of experiment V2/V4 from the magnitude of experiment V1/V3 and subsequently dividing it by the magnitude of the erosion parameters of experiment V2/V4, see Equation 5.5 and Equation 5.6. In these equations α stands for V1/V3 and β for V2/V4. The magnitude of the erosion parameters are given in Table 5.7 and Table 5.8. In Table 5.9 the decrease in dune erosion between experiments V1 & V2 is given. Between experiments V3 & V4 this information is given in Table 5.10. The decrease in dune erosion is visualized in Figure 5.14.

$$\delta_{\overline{\Delta R^*}}(t) = \frac{\overline{\Delta R^*}(t,\alpha) - \overline{\Delta R^*}(t,\beta)}{\overline{\Delta R^*}(t,\beta)} \quad \text{with t = [15, 30, 90]} \quad \alpha = \text{V1, V3} \quad \beta = \text{V2, V4} \quad (5.5)$$

$$\delta_{\overline{A}}(t) = \frac{\overline{A}(t,\alpha) - \overline{A}(t,\beta)}{\overline{A}(t,\beta)} \quad \text{with t = [15, 30, 90]} \quad \alpha = \text{V1, V3} \quad \beta = \text{V2, V4} \quad (5.6)$$

Time	$\delta_{\overline{\Delta R^*}}$ [%]		$\delta_{\overline{A}}$ [%]	
[min]	Delta Basin	XBeach	Delta Basin	XBeach
15	-18.6	-28.8	-2.7	-21.5
30	-11.2	-40.3	-6.2	-24.9
90	-0.9	-38.3	4.1	-31.3

Table 5.9: Decrease in the erosion of dune sections D1 & D2 between experiments V1 & V2

Time	$\delta_{\overline{\Delta R^*}}$ [%]		$\delta_{\overline{A}}$ [%]	
[min]	Delta Basin	XBeach	Delta Basin	XBeach
15	-32.6	-32.2	-13.9	-16.2
30	-21.6	-40.4	-6.9	-19.3
90	-6.5	-39.0	0.2	-28.6

Table 5.10: Decrease in the erosion of dune section D11 between experiments V3 & V4

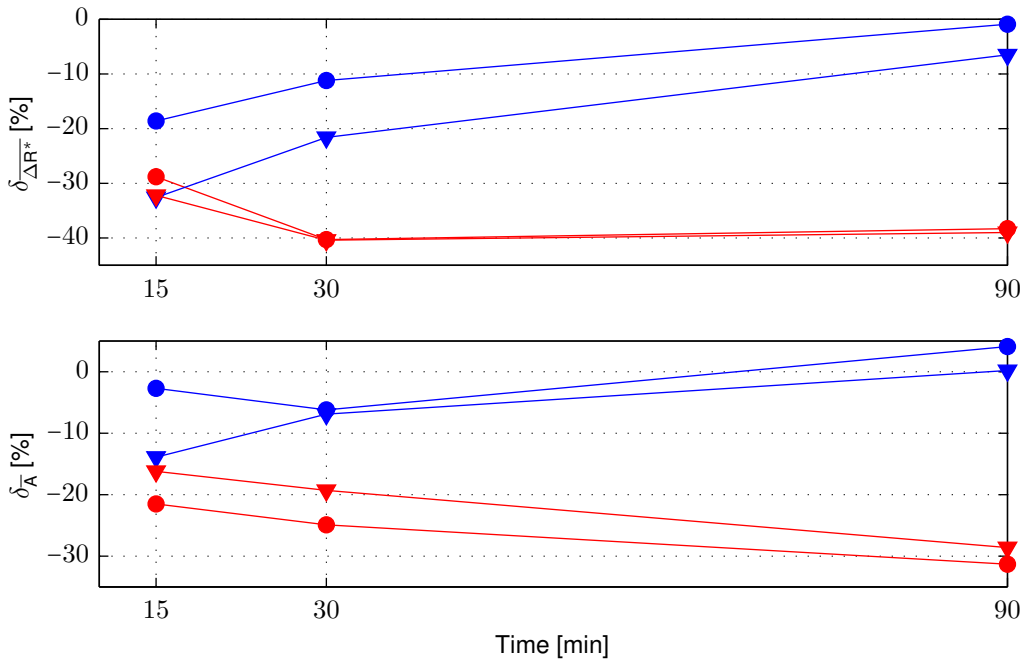

Figure 5.14: Comparison of the decrease in dune erosion between experiment V1 & V2 (T_p = 2.07 s & T_p = 1.55 s respectively) and experiments V3 & V4 (T_p = 2.07 s & T_p = 1.55 s respectively). Upper panel: Decrease in $\overline{\Delta R^*_{Argus}}$ between experiments V1 & V2 (●) and between experiments V3 & V4 (▼). Decrease in $\overline{\Delta R^*_{Pred}}$ between experiments V1 & V2 (●) and between experiments V3 & V4 (▼). Lower panel: Decrease in $\overline{A_{WP}}$ between experiments V1 & V2 (●) and between experiments V3 & V4 (▼). Decrease in $\overline{A_{Pred}}$ between V1 & V2 (●) and between V3 & V4 (▼).

The predicted decrease in the mean dune crest retreat $\delta_{\overline{\Delta R^*}}$ between experiment V1 & V2 and V3 & V4 are almost identical, see the upper panel of Figure 5.14. Regarding the predicted $\delta_{\overline{A}}$ the differences between experiment V1 & V2 and V3 & V4 are also minor, see the lower panel of Figure 5.14. This indicates that the configuration of dunes and hard structures had little influence on the decrease of the dune erosion. Throughout the experiment both the measured $\delta_{\overline{\Delta R^*}}$ and $\delta_{\overline{A}}$ decreases. This is consistent with research on the effect of the wave period on dune erosion (Van Gent *et al.*, 2008). In the lower panel of Figure 5.14 it is clearly visible that the predicted $\delta_{\overline{A}}$ increases in time. In the upper panel of Figure 5.14 the predicted $\delta_{\overline{\Delta R^*}}$ increases between t = 15 min & t = 30 min. Between t = 30 min & t = 90 min a very small decrease in the predicted $\delta_{\overline{\Delta R^*}}$ is observed. This decrease is negligible compared to the decrease in the measured $\delta_{\overline{\Delta R^*}}$. The predicted values of $\delta_{\overline{\Delta R^*}}$ are much higher than the measured $\delta_{\overline{\Delta R^*}}$. Generally the influence of the wave period on dune erosion increases in XBeach. This indicates that the effect of the wave period on dune erosion is not simulated correctly by XBeach for 2DH models with a large depth scale n_d = 60.

5.5 Discussion

5.5.1 Disturbing processes

During the experiments processes were observed which affected the morphological development. A longshore variation in wave height was present in all experiments. This resulted in longshore variations in the bathymetry. Gully formation had a profound impact on the development of additional erosion near the hard structures. At the lateral boundaries of the model the wave damping beaches caused dunes within their region of influence to receive less wave energy which consequently resulted in less erosion. The longshore current in front of the connection tends to refract the waves away from the dunes next to the structure, see Subsubsection 2.5.2.3. This wave-current interaction is not simulated by XBeach. It is however assumed that the absence of the wave-current interaction in XBeach will only have a minor influence on the development of additional erosion near the structures.

5.5.2 Boundary condition behaviour

In Section 3.6 it was already mentioned that under certain conditions Neumann boundaries show unwanted behaviour. Often a flow of water through the model boundaries was generated. In extreme cases the water level in the model raised which accelerated the dune erosion process. The parameter epsi (Section 3.6) can prevent the water level to rise beyond a certain threshold. However a small and consistent current between the model boundaries influences the morphological development of the coast. This current was also observed for normally incident waves under certain conditions.

The exploratory simulations of experiment V3 furthermore showed that well behaving Neumann boundaries produce a similar morphological response compared to models with Wall boundaries. However applying the same boundary settings for experiment V1 resulted in high current velocities at right model boundary. These velocities rapidly eroded the adjacent dunes in section D2. Therefore the more rigid and stable Wall boundaries are preferred above Neumann boundaries in the case of normally incident waves.

5.5.3 XBeach stability for large depth scales

The stability of XBeach for large depth scales n_d = 60 proved to be highly dependent on the computational grid. The simulations used in the comparison have an onshore grid size of dx_{min} = 0.05 m. To improve the accuracy of the prediction the onshore grid size was reduced to dx_{min} = 0.025 m. When ±55% of the simulation was completed local scour holes in front of the dunes and in the dune revetment breach (B11) developed. As the simulation continued the scour depth reached the concrete floor at a depth of -0.45 m. Avalanching and sediment transport were expected to fill the scour hole but they did not. This behaviour is caused by a wrong prediction of the sediment concentration at the waterline.

In exploratory simulations of experiment V1 an offshore scour hole developed at the start of the simulation. The scour hole development it proved to be related with the grid spacing in y-direction. Depending on the computational grid can become unstable for large depth scales. This results in scour holes which continue to grow without any restraints until it reaches a hard layer.

5.6 Conclusions

5.6.1 Breach sections B1, B2 & B3

The erosion in a dike breach is a function of the breach width and the wave period. XBeach predicts the erosion to increase for a smaller breach width, see Figure 5.6. This is contributed to the fraction of sediment volume lost to the scour hole in front of the adjacent dikes compared to the total amount of eroded sediment. Wider breaches supply more sediment to the foreshore

than narrower breaches. Therefore wider breaches lose relatively less sediment to the scour holes than narrower breaches. Consequently this results in less erosion in wider breaches. When the wave period increases the breach erosion also increases. This is consistent with research on the effect of the wave period on dune erosion (Van Gent *et al.*, 2008).

The erosion in the dike breaches (B1, B2 & B3) during the Delta Basin experiments was disturbed by various physical processes. It was influenced by a longshore variation in wave height and gully formation. Since these physical processes are not modeled by XBeach no quantitative comparison of the erosion in the breaches was made.

5.6.2 Dune revetment sections DR11 & DR12

XBeach underestimates the erosion above the dune revetment. An explanation for these large differences between measurements and prediction is that to erode the dunes above the revetment waves must reach the dune front. Therefore wave runup is an important process in the development of the erosion above the revetment. Currently XBeach only simulates long wave runup. Therefore it is concluded that in agreement with the testbed report (Deltares, 2010) wave runup of short waves should also be included in the avalanching algorithm.

5.6.3 Breach in a dune revetment B11

The erosion in the revetment breach (B11) is predicted well. The predicted dune crest retreat shows a close resemblance with the measurements. The erosion volume is slightly underestimated. This is caused by a different shape of the predicted profile, see Figure 5.10. The comparison between a dune revetment breach (B11) and a breach in a dike (B2) with an equal width revealed that the erosion in revetment breach B11 is less than the erosion in dike breach B2, see Figure 5.11. This is associated with the fact that the foreshore in front of the revetment raised more than the foreshore in front of the dike, see Figure 5.12. Consequently the wave height in B11 is less than in B2.

5.6.4 Dunes

For experiments V1 & V3 with a wave period of T_p = 2.07 seconds the predictive capabilities of XBeach are very good. In experiments V1 & V3 $\overline{z_{b,Pred}}$ above SSL shows a close resemblance with $\overline{z_{b,WP}}$, see the lower panel of Figures 5.19 and 5.21. The predicted mean erosion volume $\overline{A_{Pred}}$ is slightly underestimated, see the middle panel of Figures 5.19 and 5.21. This is explained by the fact that the foreshore in XBeach raised more than in the experiments. The development in time of $\overline{A_{Pred}}$ is simulated well by XBeach. For both experiments $\overline{\Delta R^*_{Pred}}$ is larger than $\overline{\Delta R^*_{Argus}}$, see the upper panel of Figures 5.19 and 5.21. This is caused by the definition of the retreat point R^*, see Figure 5.13. The difference with the mean dune crest retreat derived from profile measurements $\overline{\Delta R^*_{WP}}$ is smaller. The development in time of $\overline{\Delta R^*_{Pred}}$ shows a close resemblance with the measured time development of $\overline{\Delta R^*_{Argus}}$.

The performance of XBeach for experiments V2 & V4 with a wave period of T_p = 1.55 seconds is relatively good. The predicted shape of the mean bottom elevation above SSL is similar to $\overline{z_{b,WP}}$ derived from the profile measurements, but has an offset in seaward direction. Offshore from x = ±19.5 m $\overline{z_{b,Pred}}$ is between the minimum and maximum measured values. In both experiments a bar developed seaward of x = ±18.5 m which was not predicted by XBeach, see the lower panel of Figures 5.20 and 5.22. The development in time of $\overline{\Delta R^*_{Pred}}$ is not simulated properly by XBeach. The predicted rate of dune crest retreat decreases too rapidly in XBeach, see the upper panel of Figures 5.20 and 5.22. Despite this the predicted $\overline{\Delta R^*_{Pred}}$ is for roughly 66% of the time within the standard deviation of the Argus measurements. The predicted mean erosion volume $\overline{A_{Pred}}$ is underestimated, see the middle panel of Figures 5.20 and 5.22. This is partially

explained by the fact that the foreshore in XBeach raised more than in the experiments. The development in time of $\overline{A_{Pred}}$ is simulated well by XBeach. Generally the performance of XBeach for experiments V2 & V4 is less than in experiments V1 & V3 but is still considered to be relatively good.

5.6.4.1 Influence of the wave period

The peak frequency of the Jonswap spectrum proved to have a relatively large influence on the amount of dune erosion predicted by XBeach. In the experiments the influence of the wave period on the amount of dune erosion decreased over time. XBeach generally shows an increase of the influence of the wave period on the amount of dune erosion in time, see Figure 5.14. Therefore it is concluded that without improvements XBeach doesn't properly simulate the effect of the wave period for 2DH models with a large depth scale (n_d = 60).

The predicted decrease in the mean dune crest retreat $\delta_{\overline{\Delta R}}$ between experiment V1 & V2 and V3 & V4 are almost identical, see the upper panel of Figure 5.14. The predicted $\delta_{\overline{A}}$ also shows only minor differences between experiment V1 & V2 and V3 & V4, see the lower panel of Figure 5.14. It is concluded that the configuration of dunes and hard structures had little influence on the decrease of the dune erosion.

5.6.5 XBeach stability for large depth scales

The stability of XBeach for small depth scales proved to be highly dependent on the calculation grid. The unrestrained depth of the scour holes prevent XBeach from being stable for large depth scales. Furthermore Neumann boundaries were often observed to generate unwanted longshore currents for normally incident waves. This influenced the morphological development of the shoreline. Much like the generation of local scour holes the location and flow velocity at the lateral boundaries seems to be random and no clear pattern can be distinguished on first sight.

5.7 Recommendations

Insights obtained from the exploratory simulations and the comparison between XBeach simulations and Delta Basin measurements are formulated in the following recommendations.

- Resolve the grid dependent stability issues of XBeach revealed by the development of deep scour holes in front of sandy sections.
- Improve the behaviour of Neumann boundary conditions.
- Improve the influence of the wave period on dune erosion for small depth scales.
- Include short wave runup in the avalanching algorithm to better predict erosion above a dune revetment.

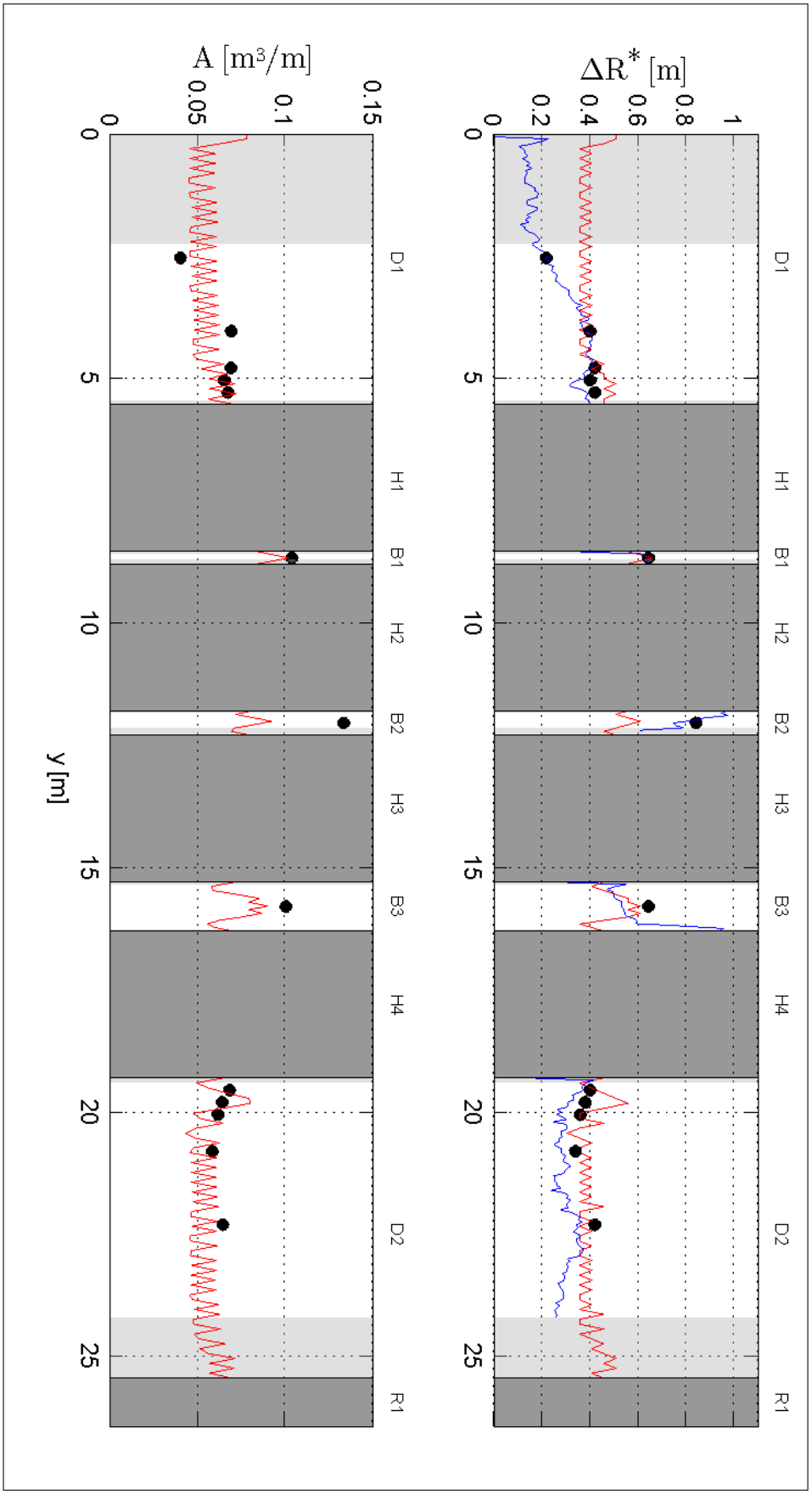

Figure 5.15: Experiment V1: Spatial comparison at the end of the experiment at t = 90 min. Upper panel: Spatial overview of the dune crest retreat ΔR^* measured by the Argus system (—), the profile measurements (•) and the XBeach prediction (—). Lower panel: Spatial overview of erosion volume A based on profile measurements (•) and the XBeach prediction (—).

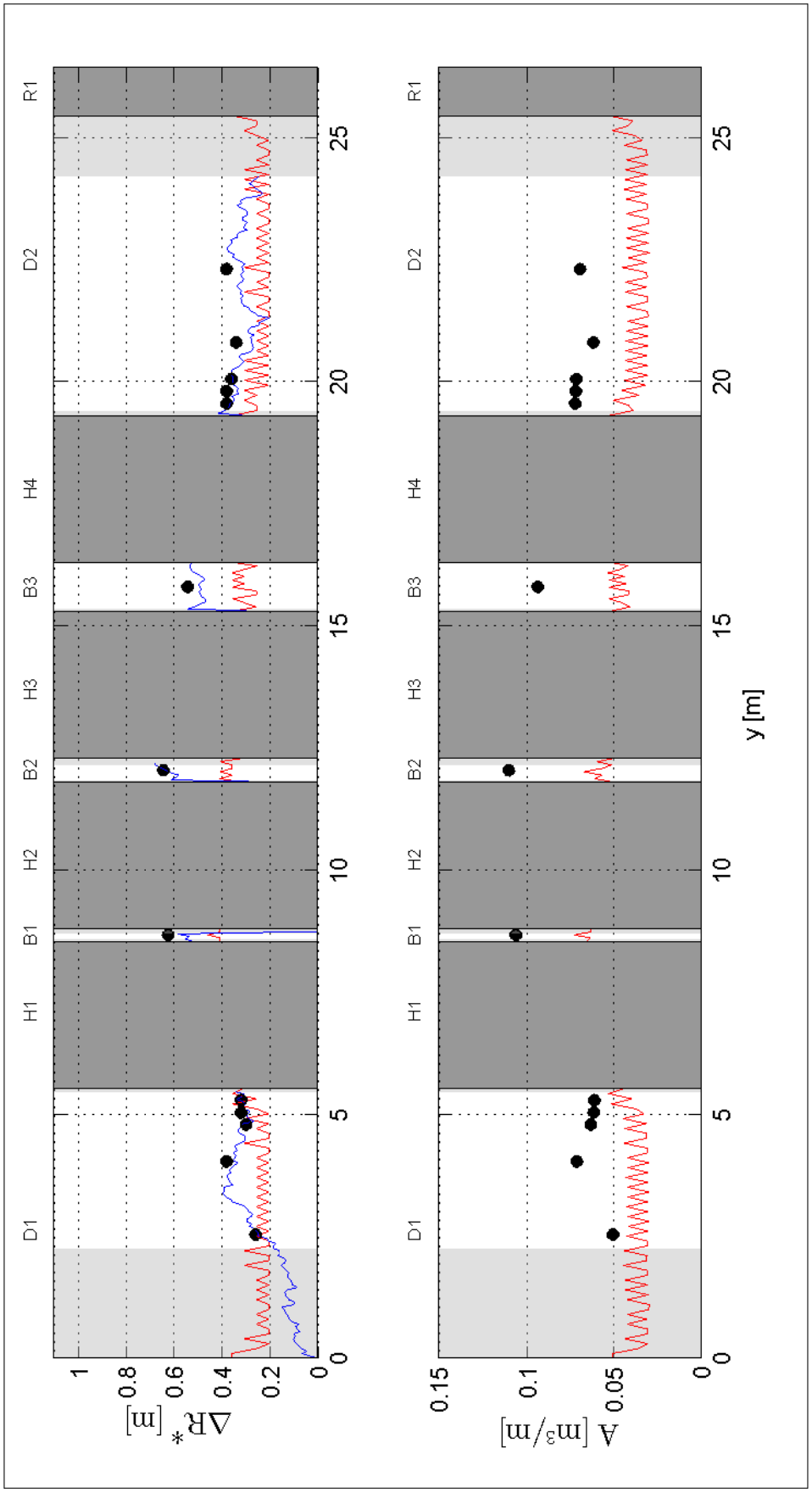

Figure 5.16: Experiment V2: Spatial comparison at the end of the experiment at t = 90 min. Upper panel: Spatial overview of the dune crest retreat ΔR^* measured by the Argus system (—), the profile measurements (•) and the XBeach prediction (—). Lower panel: Spatial overview of erosion volume A based on profile measurements (•) and the XBeach prediction (—).

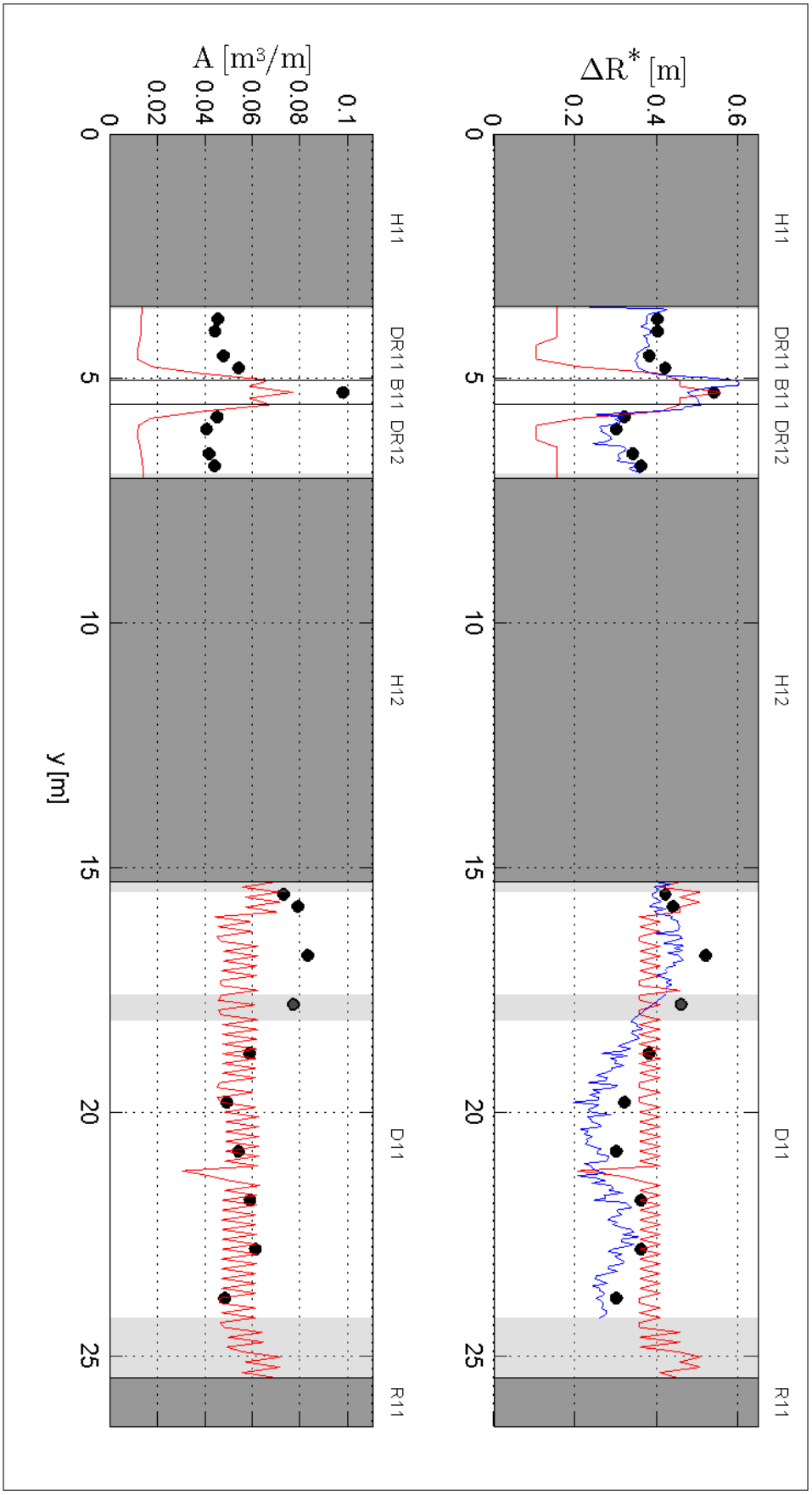

Figure 5.17: Experiment V3: Spatial comparison at the end of the experiment at t = 90 min. Upper panel: Spatial overview of the dune crest retreat ΔR^* measured by the Argus system (—), the profile measurements (•) and the XBeach prediction (—). Lower panel: Spatial overview of erosion volume A based on profile measurements (•) and the XBeach prediction (—).

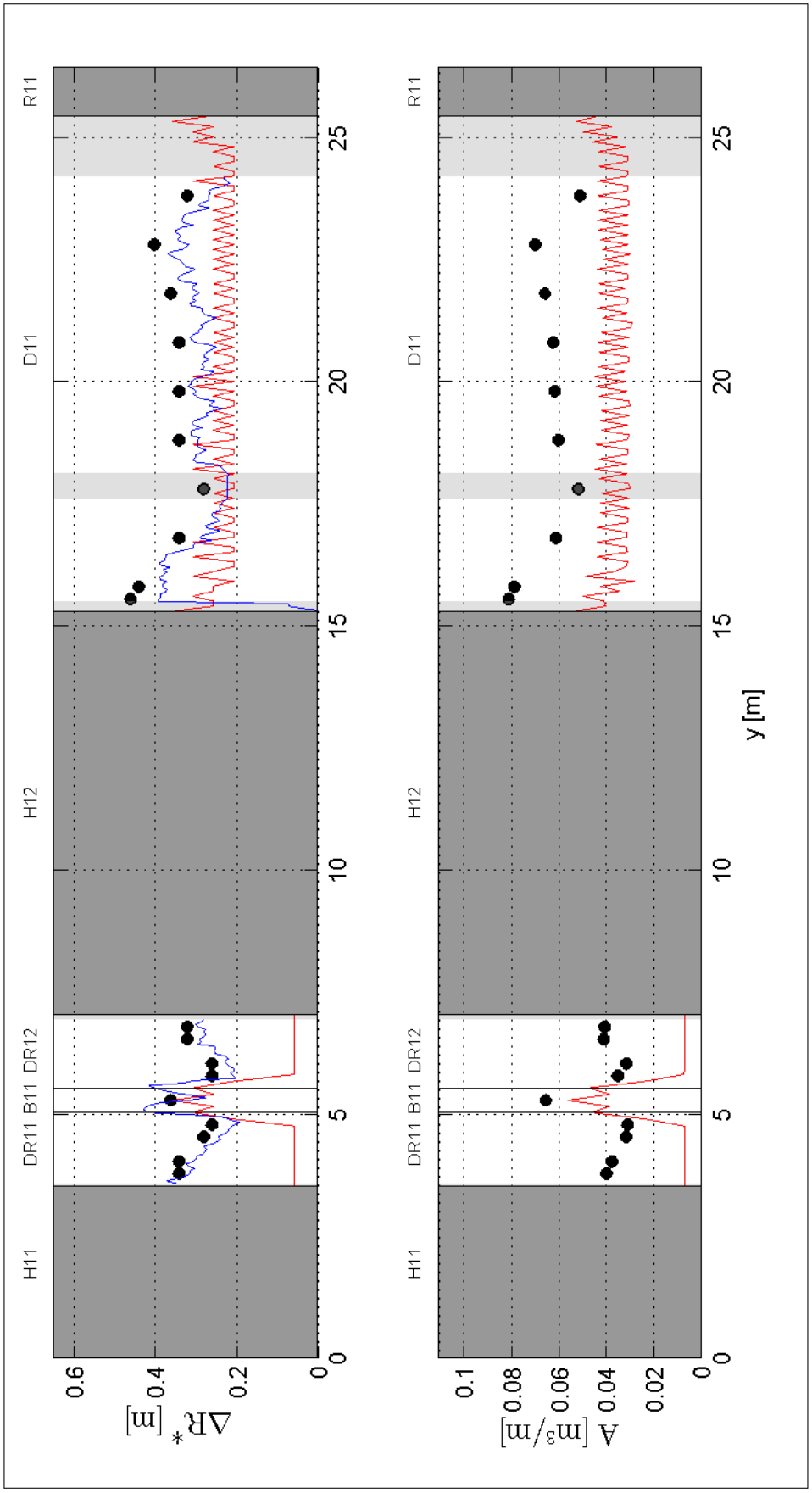

Figure 5.18: Experiment V4: Spatial comparison at the end of the experiment at t = 90 min. Upper panel: Spatial overview of the dune crest retreat ΔR^* measured by the Argus system (—), the profile measurements (•) and the XBeach prediction (—). Lower panel: Spatial overview of erosion volume A based on profile measurements (•) and the XBeach prediction (—).

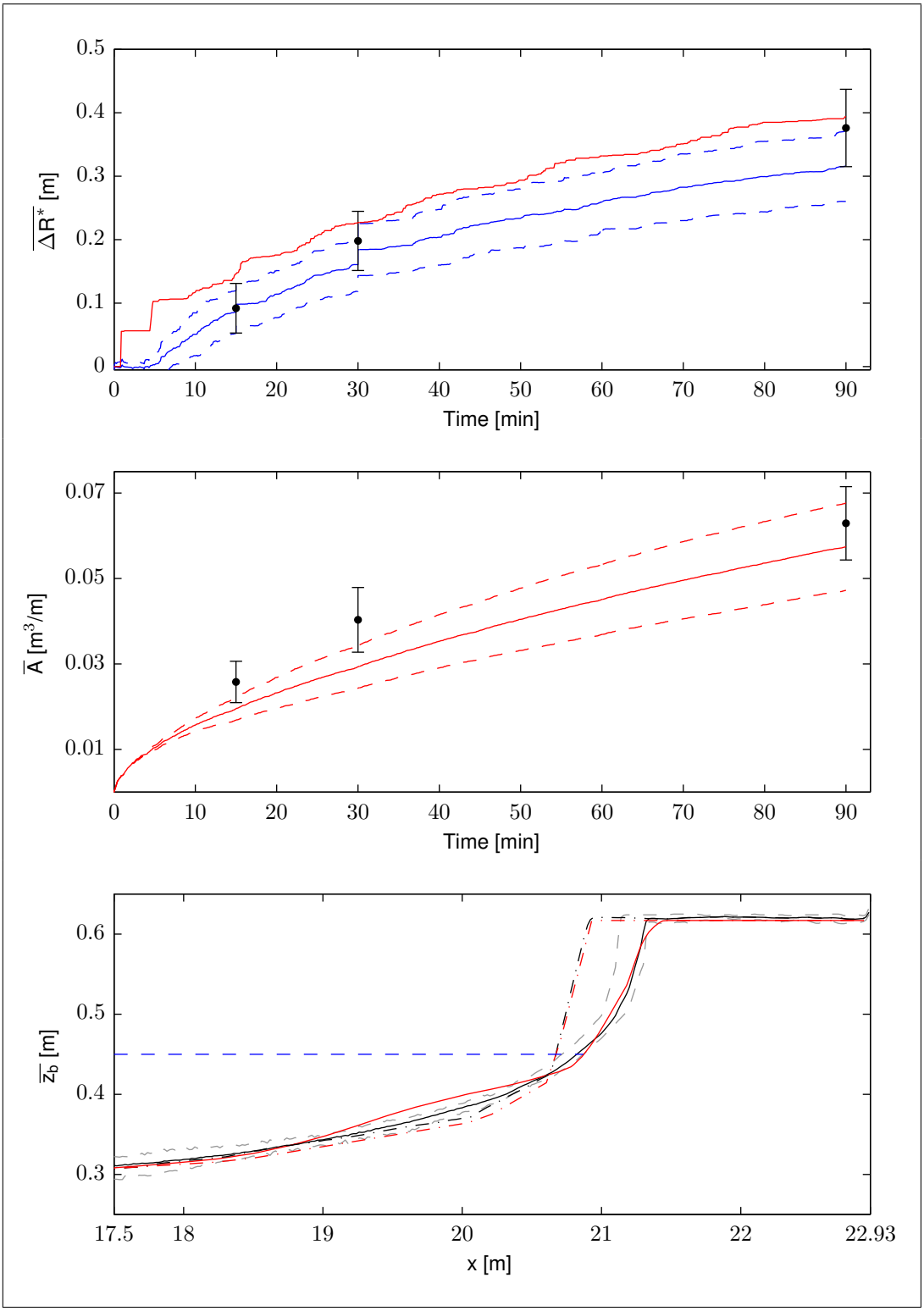

Figure 5.19: Mean erosion parameters of D1 & D2 in Experiment V1. Upper panel: Mean dune crest retreat $\overline{\Delta R^*}$ of 1. Argus measurements (—) and its standard deviation (– –), 2. XBeach (—), 3. Profile measurements (•) and its standard deviation (whiskers). Middle panel: Mean erosion volume $\overline{A}$ of 1. XBeach (—) and its standard deviation (– –), 2. Profile measurements (•) and its standard deviation (whiskers). Lower panel: Mean final bottom elevation $\overline{z_b}$ of XBeach (—) and profile measurements (—), the initial bottom elevation of XBeach (–·–) and profile measurements (–··–), SSL (– –) and minimum & maximum measured elevation (– –).

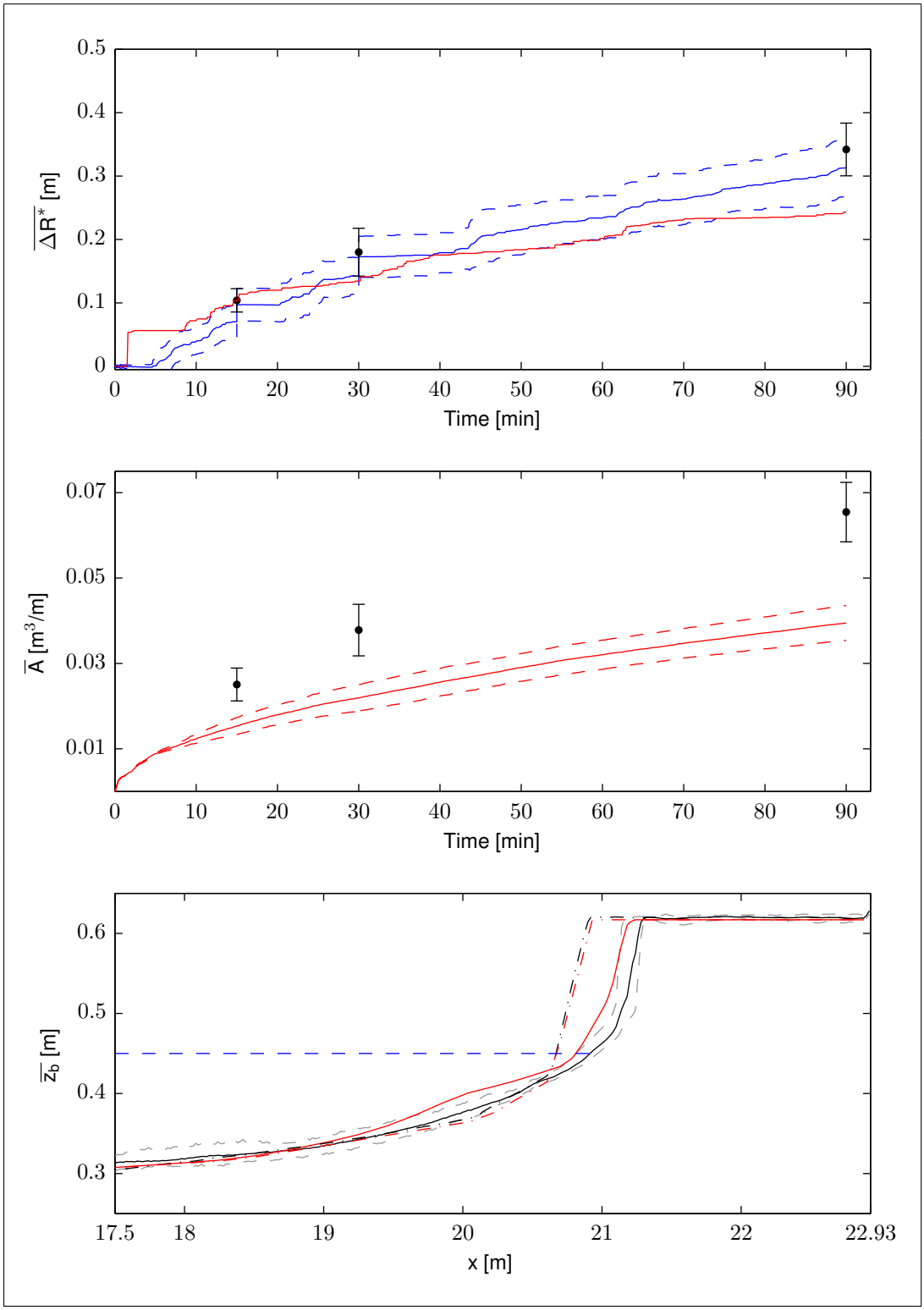

Figure 5.20: Mean erosion parameters of D1 & D2 in Experiment V2. Upper panel: Mean dune crest retreat $\overline{\Delta R^*}$ of 1. Argus measurements (—) and its standard deviation (– –), 2. XBeach (—), 3. Profile measurements (•) and its standard deviation (whiskers). Middle panel: Mean erosion volume $\overline{A}$ of 1. XBeach (—) and its standard deviation (– –), 2. Profile measurements (•) and its standard deviation (whiskers). Lower panel: Mean final bottom elevation $\overline{z_b}$ of XBeach (—) and profile measurements (—), the initial bottom elevation of XBeach (–·–) and profile measurements (–·–), SSL (– –) and minimum & maximum measured elevation (– –).

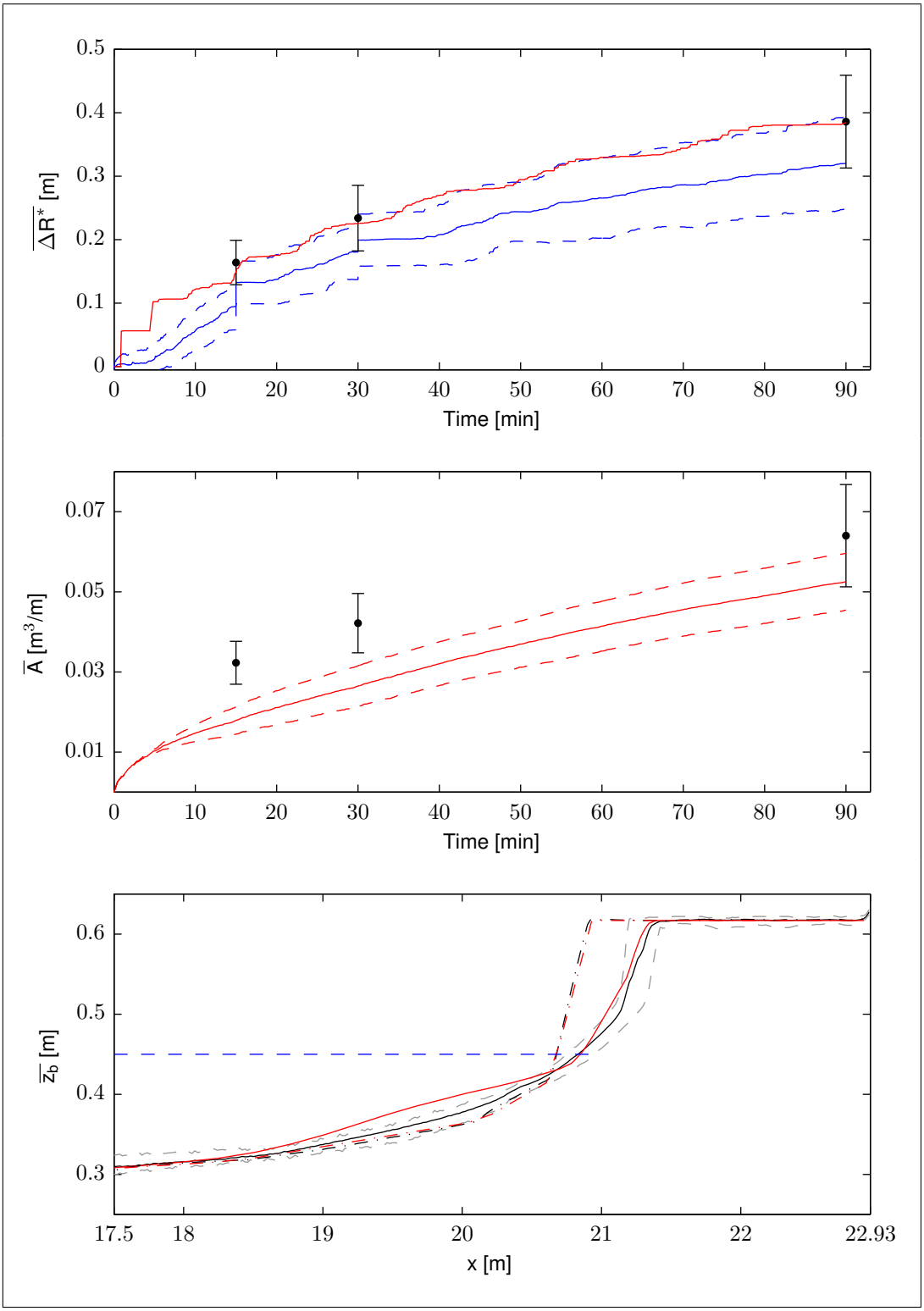

Figure 5.21: Mean erosion parameters of D11 in Experiment V3. Upper panel: Mean dune crest retreat $\overline{\Delta R^*}$ of 1. Argus measurements (—) and its standard deviation (– –), 2. XBeach (—), 3. Profile measurements (•) and its standard deviation (whiskers). Middle panel: Mean erosion volume $\overline{A}$ of 1. XBeach (—) and its standard deviation (– –), 2. Profile measurements (•) and its standard deviation (whiskers). Lower panel: Mean final bottom elevation $\overline{z_b}$ of XBeach (—) and profile measurements (—), the initial bottom elevation of XBeach (– · –) and profile measurements (– · –), SSL (– –) and minimum & maximum measured elevation (– –).

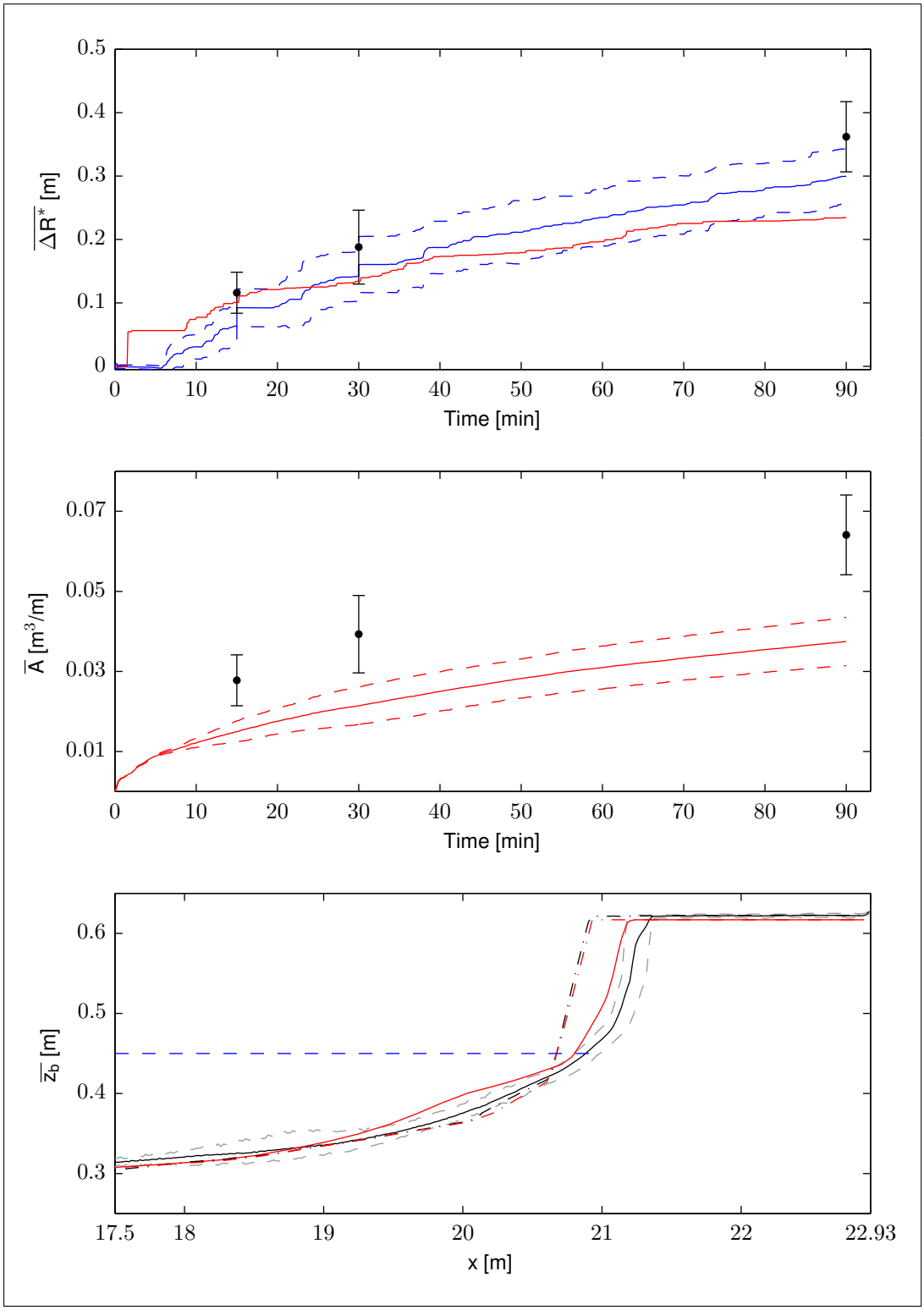

Figure 5.22: Mean erosion parameters of D11 in Experiment V4. Upper panel: Mean dune crest retreat $\overline{\Delta R^*}$ of 1. Argus measurements (—) and its standard deviation (– –), 2. XBeach (—), 3. Profile measurements (•) and its standard deviation (whiskers). Middle panel: Mean erosion volume $\overline{A}$ of 1. XBeach (—) and its standard deviation (– –), 2. Profile measurements (•) and its standard deviation (whiskers). Lower panel: Mean final bottom elevation $\overline{z_b}$ of XBeach (—) and profile measurements (—), the initial bottom elevation of XBeach (– · –) and profile measurements (– · –), SSL (– –) and minimum & maximum measured elevation (– –).

6 Conclusions & Recommendations

6.1 Conclusions

Storm impact on a dune-dike system

During a storm dunes erode and provide sediment to the beach. The foreshore rises and the wave height in front of the dunes decreases. Subsequently the wave-induced water level setup increases. The surface of seawalls prevent erosion by cutting off the supply of sediment to the beach. Waves in front of a seawall remain high throughout the storm and can even increase. Subsequently the wave-induced water level setup decreases.

Over the transition the amount of sediment available for erosion with respect to the dunes decreases. The longshore distance over which the supply of sediment changes depends on the shape and size of the connection. The longshore gradient in the sediment supply causes a difference in elevation of the foreshore. The difference in wave-induced water level setup between dunes and seawalls cause a water level gradient over the transition. The water level gradient drives a current which transports sediment from the dunes to the seabed in front of the seawall. The loss of sediment to the dike profile causes the foreshore of dunes near the connection to rise slower. More and higher waves reach the dunes near the connection during the storm which results in more erosion, see Figure 2.5.

Obliquely incident waves generate a longshore current which transports sediment along the shore. The velocity and transport capacity of the longshore current depend on the dissipation of wave energy. Seawalls reflect incoming waves and the dissipation of wave energy is limited. Consequently the velocity and transport capacity of the longshore current is limited. In a dune transect the dissipation of wave energy and hence the transport capacity of the longshore current is larger. Subsequently there is a longshore gradient in transport capacity in the transition zone.

The amount of additional erosion near structures depends on the angle of wave incidence with respect to the shore. Dunes situated downstream of the connection experience a significant increases in erosion (Steetzel, 1993). Near the upstream connection the decreasing transport capacity of the longshore current causes sediment to be deposited on the seabed in front of the structure. Sediment will pile up against the structure resulting in less erosion near the connection compared to dunes under identical longshore uniform conditions.

Model behaviour of a dune-dike system

The behaviour of a dune-dike system was investigated with exploratory 2DH simulations of a simple closed abrupt connection between dunes and a dike. Dune erosion is quantified by the retreat point R* and the erosion volume A. The behaviour of an undisturbed dune and dike transect is modeled with 1D models. Undisturbed means that there is no influence of a dune-dike connection on process behaviour.

The dune erosion process is simulated correctly by XBeach. After the storm the beach has become wider. The dune foot has moved in landward direction while the waterline moved seaward. The vertical position of the dune foot hardly changed. The behaviour of a dike transect during a storm is modeled well in a qualitative sense. The erosion depth near the toe of a structure is underestimated. This is likely to be caused by an underestimation of the suspended sediment concentration near the toe of the dike (Deltares, 2010).

XBeach predicts additional erosion to develop next to the dune-dike connection. The longshore variation in wave height, wave force F_x and wave-induced water level setup in the transition zone are predicted by XBeach. The resulting water level gradient drives the longshore current in the transition zone, see Figure 3.23. In a situation with normally incident waves the dune crest retreat ΔR^* increased with 24.7% next to the connection. The maximum increase of the erosion volume A near the connection is predicted to be 22.2%, see Figures 3.20 and 3.21 respectively.
The mean transect of the 2DH (270) Dune model with wall boundaries and with Neumann boundaries is identical. This indicates that the lateral boundaries have no effect on the amount of erosion. Although the mean transect of the 2DH (270) models shows more erosion than the 1D Dune model the differences in the bottom profile are little. The longshore current can have a profound impact on the development of additional erosion near structures. XBeach predicts dune erosion of an undisturbed dune stretch in a situation with obliquely incident waves to be more than for normally incident waves, see Figure 3.30. The dune crest retreat increased with 16.5% and the erosion volume with ±15%. This is associated with additional stirring by the longshore current (J.A. Roelvink 2011, pers. comm. 7 September).

When the dunes are situated upstream of the connection sediment will pile up against the structure. Consequently dune erosion next to the connection is less than the erosion in an undisturbed dune stretch. The influence of the dune-dike connection on the additional erosion is isolated from the effect of the longshore current. In this case XBeach predicts the dune retreat near the connection to be 35.4% less than in the undisturbed dune stretch. The erosion volume is predicted to be 32.1% less near the connection, see Figures 3.33 and 3.34. The combined effect of the connection and the longshore current results in a decrease of ΔR^* near the connection of 24.7%. The erosion volume decreases with 22.2%, see Figures 3.35 and 3.36.
In the transition zone there is a gradient in the velocity and transport capacity of the longshore current. Sediment transported by the longshore current is deposited on the seabed in front of the structure. As the foreshore in front of the structure rises the velocity and transport capacity of the longshore current increases. Consequently the sediment is deposited further downstream of the connection.

When dunes are situated downstream of the connection the erosion next to the connection increases significantly. For the isolated effect of the dune-dike connection XBeach predicts the maximum increase of ΔR^* next to the connection to be 56.6%. The erosion volume increased with 64.7%, see Figures 3.47 and 3.48. This is caused by the increasing velocity and transport capacity of the longshore current. The eroded sediment is partially deposited on the foreshore downstream of the connection. Waves in this deposition area break sooner and dunes behind it show less erosion than an undisturbed dune stretch. XBeach predicted dunes in the deposition area to show 28.3% less retreat and a decrease of 22.9% in the erosion volume. For the combined effect of the connection and the longshore current the maximum increase of ΔR^* next to the connection is 82.5%. The maximum increase of the erosion volume is 89.4%, see Figures 3.49 and 3.50.

Experiments in the Delta Basin
The influence of structures on dune erosion was investigated in a series of pilot experiments. The experiments were carried out with normally incident long-crested waves and were aimed at 4 different closed abrupt connections between a dune and a structure. Two configurations of dunes and hard structures were investigated. Each configuration was tested with 2 different wave peak periods T_p. The experiments proved the development of additional erosion near structures. The connections investigated in the experiments were:

1 The connection between a dike and an unprotected dune,

2 The connection between a dike and a dune that is protected by a dune revetment,
3 A breach in a dike with a body of sand,
4 A breach in a dune revetment.

A large number of measurements were taken before, during and after an experiment. To measure the morphological evolution use was made of a wheel profiler, 6 Argus video cameras and a hand-held surface scanner. The Argus video system measured among others the dune crest position every 6 seconds from which the dune crest retreat ΔR^*Argus was derived. From the wheel profiler measurements the erosion volume A_{WP} and the dune crest retreat ΔR^*_{WP} were derived. These measurements were used in the model-data comparison. The hydrodynamics were measured using two types of wave gauges and electro-magnetic flow meters. The wave height measurements were used to calibrate the hydrodynamic conditions in XBeach.

Analysis of the measurements revealed a longshore variation in wave height during the experiments. At the center of the basin the waves were largest. At the right side wall they were smaller. This caused a longshore variation in dune erosion. In some cases gully formation increased the amount of additional erosion near structures. The amount of additional erosion fell well within the standard deviation of the measurements. The effect of additional erosion was very local. Various disturbing processes made the experiments unsuitable to derive a reliable quantification of the additional dune erosion near structures.
Due to the longshore variation in dune erosion statistical parameters were used to compare measurements and prediction. The used parameters were the mean, the standard deviation, the minimum and the maximum of the dataset. Disturbances in space and time were omitted from the model-data comparison.

Model-data comparison
The measurements of the experiments are compared with XBeach predictions. The predictive capabilities of XBeach proved to be good. The measured wave height H_{m0} was used to calibration the wave height in XBeach. In XBeach the wave height is controlled by the breaker parameter γ in the Roelvink formulation for the wave dissipation model (Roelvink *et al.*, 2010). The best representation of the wave height H_{m0} in the Delta Basin is given by $\gamma = 0.54$. This is close to the default value of 0.55.

In XBeach the erosion in a dike breach is a function of the breach width and the wave period, see Figure 5.6. The erosion increases for a smaller breach width. This is associated with the fraction of sediment volume lost to the scour hole in front of the adjacent dikes compared to the total amount of eroded sediment. Wider breaches supply more sediment to the foreshore than narrower breaches. Therefore wider breaches lose relatively less sediment to the scour holes which results in less erosion in wider breaches. The breach erosion increases for an increasing wave period. The erosion in dike breaches (B1, B2 & B3) during the Delta Basin experiments was disturbed. It was influenced by the longshore variation in wave height and gully formation. Therefore no quantitative comparison of the erosion in the breaches was made.

In dune revetment sections large differences between measurements and prediction were observed. XBeach underestimates the erosion above the dune revetment, see Figure 5.9. To erode the dunes above the revetment waves must reach the dune front. Therefore wave runup is an important process for erosion above the revetment. Currently XBeach only simulates long wave runup.

The erosion in the revetment breach (B11) is predicted well. The predicted dune crest retreat

shows a close resemblance with the measurements. The erosion volume is slightly underestimated, see B11 in the upper and lower panel of Figures 5.17 and 5.18 respectively. This is caused by a different shape of the predicted profile. The comparison between a dune revetment breach (B11) and a dike breach (B2) with an equal width revealed that the erosion in breach B11 is less than breach B2, see Figure 5.11. This is associated with the fact that the foreshore of the revetment raised more than the foreshore of the dike. Consequently the wave height in B11 is less than in B2.

For experiments V1 (Dune stretch D1 & D2) and V3 (Dune stretch D11) with a wave period of T_p = 2.07 seconds the predictive capabilities of XBeach are very good. In experiments V1 & V3 the predicted bottom elevation $\overline{z_{b,Pred}}$ above SSL shows a close resemblance with the measured bottom elevation $\overline{z_{b,WP}}$, see the lower panel of Figures 5.19 and 5.21. The predicted mean erosion volume $\overline{A_{Pred}}$ is slightly underestimated, see the middle panel of Figures 5.19 and 5.21. This is explained by the fact that the foreshore in XBeach raised more than in the experiments. The development in time of $\overline{A_{Pred}}$ is simulated well by XBeach. Also the development in time of the predicted mean dune crest retreat $\overline{\Delta R^*_{Pred}}$ shows a close resemblance with the measured time development of $\overline{\Delta R^*_{Argus}}$, see the upper panel of Figures 5.19 and 5.21.
The performance of XBeach for experiments V2 (Dune stretch D1 & D2) and V4 (Dune stretch D11) with a wave period of T_p = 1.55 seconds is relatively good. The predicted shape of the mean bottom elevation above SSL is similar to $\overline{z_{b,WP}}$ derived from the profile measurements, but has an offset in seaward direction. In both experiments a bar developed seaward of x = ±18.5 m which was not predicted by XBeach. The development in time of $\overline{\Delta R^*_{Pred}}$ is not simulated properly by XBeach. The predicted rate of dune crest retreat decreases too rapidly in XBeach. The predicted mean erosion volume $\overline{A_{Pred}}$ is underestimated. This is partially explained by the fact that the foreshore in XBeach raised more than in the experiments. The development in time of $\overline{A_{Pred}}$ is simulated well by XBeach. Generally the performance of XBeach for experiments V2 & V4 is less than in experiments V1 & V3 but is still considered to be relatively good.

The peak frequency of the Jonswap spectrum proved to have a relatively large influence on the amount of dune erosion predicted by XBeach. The effect of the wave period for 2DH models with a large depth scale (n_d = 60) is not properly simulated by XBeach. The configuration of dunes and hard structures has little influence on the effect of the wave period. The stability of XBeach for small depth scales is highly dependent on the calculation grid. Neumann boundaries can generate unwanted longshore currents in a situation with normally incident waves.

6.2 Recommendations

Modeling dune erosion near seawalls

- Resolve the grid dependent stability issues of XBeach revealed by the development of deep scour holes in front of sandy sections.
- Improve the behaviour of Neumann boundary conditions.
- Improve the influence of the wave period on dune erosion for small depth scales.
- Include short wave runup in the avalanching algorithm to better predict erosion above a dune revetment.

Future research to additional dune erosion near structures

- Measure the wave height along a longshore transect at the shoreline and at various distances from it. Preferably measure the surface elevation of the entire model domain with for instance laser altimeters suspended from the roof of the building.

- Limit the longshore variations in wave height as much as possible. Measure the wave height in a longshore transect at the wave board and at various distances from it.
- Use reliable velocity meters and measure the current velocities along a longshore transect at various distances from the shoreline.
- Increase the density of velocity meters in front of the connection to accurately measure the longshore current in front of it.
- Prevent the development of gully formation by either preventing waves from running over the dunes and dikes or prevent water on the dune and dike surface to flow back to the wave basin.
- Investigate one connection per test to be constructed at the center of the model domain to eliminate the mutual influence of connections.
- Investigate the influence of the angle of wave incidence and the shape of the connection on the development and magnitude of the additional erosion near hard structures.

References

Boers, M., 2008. *Duinen als Waterkering: Inventarisatie van kennisvragen bij waterschappen, provincies en rijk*. Tech. rep., Deltares, Delft. Projectnumber H5019.10. 2

Boers, M., P. van Geer and M. van Gent, 2011. *Dike and dune revetment impact on dune erosion*. Tech. rep., Deltares, Delft. Proceedings of the Coastal Sediments 2011. 3, 58, 63, 69

Boers, M., I. van der Werf and P. van Geer, 2008. *Dune and Dike Connections: Pilot experiments in the Vinjé Wave Basin*. Tech. rep., Deltares, Delft. Projectnumber H5019.50. 9, 55, 58, 59, 60, 61, 64, 65, 67, 70

Bosboom, J. and M. Stive, 2010. *Coastal Dynamics 1*. Delft University of Technology, Faculty of Civil Engineering and Geosciences. Lecture notes CT4305. 6, 7, 10, 12, 13, 15, 16, 17

Brandenburg, P., 2010. *Scale dependency of dune erosion models, performance assessment of the DUROS and XBeach model for various experiment scales*. Master's thesis, University of Twente. 78

Deltares, 2010. *XBeach testbed report*. Tech. rep., Deltares, Delft. Revision: 1241. VIII, 29, 30, 52, 88, 98, 109

Expertisenetwerk Water Veilig, 2007. *Technisch Rapport Duinafslag*. Beoordeling van de veiligheid van duinen als waterkering ten behoeve van Voorschrift Toetsing op Veiligheid 2006. Expertisenetwerk Water Veilig. 3, 5

Geer, P. van, M. Boers and M. van Gent, 2009. *Measurements on the interaction between dunes and dikes during extreme storm events*. Tech. rep., Deltares, Delft. Proceedings of Coastal Dynamics, Paper 84. 62

Gent, M. van, J. van Thiel de Vries, E. Coeveld, J. de Vroeg and J. van de Graaff, 2008. *Large-scale dune erosion tests to study the influence of wave periods*. Tech. rep., Deltares, Delft. Coastal Engineering, 55(12): 1041-1051. 95, 96, 98

Holthuijsen, L., 2007. *Waves in oceanic and coastal waters*. Cambridge University Press. ISBN: 978-0-521-86028-4. 10, 11

Holthuijsen, L., N. Booij and T. Herbers, 1989. *A prediction model for stationary short-crested waves in shallow water with ambient currents*. Tech. rep., Delft University of Technology, Delft. Coastal Engineering, 13(1989): 23-54. 19

Massel, S. R., 1996. *Ocean surface waves: Their physics and prediction*, chap. 9, pages 393–425. World Scientific Publishing Co. Pte. Ltd. ISBN: 9810216866. 61

Ministerie van Verkeer en Waterstaat, 2007. *De veiligheid van de primaire waterkeringen in Nederland*, chap. 6, pages 179–213. Voorschrift Toetsing op Veiligheid voor de derde toetsronde 2006-2011. Ministerie van Verkeer en Waterstaat, Den Haag. ISBN: 978-90-369-5762. 2

Rijkswaterstaat, 2004. *Waterwijzer 2004 - 2005: Feiten en cijfers waterbeheer in Nederland*. Ministerie van Verkeer en Waterstaat. 1

Rijn, L. van, P. Tonnon, A. Arcilla-Sanchez, I. Caceras and J. Grüne, 2008. *Scaling laws for beach and dune erosion processes*. Tech. rep., WL | Delft Hydraulics, Delft. Projectnumber H2178. 60

Roelse, P., 1993. *Eindconstructies van dijken en duinvoetverdedigingen in Zeeland*. Tech. rep., Ministerie van Verkeer en Waterstaat, Middelburg. Werkdocument GWWS-93.843X. 7, 9

Roelvink, J., A. Reniers, A. van Dongeren, J. van Thiel de Vries, J. Lescinski and R. McCall, 2010. *XBeach Model Description and Manual*. Unesco-IHE Institute for Water Education and Deltares and Delft University of Technology. Version 6. IX, 19, 82, 111

Roelvink, J., A. Reniers, A. van Dongeren, J. van Thiel de Vries, R. McCall and J. Lescinski, 2009. *Modeling storm impacts on beaches, dunes and barrier islands*. Tech. rep., UNESCO-IHE Institute for Water Education, Delft. Coastal Engineering, 56(2009): 1133-1152. 19, 20, 21

Steetzel, H., 1987. *Modelonderzoek duinvoetverdedigingen: Systematisch onderzoek naar de werking van duinvoetverdedigingen; modelonderzoek op grote schaal in de Deltagoot*. Tech. rep., WL | Delft Hydraulics, Delft. Projectnumber H298.01. 29, 30

—, 1993. *Effect bebouwing op de mate van duinafslag: Een eerste verkenning inzake bebouwingseisen voor de zeereep*. Tech. rep., WL | Delft Hydraulics, Delft. Deel 1: Verslag bureaustudie. VII, 8, 9, 10, 32, 109

—, 1995. *Toetsing aansluitconstructies: Advies formulering toetsingsregels voor de vormgeving van de aansluiting tussen de verschillende waterkeringsconstructies*. Tech. rep., WL | Delft Hydraulics, Delft. 2, 8, 9, 55

Technische Adviescommissie voor de Waterkeringen, 1995. *Basisrapport Zandige Kust*, chap. 3, pages 45–49. Ministerie van Verkeer en Waterstaat. ISBN: 90-36-93-704-3. 1, 2

Tilmans, W., 1981. *Onderzoek naar duinafslag tijdens superstormvloed: Toetsing van de resultaten van het twee-dimensionale modelonderzoek door middel van onderzoek in een drie-dimensionaal model*. Tech. rep., WL | Delft Hydraulics, Delft. Projectnumber M1653. 55

van Thiel de Vries, J., 2009. *Dune erosion during storm surges*. Ph.D. thesis, Delft University of Technology. 5, 6, 16, 21, 27, 32

van Thiel de Vries, J., A. van Dongeren, R. McCall and A. Reniers, 2010. *The effect of the longshore dimension on dune erosion*. Tech. rep., Deltares, Delft. 32nd International Conference on Coastal Engineering. 5, 22

Vellinga, P., 1986. *Beach and dune erosion during storm surges*. Ph.D. thesis, Delft University of Technology. 1, 60

Wenneker, I., A. van Dongeren, J. Lescinski, J. Roelvink and M. Borsboom, 2010. *A Boussinesq-type wave driver for a morphodynamical model to predict short-term morphology*. Tech. rep., Deltares, Delft. Coastal Engineering, 58(2011): 66-84. 52